SPIN ZERO WINDOWS TO NEW PHYSICS

Memoria de Tesis Doctoral realizada por

ROCÍO DEL REY BAJO

presentada ante el Departamento de Física Teórica
de la Universidad Autónoma de Madrid
para la obtención del Título de Doctora en Ciencias.

Tesis Doctoral dirigida por

BELÉN GAVELA LEGAZPI

Catedrática del Departamento de Física Teórica
de la Universidad Autónoma de Madrid.

UAM
UNIVERSIDAD AUTONOMA
DE MADRID

ift Instituto de Física Teórica
UAM-CSIC

– Madrid, febrero de 2018 –

Rocío del Rey Bajo: *Spin zero windows to New Physics,* – Madrid, febrero de 2018
SUPERVISORA: Belén Gavela Legazpi

PUBLICATIONS

This thesis is based on the following scientific articles:

JOURNAL ARTICLES IN THIS THESIS

[1] **Non-linear Higgs portal to Dark Matter**.
I. Brivio, B. Gavela, L. Merlo, K. Mimasu, J.M. No, R. del Rey and V. Sanz
JHEP 04 (2016), p. 141. and *arXiv: 1511.01099 [hep-ph]*

[2] **ALPs Effective Field Theory and Collider Signatures**.
I. Brivio, B. Gavela, L. Merlo, K. Mimasu, J.M. No, R. del Rey and V. Sanz
Eur. Phys. J. C77.8 (2017), p. 572. and *arXiv: 1701.05379 [hep-ph]*

[3] **The Axion and the Goldstone Higgs.**
I. Brivio, B. Gavela, S. Pascoli, R. del Rey, S. Saa
arXiv: 1710.07715 [hep-ph]

PROCEEDINGS

[4] **Non-linear Higgs portal to Dark Matter**.
51st Rencontres de Moriond on Electroweak Interactions and Unified Theories
La Thuile, Italy, March 12-19, 2016
arXiv: 1605.06388 [hep-ph]

[5] **ALPs EFT & Collider Signatures**.
13th Patras Workshop on Axions, WIMPs and WISPs
Thessaloniki, Greece, May 15-19, 2017
arXiv: 1711.04517 [hep-ph]

AGRADECIMIENTOS

Da vértigo llegar a este punto y echar la vista atrás, pensando de una en una en todas las personas que me habéis acompañado en este proceso duro a la par que gratificante.

Una tesis que empezó con una puerta entornada dejando entrever lo que hay detrás: la puerta era la de Belén, quien me invitaba seguir haciendo física. A ti te agradezco profundamente innumerables cosas, desde la oportunidad de hacer investigación hasta el acompañamiento en los momentos de mayor inseguridad. Tu perspectiva, tus consejos y tu exigencia me llevan a estar aquí con mucha más confianza de la que nunca imaginé que tendría. Pero sobre todo te agradezco que compartas y contagies tu gusto por aprender, es inspirador ver esa pasión en alguien que lleva tantos años en haciéndolo. Considero una suerte haber vivido contigo esta incursión en el mundo de los axiones a la que me invitaste hace cuatro años y en la que he disfrutado mucho. Pero porque la física no lo es todo, y eso siempre lo has entendido, gracias también por apoyar mis aspiraciones en el mundo educativo y facilitarme mis primeros pasos en el camino que seguiré ahora.

Quiero agradecer a las personas que me han enseñado el día a día de la física: las cuentas, el rigor y la honestidad. Una gran parte de mi trabajo ha salido adelante gracias a Josemi, con quien he tenido las larguísimas conversaciones de skype gracias a las cuales me he atrevido con el mundo de las simulaciones, que ha ampliado enormemente mis posibilidades de hacer física. Has estado siempre accesible y me has repetido varias veces las mismas respuestas sin desesperar ni un poquito. Tanto los trabajos que hemos hecho juntos como las cenas en Sussex y el par de conferencias que hemos compartido me harán lamentar que nuestro futuro solapamiento en Madrid no vaya a ser más largo.

De la misma manera quiero agradecer a Luca por los quebraderos de cabeza compartidos respecto a las partes más teóricas de mi trabajo. Pero sobre todo porque gracias a tu insistencia en los Pheno-coffees he aprendido sobre muchas cosas no centrales en mi trabajo, pero que me han abierto las miras y han ejercitado mi capacidad de aprender. Gracias también por tu sangre germana, que ha mantenido nuestras carpetas compartidas a salvo del caos.

Otra persona que ha acompañado mis proyectos científicos ha sido Verónica, en quien admiro el entusiasmo con el que acoge las ideas de los demás, pero sobre todo por el entusiasmo con el que hace física. No hay más que ver tu charla en el Workshop de Invisibles 2017, en la que lo decías claramente: “It has to be fun, guys!”. Gracias a Enrique porque tu puerta estaba siempre abierta, y por toda la física que he aprendido de ti, desde las clases en el máster hasta las explicaciones todos los viernes en el Pheno-Coffee. Quiero agradecer también a las otras personas que me han acogido en el mundo científico, en concreto en mis estancias en Berkeley: Zoltan Ligeti y Mary K Gaillard.

Volviendo al día a día, quiero agradecer a Ilaria, que ha ejercido excelentemente su rol de *hermana mayor de doctorado* compartiendo conmigo todo lo que sabía, y dándome la tranquilidad

de decir mis preguntas en voz alta por simples que parecieran. Eres además todo un ejemplo a nivel de comunicación científica: todavía veo en mis diapositivas atisbos de tu claridad. A mis otros hermanos de doctorado también tengo mucho que agradecerles. A Pablo porque le hemos dado muchas (y cuando digo muchas son muchas) vueltas a nuestros infinitos, y a día de hoy seguimos compartiendo la intriga de si se cancelarán. Pero sobre todo porque lo que sí es infinita es tu curiosidad: gracias por poder presenciarla y compartirla, viendo cómo te permite enfrentarte a lo desconocido sin miedo. Agradezco a Sara por lo que hemos compartido en las conferencias: tanto el nerviosismo que nos ha llevado a practicar varias veces las charlas juntas y buscarnos en el público, como la diversión y el cansancio –no todos los días puede una esquiar y estar en siete charlas de física en un mismo día.

Gracias a todas las personas del ift y el departamento que han hecho de este periodo una experiencia más agradable a diario. Al DiscoChino, Víctor, Miguel y Mario: no era consciente de lo que apreciaba vuestra presencia hasta que os marchasteis. Me ayudasteis a cambiar mi fumeteo de por la mañana por un delicioso café en buena compañía, y con vosotros aquí las comidas eran otra cosa. En concreto, gracias a Víctor, que además has sido todo un ejemplo como profesor y como divulgador. Gracias a otras personas con las que he compartido comidas: Maria José, gracias porque tus conversaciones son "de verdad", y gracias a eso me he sentido más presente en el ift. Gracias a Carlos Pena por la oportunidad de hacer divulgación, combinando la tesis con mi gusto por enseñar. Siempre diré que los momentos en los que más disfruto la tesis son aquellos en los que le explico lo que hago a alguien que no sabe pero tiene interés. Al equipo de secretaría porque siempre respondéis a todo con una sonrisa, y en concreto a Isabel, por la atención y el cuidado a cada uno de los que pasamos por aquí y a Rebeca por alguna conversación más larga "sobre cosas de la vida". Gracias también al equipo del departamento, tanto a Ana como a Javier, que hacen un trabajo excelente de poner orden en nuestras vidas.

Habiendo puesto las miras en la facultad quiero agradecer a mis amigos y compañeros físicos, los antarianos, con los que tantas comidas, conversaciones y horas de estudio he compartido. Javi, Pepe, Jose Manuel y Jorge: gracias a vosotros la facultad ha sido un lugar realmente familiar, y los años de carrera han sido muy divertidos. Gracias también a la gente de la Malasaña, de la FEL y de las asambleas, con quien he sentido la potencia de la gestión comunitaria. Ojalá estas prácticas se extiendan más un día pronto.

Aunque no siempre ha facilitado el desarrollo de esta tesis por la cantidad de dudas que me ha generado, hay todo un ámbito de mi vida que me ha hecho crecer mucho como persona y situar esta tesis en un mundo más amplio. Se trata de mis compañeros y compañeras de asambleas varias y otros aliados en el acto de tratar de tener una mirada crítica a un mundo enfermo, por dolorosa que sea, pero sobre todo en el acto de tratar de construir un mundo que merezca ser vivido. A los salmones, por el libro de Oblomoff: porque confiasteis en mí y porque me hizo pensar mucho sobre el sentido de todo esto. Pero gracias sobre todo por las conversaciones sesudas y por las personales. A los chicos –Ángel, Raúl y Jorge– gracias porque sois amigos, porque sois barrio. A las compas de Nosaltres porque sois un ejemplo. A los habitantes de los pueblos que he visitado, gracias por regalarme ese horizonte. Y a Quique, gracias por el cariño, la sinceridad y el flamenco. Entre todos habéis mantenido mi mente despierta y mi corazón encendido.

Gracias a las Rudas –Silvia y Guiliana– que habéis dado la vuelta a mi vida en este último medio año. Gracias por darme de nuevo un hogar (mientras que yo andaba en Mérida sin poder haceros ni caso). Si solo hubiera sido una casa donde escribir la tesis os podría agradecer el *protocolo tesis* (¡oh, no! ya se me acaba), el super ambiente de trabajo que hay en casa o el tener ganas de seguir en Madrid por lo menos hasta otoño terminando mis proyectos de física. Pero es no es más que una ínfima parte de lo que se cuece en esta casa. Gracias a vosotras vuelvo a tener una nevera con comida *compartida*, platos ricos sobre la mesa a diario, invitados a cenar, invitados a dormir, una conversación agradable cada vez que nos encontramos por cualquier rincón de la casa, una sonrisa, una risa... y dos amigas. Este hogar ha sido un pilar esencial estos últimos meses.

Gracias a las compañeras de Malasartes, *aka* equipo salmonete, por acogerme comprensivamente en clase y en la compañía en mis idas y venidas. Quizá sin saberlo, me habéis ayudado a salir a flote en alguno de los momentos más dificiles de estos cuatro años. En concreto, gracias a Rous por tanto amor.

Quiero agradecer a otras personas que me han acompañado de diferentes maneras en los últimos tiempos. Natxo, durante el TFM me tocó vivir los meses de mayor inseguridad, pero mantuviste viva la chispa de la curiosidad y el gusto por la investigación. Carmen, has sido más soporte de lo que te imaginas: gracias. Elena, has sido "la amiga que me he echado en el barrio", algo verdaderamente importante para mi. A los habitantes de Carnero: gracias, Peri, por tu cariño por ser un super compañero de piso. Gracias, Chevo, porque seguir ahí en la distancia, y por aquel mes de ensueño en casa que siempre recordaremos. María, gracias a ti Carnero ha seguido siendo hogar cuando podía haber dejado de serlo. Quiero dar las gracias a Diego, por enseñarme a ser autodidácta, porque gracias a tí ahora tengo la guitarra y el euskara. Y termino agradeciendo especialmente a Paloma, Manuel, María y Paula el haberme querido como familia. Me habéis abierto las puertas y me habéis arropado, en un acto de valor incalculable. Y gracias a todas las que no nombro pero que se saben partícipes de esto de una manera u otra.

Quiero un huequito especial en estos agradecimientos para Kike, con quien no solo he compartido las alegrías y miserias del mundo de la investigación si no además el interés por la naturaleza, la educación y la montaña. Y chapas muy largas y a veces muy rápidas para mantenernos al día en la distancia. También quiero otro huequito para Miguel, porque hay un amor que no se olvida, y porque no hay nadie que muestre más entusiasmo que tú cuando les hablo de mi tesis. Gracias también a Dani, porque me acompañas desde hace muchísimos años (¡más de diez!) de una manera sencilla pero tremendamente especial.

Adrián, hay tantos de estos agradecimientos que se relacionan contigo, que no sé por dónde empezar. Gracias por ser familia en lo que al día a día se refiere: esta tesis ha salido adelante en gran parte gracias a la estabilidad de nuestra vida en común. Gracias también por el horizonte, que me ha dado la fortaleza de seguir en esto hasta el final, a pesar de que a veces pareciera que nunca iba a llegar. Contigo he compartido las ansias de transformación mientras que me embarcaba en este proyecto que implicaba permanecer. Eres la persona que atraviesa muchísimas de mis contradicciones, y quiero agradecerte por seguir en pie en ese lugar tan difícil que ocupas.

Indra, no deberías preocuparte estar o no estar en estos agradecimientos porque donde estás innegablemente es en mi vida. La has transformado de maneras que ni te imaginas con una inyección de alegría, amor, cuidado y ganas de vivir. En concreto, has acompañado el final de esta tesis a todos los niveles: has compartido conmigo los momentos de frustración con el cariño que te caracteriza, has alimentado la ilusión y el orgullo por mi trabajo con tu sonrisa y enorme empatía y has mantenido vivo a este cuerpo lleno de necesidades y deseos, con comida, descanso y pura vida en la montaña. Y ahora tienes toda mi confianza, compañero. Pero esto va más allá de la tesis, y lo sabes de sobra. Gracias porque he perdido un poco el miedo al cambio contigo. Sonrío a las aventuras que busquemos en este final de etapa que estamos compartiendo, y miro sin miedo para adelante sin dejar de disfrutar de cada instante del presente, con verdadera curiosidad de adonde nos llevará esto.

A mis amigas quiero agradeceros por ser constantes. Por estar siempre ahí: mes tras mes, año tras año. Por saber mutar y transformarnos para crecer juntas. Diez años de noches en la calle, tardes al sol, viajes apretujadas en mi coche, conversaciones sobre las cosas más fundamentales de la vida. Diez años de escuchas y preocupaciones sinceras... y tantas otras cosas que quedan por venir. Gracias Andrea por tu atención y confianza en que saldría adelante; Ana, gracias por tu decir las cosas difíciles cuando hacía falta; Marina, por tu contagiosa energía y gracias, Marta, por tu capacidad para escuchar.

Quiero dar muchas muchas gracias a mi familia. A mi abuelita, gracias por mantener el quererme tanto y por ser un ejemplo de fortaleza. Paula, a veces me sorprendo al ver que incluso en la distancia pensamos parecido y vivimos parecido. Gracias por todo lo que hemos aprendido juntas, y más recientemente por los momentos de profunda comprensión de los procesos vitales la una de la otra que a veces parecen ir en paralelo. A ti, papá, por tener buenos consejos cuando los he buscado, respetar mis decisiones cuando no pregunto, y porque me apoyas incondicionalmente en mis certezas y en mis dudas. Y a ti, mamá, porque me acompañas día a día, me escuchas en cada decisión difícil que tengo que tomar y por el mismo apoyo incondicional que le agradezco a papá. A ambos por la educación que me habéis dado: gracias a vosotros conozco los frutos del esfuerzo y del compromiso.

De no haber compartido esto con todas vosotras, no diré que no hubiera sido posible, pero sé seguro que no hubiera tenido sentido.

CONTENTS

ACRONYMS

ALP axion-like particle

BSM beyond the Standard Model

CKM Cabibbo-Kobayashi-Maskawa

CMB cosmic microwave background

CPV CP violation

DM dark matter

EDM electric dipole moment

EFT effective field theory

EOM equation of motion

EW electroweak

EWSB electroweak symmetry breaking

GB Goldstone boson

GC globular cluster

ggF gluon-gluon fusion

HB horizontal branch

HDM hot dark matter

HEFT Higgs effective field theory

HL-LHC high-luminosity LHC

LHC Large Hadron Collider

LSW light-shining-through the wall

MACHO massive astronomical compact halo object

MOND modified Newtonian dynamics

MSSM minimal supersymmetric Standard Model

NDA naive dimensional analysis

nEDM neutron electric dipole moment

NGB Nambu-Goldstone boson

NLO next-to-leading order

NNLO next-to-next-to leading order

NP new physics

pGB pseudo-Goldstone boson

PQ Peccei-Quinn

PQWW Peccei-Quinn-Weinberg-Wilczek

QCD Quantum Chromodynamics

QED Quantum Electrodynamics

SM Standard Model

SMEFT Standard Model effective field theory

SSB spontaneous symmetry breaking

UV ultra-violet

VBF vector-boson fusion

WIMP weakly-interacting massive particle

Part I

INTRODUCTION

MOTIVATIONS AND PURPOSE

Until very recently all known elementary particles were either fermions or vector gauge bosons, but the discovery in 2012 of a spin zero resonance at the Large Hadron Collider (LHC) changed this picture with the inclusion of a new (possibly elementary) scalar identified as the boson of the Higgs mechanism. This completed the discovery of the fundamental particles of the Standard Model of particle physics (SM). The question is whether the discovery of the Higgs particle not only culminates an essential quest of humankind but also heralds new territory to explore.

Indeed, there are still uncomfortable yet exciting hints suggesting that the SM picture is incomplete. On the one hand, a set of experimental observations cannot be accounted for in this theory. Plausibly beyond the realm of particle physics lies the problem of "Dark Energy", the common name for the unknown mechanism behind the accelerated expansion of the universe which confronts cosmological models. However, particle physics has its own pressing issues:

- **Neutrino masses and mixings.** Neutrino masses can be accommodated by Dirac mass terms in the SM Lagrangian through Yukawa interactions, as for the rest of the SM fermions. However, unless the ad-hoc assumption of a global $B - L$ invariance is required, gauge invariance allows in addition another type of mass terms, Majorana masses, which can additionally elegantly explain their smallness. Which is the extension that describes massive neutrinos, and the question whether they are of Dirac or Majorana nature remains one of the open questions in particle physics.
- **Dark Matter:** The most appealing explanation of 27% of the matter of the universe is an unknown type of particle or particles, a fascinating realm that needs to be identified, with candidates' masses ranging $10^{-22} - 10^{18}$ GeV.
- **Matter-antimatter asymmetry,** or the question of why the observed universe is made of matter. Explanations based on imposing initial conditions are difficult to reconcile with the ideas of inflation, which is a strong candidate to account for the evolution of the early universe. Microphysics could alternatively explain the asymmetry, but the SM alone is largely insufficient.

Furthermore, anomalies have appeared in different realms of particle physics, from neutrinos to hadronic data (for instance, the present ones involving several observables B meson decays), although none are significant enough to claim the discovery of new physics (NP).

In addition to the experimental hints, the SM also raises some theoretical concerns on its structure, of which the most worrysome manifest themselves in the form of fine-tunings which are to be imposed on some of the parameters of the Lagrangian:

- **The flavour puzzle** concerns the large hierarchy between the size of the Yukawa couplings which determine the fermion masses in the SM, with ratios as large as $m_\tau/m_e \sim 10^3$ for the charged leptons and $m_t/m_u \sim 10^5$ for the quarks. Although chiral symmetry protects the small numbers involved, their stringent adjustment calls for some rational explanation if a true understanding is desired.

- **The electroweak hierarchy problem,** or why the Higgs particle "is so light". The fact that the Higgs is a spin zero particle means that its mass is not protected by gauge symmetries, but on the contrary very sensitive to possible high-energy extensions of the SM. Radiative corrections to its mass would then force a tuning between parameters to explain its electroweak-scale value of 125 GeV.
- **The strong CP problem:** A combination of the QCD topological angle in $\sim \theta G_{\mu\nu}\tilde{G}^{\mu\nu}$ and electroweak sources of CP violation in the quark mass matrices is expected to show up in measurements of the electric dipole moment of the neutron, but experiments constrain this combination to $\bar{\theta} \lesssim 10^{-10}$. Such a strong fine-tuning calls as well for a dynamical explanation.

Although apparently of very different nature, two or more of these problems may in fact be related: some proposals extend the matter content of the SM solving various problems simultaneously. Conversely, the solutions to one problem may aggravate another: e.g. the EW hierarchy problem may feed the strong CP problem as most theories devised to solve the former induce unacceptably large quantum corrections to $\bar{\theta}$.

This thesis pays special attention to fine-tunings such as those characterising the strong CP problem and the electroweak (EW) hierarchy problem. In the past, symmetry principles have proven fruitful in solving fine-tuning issues. A guidance in the approach based on symmetries is provided by 't Hooft's naturalness criterion [6], according to which a physical parameter is allowed to be very small only if taking it to zero increases the symmetry of the system. From this perspective, small parameters may be explained by approximate symmetries, serving as guideposts of symmetries yet undiscovered. For instance, the lightness of pions with respect to other QCD bound states is understood on account of the almost exact realisation of a chiral flavour symmetry of quarks, slightly broken by the quark masses.

Symmetries may however be hidden. A symmetry may be exact at the level of the Lagrangian but not apparent in the observed spectrum, in which case it is said to be *spontaneously broken*. In scenarios where the Lagrangian has an enlarged continuous symmetry (global or gauge) which breaks spontaneously, there is one massless particle predicted for each broken generator: a Goldstone boson. They are a tell-tale of hidden symmetries. These and other spin zero particles appear amongst the scalars and pseudoscalars in beyond the SM (BSM) solutions to some of the aforementioned problems. Hence, the Higgs boson may not be the last but rather the first of a completely new sector of particles yet to be explored: *the spin zero window to new physics*.

This thesis is structured around solutions to some of the problems of the SM which happen to require extra scalars and/or pseudoscalars. In a first step, a theoretical proposal deals with two fine-tuning problems simultaneously: the strong CP problem and the EW hierarchy problem, studying the minimal extension of composite Higgs models which allows to implement the axion solution to the strong CP problem. In a second, more phenomenological step, the search for GBs in general will be tackled, using and developing the tool of effective Lagrangians to identify novel experimental proposals in the search for axions and axion-like particles (ALPs) at colliders. A third step of the exploration of the spin zero sector will concentrate on the case of scalar dark matter (DM), reconsidering the phenomenological

status of the Higgs portal scenario in the light of a more general formulation of effective field theories (EFTs), and of new LHC signatures.

In the theoretical and model-building part of this work we concentrate on a minimal implementation of two Goldstone boson (GB) solutions to fine-tuning problems. The strong CP problem may find its solution in the axion, the GB associated to the $U(1)_A$ Peccei-Quinn symmetry [7] which would explain the non-observation of the $\bar{\theta}$ parameter (and which is additionally an excellent candidate for DM). Assuming only the gauge symmetries of the SM, the axion physics scale f_a is phenomenologically constrained by astrophysics to be in general many orders of magnitude larger than the observed EW scale. These two scales are not watertight though, as they communicate through the scalar potential, and quantum corrections tend to raise the latter to values of $\mathcal{O}(f_a)$. Thus, one of the major drawbacks of the most extended axion solutions –*invisible axion models*– is that they are strongly fine-tuned from the point of view of the EW hierarchy problem. This is an example of solution to one fine-tuning problem which aggravates another. There exist, however, a class of solutions to the EW hierarchy problem based endowing the Higgs itself with a pseudo-Goldstone boson (pGB) character. The small scale, in this case the mass of the Higgs particle, is protected from putative higher scales via its Goldstone boson ancestry [8]. We will propose and study a setup in which composite Higgs models are minimally extended to implement PQ symmetry solving the strong CP problem. A recurrent characteristic in composite Higgs models is the presence by construction of vectorial exotic fermions, much as in KSVZ invisible axion theories [9, 10]: we take advantage of this fact and it will be shown that an extra complex scalar is enough to make the composite Higgs models PQ invariant. Associated phenomenological predictions will be determined as well.

More in general, GBs are relevant particles to study from the point of view of the problems of the SM, as many extensions of the SM feature one or several spontaneously broken global $U(1)$ symmetries. In consequence, it seems desirable to remain agnostic about the type of GBs or pGBs that we may find in Nature. Thus, we move on to engage in a general study of the couplings of ALPs to the SM fields, with the aim of reviewing the status of ALP phenomenology, and leading us to explore a novel experimental path in the search for GBs. The model-independent way of formulating the exploration of new physics (NP) in low-energy data is provided by the use of effective Lagrangians: a *linear* expansion is used when assuming linear realizations of electroweak symmetry breaking (EWSB) [11, 12] , while *non-linear* expansions–sometimes called *chiral*– are the optimal instrument to treat regimes which are not necessarily weakly interacting, as the composite Higgs scenarios previously mentioned [13–15]. The leading and next-to-leading order interactions of ALPs in the context of the linear Lagrangian were formulated long ago [16], while the non-linear effective basis was lacking, and will be developed here.

The use of effective field theories is specially well-suited for phenomenologically-oriented studies, as it gives an idea of the amount and type of experiments which are needed to truly span the independent directions in parameter space. Up to now, phenomenological analyses concentrated on ALP couplings to photons, gluons and fermions, which dominate at low energies and determine, for instance, astrophysical constraints for light ALPs. However, the $SU(2)_L \times U(1)_Y$ invariant formulation of their interactions in EFTs brings up, together with

the coupling to photons, ALP couplings to the other EW gauge bosons, irrespectively of whether the expansion is linear or chiral, and to the Higgs in the latter case. Interesting phenomenological proposals have been very recently developed to test some of these couplings, both in the context of low-energy probes via one-loop contributions to rare meson decays able to test axion coupling to $W^{\pm}$ bosons [17], and of high-energy observables at LHC involving Z boson-mediated axion production [18]. We will identify novel channels which stem from the effective theory formulation. The high-energies and momenta made now accessible by LHC allow a serious exploration of derivative couplings in all generality and of axions with masses beyond the reach of low-energy probes. The new searches that we propose at the LHC may be essential in the quest for Goldstone bosons.

Spin zero particles are strongly motivated by other problems mentioned above. DM can be explained not only by axions with mostly derivative couplings (non-thermally produced through mechanisms such as the misalignment mechanism and others). Scalars with polynomial couplings to the SM fields thermally produced in the early universe are also viable candidates to this major observational puzzle. The renormalisable interactions of DM scalar candidates with the SM fields take place through couplings with the Higgs in a very tightly constrained scenario called *the Higgs portal* [19]. Again from an EFT perspective, the question here raised is what do leading order interactions between a scalar DM and the SM look like in non-linear realisations of EWSB, *i.e.* the *non-linear Higgs portal*. We will study the linear and non-linear effective interactions of a real scalar particle with the SM fields and explore its phenomenological consequences at colliders, together with its cosmological implications tested in DM observables such as relic density and direct detection.

The Higgs may have opened the window to an intriguing new territory where we may find scalars and pseudoscalars, of (pseudo)Goldstone nature or not, playing an essential role in solving some of the pressing open questions of the SM. The impressive experimental developments of the recent years, exploited in this thesis in the context of spin zero particles, should bring us closer to the solid theoretical construction longed for by particle physics. Hopefully, this thesis serves as a stepping stone in this quest.

Chapters 1-4 present the state of the art. The original contributions of this thesis are reported in Chapters 5, 6 and 7.

OBJETIVO Y MOTIVACIÓN

Hasta recientemente, todas las partículas fundamentales conocidas eran fermiones o bosones gauge, pero el descubrimiento en 2012 de una resonancia de spin cero en el LHC cambió el panorama con la inclusión de un nuevo escalar (posiblemente elemental) identificado como el bosón de Higgs. Este acontecimiento completó el descubrimiento del Modelo Estándar (ME) tal y como lo conocemos hoy. La pregunta ahora es si el descubrimiento del Higgs culmina una búsqueda esencial de la humanidad o, al contrario, anuncia la existencia de nuevo territorio aún por explorar.

En efecto, existen una serie de pistas incómodas aunque emocionantes que sugieren que el ME está aun incompleto. Por un lado se encuentran una serie de observaciones que no se explican en esta teoría. Posiblemente mas allá de la esfera de la física de partículas se halla el problema de la "energía oscura", el nombre que se da al mecanismo desconocido que pueda explicar la expansión del universo, y que a día de hoy confronta a los modelos cosmológicos. Pero la propia física de partículas tiene sus cuestiones urgentes a las que dar respuesta.

- **Masas y parámetros de mezcla de los neutrinos.** Las masas de los neutrinos se pueden acomodar con términos de masa de Dirac en el Lagrangiano del ME, mediante acoplos de tipo Yukawa, como para el resto de los fermiones. Sin embargo, salvo si se asume la existencia ad-hoc de simetría global $B - L$, también se podría escribir otro tipo de término de masa, una masa de Majorana, que podría además explicar la ligereza de los neutrinos. Cuál es la extensión que describe a neutrinos con masa, y si son partículas de tipo Dirac o Majorana sigue siendo una pregunta abierta en la física de partículas.
- **Materia Oscura:** La explicación más atractiva del 27% de la materia del universo es un tipo de partícula desconocida, un ámbito fascinante con candidatos cuyas masas abarcan de los 10^{-22}GeV hasta los 10^{18} GeV.
- **Asimetría materia-antimateria,** o la pregunta de por qué el universo observado está hecho de materia. Las explicaciones basadas condiciones iniciales impuestas son difíciles de reconciliar con las ideas de inflación, un candidato fuerte para explicar la evolución del universo temprano. Se podría explicar mediante física de partículas, pero el ME por si sólo es altamente insuficiente.

Además de estas pistas observacionales, el establecimiento del ME suscita algunas preocupaciones respecto a su estructura o consistencia teórica, de entre las cuales las más preocupantes aparecen en forma de ajustes finos que se deben imponer sobre algunos parámetros del Lagrangiano.

- **El problema del sabor** concierne a la gran jerarquía entre el tamaño del los acoplos de Yukawa que determinan las masas de los fermiones, con proporciones de hasta $m_\tau/m_e \sim 10^3$ en el caso de los leptones cargados y $m_t/m_u \sim 10^5$ en el caso de los quarks. Aunque los números pequeños implicados están protegidos por una simetría quiral, falta una explicación de estos valores si se desea un verdadero conocimiento.
- **El problema de la jerarquía electrodébil,** o la pregunta de por qué el Higgs "es tan ligero". El hecho de que sea una partícula de espín cero hace que su masa no esté prote-

gida por las simetrías gauge, si no que, al contrario, sea muy sensible a extensiones del ME a altas energías que se comuniquen con el Higgs. Las correcciones radiativas a su masa, cuadráticas en la escala de nueva física, forzarían un ajuste entre parámetros para explicar su valor experimental de 125 GeV.

- **El problema CP fuerte:** una combinación del ángulo θ de las interacciones fuertes y fuentes de violación de CP en el mecanismo que da masas a los quarks debería aparecer en medidas del momento dipolar eléctrico del neutrón, pero está acotada experimentalmente a 10^{-10}. Un ajuste tan fino también requiere una explicación dinámica.

Aunque aparentemente de naturaleza muy diferente, dos o más problemas de entre los mencionados anteriormente pueden estar relacionados. Algunas propuestas para extender el contenido del ME solucionan varios problemas al mismo tiempo. En cambio, las soluciones a un problema pueden agravar otro de ellos. Por ejemplo, el problema de la jerarquía electrodébil (ED) puede empeorar el problema CP fuerte ya que muchas teorías diseñadas para solucionar el primero inducen correcciones inaceptables al parámetro θ.

Esta tesis presta especial atención a problemas de ajuste fino como el problema CP fuerte y el problema de la jerarquía ED. En el pasado, el uso del principio de simetría ha resultado fructífero en el contexto de los problemas de ajuste fino. El principio de naturalidad de t'Hooft [6] proporciona una guía en este sentido. Según éste, es natural que un parámetro físico sea pequeño siempre y cuando el llevarlo a cero aumente la simetría del sistema. Desde esta perspectiva, los parámetros pequeños se pueden explicar mediante simetrías aproximadas, sirviendo de indicadores de simetrías aún por descubrir. Por ejemplo, la ligereza de los piones con respecto a los demás estados ligados de las interacciones fuertes se puede entender por medio de la realización casi exacta de una simetría quiral de sabor para los quarks, que solo está rota ligeramente por las masas de los mismos.

No obstante, una simetría puede estar escondida, pudiendo ser exacta a nivel del Lagrangiano pero no apareciendo en el espectro observado. En este caso se dice que la *simetría está espontáneamente rota*. En escenarios en los que el Lagrangiano tiene una simetría continua ampliada, global o local, que se rompe espontáneamente, hay un bosón de Goldstone (BG –o BBG en plural–) sin masa por cada generador roto. En consecuencia, estos BBG se convierten en indicadores de simetrías escondidas. Tanto los bosones de Goldstone como otras partículas de espín cero aparecen entre los escalares y pseudoescalares de teorías más allá del ME (MAME) que ponen solución a algunos de los problemas anteriormente mencionados. Por todo ello, el Higgs puede no ser el último si no más bien el primero de un sector de partículas aún por explorar: *la ventana de espín cero a nueva física*.

En el marco de esta tesis se estudiarán soluciones a los problemas de ajuste fino en las que aparecen simetrías espontáneamente rotas y bosones de Goldstone. En un primer paso, una propuesta teórica se enfrenta a dos problemas de ajuste fino de manera simultánea: el problema CP fuerte y el problema de la jerarquía ED; estudiaremos la extensión mínima de los modelos de Higgs compuesto que permita también implementar el axión como solución al problema CP fuerte. En un segundo paso más fenomenológico, se abordará la búsqueda de BBG en general, utilizando y desarrollando la herramienta de los Lagrangianos efectivos para identificar nuevas propuestas experimentales en la búsqueda de axiones y partículas-tipo-axión (PTA –o PPTA en plural–). Un tercer paso en la exploración del sector de espín

cero se concentrará en el caso de un candidato escalar a materia oscura (MO), reconsiderando el estatus fenomenológico del escenario llamado portal de Higgs a la luz de una formulación más general de las teorías efectivas de campos (TEC) y de nuevas señales en el LHC.

En la parte teórica, de construcción de modelos, de esta tesis nos concentramos en una implementación mínima de dos soluciones a problemas de ajuste fino en las que aparecen BBG. El problema CP fuerte puede encontrar su solución en el axión, el BG asociado a la rotura de la simetría $U(1)_A$ Peccei Quinn (PQ) [7], que explicaría la no-observación del parámetro $\bar{\theta}$ (y que es, además, un candidato excelente a MO). Asumiendo solamente las simetrías gauge del ME, la escala física del axión está constreñida fenomenológicamente por medidas de astrofísica a ser, en general, muchos órdenes de magnitud mayor que la escala ED. Sin embargo, estas dos escalas se pueden comunicar mediante acoplos en el potencial escalar, y por efectos cuánticos, la segunda de estas dos escalas puede verse inflada hasta valores de $\mathcal{O}(f_a)$. Así pues, uno de los mayores inconvenientes de las soluciones más extendidas basadas en axiones –*los modelos de axión invisible*– es que tienen un fuerte ajuste-fino entre parámetros desde el punto de vista del problema de la jerarquía ED. Este es un ejemplo de una solución a un problema de ajuste fino que agrava otro problema diferente. Sin embargo, existen soluciones al problema de la jerarquía ED que convierten al propio Higgs en un bosón de Goldstone. La escala pequeña, en este caso la masa de la partícula de Higgs, está protegida de las escalas altas putativas mediante una ascendencia de BG [8]. Propondremos y estudiaremos un montaje en el que los modelos de Higgs compuesto se extienden mínimamente para implementar la simetría PQ, resolviendo el problema CP fuerte. Una característica recurrente de los modelos de Higgs compuesto es la presencia por construcción de fermiones vectoriales exóticos, una característica compartida con los modelos de axión invisible tipo KSVZ [9, 10]: nos beneficiamos de este hecho y mostraremos que basta con añadir un escalar complejo al espectro de los modelos de Higgs compuesto para hacerlos invariantes PQ. Se determinarán también las señales fenomenológicas asociadas.

Más en general, tiene interés estudiar los BBG desde el punto de vista de los problemas del ME porque hay muchas extensiones del ME que cuentan con simetrías $U(1)$ espontáneamente rotas. In consecuencia, parece deseable mantenerse agnóstico respecto al tipo de BBG que podamos encontrar en la Naturaleza. Así pues, pasamos a desarrollar un estudio general de los acoplos de las PPTA a los campos del ME, con el objetivo de revisar el estado fenomenológico de las PPTA que nos llevará a explorar un camino novedoso en la búsqueda de BBG. La forma de plantear, con independencia de modelos concretos, la exploración de nueva física (NF) en datos tomados a baja energía es utilizando Lagrangianos efectivos: se usa una expansión *lineal* cuando se asumen realizaciones lineales de la rotura de la simetría electrodébil (RSED) [11, 12], mientras que la expansión *no lineal* –también llamada en ocasiones expansión *quiral*– es el instrumento óptimo para tratar con regímenes que no se caractericen necesariamente por tener una interacción débil, como los modelos de Higgs compuesto previamente mencionados [13–15]. El orden dominante y el segundo orden de las interacciones de las PPTA en el contexto del Lagrangiano lineal se formularon hace años [16], mientras aún faltaba la base efectiva no-lineal, que se desarrollará aquí.

El uso de las teorías efectivas de campos es especialmente adecuado para estudios orientados fenomenológicamente, pues dan una idea de cuánta información y de qué tipo de

experimentos son necesarios para realmente abarcar las direcciones independientes del espacio de parámetros. Hasta ahora, los estudios fenomenológicos se han basado en los acoplos de las PPTA a fotones, gluones y fermiones, que dominan a bajas energías y determinan, por ejemplo, cotas astrofísicas para PPTA ligeras. Sin embargo, una formulación invariante $SU(2)_L \times U(1)_Y$ de sus interacciones en una TEC hace aparecer, junto con los acoplos a fotones, acoplos de las PPTA a los otros bosones gauge ED, independientemente de si la expansión es lineal o quiral, y acoplos al Higgs en el segundo caso. Se han desarrollado recientemente propuestas fenomenológicas interesantes para poner a prueba algunos de estos acoplos, tanto en el contexto de experimentos a baja energía por medio de contribuciones a un loop a decaimientos raros de mesones, que son sensibles a las interacciones de axiones con bosones $W^{\pm}$ [17], como en observables a alta energía en el LHC que involucran producción de axiones mediada por bosones Z [18]. En esta tesis se identificarán canales nuevos derivados de la formulación efectiva de la teoría. Las altas energías y momentos que son accessibles ahora gracias al LHC permiten una exploración seria de los acoplos derivativos en general, y de axiones con masas más allá del alcance de los experimentos a baja energía. Las nuevas búsquedas que proponemos en el LHC pueden ser esenciales en la búsqueda de bosones de Goldstone.

Las partículas de espín cero están fuertemente motivadas por otros de entre los problemas mencionados arriba. La MO se puede explicar no solo mediante axiones con acoplos principalmente derivativos (producidos no-térmicamente por mecanismos como el mecanismo de desalineación, y otros). Otros candidatos viables a este rompecabezas observacional son escalares con acoplos polinómicos al ME, producidos térmicamente en el universo temprano. Las interacciones renormalizables de un candidato a MO escalar con el ME tienen lugar mediante acoplos con el Higgs en un escenario altamente constreñido llamado el *portal escalar de Higgs* [19]. De nuevo desde la perspectiva de la TEC, la pregunta que nos planteamos es cuál es la forma de las interacciones dominantes entre una MO escalar y el ME en realizaciones no lineales de RSED, es decir, el *portal de Higgs no lineal*. Estudiaremos las interacciones efectivas lineales y no lineales de una partícula escalar real con los campos del ME y exploraremos sus consecuencias fenomenológicas en aceleradores de partículas, junto con sus implicaciones cosmológicas puestas a prueba en observables de MO como su abundancia cosmológica y en búsquedas de detección directa.

El Higgs puede haber abierto la ventana a un territorio intrigante donde podemos encontrar escalares y pseudoescalares, de naturaleza (pseudo)Goldstone o no, desempeñando un papel esencial a la hora de resolver algunos de las urgentes preguntas abiertas del ME. Los impresionantes desarrollos experimentales de los últimos años, explotados en esta tesis en el contexto de las partículas de espín cero, deberían acercarnos a la sólida construcción teórica añorada por los físicos de partículas. Esperemos que esta tesis sirva como un peldaño en esta búsqueda.

Los capítulos 1-4 presentan en estado del arte. Las contribuciones originales de esta tesis se encuentran con los capítulos 5, 6 and 7

Part II

FOUNDATIONS

1 THE HIGGS AS A GOLDSTONE BOSON

The discovery of the Higgs in 2012 [20, 21] completed the Standard Model of particle physics (SM) as we know it today. In apparently concluding this quest, it simultaneously initiated an excursion into a new territory, as the Higgs is up to now the only fundamental (possibly elementary) scalar in the theory of particle interactions. This may be regarded as good news, although it places simultaneously a heated debate at the heart if the particle physics community: is the SM a low-energy effective description of underlying fundamental interactions? One hint pointing to additional physics is the fact that the SM may face the EW hierarchy problem. If there exists any putative new physics scale above the electroweak scale to which the Higgs particle is sensitive, it should not be not far from the TeV scale. The hierarchy problem can be expressed as the instability of the value of the Higgs boson mass with respect to radiative corrections, in presence of a physical cut-off at energies far above the EW scale.

This chapter reviews the EW sector of the SM and its possible problems in terms of naturalness, before exploring solutions to explain the lightness of the Higgs. In particular, proposals that consider the possibility that the Higgs has a Goldstone boson ancestry which protects its mass from higher-order corrections will be explored.

1.1 SPONTANEOUS SYMMETRY BREAKING IN THE STANDARD MODEL

1.1.1 *Spontaneous symmetry breaking*

A physical system is said to possess a symmetry when the physics remains unchanged under a certain transformation. The transformation can be global (it is the same throughout spacetime) or gauge (when the transformation is local). For instance, the SM is built as the set of interactions which are invariant under the product of three unitary gauge groups $SU(3)_C \times SU(2)_L \times U(1)_Y$. The fields of the SM have definite transformation properties under these three gauge groups which are summarized in Tab. 1.1, while B-L ("baryon minus lepton number") is an example of an accidental global symmetry of the SM Lagrangian.

Symmetries can also be classified according to whether they are exact, or broken in different ways:

- A given symmetry may be broken *explicitly*. Sometimes it is useful to detect broken symmetries when they are *approximate* or "almost present", i.e. when they are explicitly broken by some "small" parameter such that, when the latter is set to zero the symmetry is recovered. All of the effects that do not respect the symmetry then have to be proportional to the symmetry-breaking parameter in the Lagrangian. One such example is isospin, which is broken by the difference in masses between the u and d quarks and also by the quark charge differences (hypercharge).

  A particularly interesting case is that of a symmetry which is exact at a classical level in the Lagrangian but explicitly broken by quantum effects. It is described as corre-

	$SU(3)_C$	$SU(2)_L$	$U(1)_Y$
$q_L = (u_L, d_L)^T$	3	2	1/6
u_R	3	1	2/3
d_R	3	1	-1/3
$l_L = (\nu_L, e_L)^T$	1	2	-1/2
e_R	1	1	-1
G^a_μ	8	1	0
W^a_μ	1	3	0
B_μ	1	1	0
Φ	1	2	1/2

Table 1.1: Transformation properties of the SM fields under the SM gauge group.

sponding to a current which is *anomalous*. An example of this is the global $U(1)_A$ axial symmetry of the Quantum Chromodynamics (QCD) Lagrangian.

- Alternatively, the Lagrangian may be exactly symmetric at both classical and quantum level, but the ground-state may not exhibit the symmetry. In field theory, the spectrum of particles is determined by the excitations over the state of lowest energy –the ground state. As a result, the symmetry of the Lagrangian is not visible in the spectrum of physical particles. For instance the spectrum may not exhibit sets of fields building up multiplets –eigenstates of the symmetries of the Lagrangian. The symmetry is said to be *spontaneously broken*, although it could arguably be considered simply a "hidden symmetry", because it remains exact. Technically the mechanism may be implemented through the non-zero vacuum expectation value of one or several scalar fields, as in the spontaneous breaking of the electroweak symmetry, or dynamically, as in the breaking of chiral symmetry by quark condensates.

The concept of symmetries is central in particle physics, both in the SM and its extensions. This chapter will present spontaneous symmetry breaking (SSB) in the Higgs mechanism of the SM and it will also be invoked as a possible explanation of the lightness of the Higgs. Next, Chapter 2 will make use of a classical $U(1)_A$ symmetry which is anomalous and also spontaneously broken to explain the extreme smallness of the QCD θ parameter.

▷ *Spontaneous breaking of a discrete symmetry*

The simplest example of a theory with a broken symmetry is that of a single scalar field $\phi(x)$, with a discrete reflection symmetry which takes $\phi(x) \to -\phi(x)$. Abbreviating the x dependence, a renormalisable ($d \leqslant 4$) Lagrangian that displays this symmetry is the $\lambda\phi^4$ Lagrangian

$$\mathcal{L} = \frac{1}{2}(\partial_\mu\phi)^2 - \frac{1}{2}\mu^2\phi^2 - \frac{\lambda}{4}\phi^4\,, \tag{1.1}$$

defined with $\lambda > 0$. The sign of μ^2 can be positive or negative, and while the case of $\mu^2 > 0$ is familiar, and describes a scalar field with mass μ which are excitations over a vacuum state $\langle\phi\rangle = 0$, it may also be the case that $\mu^2 < 0$. In this case, the ground state $\langle\phi\rangle$ which minimises the potential $V(\phi) = \mu^2\phi^2/2 + \lambda\phi^4/4$ is a constant field which takes two values,

$$\frac{dV(\phi)}{d\phi} = 0 \quad \to \quad \langle\phi\rangle \equiv \pm v = \pm\sqrt{-\mu^2/\lambda}\,. \tag{1.2}$$

The spectrum corresponds to excitations over the vacuum. Choosing one of the options, e.g. $\langle\phi\rangle = v$ (the physics is completely equivalent at $\langle\phi\rangle = -v$) the Lagrangian can be rewritten as a function of the fluctuations $\eta(x)$ around the vacuum expectation value (vev) $\langle\phi\rangle$, by making the change of variables $\phi(x) = v + \eta(x)$:

$$\mathcal{L} = \frac{1}{2}(\partial_\mu\eta)^2 + \frac{1}{2}(2\mu^2)\eta^2 - \mu\sqrt{\lambda}\eta^3 - \frac{\lambda}{4}\eta^4 + \frac{1}{2}\frac{\mu^4}{\lambda}\,. \tag{1.3}$$

This Lagrangian describes a scalar field η with a *positive* mass $m_\eta = \sqrt{-2\mu^2} > 0$. Additionally, the reflection symmetry is no longer apparent in terms of the η field (e.g. in the η^3 terms), since one of the two minima of the potential was selected. The symmetry is *spontaneously broken*, or rather hidden, as it is not apparent in the physics which is described by the perturbations around the ground state, but it is there in the Lagrangian. The dynamics of spontaneous symmetry breaking was originally developed in analogy to the Ginzburg-Landau theory describing a superconducting phase transition [22], since it implements a potential analogous to the scalar potential described here.

▷ *Spontaneous breaking of continuous symmetries and Goldstone's theorem*

Spontaneous symmetry breaking of continuous symmetries is emblematically studied in the context of N real scalar fields, $\Phi = \{\phi_1, \ldots, \phi_N\}$, described by the Lagrangian which is invariant under $\phi_i \to R_{ij}\phi_j$. One particular case of a Lagrangian with such symmetry is for $N = 2$ the Lagrangian for a complex field $\Phi = \phi_1 + i\phi_2$,

$$\mathcal{L} = (\partial_\mu\Phi)^*(\partial^\mu\Phi) - \mu^2|\Phi|^2 - \lambda|\Phi|^4\,, \tag{1.4}$$

which is invariant under a $O(2) \sim U(1)$ symmetry $\Phi \to e^{i\alpha}\Phi$. The potential is represented in Fig. 1.1 Again, we concentrate on the case where $\mu^2 < 0$, for which minimising the potential gives a ground-state which is a circle in the ϕ_1, ϕ_2 plane of radius $v/\sqrt{2}$,

$$|\langle\phi\rangle|^2 = \phi_1^2 + \phi_2^2 = \frac{v^2}{2} \quad \text{with} \quad v^2 = -\frac{\mu^2}{\lambda}\,. \tag{1.5}$$

The fact that the manifold has degenerate minima is consistent with the fact that the choice of one particular vacuum is physically equivalent to any other, since they are related by a symmetry in the Lagrangian.

Again, it is physically illustrative to expand the field around the minimum, and a clear way given the minimum configuration is in terms of polar coordinates. Under the replacement $\Phi(x) = (v + \rho(x))e^{i\varphi(x)/v}/\sqrt{2}$, the Lagrangian reads

$$\mathcal{L} = \frac{1}{2}(\partial_\mu \rho)(\partial^\mu \rho) + \frac{1}{2}(v+\rho)^2 \frac{\partial_\mu \varphi \partial^\mu \varphi}{v^2} + \mu^2 \rho^2 + \dots , \tag{1.6}$$

where the dots stand for cubic and quartic terms in ρ and in powers of $\partial_\mu \varphi$. The relevant fact about this Lagrangian is that, while it contains a kinetic term for both the ρ and φ, only ρ has a mass! The ground state of a Lagrangian with a spontaneously broken global continuous symmetry possesses a massless excitation, which is called a Goldstone boson (GB) and it is the angular component φ which appears massless. What is more, the interactions of φ are all derivative, i.e. proportional to $\partial_\mu \varphi$. As a consequence, the interactions in terms of the excitations around the minimum are invariant under a shift transformation of the GB,

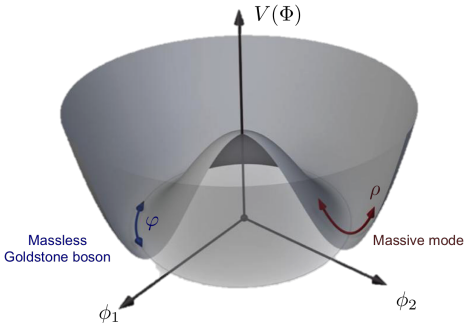

Figure 1.1: Scalar potential symmetric under $O(2) \sim U(1)$, showing the massless Goldstone excitation and the massive field that remain after the spontaneous breaking of the symmetry.

$$\varphi(x) \to \varphi(x) + C\,. \tag{1.7}$$

The Lagrangian is said to possess a shift symmetry.

This is a particular case of the Goldstone theorem [23–25], first realised by Yoichiro Nambu and generalised by Jeffrey Goldstone. It can be stated in simple words as follows:

> Consider a system whose Lagrangian is invariant under an n-dimensional set of continuous, global transformations. If the vacuum of the theory is invariant under the action of only k among the n generators, then there must exist $n-k$ spinless particles of zero mass.

A simple proof at a classical level [1] can be given for a toy model consisting of an arbitrary number of scalar fields $\phi_i(x)$ whose Lagrangian $\mathcal{L} = (\partial_\mu \phi_i)^2/2 - V(\phi_i)$ has a vacuum state corresponding to a constant $\langle \phi_i \rangle$ such that

$$\frac{\delta}{\delta \phi_i} V(\phi_i)\Big|_{\phi_i = \langle \phi_i \rangle} = 0\,. \tag{1.8}$$

Assume that the Lagrangian is invariant under a global symmetry group $\mathcal{G}$, spanned by n generators, T^a_{ij} with $a \in [1, \dots, n]$. An infinitesimal transformation under $\mathcal{G}$ can be parametrised by the parameters ϵ^a, with the fields transforming as $\phi_i \to \phi_i + i\epsilon^a T^a_{ij}\phi_j$. In particular, the invariance of the scalar potential reads

$$V(\phi_i + i\epsilon^a T^a_{ij}\phi_j) - V(\phi_i) = i\epsilon^a \frac{\delta V}{\delta \phi_i} T^a_{ij}\phi_j = 0 \quad \forall \epsilon^a\,. \tag{1.9}$$

1 Goldstone's theorem is however more general and can be proven to all orders in perturbation theory [25].

Differentiating the previous expression with respect to ϕ_k, and evaluating in the vacuum $\phi_i = \langle\phi_i\rangle$ results in

$$\frac{\delta^2 V}{\delta\phi_k\delta\phi_i}T^a_{ij}\phi_j + \frac{\delta V}{\delta\phi_i}T^a_{ik} = 0 \quad \xrightarrow[\phi_i=\langle\phi_i\rangle]{} \quad \left.\frac{\delta^2 V}{\delta\phi_k\delta\phi_i}\right|_{\phi_i=\langle\phi_i\rangle} T^a_{ij}\langle\phi_j\rangle = 0\,, \tag{1.10}$$

where Eq. (1.8) has been used. The condition that the vacuum is invariant only under a smaller group $\mathcal{H}$, spanned by k amongst the n generators of $\mathcal{G}$ can be expressed as

$$\begin{aligned} T^a_{ij}\langle\phi_j\rangle &= 0 \;\forall i \quad a \in [1,\dots,k] \\ \exists i \quad T^a_{ij}\langle\phi_j\rangle &\neq 0 \qquad a \in [k+1,\dots,n]\,. \end{aligned} \tag{1.11}$$

It follows from Eqs. (1.10) and (1.11) that the second derivative of the scalar potential has $n-k$ zero eigenvalues. Since the excitations around the vacuum, $\pi_i(x) \equiv \phi_i(x) - \langle\phi_i\rangle$, must satisfy the equations of motion (EOM), which for a scalar field in absence of interactions is the Klein Gordon equation,

$$\left(\delta_{ij}\Box + \left.\frac{\delta^2 V}{\delta\phi_k\delta\phi_i}\right|_{\phi_i=\langle\phi_i\rangle}\right)\pi_j(x) = 0\,, \tag{1.12}$$

where the second term defines the particle mass. The vacuum state of this system is such that $(n-k)$ of the excitations are massless. These are the Goldstone bosons (sometimes also referred to as Nambu-Goldstone bosons) of the theory. The Lagrangian cannot depend directly on the fields, but can only contain *derivative* interactions of these, giving it its well-known shift symmetry. A small explicit breaking of $\mathcal{G}$ would translate in a small mass for one or more of the GBs, in which case they are denominated pseudo-Goldstone bosons (pGB).

As anticipated above, the spontaneous breaking of a global symmetry is going to be used in this thesis in two different contexts giving rise to GBs: in the most popular solution to the strong CP problem, the Peccei Quinn mechanim, the GB associated to the SSB of $U(1)_{PQ}$ is the axion, as we will see in Chaps. 2 and 3. However, the axion is not going to be completely massless because a small breaking at the quantum level of $U(1)_{PQ}$ by non-perturbative QCD effects gives it a small mass. In a different realm, it is possible to justify the light mass of the Higgs defining it as the pGB associated to the spontaneous breaking of some larger global symmetry group $\mathcal{G}$ to another $\mathcal{H}$, which contains the the SM symmetry group.

▷ *Spontaneous breaking of gauge symmetries: the Higgs mechanism*

Finally, let us consider the spontaneous breaking of local symmetries, the Higgs mechanism constituting the final step in describing the weak sector of the SM. It was discovered by three independent groups in 1964: Brout-Englert [26], Higgs [27] and Guralnik-Hagen-Kibble [28]. How can a process which involves the appearance of massless excitations result in explaining the masses of the gauge bosons in the SM? The point is that, in the local case, the Goldstone bosons do not reveal themselves as massless excitations, but rather as the longitudinal components of the vector bosons associated to the broken generators; in other words, these gauge bosons acquire a mass.

Consider the simple case of a $U(1)$ abelian gauge symmetry spontaneously broken, as it suffices to illustrate the main characteristics of the setup. A Lagrangian describing a complex scalar with such symmetry is

$$\mathcal{L} = -\frac{1}{4}F_{\mu\nu}F^{\mu\nu} + (D_\mu\phi)^*(D^\mu\phi) - \mu^2|\phi|^2 - \lambda|\phi|^4\,, \tag{1.13}$$

where the covariant derivative reads $D_\mu\phi = (\partial_\mu + igA_\mu)\phi$, and where the local $U(1)$ transformation corresponds to

$$\phi(x) \to e^{i\alpha(x)}\phi(x)\,, \quad A_\mu \to A_\mu(x) - \frac{1}{g}\partial_\mu\alpha(x)\,. \tag{1.14}$$

Once again, the symmetry may be spontaneously broken if $\mu^2 < 0$, the minimum of the potential occurring for a circle of $|\phi| = v/\sqrt{2}$ as in Eq. (1.5) for the global case. However, expanding now the field around the minimum, $\phi(x) = (v + \rho(x))e^{i\varphi(x)/v}/\sqrt{2}$, and replacing the Lagrangian, Eq. (1.13) will give a different result due to the replacement of the derivative with the covariant derivative, $\partial_\mu \to D_\mu$, in this gauge case:

$$\mathcal{L} = -\frac{1}{4}F_{\mu\nu}F^{\mu\nu} + \frac{1}{2}(\partial_\mu\rho)(\partial^\mu\rho) + \frac{(v+\rho)^2}{2}\left(gA_\mu + \frac{\partial_\mu\varphi}{v}\right)^2 - \mu^2\frac{(v+\rho)^2}{2} - \lambda\frac{(v+\rho)^4}{4}\,. \tag{1.15}$$

Again a mass term results for the radial component ρ and no mass term for φ, but the interesting characteristic of this Lagrangian is the mass term for the gauge boson $\frac{v^2g^2}{2}A_\mu A^\mu$ that results from the third term in Eq. (1.15). However, a non-physical mixing between the gauge boson and φ, the coupling $vgA_\mu\partial^\mu\varphi$, also stems from this term, indicating that the physical bosons are an admixture of A_μ and $\partial_\mu\varphi$. A simple gauge transformation

$$A_\mu \to A_\mu - \frac{1}{gv}\partial_\mu\varphi \tag{1.16}$$

eliminates completely the presence of φ from the Lagrangian, which is now expressed in the unitary gauge as:

$$\mathcal{L} = -\frac{1}{4}F_{\mu\nu}F^{\mu\nu} + \frac{1}{2}(\partial_\mu\rho)(\partial^\mu\rho) + g^2\frac{(v+\rho)^2}{2}A_\mu A^\mu - \mu^2\frac{(v+\rho)^2}{2} - \lambda\frac{(v+\rho)^4}{4}\,. \tag{1.17}$$

It seems that one field, the would-be GB has completely disappeared! However the number of degrees of freedom has not changed, as it has to be expected. Initially there were two real scalar degrees of freedom –those of the complex field ϕ– plus a massless gauge boson (which has two transverse polarisations), while in Eq. (1.17) there are still four degrees of freedom, one in the ρ and three in the massive gauge boson, which now has the two transverse plus a the longitudinal polarisation. It is colloquially said that the gauge boson has *eaten* the Goldstone boson in getting its mass.

The Higgs mechanism in the SM is a generalisation of the procedure described above to the case of a local $SU(2)$ symmetry.

1.1.2 *The Higgs mechanism in the Standard Model*

For completeness we will here outline the setup and the main results of the Weinberg-Salam theory [29, 30] which describes the unification of electromagnetic and weak interactions in a $SU(2)_L \times U(1)_Y$ gauge-invariant formulation which is spontaneously broken via the Higgs mechanism [26–28] to $U(1)_{em}$ [31]. The Higgs boson field is a new scalar doublet of $SU(2)_L$, that is, a field containing four degrees of freedom. This setup explains the masses of the three gauge bosons mediating the weak interactions, and at the same time allows to give mass to the SM fermions via direct Yukawa interactions to the SM fermions. Explicit mass terms for the $SU(2)_L$ gauge bosons would not be acceptable because they are non-gauge invariant, which ultimately would result in a non non-renormalizable theory [32]. The Higgs mechanism allows instead the presence of gauge boson (and fermion) masses, while preserving renormalisability, as the $SU(2)_L \times U(1)_Y$ gauge symmetry is exact.

The Higgs doublet is commonly written as

$$\Phi = \begin{pmatrix} \Phi^+ \\ \Phi^0 \end{pmatrix} , \tag{1.18}$$

with hypercharge $Y_\Phi = 1/2$. Its covariant derivative reads

$$D_\mu \Phi = \partial_\mu \Phi + \frac{ig}{2} W_\mu^a \sigma^a \Phi + \frac{ig'}{2} B_\mu \Phi \,., \tag{1.19}$$

where g and g' are respectively the $SU(2)_L$ and $U(1)_Y$ gauge coupling constants, and σ^a are the Pauli matrices. The Higgs scalar Lagrangian is given by

$$\mathcal{L}_\Phi = (D_\mu \Phi)^\dagger (D^\mu \Phi) + \mu^2 \Phi^\dagger \Phi - \lambda (\Phi^\dagger \Phi)^2 \,, \tag{1.20}$$

with $\mu^2 > 0$. [2] It is invariant under the $SU(2)_L$ gauge transformation $\Phi \to e^{i\sigma^a \alpha_a(x)/2} \Phi$, with $\alpha_a(x)$ a set of real parameters that define the transformation, which is a generalisation to $SU(2)$ of the gauge transformation defined in Eq. (1.14) for $U(1)$. This Lagrangian results in a non-zero vev for the radial component of Φ,

$$|\langle \Phi \rangle|^2 = v^2 = \frac{\mu^2}{\lambda} \approx (246\,\mathrm{GeV})^2 \,, \tag{1.21}$$

breaking the $SU(2)_L \times U(1)_Y$ gauge group down to $U(1)_{em}$ in a process known as electroweak symmetry breaking (EWSB). As in the previous examples, one of the bosons, called h gets a mass m_h and a vev v, while now there will be three would-be GBs. The value of v^2 in Eq. (1.21) is fixed by the Fermi constant $v = (\sqrt{2} G_F)^{-1/2}$. This is the typical scale of the $SU(2)_L$ interactions and referred to as the electroweak (EW) scale.

2 Notice that the notation has been changed with respect to that of Eqs. (1.1) and (1.13) in that now it is the case $\mu^2 > 0$ which gives a non-trivial vev to the scalar field, since the sign of μ^2 has been changed at the level of the Lagrangian.

The excitations of the Higgs field are expressed as an expansion around the vev v and can be parametrised in polar coordinates,

$$\Phi(x) \;=\; \frac{v+h(x)}{\sqrt{2}}\mathbf{U}(x)\begin{pmatrix}0\\1\end{pmatrix}, \quad \text{with} \quad \mathbf{U}(x)=e^{i\pi^a(x)\sigma^a/v}, \tag{1.22}$$

$\mathbf{U}(x)$ being a unitary matrix and $\pi^a(x)$ denoting the three would-be GBs. The physical Higgs field h becomes massive,

$$m_h^2 = 2\mu^2, \tag{1.23}$$

and $\pi^a(x)$ give masses to three of the four gauge bosons of the $SU(2)_L\times U(1)_Y$ gauge group. In the unitary gauge ($\mathbf{U}(x)=\mathbb{1}$) the $\pi^a(x)$ fields are eliminated from the Lagrangian and the Higgs kinetic term reads

$$(D_\mu\Phi)^\dagger(D^\mu\Phi)=\frac{1}{2}\partial_\mu h\partial^\mu h+\frac{(v+h)^2}{4}g^2W_\mu^+W^{-\mu}+\frac{(v+h)^2}{8}(g^2+g'^2)Z_\mu Z^\mu, \tag{1.24}$$

where

$$W_\mu^\pm\equiv\frac{W_\mu^1\mp iW_\mu^2}{\sqrt{2}}, \quad Z_\mu\equiv\frac{gW_\mu^3-g'B_\mu}{\sqrt{g^2+g'^2}} \quad \text{and} \quad A_\mu\equiv\frac{g'W_\mu^3+gB_\mu}{\sqrt{g^2+g'^2}}. \tag{1.25}$$

According to Eq. (1.24), the masses of the gauge bosons follow as

$$m_W=\frac{gv}{2}, \qquad m_Z=\frac{\sqrt{g^2+g'^2}v}{2}=\frac{1}{\cos\theta_W}m_W, \tag{1.26}$$

while the photon A_μ remains massless. In the last step of Eq. (1.26) the auxiliary Weinberg angle is defined, relating the electromagnetic coupling e to the gauge couplings of $SU(2)_L$ and $U(1)_Y$,

$$e=g\sin\theta_W=g'\cos\theta_W, \quad \text{with} \quad \tan\theta_W=\frac{g'}{g}. \tag{1.27}$$

It is not a prediction of the SM but measured to $\sin^2\theta_W\approx 0.23$ [33].

For completeness we include here the rest of interactions of the Higgs in the SM, in particular the Yukawa Lagrangian of the Higgs reads

$$\mathcal{L}_{\text{Yuk.}}=-\bar{q}_L\Phi Y_d d_R-\bar{q}_L\tilde{\Phi}Y_u u_R-\bar{l}_L\Phi Y_e e_R+\text{h.c.}, \tag{1.28}$$

where Y_u, Y_d and Y_e are 3×3 Yukawa matrices in flavour space, since q_L, u_R, d_R, l_L and e_R contain three copies of quarks and leptons respectively (called the three families), and

$$\tilde{\Phi}=i\sigma^2\Phi^*=\begin{pmatrix}\Phi^{0*}\\-\Phi^-\end{pmatrix}, \tag{1.29}$$

with $\Phi^-=(\Phi^+)^*$. When the Higgs takes a vev, by repacing $\Phi\to\langle\Phi\rangle=(0,v)^T/\sqrt{2}$ the mass matrices for the quarks and the charged leptons $M_i=Y_iv/\sqrt{2}$ are obtained. These matrices

are in general non-diagonal but can be diagonalised through unitary transformations on each of the quarks:

$$\psi_L \to V_L^{\psi}\psi_L\,, \qquad \psi_R \to V_R^{\psi}\psi_R\,, \tag{1.30}$$

where V_L^{ψ} and V_R^{ψ} are 3×3 unitary matrices. This transformation leads also to diagonal couplings with the Higgs excitation $(m_i/v)h\bar{\psi}\psi$. That is, the Higgs couplings remain flavour diagonal. In contrast, the mass diagonalisation process uncovers flavor-changing charged currents via $W^{\pm}$ exchange. The kinetic terms of the fermions $\bar{\psi}i\not{D}\psi$ include the interactions of the fermions with the gauge bosons via the presence of the latter in the covariant derivative. While the transformation in Eq. (1.30) has no impact on the neutral currents (the interactions of the fermions with the photon and Z_μ), the fact that the charged currents now connect different generations results in flavor-changing charged currents at tree-level once Eq. (1.30) is applied,

$$\mathcal{L}_{CC} \supset -\frac{g}{\sqrt{2}}\left\{W_\mu^+\ \left[\bar{u}_i\gamma^\mu P_L d_j\ V_{CKM}^{ij} + \bar{\nu}_i\gamma_\mu P_L e_j U_{PMNS}^{ij}\right] + \text{h.c.}\right\}\,, \tag{1.31}$$

controlled by the Cabibbo-Kobayashi-Maskawa (CKM) matrix [34, 35],

$$V_{CKM} \equiv (V_L^u)^\dagger V_L^d\,, \tag{1.32}$$

in the quark sector, and the Pontecorvo-Maki-Nakagawa-Sakata (PMNS) matrix [36, 37],

$$U_{PMNS} \equiv (V_L^\nu)^\dagger V_L^e\,, \tag{1.33}$$

in the lepton sector. For three quark generations the CKM matrix can be parametrised with three physical mixing angles and one CP-odd phase δ on which all CP-violating and flavour-changing processes depend. In the lepton case, flavor-changing effects would have been absent if neutrinos had been exactly massless: in this case, it is possible to choose $V_L^\nu = V_L^e$ in order to compensate for the charged leptons rotation and $U_{PMNS} = \mathbb{1}$. Nonetheless, the phenomenon of neutrino oscillations has been firmly established experimentally, and U_{PMNS} measures the mixing angles in neutrino oscillations. The observed pattern of leptonic mixing angles is very different from that of the quarks sector: two angles are large (one being nearly maximal) and the third is only one order of magnitude smaller. Additionally, two other phases apart from the analogous to δ are physical if neutrinos are Majorana particles. No significant constraint is currently available on the three complex phases.

These pages have outlined the main building blocks on which the EW sector of the SM is constructed. It was confirmed by the discovery at the LHC of the scalar boson responsible for the Higgs mechanism, announced simultaneously by the ATLAS [21] and CMS [20] experiments currently operating at CERN, with a mass near 125 GeV. Given the Higgs mass, the dominant production channel is gluon-gluon fusion (ggF) via a loop of tops, since it benefits from the absence of weak interaction couplings and from the presence of the (large) top Yukawa coupling, followed by vector-boson fusion (VBF) and associated production with a vector boson (VH) or with a $t\bar{t}$ pair (ttH), see Fig. 1.2. The Higgs was found via its radiative decay to two photons $h \to \gamma\gamma$ (again via a top loop as in the ggF production) and via $h \to ZZ^* \to 4l$. Although the branching fraction corresponding to these decays are up to

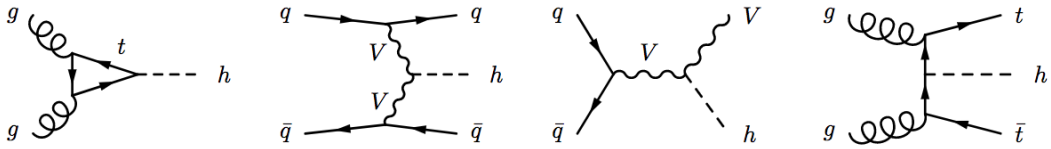

Figure 1.2: Feynman diagrams for the dominating Higgs production modes at the LHC: gluon-gluon fusion (ggF), vector-boson fusion (VBF), associated production with a gauge boson (VH) and with a $t\bar{t}$ pair (ttH). In the two central diagrams, $V = \{Z, W^{\pm}\}$.

two orders of magnitude smaller than the dominant one (eg. $h \to b\bar{b}$) they are the cleanest ones at the LHC benefitting from low backgrounds. As of today, the Higgs resonance has been observed in a diversity of channels: WW^*, $\tau^+\tau^-$, $b\bar{b}$, and is being searched for in others such as $\mu^+\mu^-$. The ATLAS and CMS combined value for the Higgs mass as measured in $\sqrt{s} = 7\,\text{TeV}$ and $\sqrt{s} = 8\,\text{TeV}$ in the $\gamma\gamma$ and $4l$ channels is [38]

$$m_h = 125.09 \pm 0.21\,(\text{stat.}) \pm 0.11\,(\text{syst.})\,\text{GeV}\,. \tag{1.34}$$

The couplings of the Higgs particle are being thoroughly tested experimentally: they must all align with the SM prediction in order for it to be recognised as the SM Higgs boson. While no significant deviations from the SM prediction have been found, these couplings are measured on average with a $10-15\%$ accuracy [33], and many are not even measured yet. While all data points to a SM-like Higgs, there is still room for new physics to be hiding in its couplings. An agnostic approach to Higgs physics is still justified.

Nevertheless, SM is a great achievement of particle physics as it predicts the masses and couplings with very few inputs. Setting aside the Higgs self-coupling λ and the fermion masses (or Yukawa interactions), the SM depends on simply four paramaters $\{g,\, g',\, m_h,\, g_s\}$ (one can chose alternatively $\{G_F,\, \alpha\}$ for the first two and v or μ for the third), where g_s is the gauge coupling constant of the strong interactions which will be presented at the beginning of Chapter 2 and α the fine-structure constant. In terms of scales the SM is characterised by two fundamental scales other than the fermion and Higgs masses: the EW scale v and the QCD scale Λ_{QCD}. QCD confinement is a dynamical process and the scale of strong interactions Λ_{QCD} is determined by dimensional transmutation. In contrast, the SM Higgs mechanism provides no *dynamical* explanation for EWSB. Additionally, whether the fields involved –the Higgs and the would-be GBs that give masses to the W and Z bosons– are elementary states or are rather composed of more fundamental particles still remains to be elucidated. Furthermore, as discussed below, if there is new physics beyond the EW scale to which the Higgs couples, the Higgs mechanism as we know it today faces some fine-tuning problems. Thus, from the theoretical model-building perspective, these hits point to the possibility of underlying fundamental physics beyond the Higgs mechanism in the SM.

1.2 IS THE STANDARD MODEL UNNATURAL?

Having found the Higgs at LHC might have put the particle physics community on the spot, as the boson of the Higgs mechanism suffers what is known as the EW hierarchy problem.

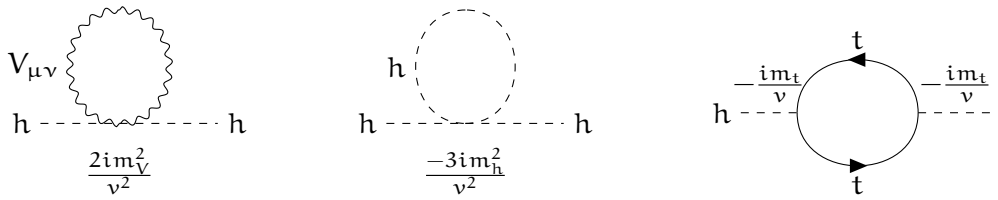

Figure 1.3: Most significant quadratically divergent contributions to the Higgs mass in the SM.

In order to discuss it, it is useful to first understand the concept of *naturalness*, which is often formulated in terms of the definition given by 't Hooft [6],

> At any energy scale μ, a physical parameter or set of physical parameters $\alpha_i(\mu)$ is allowed to be very small only if the replacement $\alpha_i(\mu) = 0$ would increase the symmetry of the system. [3]

While for dimensionless parameters *small* can be interpreted as "substantially smaller than one", for dimensionful parameters it is the relative size with respect to a larger scale (for instance 't Hooft compares electron mass at a certain scale with the scale itself). Additionally, two numbers which are much closer together than each number's absolute value, unless forced to be so by a symmetry, are also considered unnatural. A SM example may be illuminating. For instance, the lightness of pions with respect to other QCD bound states is understood on account of the almost exact realisation of a chiral flavour symmetry of quarks, slightly broken by the quark masses. In this sense it is technically natural.

Indeed, the electroweak hierarchy problem receives different formulations but it refers to the smallness of the Higgs mass with respect to some higher ultraviolet (UV) physics scale to which the Higgs particle may be sensitive. From a technical point of view, the problem arises essentially from the quadratic sensitivity of the Higgs mass to higher scales. If the SM is interpreted as an effective theory, when loop corrections of the self-energy of the Higgs scalar are computed, see Fig. 1.3, the result obtained is proportional to the UV cut-off scale squared (Λ^2),

$$\Delta m_h^2 = \frac{3G_F}{4\sqrt{2}\pi^2}(2m_W^2 + m_Z^2 + m_h^2 - 4m_t^2)\Lambda^2\,, \tag{1.35}$$

where m_t is the top quark mass. The larger the scale of new physics Λ, the larger the bare Higgs mass has to be to cancel the corrections Δm_h^2 in Eq. (1.35), so as to yield the physical mass of 125 GeV. One can demand that the correction is no larger than the physical mass, $\Delta m_h^2 < (125\,\text{GeV})^2$, which would suggest that the UV physics scale cannot be far from the TeV. [4]

However, when dozens of LHC searches have failed to find new physics effects up to energy scales of 10 TeV, the problem itself may need to be questioned. Should naturalness be

3 This is idea is sometimes referred to as *technical naturalness*, as opposed to *naturalness* which would require all parameters being of order one, even if taking them to zero increases the symmetry of the system.

4 Already in 1976 Gildener [39] and Weinberg [40] discussed the so-called hierarchy problem in relation to the Higgs mass in the context of grand-unified theories, and Susskind in 1978 [41], used it as a primary motivation for his proposal of technicolor. The latter, however, gave full credit to Wilson for having pointed out the conceptual difficulty linked to the existence of fundamental scalar particles almost ten years earlier, in Ref. [42].

such a strong guidance in particle physics? It may be disregarded, considering it a simple matter of theoretical consistency: maybe we should simply learn to live with fine-tunings and not seek in them indicators for new physics (NP). However, the EW hierarchy problem has *de facto* become one of the strongest motivations for physics beyond the Standard Model (BSM). It is true that in the past naturalness principles have lead the way to more fundamental explanations of Nature. A historical revision of naturalness arguments [43] brings three examples in which the presence of an unnatural number signalled that a theory had reached its limits and some new effect had to show up beyond a certain energy. Two of the examples, the electron mass and the charged pion mass difference, were found to be naturalness problems only after the new processes had been observed (the positron and ρ-meson, respectively). The third example lead to the prediction of the charm quark, since some new physics scale had to control the kaon mass difference:

$$\frac{M_{K_L^0} - M_{K_S^0}}{M_{K_L^0}} = \frac{G_F^2 f_K^2}{6\pi^2} \sin^2\theta_c \Lambda^2 \tag{1.36}$$

where $f_K = 114\,\text{MeV}$ is the kaon decay constant and $\sin\theta_c = 0.22$ is the Cabibbo angle. Experimentally, the left-hand side was determined to be less than 7×10^{-5}, and this was used by Lee and Gaillard to successfully predict that the charm quark's mass had to be less than a few GeV [44]; indeed, before reaching this energy scale a new particle (the charm quark with mass $m_c \approx 1.2\,\text{GeV}$) modifies the short-distance behaviour of the theory, implementing the so-called GIM mechanism [45], which suppresses the quantity in Eq. (1.36) through a dependence on the the top and charm mass squared difference (see footnote 3 in Sect. 2.2.2).

Although the electroweak hierarchy problem still stands as one of the fine-tuning problems of the Standard Model, it should be formulated with care. It was historically first taken seriously in the context of grand unified theories (see footnote 4), but is normally presented nowadays mentioning the Planck mass ($\mathcal{O}(10^{19}\,\text{GeV})$) as the scale where the SM necessarily breaks down. However, as of today, the theory of quantum gravity is still not settled, and it may be wiser to formulate the EW hierarchy problem, then, as the question of why the Higgs mass is so light *in the presence of new physics that couples to the Higgs*. No such physics has been up to now required by data, and so it is not completely excluded that the hierarchy problem is not a problem at all. Nonetheless, the Standard Model has other pressing issues which call for extensions that *do* feed the EW hierarchy problem. For instance, Majorana neutrinos to explain the lightness of neutrinos typically have masses of $\mathcal{O}(10^{12}\,\text{GeV})$ in the standard type-I see-saw mechanism, and axions, which can simultaneously result from solving the strong CP problem and explain Dark Matter tend to appear in BSM theories with a new physics scale at around $10^{9-12}\,\text{GeV}$, as it will be discussed in Chapter 2. In light of these and other high-energy extensions of the SM, the electroweak hierarchy problem would remain to be solved.

Before moving on to discuss possible solutions to the EW hierarchy problem in the remaining pages of this chapter, let us remind yet another theoretical concern of the SM. The Yukawa interactions that give mass to the SM fermions rely on a set of 22 parameters that describe the very different masses and mixings of the quarks and leptons. It becomes even more intriguing when one notices that, including neutrinos, the masses of quarks and leptons span 12 orders of magnitude. To be consistent on the definition of naturalness, when one takes the fermion masses to zero one does recover an enhanced symmetry, namely the

chiral symmetry. In this sense, we will not call this a naturalness problem, even if it calls for a rationale of some sort. Simply the question of whether there exists a more economical formulation which would explain the values of these parameters (alike to the way in which gauge invariance and renormalisability allow to describe the strong and weak interactions in terms of just four parameters) is already a theoretical challenge.

Finally, as already mentioned, the theory of strong interactions has its own small parameter in the form of a dimensionless CP violating phase. If included in the Lagrangian of QCD (according to Gell-Mann's principle, which states that "Everything which is not forbidden is compulsory" [46]), experimentally one finds that its value together with CP violating contributions from the EW interactions cancel to one part in 10^{10}, giving rise to what is called the strong CP problem. In Chapter 2 we will describe in detail the implications of this problem and its possible solutions.

1.3 THE HIGGS AS A GOLDSTONE BOSON

What is the symmetry that may stabilise the Higgs mass m_h against large radiative corrections? When advocating the presence of a new symmetry, the Higgs will be accompanied by new physical states which build up the multiplet under a given symmetry. In some BSM theories, the new physics is weakly interacting, and electroweak symmetry breaking is *linearly* realised. One paradigmatic example of this are supersymmetric models, where the presence of the new particles required to implement the symmetry translates to a protection of the Higgs mass term as the loop contribution of these patterns cancels the quadratic sensitivity of the Higgs mass discussed earlier. In another class of solutions, a Goldstone boson ancestry of the Higgs is argued to explain its lightness, with the Higgs being a pGB. Often –but not necessarily– this is achieved in models where strongly interacting new physics generate EWSB dynamically. It is sometimes said that EWSB is *non-linearly* realised. Popular representatives of these theories are composite Higgs models and little Higgs models, that descend from technicolor. For this reason we first present a brief description of *technicolor* as an illustrative example before moving on to more realistic setups.

1.3.1 *Technicolor: an alternative path to EWSB*

The technicolor ansatz [41, 47] was inspired by QCD and constructed as a parallel to the usual color dynamics, just translated at higher scale: one assumes the existence of some new strong interacting sector at a scale Λ_{TC}, that exhibits a global chiral symmetry $\mathcal{G} = SU(2)_L \times SU(2)_R$. Suppose, to begin with, that there is no electroweak interaction. As in QCD, the invariance under $\mathcal{G}$ can be spontaneously broken by a vacuum condensate of new fermion fields down to a diagonal $\mathcal{H} = SU(2)_{L+R}$. Then three Goldstone bosons, analog of the pions, are produced: the "technipions" $\pi^a_{TC}(x)$. For instance, the simplest models included new massless quarks, (T, B), and a new confining gauge group that is responsible for the formation of quark condensates;

$$\langle \bar{T}_L T_R \rangle \neq 0\,, \quad \langle \bar{B}_L B_R \rangle \neq 0 \quad \xrightarrow[SU(2)_R \times SU(2)_L \to SU(2)_V]{} \quad \pi^+_{TC}, \pi^-_{TC}, \pi^0_{TC}\,, \tag{1.37}$$

where the technipions are not fundamental degrees of freedom, but rather massless bound states which have a decay constant f_{TC} (which must satisfy $4\pi f_{TC} \geqslant \Lambda_{TC}$ [48]). This is analogous to the breaking of the chiral flavour symmetry in QCD by the quark condensate $\langle\bar{\psi}\psi\rangle \neq 0$ which gives rise to the pions with a decay constant f_π, but simply at a larger scale. One now "turns on" the EW interactions, by gauging the subgroup $SU(2)_L$ and adding an extra local $U(1)_Y$ to the symmetries of the theory. In this case, the Lagrangian acquires a global invariance under $\mathcal{G} = SU(2)_R \times SU(2)_L \times U(1)_Y$, where the last two components are also local and coincide with the EW gauge group. When the latter is spontaneously broken by the techniquark condensate, the technipions can be eaten by the gauge bosons, finally producing the three massive states $W^\pm$ and Z. The mass of the W turns out to be

$$m_W = \frac{g f_{TC}}{2}\,, \tag{1.38}$$

which reproduces the physical mass if f_{TC} is identified with v, see Eqs. (1.21) and (1.26). In fact, if the EW symmetry was not already broken at the QCD confinement scale, the quark condensate would break $SU(2)_L$ and give the W boson a mass proportional to f_π, which of course is too small to explain the observed value of ~ 80 GeV.

The main interest of this model is that it does not suffer from any hierarchy problem: the scale v is not defined by the expectation value of a scalar, but is rather generated dynamically, by the formation of condensates of techniquarks. In the original proposal there is no Higgs boson though, which we now know exists. Nevertheless, there exists a way in which to still use the technicolor ideas are still fruitful, extending them to include the fundamental scalar boson found at the LHC, as we will discuss next.

1.3.2 *A Goldstone Higgs*

Indeed, some variants of the strong interacting ansatz "predict" the existence of a light Higgs resonance in the spectrum. In the best known of such scenarios, originally proposed in Refs.[49–53], the SM Higgs particle is substituted by a composite scalar degree of freedom that, being a pseudo-Goldstone boson of a larger symmetry group which breaks spontaneously at a scale of $\mathcal{O}$(TeV), cannot acquire a large mass. Besides this light Higgs-like scalar particle, these models still present a strongly interacting sector at the TeV scale, while they may correct at lower energies the size of SM couplings.

The key idea to overcome the shortcomings of pure technicolor models is to separate the characteristic scale of the composites, f_{TC} in the those models, which we will now call f, from the electroweak scale v. This is achieved splitting the symmetry breaking process in two stages, that can be essentially outlined as follows:

1. in the first step, a mechanism similar to that of technicolor is at work: some strong interacting sector exists at the scale Λ_s, invariant under the global symmetry $\mathcal{G}$ which is spontaneously broken down to the subgroup $\mathcal{H} \supset SU(2)_L \times U(1)_Y$. Consequently, $n = (\dim\mathcal{G} - \dim\mathcal{H})$ Nambu-Goldstone bosons are produced, that are composite states of the heavy resonances and are characterized by a scale f. There shall be a group of four among these that transforms as a doublet under $SU(2)_L$, which must survive as physical degrees of freedom at the end of this first phase, since together they are going

to play the role of the four components of the Higgs doublet in the next step. The other ones, if there are, can be eliminated from the spectrum, for example by gauging a convenient subgroup of $\mathcal{G}$. At this stage $SU(2)_L \times U(1)_Y$ is not spontaneously broken, unlike in technicolor.

With the conditions just pointed out, the minimal group that can be chosen is [54] $\mathcal{G} = SO(5)$, to be broken into $\mathcal{H} = SO(4)$, in which case only four GB appear, just as needed at low energies: the three longitudinal components of the $W^\pm$ and Z bosons, plus the Higgs ancestor. Other interesting possibilities considered in the literature include $\mathcal{G}/\mathcal{H} = SO(6)/SO(5)$, $SU(3)/SU(2)$, $SU(5)/SO(5)$ [55].

Up to here, the Higgs is massless. Some physical effect must then convert it in a pGB, giving it a small mass compared to the overall ~TeV scale of the theory. There must be some source of explicit violation of $\mathcal{G}$, and the way in which such explicit breaking is performed is very model-dependent.

2. In a second step the source of explicit breaking of $\mathcal{G}$ should act for the scalar doublet produced in the previous stage to develop a potential: EWSB takes place. A Coleman Weinberg potential may be generated for example by loops of "technifermions" with $\mathcal{G}$-breaking mass terms. If some specific conditions are verified, the minima of this potential can be non-trivial and thus the vacuum can finally break $SU(2)_L \times U(1)_Y$ down to $U(1)_{em}$, just as it happens in a typical Higgs model. It also provides a mass for the physical scalar resonance h.

The Higgs mass is controlled by the size of $\mathcal{G}$-breaking terms. It is techically natural in that it is protected by the global symmetry: if the $\mathcal{G}$-breaking interactions are taken to zero, the larger symmetry is recovered, thus avoiding the electroweak hierarchy problem. Although this is the principle behind so-called *composite Higgs* models, the Higgs does not necessarily have to be composite. It can be an elementary field with a Goldstone nature, as we will see next.

At this point, an overview of the scales involved in Goldstone Higgs constructions is pertinent:

- The electroweak scale v.
- The Goldstone-boson scale f associated to the (pGB) Higgs h, whose value does not need to coincide with the EW scale fixed by the $W^\pm$ mass v, and is typically expected to be in the TeV range, $f \gtrsim 500$ GeV [54, 56]. It is the analogous of f_π in QCD.
- The scale Λ_s of the high-energy strong dynamics responsible for the pseudo-Goldstone boson nature of the Higgs field, with $\Lambda_s \leqslant 4\pi f$ [57], and in consequence approximately in the $1 - 10^2$ TeV range. This is the overall scale of the global theory and, as such, this sets intuitively the scale of masses expected for the exotic fermions, much as in QCD the overall scale of the theory corresponds to the proton mass.

The splitting between v and f is a measure of the degree of misalignment beween the vacuum of the theory after the $\mathcal{G}/\mathcal{H}$ breaking and the vev of the physical Higgs boson, which is related to the $W^\pm$ and Z masses. The presence of v/f factors in the theory constitutes a fine-tuning in composite Higgs models.

1.3.3 *The minimal* SO(5)/SO(4) *linear σ model for a Goldstone Higgs*

In the most economical realisation of GB Higgs models, the Higgs and the longitudinal degrees of freedom of the electroweak bosons originate as the GBs from a global $SO(5)$ symmetry [54, 56] spontaneously broken to $SO(4)$ at some high scale Λ_s, and the gauge group is just the SM one. The low-energy dynamics of such models is commonly studied using an effective non-linear approach that assumes strongly interacting physics underlying the composite scalar sector (a seminal work can be found in Ref. [56]). However. a renormalisable model also exists, which in its scalar part is a linear sigma model, including a new scalar particle σ, singlet under the gauge group [58, 59]. While the scalar part of the linear σ model for the composite Higgs is quite model-independent as far as $SO(5)$ is contained in a given theory, the fermionic part is rather model-dependent.

In this model, the four would-be GBs (which will become the longitudinal components of the W and Z bosons), the Higgs and the σ field are embedded in the fundamental representation of $SO(5)$

$$\phi = (\pi_1\,,\,\pi_2\,,\,\pi_3\,,\,h\,,\,\sigma)^T\,. \tag{1.39}$$

Being GBs, their interactions are characterised by the GB-scale f, which cannot be far from the the scale which at which the spontaneous $SO(5)/SO(4)$ breaking takes place ($\Lambda_s \leqslant 4\pi f$ [57]). Below, the fields π_i will sometimes be referred to as "pions". Furthermore, the model includes exotic fermion representations with couplings that break $SO(5)$ softly.

The potential, with broken $SO(5)$ but preserved $SO(4)$, can be written as

$$V(h,\,\sigma) = V_{SO(5)}(\phi) + V_{\cancel{SO(5)}}(h,\,\sigma)\,, \tag{1.40}$$

where $V_{SO(5)}(h,\,\sigma)$ is a generalisation to $SO(5)$ of the potential of the linear sigma model of QCD,

$$V_{SO(5)}(\phi) = \lambda\left(\phi^T\phi - f^2\right)^2\,, \tag{1.41}$$

and $V_{\cancel{SO(5)}}(h,\,\sigma)$ includes the renormalisable operators required to cancel the divergences of the Coleman-Weinberg potential (see Ref. [59])

$$V_{\cancel{SO(5)}}(h,\,\sigma) = \alpha f^3\sigma - \beta f^2 h^2\,, \tag{1.42}$$

where α and β break obviously $SO(5)$ explicitly. In the unitary gauge (where the longitudinal components of the W and the Z are not explicit), the potential can be parametrised as

$$V(h,\,\sigma) = \lambda(h^2 + \sigma^2 - f^2) + \alpha f^3\sigma - \beta f^2 h^2\,. \tag{1.43}$$

This potential has a non-trivial minimum, providing a mass for h and breaking the SM electroweak symmetry at a scale $v \neq f$. The important feature of GB Higgs models shows up in the expression of the Higgs mass, which after diagonalisation reads [5]

$$m_h^2 = 2\beta v^2 + \mathcal{O}\left(\frac{\beta}{4\lambda}\right)\,. \tag{1.44}$$

5 It is possible by construction for the physical σ to be lighter than the pGB Higgs, however, the authors show that this option requires an uncomfortable fine-tuning of the α and β parameters in the potential.

Another important characteristic of this class of models is that the mechanism of *partial compositeness* is typically implemented: the SM fermions do not have direct couplings to the Higgs (included in the scalar five-plet from Eq. (1.39)) but rather couple to it via a mixing with the exotic fermions. This gives rise to a seesaw-like mechanism in the generation of all low-energy fermion masses: the heavier the exotic fermions the lighter the light fermions. It is quite model-dependent and we do not develop it further here; however, the work presented in Chapter 5 of this thesis will describe in detail and use one particular implementation and present a large number of alternative setups.

The model can be considered either as an ultimate theory describing elementary fields (instead of composite ones), or as a renormalisable version of a deeper dynamics, much as the linear σ model is to QCD; in the limit of very heavy σ mass, the non-linear regime is reached. The σ mass can range from few hundred of GeV to infinitely heavy in the strong interacting regime. The latter avoids fine-tuning issues by construction. This mass scale is absent in non-linear realizations, which are akin to a very heavy σ decoupled from the spectrum, much as the chiral Lagrangian for QCD with a light pion decay constant f_π corresponds to the infinite mass limit of the σ particle in the renormalizable linear sigma model for QCD.

1.4 MODEL-INDEPENDENT APPROACH: SMEFT AND HEFT EFFECTIVE FIELD THEORIES

In the previous subsection we referred to explicit models in which the Higgs may have a GB ancestry and/or may eventually be a composite object arising from a strongly interacting dynamics at higher energies. In the last part of this chapter we present the *effective field theory* (EFT) formalism which is used to study the low-energy dynamics in a model-independent way, exploiting the fact that in order to study the physics at a given energy scale one does not need to know the specificities of the theory at a higher scale. The robustness of EFTs relies on the fact that they only assume invariance under the established low-energy symmetries.

A paradigmatic example of an EFT can be found in the SM example known as the Fermi theory, which describes the particle interactions responsible for beta decay with an operator constructed out of four fermions. When constructed, the only requirement was electromagnetic invariance, being the only symmetry established at the time. For instance the decay $n \to p e^- \bar{\nu}_e$, interpreted in terms of quarks, can be described by the operator

$$\mathcal{L}_{\text{Fermi}} = -\frac{G_F}{\sqrt{2}} \left(\bar{u}\gamma_\mu(1-\gamma_5)V_{ud}\,d\right)\left(\bar{e}\gamma_\mu(1-\gamma_5)\nu_e\right) . \tag{1.45}$$

V_{ud} is the $(1,1)$ element of the CKM matrix defined in Eq. (1.32), although Eq. (1.45) can be trivially generalised to any four fermions. Nowadays we know that a more fundamental theory, that of $SU(2)_L \times U(1)_L$ weak interactions, lies behind the Fermi interactions and in fact, the latter can be obtained as a low-energy limit of the former. In terms of weak interactions, beta decay is described via the s-channel exchange of a virtual W boson, but the Fermi theory is a valid description up to the electroweak scale, which is referred to as the cut-off scale. Indeed, the amplitude in terms of the weak interactions would contain a vector boson propagator which can be Taylor expanded for low momentum with respect to this cutoff scale,

$$\frac{-g_{\mu\nu} + p_\mu p_\nu / m_W^2}{p^2 - m_W^2} \xrightarrow[q^2 \ll m_W^2]{} \frac{g_{\mu\nu}}{m_W^2} . \tag{1.46}$$

Implementing this replacement in the expression for the amplitude in the weak theory one obtains exactly the four-particle interaction in Eq. (1.45) by identifying

$$\frac{G_F}{\sqrt{2}} = \frac{g^2}{8m_W^2}\,, \tag{1.47}$$

The lesson is that the knowledge at the electroweak scale was not necessary to describe the interactions of the fermions orders of magnitude below. Neither the EW-scale fields, the W bosons, nor the EW-scale symmetries are present in the contact-interaction of Eq. (1.45): in this case $SU(2)_L \times U(1)_Y$ is not a symmetry of Eq. (1.45) while $U(1)_{em}$ is manifestly conserved. In spite of its simplicity, it was nevertheless most useful in setting the basis that ultimately led to the discovery of the $SU(2)_L \times U(1)_Y$ gauge theory.

In general, an EFT is expressed as a sum of operators $\mathcal{O}_i$ constructed out of the low-energy fields and which must respect the symmetries of the low-energy regime,

$$\mathcal{L} = \sum_i c_i \mathcal{O}_i^{(d_i)}\,, \tag{1.48}$$

where the arbitrary coefficients, c_i, encode the high-energy physics and have to be determined phenomenologically at low energy. The tower of operators is usually organised according to their dimension, $[\mathcal{O}_i] = d_i$. The dimension fixes the powers of the NP scale Λ inside the coefficients c_i:

$$c_i \sim \frac{1}{\Lambda^{d_i-4}}\,, \tag{1.49}$$

much as the Fermi coupling G_F is suppressed by powers of $m_W \sim v$. Often, and in what follows below, the coefficients are left dimensionless and the powers of the new physics scale are made explicit in the expansion in Eq. (1.48).

At each order $k = d_i - 4$ there is a finite set of operators that can be used to compute all physical quantities at an energy E, and the error made by including interactions only up to order k instead of the full expansion is of the order $(E/\Lambda)^k$. The result given by the EFT is thus better the farther apart that E and Λ are. As the energy of the observable is raised, the effective field theory ceases to be valid, and it is said to break down as E approaches Λ, since then the new particle states can begin to be produced.

There are two kinds of EFTs for the SM, depending on the assumptions of the new physics involved and they are constructed with the use of either *linear* or *non-linear* Lagrangians. They differ in the choice of the low-energy fields which are used to construct the operators –the building blocks–, and in the organisation of the towers of operators –the counting–, while in both cases the symmetry group is the SM one. They give rise to what is known as the *Standard Model effective field theory* and the *Higgs EFT* respectively.

1.4.1 *Linear effective Lagrangians: the Standard Model effective field theory*

The Standard Model effective field theory (SMEFT) is characterised by the fact that the Higgs scalar degrees of freedom –the physical Higgs particle $h(x)$ and the longitudinal components

of the W and Z: $\pi^a(x)$– are part of an exact doublet at low energies. They are encoded in the Lagrangian as it was defined in Eq. (1.22):

$$\Phi(x) \;=\; \frac{v+h(x)}{\sqrt{2}}\mathbf{U}(x)\begin{pmatrix}0\\1\end{pmatrix}, \quad \text{with} \quad \mathbf{U}(x)=e^{i\pi^a(x)\sigma^a/v}. \tag{1.50}$$

A Higgs particle h of this type has interactions in powers of $(v+h)^n$. Apart from the Higgs, the operators are constructed out of the SM fields: $W_{\mu\nu}$, $B_{\mu\nu}$, $G_{\mu\nu}$ and the fermions, and the operators are organised in a tower of canonical mass dimensions.

The *leading order* (LO) Lagrangian is defined by having canonical mass dimension four ($d=4$): it is the SM Lagrangian. The higher order interactions $d \geqslant 5$ will encode the new physics effects:

$$\mathcal{L}_{\text{SMEFT}} = \mathcal{L}_{\text{SM}} + \frac{1}{\Lambda}\mathcal{L}^{(d=5)} + \frac{1}{\Lambda^2}\mathcal{L}^{(d=6)} + \dots . \tag{1.51}$$

Only one dimension five operator can be constructed out of the SM fields, it is the Weinberg operator [60] $\mathcal{O}_{d=5} = \frac{1}{2}\left(\bar{l^c}_L\tilde{\Phi}^*\right)\left(\tilde{\Phi}^\dagger l_L\right)$ (where the contraction in flavour space is not made explicit and the charge-conjugate spinor is denoted $\psi^c \equiv C\bar{\psi}^T$). This operator violates $B-L$ ("baryon minus lepton number") symmetry and leads to Majorana neutrino masses and is strongly suppressed by the smallness of neutrino masses. Conversely, a plethora of operators compose the $d=6$ basis [11, 12], which is referred to as the *next-to-leading order* (NLO) in the SMEFT Lagrangian. [6] There has been a large effort in the particle physics community to search for effects of new physics in these interactions.

This kind of Lagrangian is typical of weakly interacting new physics. However, strongly interacting scenarios, as the ones involved in composite Higgs and some GB Higgs models, are rather described by a different setup: that of *chiral* or *non-linear* Lagrangians.

1.4.2 *Non-linear effective Lagrangians: the Higgs effective field theory*

The paradigmatic example of non-linear (or chiral) effective Lagrangians is the *non-linear* σ-*model* of QCD, which was introduced for the first time in 1960 as a description for low energy strong interactions [61], that is, the chiral Lagrangian for QCD pions. It is reproduced in the context of the EW interactions in the *EW chiral Lagrangian*.

A milestone in the path towards the chiral description of a light, dynamical Higgs is represented by the formalism mainly developed by T. Appelquist and A. Longhitano in the early 80s [62–64]. They considered the possibility of a Higgs so heavy that it could be integrated out from the low energy Lagrangian, and therefore built a complete basis of chiral operators describing a "Higgsless" scenario. Although this model does not seem realistic anymore, their work represents the starting point to build the chiral Lagrangian we are interested in now. This work was extended to include a light Higgs [1, 14, 15, 65–76] in what has come to be known as the Higgs effective field theory (HEFT)

The chiral effective Lagrangian HEFT, which describes, in the context of generic non-linear realizations of EWSB, the interactions among SM gauge degrees of freedom, SM fermions

6 Indeed, in an abuse of notation, often the $d=6$ is referred to as the NLO Lagrangian, and the $d=8$ as the *next-to-next-to leading order* (NNLO) in particular when considering only bosonic interactions.

and a light Higgs resonance, consists of all operators invariant under Lorentz and SM gauge symmetries and written in terms of the SM spectrum with the only exception of the Higgs doublet, whose four degrees of freedom are distributed in two separate sets.

- On one side, the unitary matrix $\mathbf{U}(x)$ from Eq. (1.50) describes only the three SM would-be Nambu-Goldstone bosons [65, 77–79] – that become the longitudinal components of the gauge bosons after EWSB:

$$\mathbf{U}(x) = e^{i\sigma_a \pi^a(x)/v}\,, \tag{1.52}$$

  whose covariant derivative reads

$$\mathbf{D}_\mu \mathbf{U}(x) \equiv \partial_\mu \mathbf{U}(x) + igW_\mu(x)\mathbf{U}(x) - \frac{ig'}{2}B_\mu(x)\mathbf{U}(x)\sigma_3\,. \tag{1.53}$$

  Two $SU(2)_L$ covariant objects are constructed and used as building blocks if the Lagrangian:

$$\mathbf{V}_\mu(x) \equiv (\mathbf{D}_\mu \mathbf{U}(x))\,\mathbf{U}(x)^\dagger\,, \qquad \mathbf{T}(x) \equiv \mathbf{U}(x)\sigma_3\mathbf{U}(x)^\dagger\,, \tag{1.54}$$

  Under $SU(2)_{L,R}$ global transformations (L, R respectively), these objects transform as

$$\mathbf{U}(x) \to L\,\mathbf{U}(x)R^\dagger\,, \qquad \mathbf{V}_\mu(x) \to L\,\mathbf{V}_\mu(x)L^\dagger\,, \qquad \mathbf{T}(x) \to L\,\mathbf{T}(x)L^\dagger\,. \tag{1.55}$$

- On the other side, the physical Higgs particle h is introduced as an independent field, a generic singlet of the SM with arbitrary couplings [14, 65, 67, 68, 80] via generic polynomial functions $\mathcal{F}_i(h)$ [80] expanded in powers of h/v,

$$\mathcal{F}_i(h) = 1 + 2a_i h/v + b_i (h/v)^2 + \dots\,, \tag{1.56}$$

  where a_i, b_i ... are constant coefficients. For particular values of these coefficients (e.g. $a_i = b_i = 1$ and all others zero), the typical SM dependence of e.g. $(v+h)^2$ is recovered.

This separation stems from the fact that in non-linear realisations of EWSB h is not part of an exact $SU(2)_L$ doublet. In other words, it does not appear in the low-energy Lagrangian as powers of $(v+h)^n$, unlike the SM Higgs particle. [7]

The HEFT building blocks can thus be chosen to be the Higgs expansion, $\mathcal{F}_i(h)$, the scalar and vector fields containing the would-be-GBs, $\mathbf{T}(x)$, $\mathbf{V}(x)$ and the gauge field strengths $G_{\mu\nu}$, $W_{\mu\nu}$ and $B_{\mu\nu}$. Finally, the SM fermions are often grouped into doublets of $SU(2)_L$ and $SU(2)_R$, $Q_{L,R} \equiv (u_{L,R}\,, d_{L,R})$, $L_L \equiv (\nu_L\,, e_L)$ and $L_R \equiv (0\,, e_R)$. The notation chosen allows an easy identification of terms breaking the custodial symmetry $SU(2)_C$ to which the global group $SU(2)_L \times SU(2)_R$ gets broken after EWSB. $SU(2)_C$ is explicitly broken by the gauging of the hypercharge $U(1)_Y$ and by the heterogeneity of the fermion masses; insertions of the scalar chiral field $\mathbf{T}(x)$, which is not invariant under transformations of the full $SU(2)_R$, account for breaking of the custodial symmetry in the effective operators.

Aside from fermionic operators, the tower of invariant operators shall be organised according to a chiral (derivative) expansion [81]. The normalization of the operators in the EW

7 For instance, in composite Higgs models it is typically sinusoidal. e.g. $\mathcal{F}_i(h) \sim \sin^2(\varphi/2f)$ [74] where φ is the light scalar singlet resulting from the global breaking, ancestor of the Higgs.

chiral Lagrangian will follow the *naive dimensional analysis* formula for the HEFT Lagrangian as discussed in Refs. [57, 82–84]. With this convention the gauge boson kinetic terms will appear canonically normalised. In addition, the strongly interacting regime would correspond to operator coefficients of $\sim \mathcal{O}(1)$.

Having settled the symmetries, building blocks and ordering of the operators, the LO Lagrangian in the in the chiral Lagrangian formalism reads

$$\begin{aligned}\mathcal{L}^{\text{LO}}_{\text{HEFT}} =& \frac{1}{2}(\partial_\mu h)(\partial^\mu h) - \frac{1}{4}G^a_{\mu\nu}G^{a\mu\nu} - \frac{1}{4}W^a_{\mu\nu}W^{a\mu\nu} - \frac{1}{4}B_{\mu\nu}B^{\mu\nu} - V(h) + \\ &- \frac{v^2}{4}\text{Tr}[\mathbf{V}_\mu\mathbf{V}^\mu]\,\mathcal{F}_C(h) + c_T\,v^2\text{Tr}[\mathbf{T}\mathbf{V}_\mu]\text{Tr}[\mathbf{T}\mathbf{V}^\mu]\mathcal{F}_T(h) + i\bar{Q}\not{D}Q + i\bar{L}\not{D}L + \\ &- \frac{v}{\sqrt{2}}\left(\bar{Q}_L\mathbf{U}\mathcal{Y}_Q(h)Q_R + \text{h.c.}\right) - \frac{v}{\sqrt{2}}\left(\bar{L}_L\mathbf{U}\mathcal{Y}_L(h)L_R + \text{h.c.}\right),\end{aligned} \tag{1.57}$$

where the dependence on x, as well as that on v of $\mathcal{F}(h/v)$, has been left implicit for brevity. The first line in Eq. (1.57) accounts for the h and gauge boson kinetic terms, and a general scalar potential $V(h)$. The first term in the second line describes the W and Z masses and their interactions with h, as well as the kinetic energy of their longitudinal components; the second term in this line is a custodial-breaking term that we will disregard in what follows, being phenomenologically extremely suppressed (for this reason sometimes it is included instead among the NLO chiral terms even if it is a two-derivative coupling). The fermion kinetic energy and Yukawa-like terms written in the mass eigenstate basis come next, with

$$\mathcal{Y}_{Q,L}(h) \equiv \mathbf{Y}_{Q,L}\mathcal{F}_{Q,L}(h)\,, \tag{1.58}$$

where $\mathbf{Y}_{Q,L}$ are 6×6 block-diagonal matrices containing the usual Yukawa couplings as defined as $\mathbf{Y}_Q = \text{diag}(Y_u, Y_d)$ and $\mathbf{Y}_L = \text{diag}(0, Y_e)$, with Y_i the same as in Eq. (1.28). This notation follows the assumption that the Yukawa-type fermion-h couplings are aligned with the fermion masses.

Furthermore, the mass parameter in front of several operators in Eqs. (1.57) should be a generic scale f, for instance that associated in specific models to a Nambu-Goldstone ancestry for the Higgs resonance (alike to f_π for QCD pions), such that $\Lambda \leqslant 4\pi f$ [57]. Instead, v –the electroweak scale– is shown as explicit mass parameter for bosons and fermions in Eq. (1.57), with $v \neq f$: this inequality is the well-known fine-tuning of the chiral electroweak Lagrangian, necessary to recover the correct scale of the gauge boson masses. It reflects as well the fine-tuning problems of specific "composite Higgs" scenarios mentioned before. For consistency, v has been then chosen as weight in all mass-related terms in those equations.

The same fine-tuning is at the origin of the $\mathcal{F}_i(h)$ functions being customarily written as generic polynomials in h/v instead of h/f, see Eq. (1.56). It can be considered that in this parametrization factors of v/f have been reabsorbed in the free parameters a_i, b_i, etc. in Eq. (1.56). Note as well that, in principle, a function $\mathcal{F}_i(h)$ can be attached to any of the operators in Eqs. (1.57). However, those attachments can be redefined away in both Higgs and fermionic kinetic terms at the price of redefining $\mathcal{F}_{Q,L}(h)$ [85]. Moreover, $\mathcal{F}_i(h)$ insertions in the gauge bosons kinetic terms can be avoided assuming that the transverse components of the gauge fields do not couple at tree level to the Higgs sector, as it has been explicitly shown in Refs. [74, 75] for composite Higgs models [8, 86, 87].

The next-to-leading interactions of the EW chiral Lagrangian with a light Higgs correspond to operators with four derivatives, according to the chiral power-counting criteria. They have been largely studied during the last decade [14, 65, 68–71, 80, 88–90] and Ref. [15] contains a non-redundant definition of the complete NLO basis.

One last comment is in order before finishing this chapter, since we will move on to presenting very different physics sectors. While the SMEFT and the HEFT are presented as formalisms to describe NP in scenarios where the only fields at low energy are the ones already discovered and included in the SM, it is possible that there are others. These may be "light", having masses at the EW scale or lower, but might have escaped detection because their couplings to the SM are very suppressed (for instance by very high NP scales). Both the *linear* and *chiral* (or *non-linear*) formulations used in the SMEFT and HEFT respectively can be extended to study effective Lagrangians of such other BSM proposals by including additionally new degrees of freedom not present in the SM, and maybe an enlarged symmetry group at low energy. In particular, this will be done in this thesis in two different contexts. In Chapter 6 we will derive the bosonic chiral Lagrangian for an extra pseudoscalar GB with derivative couplings, $a(x)$, and study the phenomenology of both the linear and non-linear Lagrangians. In addition, Chapter 7 will present the extension of the SM with an extra scalar SM singlet, $S(x)$, studying it in the context of Dark Matter as the non-linear Higgs portal.

2

THE STRONG CP PROBLEM

The Standard Model includes another sector of gauge interactions apart from the electroweak sector: the interactions known as the strong interactions or QCD. While the electroweak sector of the SM gauge group $SU(3)_C \times SU(2)_L \times U(1)_Y$ was presented in Chapter 1 together with some of its theoretical concerns, strong interactions of the SM have their own fine-tuning problems. We move on to presenting the QCD interactions and the strong CP problem.

2.1 CP VIOLATION IN QCD

The SM Lagrangian has come to elegantly describe strong interactions with just one non-abelian gauge group $SU(3)_C$ characterizing the coupling of quarks, q, fermions in the fundamental representation of the group, through the action of gluons, the massless gauge bosons in the adjoint, see Tab. 1.1. The Lagrangian of QCD is simply

$$\mathcal{L}_{QCD} = \bar{q}(i\not{D} - M)q - \frac{1}{4}G^a_{\mu\nu}G^{a\mu\nu} \tag{2.1}$$

where the covariant derivative relevant to QCD interactions reads $D_\mu = \partial_\mu + ig_s G^a_\mu t^a$, g_s being the strong coupling constant, with $t^a = \lambda_a/2$ matrices (λ_a being the Gell-Mann matrices) satisfying $[t^a, t^b] = if^{abc}t^c$. $G^a_{\mu\nu}$ is the gluon field strength tensor, which can be written in terms of the gluon –the QCD vector boson– G^a_μ and of the $SU(3)$ structure constants, f^{abc} as

$$G^a_{\mu\nu} = \partial_\mu G^a_\nu - \partial_\nu G^a_\mu - g_s f^{abc} G^b_\mu G^c_\nu \,. \tag{2.2}$$

The quarks, q are six triplets under $SU(3)$, whose LH and RH components are respectively three $SU(2)_L$ doublets and six singlets, see Tab. 1.1. The Yukawa interactions (see Eq. (1.28)) generate in general non-diagonal and complex mass matrices for the quarks, which can however be diagonalised through the unitary transformations of Eq. (1.30) without any other effect in the QCD Lagrangian (2.1), so

$$M = \text{diag}(m_i e^{i\delta_i}) \tag{2.3}$$

and thus, the mass term can be expanded as

$$\bar{q}Mq = \sum_i m_i e^{i\delta_i} \bar{q}_{iL} q_R + \text{h.c.} \tag{2.4}$$

$$\simeq m_i \bar{q}_i q_i + i\delta_i m_i \bar{q}_i \gamma_5 q_i \,. \tag{2.5}$$

While $\bar{q}_i q_i$ is CP-even, $i\bar{q}_i\gamma_5 q_i = i(\bar{q}_{iL}q_{iR} - \bar{q}_{iR}q_{iL})$ is CP-odd. The extent to which CP is violated through this mechanism is weighted by the phases in the mass matrix.

There exists a second term in the QCD Lagrangian associated to CP violation (CPV), known as the QCD θ-term:

$$\mathcal{L}^\theta_{QCD} = \mathcal{L}_{QCD} + \theta_{QCD}\frac{\alpha_s}{8\pi}G^a_{\mu\nu}\tilde{G}^{a\mu\nu} \,, \tag{2.6}$$

with $\tilde{G}^a_{\mu\nu} = \frac{1}{2}\epsilon_{\mu\nu\rho\sigma}G^{a\rho\sigma}$ the dual field strength tensor and $\alpha_s = g_s^2/4\pi$. This term violates parity but conserves charge conjugation. One might be tempted to exclude it from the QCD Lagrangian due to the fact that it is actually a total divergence,

$$G_{\mu\nu}\tilde{G}^{\mu\nu} = \partial_\mu K^\mu\,, \quad K^\mu = \epsilon^{\mu\nu\rho\sigma}A^a_\nu\left[\partial_\rho A^a_\sigma - \frac{g_s}{3}f_{abc}A^a_\nu A^b_\rho A^c_\sigma\right]\,. \tag{2.7}$$

The volume integral on the Lagrangian density $\theta G\cdot\tilde{G}$ can be transformed to a surface integral via Gauss' theorem, which evaluated at spacial infinity would normally give zero. Indeed, that is the case for the analogous term $F_{\mu\nu}\tilde{F}^{\mu\nu}$ in the Lagrangian of Quantum Electrodynamics (QED), where the gauge fields can adopt configurations that die fast enough at infinity for the integral in the action to vanish. However, in the case of QCD the gluon field equations are solved by instantons, field configurations whose integral does not vanish at infinity, meaning that this term is actually physical. [1]

▷ *The $U(1)_A$ problem.*

The relevance of instantons and of this term was established in solving the $U(1)_A$ problem [91], which explains why one of the mesons, which based on classical chiral symmetry arguments was expected to be massless, is in fact as heavy as the proton, the η'.

To illustrate the problem consider the case of two quark families. Since $m_u, m_d \ll \Lambda_{QCD}$, where Λ_{QCD} refers to the confinement scale of the strong interactions, there is an approximate $U(2)_L \times U(2)_R$ symmetry in the Lagrangian of Eq. (2.1) that would become exact in the massless limit. The vectorial part of this symmetry, $U(2)_V$, is manifestly realised in nature. The axial part, $U(2)_A$ is spontaneously broken by the non-vanishing value of the QCD quark condensate, $< \bar{q}q > \neq 0$. According to the Goldstone theorem, see Sect. 1.1.1, for any spontaneously broken symmetry in a relativistic theory there will be as many massless particles, Nambu-Goldstone Bosons (NGBs), as broken symmetry generators. Thus, four massless NGBs are naively expected. If we turn on the quark masses, the NGBs get small masses, proportional to those of the quarks, responsible for the breaking of the symmetry. In particular, $m_\eta \leqslant \sqrt{3}m_\pi$ should be the mass of the fourth companion of the pions [92].

Generalising the problem to 3 quark families it is the η' that is expected to be almost massless, but in fact nothing of the sort is found! The generators of $U(3)_A$ can be decomposed into $SU(3)_A \times U(1)_A$, and the eight pseudo-NGBs associated to the $SU(3)_A$ part of this symmetry had been found, but not the η'. Historically, this question of the missing pNGB was dubbed as the $U(1)_A$ problem [93–95].

The solution to the $U(1)_A$ problem was found by 'tHooft [96, 97], who pointed out that as a consequence of the Adler-Bell-Jackiw (ABJ) anomaly [98–100] and of the non-trivial properties of the QCD vacuum, the axial current is not conserved. The $U(1)_A$ was not a symmetry

1 An equivalent term can be written for the weak vector bosons $\theta_L W_{\mu\nu}\tilde{W}^{\mu\nu}$. However, there is no weak CP problem because it can be rotated away through a vectorial rotation on the quarks thanks to the chiral nature of $SU(2)_L$.

of the Lagrangian to start with, and consequently one should not expect a Goldstone boson associated to its breaking. Indeed, under a chiral transformation of a quark:

$$U(1)_A \ : \ q \to e^{-i\gamma_5\beta} q \quad \Rightarrow \quad \begin{cases} q_L \to e^{i\beta\gamma_5} q_L \\ q_R \to e^{-i\beta\gamma_5} q_R \end{cases} \tag{2.8}$$

the associated current $j_5^\mu = \bar{q}\gamma^\mu\gamma_5 q$, with $P_{R,L} = (\mathbb{1} \pm \gamma_5)/2$ is not conserved. In the massless quark limit

$$\partial_\mu j_5^\mu = \frac{\alpha_s}{4\pi} G^a_{\mu\nu} \tilde{G}^{a\mu\nu} , \tag{2.9}$$

such that, in general,

$$\delta\mathcal{L} = \beta \partial_\mu j_5^\mu \tag{2.10}$$

(or any other current). It is through the coupling of the η meson to this current, and the non-perturbative effects of the instantonic field solutions that a potential is generated for the fourth meson, giving it a surprisingly large mass: the "scale of the m_η" is set by the QCD confinement scale, Λ_{QCD}, which is in the hundreds of MeV.

The discovery of instantons explaining the large mass of the η' meson verifies that $G \cdot \tilde{G} = G^a_{\mu\nu} G^{a\mu\nu}$ cannot be neglected as a total derivative, thus the complete $\mathcal{L}^\theta_{QCD}$ from Eq. (2.6) must be considered. To understand the implications of this let us illustrate its consequences in the Lagrangian of QCD with one quark of mass $M = me^{i\delta}$,

$$\mathcal{L}_q = \bar{q}\not{D} q + m(\bar{q}q + i\delta\bar{q}\gamma_5 q) + \theta_{QCD}\frac{\alpha_s}{8\pi} G^a_{\mu\nu}\tilde{G}^{a\mu\nu} + \mathcal{O}(\delta^2) , \tag{2.11}$$

where we will continue only to first order in the CP phase δ for clarity although the results hold to all orders in δ. If the quark were massless, a simple $U(1)_A$ rotation $q \to e^{i\theta_{QCD}\gamma_5/2} q$ would remove the last term from the Lagrangian in Eq. (2.11), as follows directly from Eqs. (2.8)- (2.10). However, the complete non-conservation of the axial current actually has an additional term proportional to the quark mass, which reads

$$U(1)_A \ : \ q \to e^{-i\gamma_5\beta} q \quad \Rightarrow \quad \partial_\mu j_5^\mu = -2mi\,\bar{q}\gamma_5 q + \frac{\alpha_s}{4\pi} G^a_{\mu\nu}\tilde{G}^{a\mu\nu} , \tag{2.12}$$

so that the transformation necessary to rotate away the θ_{QCD} parameter in fact only moves it to the quark mass term,

$$U(1)_A\,(\beta = -\theta_{QCD}/2) \quad \Longrightarrow \quad \delta\mathcal{L}_q = im\theta_{QCD}\bar{q}\gamma_5 q - \theta_{QCD}\frac{\alpha_s}{8\pi} G^a_{\mu\nu}\tilde{G}^{a\mu\nu} . \tag{2.13}$$

Indeed, the two CP violating parameters of the QCD Lagrangian, namely the phase in the quark mass matrix and the θ_{QCD} parameter are connected, and it is one combination of these that is actually physical, called $\bar{\theta}$.

To identify $\bar{\theta}$ in the SM we go back to the QCD Lagrangian with six massive quarks and the $\theta G \cdot \tilde{G}$ term from Eq. (2.6). By rotating each quark chirally proportional to the phase in its mass

$$q_i \to e^{-i\gamma_5\delta_i/2} q_i \quad \Longrightarrow \quad \delta\mathcal{L}^\theta_{QCD} = \sum_i \left(-im_i\delta_i\bar{q}_i\gamma_5 q_i + \delta_i \frac{\alpha_s}{8\pi} G^a_{\mu\nu}\tilde{G}^{a\mu\nu} \right) . \tag{2.14}$$

and $\mathcal{L}^{\theta}_{QCD}$ becomes

$$\mathcal{L}^{\theta}_{QCD} = \bar{q}_i(i\not{D} - m_i)q_i + \frac{1}{4}G^a_{\mu\nu}G^{a\mu\nu} + \left(\theta_{QCD} + \sum_i \delta_i\right)\frac{\alpha_s}{8\pi}G^a_{\mu\nu}\tilde{G}^{a\mu\nu}\,. \tag{2.15}$$

The ultimate CP violating parameter is thus

$$\bar{\theta} \equiv \theta_{QCD} + \mathrm{ArgDetM}\,, \tag{2.16}$$

where $\mathrm{ArgDetM} = \sum_i \delta_i$ simply accounts for the sum of all of the phases in the quark mass matrices. In summary, $\bar{\theta}$ may be written as the coefficient of $G\tilde{G}$ as in Eq. (2.15) or as a physical phase in the quark masses.

In order to estimate the CP violating effects of $\bar{\theta}$ in the SM it is customary to express the contribution of $\bar{\theta}$ in the quark mass matrix in a basis where the Lagrangian has no $G\cdot\tilde{G}$ term. This can be accomplished by rotating the $\bar{\theta}$ parameter to the quark mass term through a chiral redefinition $q_i \to \exp(i\gamma_5\phi_i/2)q_i$ which is different for each quark flavor, in such a way that $\bar{\theta}G\cdot\tilde{G} \to 0$. Since $\bar{\theta}G\cdot\tilde{G}$ is a flavor singlet, the resulting axial coupling shall be so too, and this is the condition used to determine the phases of the rotations ϕ_i. To the lowest order in $\bar{\theta}$ and with three flavours for illustration the CP-violating Lagrangian is

$$\delta\mathcal{L}_{CP} = -i\bar{\theta}\,\lambda\,(\bar{u}\gamma_5 u + \bar{d}\gamma_5 d + \bar{s}\gamma_5 s)\,, \tag{2.17}$$

where

$$\lambda = \frac{m_u m_d m_s}{m_u m_d + m_u m_s + m_d m_s}\,. \tag{2.18}$$

Contributions of the heavy quarks to Eqs. (2.17) and (2.18) are subdominant. Notice that this goes to zero in the correct limits, *i.e.* when $\bar{\theta} = 0$ or if any of the light quarks were massless, $m_i = 0$. This formula reflects explicitly the fact that one single massless quark would have been enough for $\bar{\theta}$ not to be physical.

2.2 THE STRONG CP PROBLEM

2.2.1 *Measuring $\bar{\theta}$: Electric dipole moment of the neutron*

The CP-violating $\delta\mathcal{L}_{CP}$ can manifest itself through the electric dipole moment of the neutron (nEDM), defined as

$$\mathcal{L} = -\frac{i}{2}d_n\,\bar{\psi}_n\sigma_{\mu\nu}\gamma_5\psi_n\,F^{\mu\nu} \tag{2.19}$$

where ψ_n is the neutron spinor field and $F^{\mu\nu}$ represents the field strength tensor associated to the photon. The measurement of this quantity is the one which sets the strongest constraints on $\bar{\theta}$.

There are many estimations of the expected size of the nEDM, d_n as a function of $\bar{\theta}$ [101–107], but they all lie in the range $|d_n/\bar{\theta}| = (0.1-2)\times 10^{-15}\,e\cdot cm$. For instance in Ref. [102], the authors computed the dominant contribution to the nEDM through the diagram in Fig. 2.1, which can be expressed in terms of the CP-even and CP-odd couplings of pions to nucleons, respectively

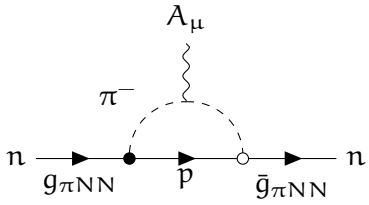

Figure 2.1: Dominating diagram contributing to the electric dipole moment of the neutron. The solid black blob indicates a CP-conserving vertex, while the empty one depicts the CP-violating interaction in $\delta\mathcal{L}_{CP}$.

$$\mathcal{L}_{\pi NN} = \bar{\psi}_N (i\gamma_5 g_{\pi NN} + \bar{g}_{\pi NN}) \sigma^a \pi^a \psi_N \,, \tag{2.20}$$

where $g_{\pi NN}$ is the pion-nucleon coupling determined from experiment and $\bar{g}_{\pi NN}$ can be computed in relation to $\bar{\theta}$. For instance, using current-algebra methods to evaluate the matrix element $\langle \pi^a N | \delta\mathcal{L}_{CP} | N \rangle$ [102, 108] yields

$$\bar{g}_{\pi NN} = -\frac{\bar{\theta}\,\lambda}{f_\pi} \frac{2(m_\Xi - m_\Sigma)}{2m_s - m_u - m_d} \simeq -0.027\,\bar{\theta}\,. \tag{2.21}$$

The logarithmic contribution to the nEDM through the diagram in Fig. 2.1 is[2]

$$d_n = \frac{e\, g_{\pi NN}\, \bar{g}_{\pi NN}}{4\pi^2 m_N} \ln\left(\frac{m_N}{m_\pi}\right) \simeq 3.6 \times 10^{-16}\,\bar{\theta}\, e \cdot cm\,. \tag{2.22}$$

Taking the latest bound on d_n [109], an order of magnitude estimate follows from $|d_n| \sim 10^{-15}|\bar{\theta}|$

$$d_n < 2.9 \times 10^{-26}\, e \cdot cm \quad (90\%\,\text{C.L.}) \quad \Rightarrow \quad |\bar{\theta}| \lesssim 10^{-11}\,. \tag{2.23}$$

As can be seen from Eq. (2.16), $\bar{\theta}$ is the sum of two terms whose origin is in principle completely unrelated. Why these two terms would add up to cancel in such a way is a mystery which has been dubbed the strong CP problem.

2.2.2 *Weak CP violation*

The truly tiny bound given in Eq.(2.23) begs for an explanation and one might naively answer that $\bar{\theta} = 0$ corresponds to an enlarged symmetry of the theory, i.e that the theta parameter is protected by CP invariance. However, even if there were no CPV in the strong interactions, CP is already violated in the weak sector. In the SM formulation, the phases from the quark mass matrices are encoded in the CKM matrix after their diagonalisation (see Eqs. (1.30)-(1.32) in Chapter 1), and CP violation in the CKM formalism has been widely confirmed by a very large number of experimental observations. Hence the smallness of $\bar{\theta}$ is not protected by the symmetry and the CPV in the electroweak interaction induces a contribution to $\bar{\theta}$ via ArgDet$M$ in Eq. (2.16).

SM predictions of CKM-induced nEDM are obtained by evaluating the amplitudes of two kinds of processes [110]: processes in which the nEDM arises from a single quark in the

2 This result is subject to an ambiguity as to which mass is to be inserted in the numerator of the logarithm, m_ρ or m_N, since finite terms are not determined by current algebra [102].

neutron, and those where it is due to the interplay of two or three quarks in the neutron. Amongst the first type, the SM does not induce nEDM at one loop: the simplest one-loop contribution to $d \to d\gamma$ or $u \to u\gamma$ through a $W^{\pm}$ loop (see Fig. 2.2a), vanishes because there remains no net CP-phase, due to the V-A structure of the weak interactions. At two loops there exists the possibility of *non-self-conjugate* diagrams as in Fig. 2.2b, which have a complex amplitude and contribute to d_n at the order of $10^{-31}\, e \cdot cm$ [111, 112]. However, it has been shown by Shabalin [113] that the sum of all the two loop diagrams leads to a vanishing electric dipole moment for the quarks. A non-vanishing contribution requires at least one more loop, which can be an additional gluon [114], see Fig. 2.2c as an example. Parametrically this results in

$$\frac{d_n}{e} \sim m_d\, \mathcal{J} \left(\frac{\alpha_S}{\pi}\right) \frac{g^4}{(2\pi)^4 M_W^4} \frac{(m_t^2 - m_c^2)(m_t^2 - m_u^2)(m_c^2 - m_u^2)(m_b^2 - m_s^2)}{M_W^6} \sim 10^{-35}\, cm\,. \quad (2.24)$$

where $\mathcal{J} = \mathrm{Im}(V_{us} V_{cb} V_{ub}^* V_{cs}^*) \sim 10^{-5}$ is the Jarlskog invariant which settles the strength of all SM CP violating processes. An equivalent computation for the up quark is subdominant. The external factor of m_d reflects the helicity-flip nature of the dipole moment operator and one can deduce the dependence of the amplitude on the internal fermion masses from the fact that GIM cancellation must be present. [3] When one considers graphs with exchanges among different valence quarks (eg. Ref. [115]), a similar prediction is obtained. However, a possible large contribution may come from those involving Penguin diagrams as the one in Fig. 2.2d; the GIM suppression being only logarithmic, they lead to a d_n as large as $10^{-30}\, e \cdot cm$ [116]. In any case, the known electroweak CPV of the SM contributes to the neutron EDM well below the already extraordinary stringent limit of less than $\mathcal{O}(10^{-26}\, e \cdot cm)$ (see Eq. (2.23)).

In contrast, CP violation in BSM proposals is typically considerably larger, arising often at one loop. Theories with extra scalars such as supersymmetry or two-Higgs doublet models may have generic complex couplings $\sigma(x)\bar{\psi}(c_v + c_a i\gamma_5)\psi$ which can contribute to neutron EDM via a one loop scalar interaction, as the total amplitude is then proportional to $\mathrm{Im}(c_v c_a^*)$. For instance, in the minimal supersymmetric extension of the SM (MSSM), there are many new sources of CP violation that can result in larger contributions to the EDM of the neutron, for example via a gluino loop. Taking the CP phases with a natural size of $\mathcal{O}(1)$, and the supersymmetry mass spectra at the TeV range, the theoretical prediction on the neutron EDM at one-loop level already exceeds the present experimental upper bound, easily resulting $\sim 10^{-22} - 10^{-24}\, e \cdot cm$ [117–119]. In order to make the theoretical prediction consistent with

3 Flavour changing processes in the SM are suppressed by ratios of the quark mass differences with respect to the W mass due to the unitarity of the quark mixing matrix. Technically this comes about in an $i \to j$ flavour-changing process when when adding the result of the loop integral $f(m_k^2/m_W^2) \times V_{kj} V_{ki}^*$ over all internal flavours k of quarks. Because of the unitarity of the CKM mixing matrix ($VV^\dagger = \mathbb{1} \Rightarrow V_{uj} V_{ui}^* + V_{cj} V_{ci}^* + V_{tj} V_{ti}^* = 0$) the result is proportional to either the internal quark mass square differences,

$$\mathcal{A} \sim V_{uj} V_{ui}^* \frac{m_t^2 - m_u^2}{m_W^2} + V_{cj} V_{ci}^* \frac{m_t^2 - m_u^2}{m_W^2}\,, \quad (2.25)$$

in which case there the process is said to be quadratically GIM supressed, or to the logarithm of the internal mass ratios,

$$\mathcal{A} \sim V_{uj} V_{ui}^* \log[m_u^2/m_t^2] + V_{cj} V_{ci}^* \log[m_c^2/m_t^2]\,, \quad (2.26)$$

in which case there is said to be logarithmic GIM supression. This was shown by Glashow, Iliopoulos and Maiani in Ref. [45] and is referred to as the GIM mechanism.

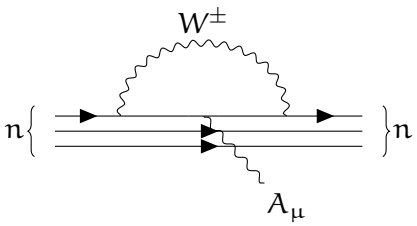

(a) Pure electroweak diagram at one loop.

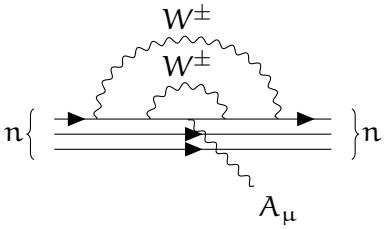

(b) Pure electroweak diagram at two loops.

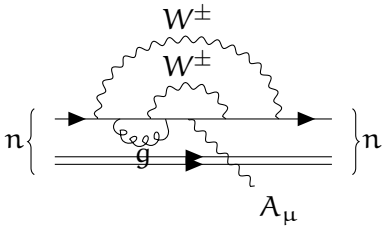

(c) Diagram with an additional gluon.

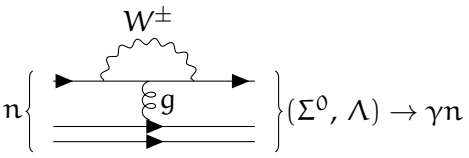

(d) Penguin diagram.

Figure 2.2: Standard Model contributions to the electric dipole moment of the neutron. Figs **(a)**, **(b)** and **(c)** correspond to processes in which only one quark is involved, while the diagram in Fig. **(d)** represents dominant processes which involve more than one quark.

the experimental data, three approaches are adopted in the literature. One possibility is to make the CP phases sufficiently small, i.e.$\leqslant 10^{-2}$. One can also assume a mass suppression by making the supersymmetry spectra heavy, i.e. in the several TeV range [119], or invoke a cancellation among the different contributions to the fermion EDMs [120], all of them not very satisfactory adjustments.

Whether we want to explain the strongly fine-tuned cancelation between the QCD vacuum phase and the phases in the quark masses, or we want to protect our theory from the large contributions to $\bar{\theta}$ that arise in many BSM solutions, a proposal is called for in order to constrain the strong CP phase to a safe level.

2.3 SOLUTIONS TO THE STRONG CP PROBLEM

The proposals to explain the strong CP problem can be classified in three types.

2.3.1 *Massless quark solutions*

One option is to consider that it was never there in the first place, *i.e.* that the SM Lagrangian *did* possess the chiral symmetry in Eq. (2.8) at the classical level, which would render the θ parameter unphysical. If there existed a massless quark, a chiral rotation would allow to reabsorb $\bar{\theta}$, as explained in Sect. 2.1. Different proposals have considered the possibility that the lightest quark (i.e. the up quark) could be massless, arguing that the meson masses could be attributed to second order effects of chiral symmetry breaking in QCD [121]. This

possibility is now ruled, see Fig. 2.3, the chiral behaviour of QCD having been confirmed by lattice computations [122].

Other interesting solutions (eg. in Refs.. [123] and [124]) can be implemented by adding exotic colored quarks to the SM spectrum. For instance, in the first one [123] K. Choi and E. Kim consider the inclusion of two exotic quarks and propose to enlarge the gauge symmetry of the SM with another confining group $SU(\tilde{N})$ with a scale larger than that of $SU(3)_C$ QCD, $\tilde{\Lambda} \gg \Lambda_{QCD}$. One new exotic massless quark Q, singlet of $SU(2)_L \times U(1)$, feels both $SU(3)_c$ and $SU(\tilde{N})$ and solves the strong CP problem of the SM. An issue arises because by considering a second confining group there are now two potentially harmful vacuum angles to absorb: θ of QCD and $\tilde{\theta}$, as they (or their combinations) would lead to undetected phenomenological consequences (i.e. the customary contributions to the neutron electric dipole moment). Only one combination can be redefined away, while the other combination would remain physical. This is easily remedied by adding a second exotic quark χ charged only under $SU(\tilde{N})$. The exotic quark content of the Choi-Kim model is then:

	$SU(3)_c$	$SU(\tilde{N})$	$SU(2)_L$
$Q_{L,R}$	$\square$	$\square$	1
$\chi_{L,R}$	1	$\square$	1

If the QCD coupling constant was switched off, the $SU(\tilde{N})$ theory would have a global $SU(4)_L \times SU(4)_R \times U(1)_L \times U(1)_R$ symmetry at the Lagrangian level. Upon chiral symmetry breaking by the $SU(\tilde{N})$ condensates, $15 + 1$ bosons would be expected: in particular one equivalent to the η' from QCD gets a mass of the scale of $\tilde{\Lambda}$, and the breaking of $SU(4)_L \times SU(4)_R \to SU(4)_V$ brings about 15 pseudo-Goldstone bosons. Turning on color interactions shows that those in non-trivial color representations get a mass of scale $\sqrt{\alpha_s}\tilde{\Lambda}$ from loops of gluons. One meson remains which is a complete singlet of $SU(3)_C$ and $SU(\tilde{N})$, and who is called the *composite axion*, since it plays a role similar to the invisible axion we will see further below, as it couples to the anomalous QCD current, and has largely suppressed couplings to the visible world proportional to $1/\tilde{f}$.

2.3.2 *Spontaneous CP breaking*

In the SM CP symmetry is *explicitly* broken by the Yukawa couplings, and CPV shows in the CKM formalism, with which experimental data is in excellent agreement. In contrast, another set of solutions to the strong CP problem are based on considering the possibility that CP is an exact symmetry of the Lagrangian at some energy, and rather *spontaneously* broken. For instance, the quark mass matrix could be real at tree-level and the CP phases might come from the complex vevs of extra Higgs scalars: this is the basis of the Nelson-Barr mechanism [125, 126] (see Ref. [127] for a review). Amongst the difficulties of these models, loop contributions to $\bar{\theta}$ have to be controlled, which requires sophisticated matter content. Also, as any discrete symmetry, these theories run into the domain wall problem, by which the energy associated to the walls between domains of different CP phases may easily exceed the closure density of the universe, unless further assumptions regarding inflation are made.

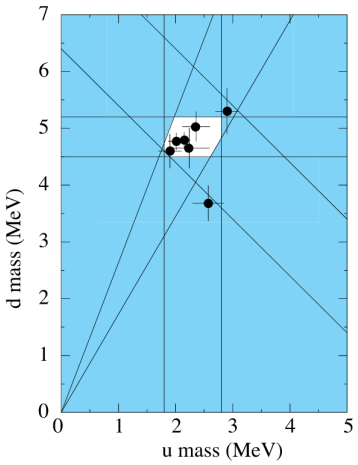

Figure 2.3: The allowed $m_u - m_d$ region [122]. Two downward sloping lines are from the bound on $(m_u + m_d)/2$ and two rising lines are from the bound on m_u/m_d, which are determined by the masses of the meson octet. Two vertical and horizontal boundaries are from the Particle Data Book bounds on $m_u = [1.5, 3.3]$ MeV and $m_d = [3.5, 6.0]$ MeV [33].

2.3.3 *The Peccei-Quinn mechanism*

The idea behind the proposal of Roberto Peccei and Helen Quinn in 1977 [7] to solve the strong CP problem is to restore a $U(1)_A$ symmetry which is to be:

- *exact* at the classical level;
- only broken *explicitly* by anomalies;
- *spontaneously* broken at a scale f_a.

The goal is that the transformation which meets these requirements will allow again to perform a rotation with

$$\partial_\mu j^\mu = \frac{\alpha_s}{4\pi} G^a_{\mu\nu} \tilde{G}^{a\mu\nu}, \tag{2.27}$$

thus rendering the $\bar{\theta}$ parameter unphysical.

In the SM the strong CP problem arose with the quark masses, *i.e.* with the Yukawa interactions, since the measured non-zero values for the SM quark masses broke the initial $U(1)_A$ symmetry classically, see Eq. (2.12). The original Peccei-Quinn (PQ) proposal modifies precisely the Yukawa interactions to make them invariant under an extra global chiral $U(1)_{PQ}$, which must also be anomalous in order to communicate with the $G \cdot \tilde{G}$ term. We remind here the Yukawa Lagrangian of the SM, responsible for the quark masses

$$\mathcal{L}_{Yuk} \supset -Y_d \bar{q}_L \Phi d_R - Y_u \bar{q}_L \tilde{\Phi} u_R + \text{h.c.}. \tag{2.28}$$

A first attempt to make the Lagrangian in Eq. (2.28) PQ invariant would set the PQ charge of u_R, Γ_{uR} different from that of d_R, Γ_{dR}. [4] However, the fact that the Yukawa interactions

4 A chiral transformation means that it has to be different for the LH and RH components, as it can then be decomposed to a vectorial plus a pure axial. As a consequence one can think about implementing PQ symmetry by just charging the scalar Higgs and the RH components of the quarks, setting the PQ charge of q_L to zero.

are mediated by Φ and $\tilde{\Phi} = i\sigma_2\Phi^*$ means that PQ invariance forces the relation $\Gamma_{uR} = -\Gamma_{dR}$. A Lagrangian with such charges is PQ symmetric, but it is not anomalous: when computing the Adler-Bell-Jackiw anomaly [98–100], the factor in front of the current in Eq. (2.27) is proportional to $\Gamma_{dR} + \Gamma_{uR}$, which cancels exactly in this setup. The simplest way to obtain an anomalous current with an exactly symmetric Lagrangian is to have two Higgs doublets, one for each of the two terms in Eq. (2.28): this is precisely the solution proposed by Peccei and Quinn, which we will present in detail in Sect. 3.1.1.

This and other PQ-type solutions to the strong CP problem all share a common feature which is the appearance of a Goldstone boson excitation, associated to the spontaneous breaking of the chiral PQ symmetry, the axion, as first noted by Weinberg and Wilczek [128, 129]. However, since the chiral symmetry is also explicitly broken by the color anomaly in Eq. (2.27), the axion is not completely massless and is rather a pseudo-GB. The axion couples to $G \cdot \tilde{G}$ and the instantons induce a potencial, and thus a mass for the axion.

Although the original solution by Peccei and Quinn is now ruled out, a plethora of axion models exist that still avoid present bounds from axion searches. Invisible axion models (amongst which the original proposals are those in Refs. [9, 10, 130, 131]) decouple the PQ-breaking scale from the EW scale –since in the original PQ proposal they were the same scale– and for this reason was excluded phenomenologically. Also, novel approaches in axion models avoid present phenomenological constraints by predicting "heavy axions" [132–137], which for instance get their mass from new gauge groups that confine at a much higher scale than QCD. The axion solution still stands as of today, and there is a broad experimental program searching for these elusive particles. In the next chapter we present the theoretical setup in detail and the experimental status of the Peccei-Quinn solution to the strong CP problem.

3 AXIONS AND AXION-LIKE PARTICLES

3.1 THE PQ SOLUTION: VISIBLE AND INVISIBLE AXIONS

▷ *Axion low-energy Lagrangian*

There exist many ways to implement the global $U(1)_{PQ}$ symmetry required in the PQ solution to the strong CP problem [7], and we will review in this section three paradigmatic solutions. However, they all share as a common feature the prediction of a pseudo-GB associated to the breaking of such symmetry: the axion [128, 129]. The transformation of the axion under $U(1)_{PQ}$ is simply to shift, as a consequence of its GB nature:

$$U(1)_{PQ} \; : \quad a(x) \to a(x) + C \quad \text{with} \quad C = \beta f_a \tag{3.1}$$

where β is the parameter of the $U(1)_{PQ}$ rotation and f_a is the PQ breaking scale (or axion scale).

Axion interactions to the SM fields are encoded in an effective Lagrangian (defined at energies well below f_a where all other d.o.f. in the different axion models are integrated out) which involves only derivative couplings of the axion,

$$\mathcal{L}_a^{eff} = \mathcal{L}_{SM} + \left(\bar{\theta} + \frac{a}{f_a}\right) \frac{\alpha_s}{8\pi} G^a_{\mu\nu} \tilde{G}^{a\mu\nu} + \frac{1}{2}\partial_\mu a \partial^\mu a + \frac{E}{N}\frac{a}{f_a}\frac{\alpha_s}{8\pi} F_{\mu\nu}\tilde{F}^{\mu\nu} + \mathcal{L}_{a\psi\psi}\,. \tag{3.2}$$

By a redefinition of the axion field, $a(x) + \bar{\theta} \to a(x)$ one can eliminate $\bar{\theta}$ without affecting the rest of the axion interactions, since they are all derivative, see Eq. (3.1). [1] The Lagrangian encoding axion-fermion interactions, $\mathcal{L}_{a\psi\psi}$ and the factors in front of $aG\cdot\tilde{G}$ and $aF\cdot\tilde{F}$ are model-dependent quantities. In particular, N and E result from the computation of the colour and electromagnetic anomaly factors [98–100] and they depend on the PQ-charged fermions in the theory.:

$$N = 2\sum_\psi (\Gamma_{\psi L} - \Gamma_{\psi R}) T(\mathcal{C}_\psi) \quad \text{and} \quad E = 2\sum_\psi (\Gamma_{\psi L} - \Gamma_{\psi R}) \mathcal{Q}_\psi^2\,. \tag{3.3}$$

They are a sum over all fermions in non-trivial color and electromagnetic representations, $\mathcal{C}_\psi$ and $\mathcal{Q}_\psi$ respectively. $\Gamma_{\psi(L/R)}$ are the PQ charges of the left and right components, the color index is defined by $\mathrm{Tr} T^a_\psi T^b_\psi = T(\mathcal{C}_\psi)\delta^{ab}$, with T_ψ the generators associated to the color representation. [2]

1 An alternative definition of f_a is sometimes used in which the anomalous coupling to gluons is proportional to $\frac{N}{f_a}$ instead of $\frac{1}{f_a}$ (see for instance Refs. [138, 139]). As a result, the mass and axion coupling to photons become proportional to N, as $(f_a)^{\text{this work}} \to (f_a)^{\text{other works}}/N$.

2 The notation that will be used in Chapter 5, inherited from Ref. [140] defines the electromagnetic and colour anomaly factors, E and N resepectively as one half of those in Eq. (3.3). However, we choose here this notation as it is more widespread (see eg. Ref. [141]).

▷ *Axion mass*

Another general characteristic of QCD axion is that its mass and axion scale f_a are related among eachother. In particular, it is through the anomalous interactions of axions with gluons in the $a\,G\tilde{G}$ coupling term that instantons give a potential to the axion. This behaviour of instantons has already appeared in Sect. 2.1 where the high mass of the η' meson with respect pseudoscalar mesons of QCD –of pseudoGoldstone boson nature– is explained on account of an analogous anomalous coupling of the η' to instantons, solving the $U(1)_A$ problem.

The axion is thus considered together with the pseudoscalar mesons of QCD [16, 142]. This can be done for instance using an extension of chiral perturbation theory (χPT) for the latter which includes the ninth pseudoscalar meson, π_9, which is dominantly the η' in QCD in the absence of axions. Its mixing with the axion becomes particularly relevant in determining the axion mass [142]:

$$\begin{aligned}\mathcal{L}_{\rm eff}^{a+\chi PT} \supset \left(\frac{a}{f_a}+\frac{\sqrt{6}\pi_9}{f_9}\right)\frac{\alpha_s}{8\pi}G_{\mu\nu}\tilde{G}^{\mu\nu} \\ \longrightarrow \quad V(a,\pi_9) = -\Lambda_{QCD}^4\cos\left(\frac{a}{f_a}+\frac{\sqrt{6}\pi_9}{f_9}\right).\end{aligned} \tag{3.4}$$

where $f_9 \sim f_\pi$ is the GB scale associated to the QCD mesons. The meson π_9 has yet another contribution to its mass that comes from the non-zero quark masses which is subdominant with respect to Λ_{QCD} but will translate into a small mass for the axion. Indeed, once the masses of the pseudoscalars are diagonalised, the axion mass and PQ breaking scale are found to be related by [16, 128, 142]

$$m_a f_a = m_\pi f_\pi \sqrt{\frac{m_u m_d}{(m_u+m_d)^2}} = m_\pi f_\pi \frac{\sqrt{z}}{(1+z)^2}\,, \tag{3.5}$$

with $z = m_u/m_d \simeq 0.56$, and where we have neglected contributions from the heavier quarks which enter as $m_u/m_s \simeq 0.029$. A precise calculation combining next-to-leading order results in chiral perturbation theory with recent Lattice QCD results yields numerically [141],

$$m_a = 5.70(7)\ \mu\text{eV}\left(\frac{10^{12}\,\text{GeV}}{f_a}\right), \tag{3.6}$$

where the error comes from the up-down quark mass ratio and from the uncertainties in meson couplings from chiral perturbation theory. This relation between the axion mass and scale is going to be present in all PQ-type solutions, and is going to determine strongly the phenomenological behaviour of QCD axions.

In fact, the axion mass receives a more general expression when the mixing of the π_9 meson with the others mesons is not neglected [142]. While the mass in Eq. (3.5) is a good approximation for the QCD case, the inclusion of these interactions [142] yields a result which has proved relevant for the study of more general axion models where the axions get a mass from other confining gauge groups:

$$m_a^2 f_a^2 = K\frac{1}{1+\frac{K}{2v^3}\text{Tr}(M^{-1})}\,, \tag{3.7}$$

M being the quark mass matrix, $v^3 \simeq m_\pi^2 f_\pi^2/2(m_u + m_d)$ and where $K \approx \Lambda_{QCD}^4$.

Two limiting cases are illuminating. The first corresponds to the QCD case where there exists *some* quark with $m_q \ll \Lambda_{QCD}$ so that the instanton effects decouple, and one recovers the well-known result for the axion mass [16, 128] in Eq. (3.5). A second limit will be used in solutions to the strong CP problem which invoke alternative confining gauge groups in which *all* the exotic quarks composing the new mesons have masses well above a new confinement scale, Λ' (see in Ref. [134] as an example). In these scenarios, the second term in the denominator of Eq. (3.7) is subdominant and the axion mass and PQ breaking scale are instead related by

$$m_a^2 f_a^2 \sim \Lambda'^4 \,. \tag{3.8}$$

▷ *Axion-photon coupling*

Finally, axion phenomenology is also going to be largely driven by axion coupling to photons. The general expression for the axion-photon coupling is [138],

$$\mathcal{L}_{a\gamma\gamma} = -\frac{1}{4} g_{a\gamma\gamma}\, a F_{\mu\nu} \tilde{F}^{\mu\nu} \tag{3.9}$$

with

$$\begin{aligned} g_{a\gamma\gamma} &= \frac{\alpha_{em}}{2\pi f_a} \left[\frac{E}{N} - \frac{2}{3}\frac{4m_d + m_u}{m_d + m_u}\right] \\ &= \frac{2.0}{10^{10}\,\text{GeV}} \frac{m_a}{\text{eV}} \left[\frac{E}{N} - 1.92(4)\right] . \end{aligned} \tag{3.10}$$

The first term inside the square brackets comes directly from the axion coupling to photons $aF \cdot \tilde{F}$ in Eq. (3.2), again redefining the axion scale to absorb N from the $aG \cdot \tilde{G}$ term. The second term is less straightforward but can be understood as coming from the diagonalisation of the pseudoscalar mass matrix, which brings about $a - \pi^0$ mixing and couples the axion to $F \cdot \tilde{F}$ through the $\pi^0 F \cdot \tilde{F}$ vertex. The numerical replacements leading to the last line are taken from the recent results by Villadoro et al. in Ref. [141]. A large part of axion searches rely precisely on the axion-photon coupling, and it is common to plot the results in the $(m_a, g_{a\gamma\gamma})$ parameter space. As we review the different models below we will give the values of E/N that determine the prediction for each model in the form of a line for each value.

We move on to reviewing the theoretical construction of the paradigmatic axion models and to studying the general dynamics of axions together with their phenomenology.

3.1.1 *The Peccei-Quinn-Weinberg-Wilczek axion*

The Peccei-Quinn-Weinberg-Wilczek (PQWW) axion is defined as embedded in the phase of the Higgs field in the SM gauge theory. With one only Higgs doublet it is not possible to make the theory classically invariant under an anomalous $U(1)_A$ symmetry (as discussed in Sect. 2.3.3): the simplest option is to add another Higgs, which allows the Lagrangian to

absorb independent chiral transformations of the u- and d- quarks (and leptons). Defining each Higgs doublet equivalently to the SM doublet in Eq. (1.22),

$$\Phi_i(x) = \frac{v_i + h_i(x)}{\sqrt{2}} e^{i\vec{\pi}_i(x)\vec{\sigma}/v_i} \begin{pmatrix} 0 \\ 1 \end{pmatrix} \qquad i = u,\, d\,, \tag{3.11}$$

σ_i being the Pauli matrices, the Peccei-Quinn Lagrangian is

$$\mathcal{L}_{\text{Yuk}} \supset -Y_d \bar{q}_L \Phi_d d_R - Y_u \bar{q}_L \tilde{\Phi}_u u_R - Y_e \bar{L}_L \Phi_e e_R + \text{h.c.}\,. \tag{3.12}$$

where there is a choice in whether $\Phi_e = \Phi_d$ or $\Phi_e = \Phi_u$. We will call them PQ-I and PQ-II respectively. The PQ transformation is

$$U(1)_{PQ} \begin{cases} \Phi_u & \to & e^{-i\Gamma_u \beta} \Phi_u \\ \Phi_d & \to & e^{i\Gamma_d \beta} \Phi_d \\ u_R & \to & e^{-i\Gamma_u \beta} u_R \\ d_R & \to & e^{-i\Gamma_d \beta} d_R \\ e_R & \to & e^{-i\Gamma_e \beta} e_R \end{cases} \tag{3.13}$$

with the charges determined to that the axion does not couple to $U(1)_Y$,

$$\Gamma_u = x\,, \quad \Gamma_d = 1/x\,, \quad \Gamma_e = \begin{cases} \frac{1}{x} \text{ in PQ-I} \\ x \text{ in PQ-II} \end{cases} \qquad \text{with} \quad x = \frac{v_d}{v_u}\,. \tag{3.14}$$

The physical axion is a linear combination of $\pi_u^3(x)$ and $\pi_d^3(x)$ which is found as the GB of $U(1)_{PQ}$, *i.e.* it is the field that absorbs the complete phase transformation (see Eq. (3.1)), the orthogonal pseudoscalar being the longitudinal component of the Z boson. This is obtained through a rotation of angle $\arctan(-x)$ on the pseudoscalar sector $(\varphi_u, \varphi_d) \equiv (\pi_u^3, \pi_d^3)$:

$$\begin{pmatrix} a_{PQ} \\ \varphi_Z \end{pmatrix} = \frac{1}{v_{EW}} \begin{pmatrix} v_d & -v_u \\ v_u & v_d \end{pmatrix} \begin{pmatrix} \varphi_u \\ \varphi_d \end{pmatrix}\,. \tag{3.15}$$

where the scale in the denominator above is

$$v_{EW} = \sqrt{v_u^2 + v_d^2} \approx 246\,\text{GeV}\,. \tag{3.16}$$

We will not specify the sub-index PQ on a_{PQ} in the remaining equations in this section for clearness in notation, but it should be kept in mind that it is a model-dependent definition and will be redefined in the different models below.

The PQWW axion mass satisfies the general relation in Eq. (3.5)

$$m_a = 3\left(x+\frac{1}{x}\right)\frac{1}{v_{EW}}\frac{\sqrt{z}}{1+z} \simeq \left(x+\frac{1}{x}\right)\times 75\,\text{keV} > 150\,\text{keV} \tag{3.17}$$

since $x+1/x>2$ for $x>0$. Observe that the general scale is set by the EW scale.

The axion coupling to photons follows from Eq. (3.10) [7]:

$$\mathcal{L}_{a\gamma\gamma} = \frac{\alpha_{ew}}{8\pi}\left[\frac{E}{N}-1.92(4)\right]N\frac{a}{v_{EW}}F_{\mu\nu}\tilde{F}^{\mu\nu} \tag{3.18}$$

$$\tag{3.19}$$

where

$$N = 3\left(x+\frac{1}{x}\right) \tag{3.20}$$

and

$$\text{PQ-I:}\quad \Phi_e = \Phi_d\,,\qquad E=\tfrac{8}{3}3\,(x+1/x)\quad\Rightarrow E/N=8/3 \tag{3.21}$$

$$\text{PQ-II:}\quad \Phi_e = \tilde{\Phi}_u\,,\qquad E=\tfrac{2}{3}3\,(x+1/x)\quad\Rightarrow E/N=2/3\,. \tag{3.22}$$

The 3 in the numerators of the last two equations comes from the contributions of the three generations of quarks in the SM. As a result, the axion coupling to photons cannot be arbitrarily supressed:

$$g_{a\gamma\gamma} > \frac{1.4\times10^{-5}}{\text{GeV}}\left[\frac{E}{N}-1.92(4)\right]. \tag{3.23}$$

However, it is rather through the axion coupling to fermions that the PQWW axion was searched for. These couplings are obtained straightforwardly from Eq. (3.12) by inverting the definition in Eq. (3.15). The result is (for instance, for PQ-I: $\Phi_e=\Phi_d$),

$$\mathcal{L}_{\text{Yuk}} = -Y_d\bar{d}_L e^{ia/xv_{EW}}d_R - Y_u\bar{u}_L e^{iax/v_{EW}}u_R - Y_e\bar{e}_L e^{ia/xv_{EW}}e_R + \text{h.c.} \tag{3.24}$$

$$= \frac{\partial_\mu a}{v_{EW}}\left[x\,\bar{u}_L\gamma^\mu u_R + \frac{1}{x}\,\bar{d}_L\gamma^\mu d_R + \frac{1}{x}\,\bar{e}_L\gamma^\mu e_R\right] + \text{h.c.} + \mathcal{O}(a^2/f_a^2)\,, \tag{3.25}$$

The second line in Eq. (3.24), obtained expanding to first order in the axion field and applying the fermion equations of motion, shows explicitly the derivative nature of axion interactions. The result for the PQ-II setup is obtained by the simple replacement $1/x\to x$ in the electron coupling.

A multitude of experiments ruled out both the long-lived ($m_a<2m_e$) and the short-lived ($m_a>2m_e$) axions. For instance, amongst the long-lived axions, one of the very relevant measurements was that of $K^+\to\pi^++\text{nothing}$, which was constrained by KEK to $\text{Br}(K^+\to\pi^++\text{nothing})<3.8\times10^{-8}$ [143]. One computation of this observable by Peccei, Bardeen and Yanagida using an effective Lagrangian [144], yields $\text{Br}_{K\to\pi a}\simeq 3\times10^{-5}(x+1/x)^2>1.2\times10^{-4}$, which is in contradiction with the experimental constraint. Another computation through penguin diagrams yields $\text{Br}^{\text{peng.}}_{K\to\pi a}\sim 10^{-5}x^2$ [145], which requires small x. This is in contradiction with results from $\Upsilon\to a\gamma$ and $J/\psi\to a\gamma$ which conversely require large values of x. These and other bounds ended up ruling out both the long-lived and short-lived PQWW axion (see Ref. [146] for a detailed discussion).

A way to save the Peccei-Quinn idea is to introduce a new scalar S which

- is a $SU(3)_C \times SU(2)_L \times U(1)_Y$ singlet,
- carries a PQ charge and possess a large vev $\langle S \rangle = v_S/\sqrt{2}$.

The axion scale f_a will be driven by v_S, which is decoupled from the EW scale. These models allow $f_a \gg v_{EW}$ in order to avoid existing experimental constraints, since the axion couplings to known particles scale as $1/f_a$, see for instance Eq. (3.24), and they receive the name of invisible axion models. The scalar singlet gets a vev from the scalar potential, and it can be written in radial coordinates as:

$$S(x) = \frac{v_S + \rho_S(x)}{\sqrt{2}} e^{i\varphi_S/v_S} \,. \tag{3.26}$$

One of the two paradigmatic models is simply an extension of the PQWW axion with this extra scalar field. It was proposed by Dine, Fischler, Sredniki [130] and Zhitnitsky [131], and it is referred to as the DFSZ axion model. The second paradigmatic model incorporates the field S and a new heavy coloured quark. It was proposed at a similar time by Kim [9], Shifman, Vainshtein and Zakharov [10] and is referred to as the KSVZ axion.

3.1.2 *DFSZ axion*

The model proposed by Dine, Fischler, Sredniki and Zhitnitsky [130, 131] is identical to the one presented in Sect. 3.1.1, except for the fact that it is supplemented with an additional scalar field, S in Eq. (3.26), singlet under the SM group but charged under the PQ symmetry, that develops an arbitrarily large vev. This way the breaking of the PQ symmetry is decoupled from the EW scale and can occur at much higher energies. The Yukawa Lagrangian of the model is the same as in Eq. (3.12) and the PQ charges of the model are again those of Eqs. (3.13) and (3.14) with the singlet transforming as

$$U(1)_{PQ} \;:\quad S \to e^{i\beta\Gamma_S} S \,, \tag{3.27}$$

where Γ_S is a free parameter, commonly chosen to be $\Gamma_S = 1$. The relevant potential for S is

$$V_S = -\mu_S^2|S|^2 + \lambda_S|S|^4 + \lambda_{\Phi S}^d|\Phi_d|^2|S|^2 + \lambda_{\Phi S}^u|\Phi_u|^2|S|^2 + \lambda_{udS}\Phi_d^\dagger\Phi_u S^2 \,, \tag{3.28}$$

the last term proportional to λ_{udS} being the one that fixes the relationship between the scalar PQ charges:

$$2\Gamma_S - \Gamma_u - \Gamma_d = 0 \,. \tag{3.29}$$

The potential V_S, together with additional terms involving the two Higgs doublets (which we do not make explicit here but can be found for instance in Ref. [130]), also gives a vev to both the Higgs doublets and the scalar S:

$$\langle \Phi_i \rangle = \frac{v_i}{\sqrt{2}} \quad (i = u,\, d) \qquad \text{and} \quad \langle S \rangle = \frac{v_S}{\sqrt{2}} \,, \tag{3.30}$$

breaking PQ symmetry spontaneously. Again, the GB associated to such breaking is the axion, which will now be a linear combination of the three neutral pseudoscalars φ_u, φ_d, φ_S. It is the component which absorbs the Peccei-Quinn transformation as in Eq. (3.1). It is found to

be [139] $a_{DFSZ} = (\Gamma_u v_u \varphi_u - \Gamma_d v_d \varphi_d + \Gamma_S v_S \varphi_S)/f_a$ and $f_a = \sum_{u,d,S} \Gamma_i^2 v_i^2$. Replacing the PQ charges with the relations derived from Eq. (3.14) and Eq. (3.29) wirth $\Gamma_S = 1$ one finds

$$a_{DFSZ} = \frac{v_d \varphi_u - v_u \varphi_d + v_S \varphi_S}{\sqrt{v_S^2 + v^2}} \xrightarrow[v_S \gg v]{} \varphi_S \tag{3.31}$$

$$v_{DFSZ} = \sqrt{v_S^2 + v^2} \xrightarrow{v_S \gg v} v_S \tag{3.32}$$

where $v = v_{EW}$. And where in order to use the definitions of m_a and $g_{a\gamma\gamma}$ from Eqs. (3.5) and (3.10) respectively we define

$$f_a^{DFSZ} = \frac{v_{DFSZ}}{N} \tag{3.33}$$

with

$$N = 3(\Gamma_u + \Gamma_d) = 6 \tag{3.34}$$

the last term applying for the choice $\Gamma_S = (\Gamma_u + \Gamma_d)/2 = 1$.

By expressing the Higgs doublets Φ_i as a function now of $a_{DFSZ} = a$ one obtains the DFSZ axion coupling to fermions:

$$\mathcal{L}_{Yuk} = -Y_d \bar{d}_L e^{ia/x v_{DFSZ}} d_R - Y_u \bar{u}_L e^{iax/v_{DFSZ}} u_R - Y_e \bar{e}_L e^{ia/x v_{DFSZ}} e_R + h.c. \tag{3.35}$$

$$= \frac{\partial_\mu a}{v_{DFSZ}} \left[x\, \bar{u}_L \gamma^\mu u_R + \frac{1}{x} \bar{d}_L \gamma^\mu d_R + \frac{1}{x} \bar{e}_L \gamma^\mu e_R \right] + h.c. + \mathcal{O}(a^2/f_a^2)\,. \tag{3.36}$$

This shows the important feature of DFSZ axions, namely that their couplings now scale with $1/v_{DFSZ} \sim 1/f_a$ instead of $1/v_{EW}$. DFSZ axions can avoid the bounds that excluded the PQWW: their couplings to fermions can be arbitrarily suppressed because we have introduced a new scale independent scale v_S which drives f_a.

The couplings to photons depends on which Higgs doublet is in the lepton Yukawa interaction: $\bar{L}_L \Phi_e e_R$ as this determines E/N in Eq. (3.10).

$$\text{DFSZ-I:} \quad \Phi_e = \Phi_d\,, \quad E = \tfrac{8}{3} N_f (\Gamma_u + \Gamma_d) \quad \Rightarrow E/N = 8/3 \tag{3.37}$$

$$\text{DFSZ-II:} \quad \Phi_e = \tilde{\Phi}_u\,, \quad E = \tfrac{2}{3} N_f (\Gamma_u + \Gamma_d) \quad \Rightarrow E/N = 2/3\,, \tag{3.38}$$

which results in

$$\mathcal{L}_{a\gamma\gamma} = \frac{\alpha_{ew}}{8\pi} \left[\frac{E}{N} - 1.92(4) \right] \frac{a}{f_a} F_{\mu\nu} \tilde{F}^{\mu\nu}\,. \tag{3.39}$$

Numerically, one obtains

$$g_{a\gamma\gamma} = \frac{5.8 \times 10^{-13}}{GeV} \left(\frac{10^9\,GeV}{f_a} \right) \left[\frac{E}{N} - 1.92(4) \right] \tag{3.40}$$

which can be compared with the PQWW prediction in Eq. (3.23) to see that there is no lower limit to the axion-photon coupling, as it can now be arbitrarily supressed with f_a. The DFSZ axion mass is also decoupled from the EW scale. According to Eq. (3.5)

$$m_a = 6\,meV \left(\frac{10^9\,GeV}{f_a} \right)\,. \tag{3.41}$$

The coupling $g_{a\gamma\gamma} \sim 1/f_a \sim m_a$ in Eq. (3.40) scales with m_a according to Eq. (3.10) and the predictions in $(m_a,\, g_{a\gamma\gamma})$ parameter space are shown in Fig. 3.1 by red lines labeled I and II for DFSZ models I and II respectively.

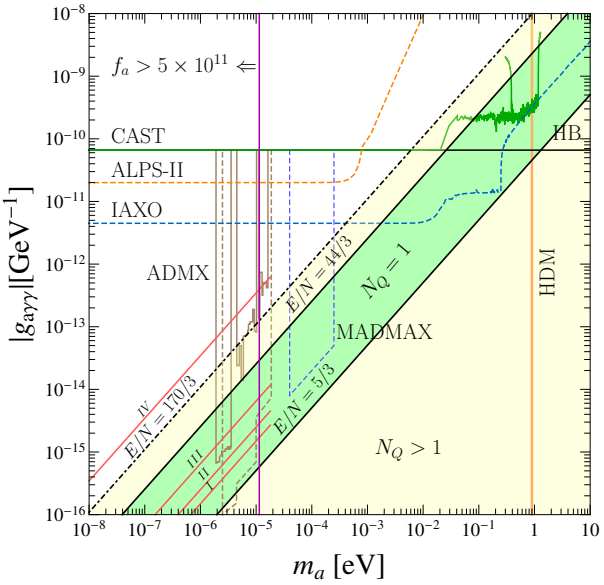

Figure 3.1: The $g_{a\gamma\gamma}$-m_a window for preferred axion models. The two lines labeled $E/N = 44/3$ and $5/3$ encompass KSVZ models with a single exotic fermion representation, while the region below $E/N = 170/3$ corresponds to allowing more than one representation. The red lines labeled from I to IV (only partially drawn so as not to clutter the figure) indicate where the DFSZ-type of models lie. Current exclusion regions are delimited by solid lines. They correspond to the 2017 CAST results [147], to the ADMX limit [148–152], to the constraints from hot DM (HDM) [153] and from horizontal branch (HB) stars [154]. The expected sensitivities for ALPS-II [155], IAXO [149, 156], ADMX [157] and MADMAX [158] are depicted with dashed lines. On the left hand side of the vertical violet line labeled $f_a > 5 \times 10^{11}$ GeV the band for KSVZ may be larger as some of the conditions are relaxed allowing more models (see footnote 3). Figure and description adapted from Ref. [140].

3.1.3 *KSVZ axion*

An alternative proposal [9, 10] also includes the scalar $S(x)$ in Eq. (3.26) in addition to new coloured quarks that transform under $U(1)_{PQ}$, while the SM fields are not PQ-charged. These are called KSVZ –or *hadronic*– axion models. The quarks Ψ are vectorial under the SM gauge group, and they obtain their mass through a Yukawa interaction with the singlet scalar S. In the original proposal a $\mathbb{Z}_2$ symmetry under which only S and Ψ_L transform was used to forbid linear S couplings to the SM fields and bare mass terms for the exotic fermions.

The renormalizable Lagrangian for the KSVZ axion model reads $\mathcal{L} = \mathcal{L}_{SM} + \mathcal{L}_{KSVZ}$ with

$$\mathcal{L}_{KSVZ} = \bar{\Psi} i \not{D} \Psi - (y_\Psi S \bar{\Psi}_L \Psi_R + \text{h.c.}) + V_S \tag{3.42}$$

$$V_S = -\mu_S^2 |S|^2 + \lambda_S |S|^4 + \lambda_{\Phi S} |\Phi|^2 |S|^2 \,. \tag{3.43}$$

It is simple to see that Eq. (3.42) is invariant under a $U(1)_A$ transformation

$$U(1)_{PQ} : \begin{cases} S & \to & e^{i\Gamma_S \beta} S \\ \Psi_L & \to & e^{i\Gamma_{\Psi_L} \beta} \Psi_L \\ \Psi_R & \to & e^{i\Gamma_{\Psi_R} \beta} \Psi_R \end{cases} \tag{3.44}$$

as long as Γ_S (which we will take to be $\Gamma_S = 1$), $\Gamma_{\Psi L}$ and $\Gamma_{\Psi R}$ are related by $\Gamma_S = \Gamma_{\Psi L} - \Gamma_{\Psi R}$. This is the desired $U(1)_{PQ}$ needed to solve the strong CP problem and the axion is now simply the phase of $S(x)$

$$a_{KSVZ} = \varphi_S \,, \tag{3.45}$$

The axion scale depends on the colour anomaly coefficient as in the previous models

$$f_a^{KSVZ} = \frac{v_S}{N} \,. \tag{3.46}$$

where $N = 1$ for the case that Ψ is a colour triplet, and can be computed from Eq. (3.3) for other colour representations. It no longer depends on the SM quarks since Ψ is the only fermion with PQ charge.

While the original KSVZ proposal only explored, for illustrative purposes, exotic fermions in the fundamental representation of $SU(3)_C$ and which were singlets of $SU(2)_L \times U(1)_Y$, many other options are viable. In fact, a recent study [140] considered hadronic axion models with the heavy quarks in arbitrary representations under the SM gauge group, $R_\Psi = (\mathcal{C}_\Psi, \mathcal{I}_\Psi, \mathcal{Y}_\Psi)$, finding a set of (fifteen) *phenomenologically preferred* axion models, in which *(i)* no Landau poles are induced below the Planck scale and *(ii)* the exotic quarks are sufficiently short lived to avoid issues with long lived strongly interacting relics. Indeed, the $SU(2) \times U(1)$ color-triplets in the original KSVZ proposal run into the problem of stability as they have no way of decaying fast enough. In general, cosmologically stable Ψs are constrained by the requirement that their present energy density does not exceed that of the DM, $\Omega_\Psi \leqslant \Omega_{DM} \sim 0.12\, h^{-2}$, h being the Hubble constant. On the other hand, if the exotic quarks are unstable and decay into SM particles, the lifetime τ_Ψ is severely constrained by cosmological observations and only lifetimes $\tau \lesssim 10^{-2}\,$s are safe with respect to cosmological issues. One option is that the exotic quarks decay to SM particles via renormalisable or effective couplings in the Lagrangian:

$$\mathcal{L}_a = \mathcal{L}_{KSVZ} + \mathcal{L}_{\Psi q} \,, \tag{3.47}$$

where $\mathcal{L}_{\Psi q}$ encodes renormalisable interactions of $\Psi_{L,R}$ to SM quarks, and there may additionally be higher order terms in an effective $\mathcal{L}_{\Psi q}^{d \geqslant 4}$. For instance $\overline{\Psi}_L \Phi^\dagger d_R$ can mediate in the decay of $R_\Psi = (3, 2, -\frac{5}{6})$. In Ref. [140] the authors find that phenomenologically preferred hadronic axions require $d \leqslant 4$ or $d = 5$ operators to mediate in the decay of the exotic quarks to the SM. This requirement can only be implemented with some particular representations and for some specific PQ charge assignments. The set of phenomenologically preferred axion models is shown in Tab. 3.1 together with the operators present in $\mathcal{L}_{\Psi q}$ for each case. [3]

The hadronic axion does not have tree-level couplings to fermions. It is searched for mainly through its coupling to photons, which is once again dependent on the PQ scale f_a, decoupled from v_{EW}.

$$\mathcal{L}_{a\gamma\gamma} = \frac{\alpha_{ew}}{8\pi}\left[\frac{E}{N} - 1.92(4)\right]\frac{a}{f_a} F_{\mu\nu}\tilde{F}^{\mu\nu} \,, \tag{3.48}$$

3 This set is computed under the assumption that PQ-breaking occurs after inflation, where the constraint that $\Omega_\Psi \leqslant \Omega_{DM} \sim 0.12\, h^{-2}$ implies $f_a \leqslant 5 \times 10^{11}$ GeV. To the right of the violet line in Fig. 3.1 the phenomenologically preferred criteria is well defined. In pre-inflationary scenarios this constraint can be relaxed, and heavier quarks are also allowed thus weakening the constraints from the Landau pole condition. Therefore for KSVZ models larger values of the axion-photon coupling become allowed within this region.

R_Ψ	$\mathcal{O}_{\Psi q}$	E/N
$R_1: (3,1,-\frac{1}{3})$	$\overline{\Psi}_L d_R$	2/3
$R_2: (3,1,+\frac{2}{3})$	$\overline{\Psi}_L u_R$	8/3
$R_3: (3,2,+\frac{1}{6})$	$\overline{\Psi}_R q_L$	5/3
$R_4: (3,2,-\frac{5}{6})$	$\overline{\Psi}_L d_R \Phi^\dagger$	17/3
$R_5: (3,2,+\frac{7}{6})$	$\overline{\Psi}_L u_R \Phi$	29/3
$R_6: (3,3,-\frac{1}{3})$	$\overline{\Psi}_R q_L \Phi^\dagger$	14/3
$R_7: (3,3,+\frac{2}{3})$	$\overline{\Psi}_R q_L \Phi$	20/3
$R_8: (3,3,-\frac{4}{3})$	$\overline{\Psi}_L d_R \Phi^{\dagger 2}$	44/3
$R_9: (\bar{6},1,-\frac{1}{3})$	$\overline{\Psi}_L \sigma d_R \cdot G$	4/15
$R_{10}: (\bar{6},1,+\frac{2}{3})$	$\overline{\Psi}_L \sigma u_R \cdot G$	16/15
$R_{11}: (\bar{6},2,+\frac{1}{6})$	$\overline{\Psi}_R \sigma q_L \cdot G$	2/3
$R_{12}: (8,1,-1)$	$\overline{\Psi}_L \sigma e_R \cdot G$	8/3
$R_{13}: (8,2,-\frac{1}{2})$	$\overline{\Psi}_R \sigma \ell_L \cdot G$	4/3
$R_{14}: (15,1,-\frac{1}{3})$	$\overline{\Psi}_L \sigma d_R \cdot G$	1/6
$R_{15}: (15,1,+\frac{2}{3})$	$\overline{\Psi}_L \sigma u_R \cdot G$	2/3

Table 3.1: R_Ψ allowing for $d \leqslant 4$ and $d = 5$ decay operators ($\sigma \cdot G \equiv \sigma_{\mu\nu} G^{\mu\nu}$) and yielding Landau poles above 10^{18}GeV. The third column lists the anomaly contribution to $g_{a\gamma\gamma}$. Results from Ref. [140].

which implies that numerically

$$g_{a\gamma\gamma} = \frac{5.8 \times 10^{-13}}{\text{GeV}} \left(\frac{10^9\,\text{GeV}}{f_a}\right) \left[\frac{E}{N} - 1.92(4)\right] . \tag{3.49}$$

For the original KSVZ model $E/N = 0$, since the exotic quark was electrically neutral. The values of E/N for the phenomenologically preferred axion models are shown in Tab. (3.1), and the prediction for these models in the $(m_a,\, g_{a\gamma\gamma})$ plane is represented by a green band in Fig. 3.1 labeled $N_Q = 1$. The authors of Ref. [140] also compute the predicted region in setups where more than one exotic fermion is included (labeled $N_Q > 1$) and find that for certain ad hoc choices of representations, $g_{a\gamma\gamma} \simeq 0$ within theoretical errors, this being the reason why the yellow-orange region in Fig 3.1 extends without limits to the bottom-right of the parameter space.

Invisible axion models face problems of fine-tuning due to the large hierarchy of scales involved. There may exist a problem with Planck scale effects breaking $U(1)_{PQ}$, for instance inducing PQ-breaking contributions to the potential. Amongst the proposals to solve this, some present PQ as an automatic or accidental symmetry [159], a consequence of some other (continuous or discrete) gauge symmetry which protects the potential at all scales. However another hierarchy exists between the electroweak scale and the axion scale and the axion scale, which is phenomenologically constrained to $10^9\,\text{GeV} \lesssim f_a \lesssim 10^{12}\,\text{GeV}$, requiring a tuning in the potential. In particular, the Higgs mass may receive contributions from PQ-scale physics, aggravating the EW hierarchy problem which was discussed in Sect. 1.2. One solution, which is proposed and explored in Chapter 5, is to implement PQ in scenarios where the Higgs is a pseudo-Goldstone boson. This can be done minimally extending known pGB Higgs models to simply include the singlet scalar S which is required to make the Lagrangian additionally

PQ-invariant, since pGB Higgs models already include exotic quarks, vectorial under the SM gauge group, as those required in hadronic axion models.

3.2 LINEAR EFFECTIVE LAGRANGIAN FOR AXIONS AND AXION-LIKE PARTICLES

There are other BSM theories which rely on (approximate) symmetries, which, if spontaneously broken, predict (pseudo) Goldstone bosons. For instance, Majorons and familons result from the spontaneous breaking of lepton number and family number symmetry, respectively. Additionally, from a top-down approach, axions and other similar particles with a shift symmetry and couplings to gauge bosons arise in the compatification of extra dimensions in string theory.

Although they may bear no relation to the strong CP problem, they are sometimes called axion-like particles (ALPs) since their properties may be similar to those of the axion, for instance in their anomalous couplings to two photons or in the fact that their couplings are shift symmetric classically. The difference is that, in the case of ALPs, the pseudo-GB mass and new scale are not necessarily related according to Eq. (3.5). Consequently, the search for ALPs should span areas of parameter space beyond this tight relationship.

A rather model-independent approach to the phenomenology of ALPs can be taken using the tool of effective field theories. Two types of EFTs exist, depending on the assumptions on the nature of the BSM physics (see Sect. 1.4): linear and non-linear Lagrangians. The dominant new physics effects in linear scenarios, where the Higgs is assumed to be an exact doublet at low energy and where the new physics is assumed to be weakly-interacting, are encoded in a $d = 5$ effective Lagrangian which includes all possible couplings of an axion or ALP to the SM fields suppressed by one power of the NP scale, f_a. Due to the pGB nature of the ALP, its couplings will be derivative.

In linear realizations of EWSB with only SM fields at low-energies, the leading order (LO) effective Lagrangian is simply the SM one, which we rewrite here for compactness in notation:

$$\mathcal{L}_{SM} \supset D_\mu \Phi^\dagger D^\mu \Phi + \sum_\psi i\bar{\psi}\not{D}\psi - \left(\bar{Q}_L\, \mathbf{Y}_D\, \Phi d_R + \bar{Q}_L\, \mathbf{Y}_U\, \tilde{\Phi} u_R + \bar{L}_L\, \mathbf{Y}_E\, \Phi e_R + \text{h.c.}\right) , \quad (3.50)$$

where $\tilde{\Phi} = i\sigma^2\Phi^*$ and $\mathbf{Y}_D$, $\mathbf{Y}_U$ and $\mathbf{Y}_E$ are 3×3 matrices in flavour space which encode the Yukawa couplings for down quarks, up quarks and charged leptons, respectively. Consider now an additional particle, singlet under the SM charges, which is a (pseudo)Nambu-Goldstone boson of a spontaneously broken symmetry at energies higher than the electroweak scale v (set by the W mass). Neglecting its mass, its couplings would be pure derivative ones because of the underlying shift symmetry. Denoting by f_a the scale associated to the physics of this ALP particle a, insertions of the latter in effective operators will be weighted down by powers of a/f_a. Focusing on interactions involving only one ALP, the next-to-leading-order (NLO) effective linear ALP Lagrangian has been determined long ago [16].

In this thesis we mostly focus on the bosonic operators involving a, determining a complete and non-redundant set. For linear EWSB realizations the most general linear bosonic Lagrangian, including only the NLO corrections involving a, is given by [16]

$$\mathcal{L}_{\text{eff}}^{\text{linear}} = \mathcal{L}^{\text{LO}} + \delta\mathcal{L}_a^{\text{lin.}}\,, \tag{3.51}$$

where now the leading order Lagrangian is the SM one plus the ALP kinetic term,

$$\mathcal{L}^{\text{LO}} = \mathcal{L}_{\text{SM}} + \frac{1}{2}(\partial_\mu a)(\partial^\mu a)\,, \tag{3.52}$$

while the NLO bosonic corrections are given by

$$\delta\mathcal{L}_a^{\text{lin.}} = c_{\tilde{W}}\mathcal{A}_{\tilde{W}} + c_{\tilde{B}}\mathcal{A}_{\tilde{B}} + c_{\tilde{G}}\mathcal{A}_{\tilde{G}} + c_{a\Phi}\mathbf{O}_{a\Phi}\,, \tag{3.53}$$

with

$$\mathcal{A}_{\tilde{B}} = -B_{\mu\nu}\tilde{B}^{\mu\nu}\frac{a}{f_a}\,, \tag{3.54}$$

$$\mathcal{A}_{\tilde{W}} = -W^a_{\mu\nu}\tilde{W}^{a\mu\nu}\frac{a}{f_a}\,, \tag{3.55}$$

$$\mathcal{A}_{\tilde{G}} = -G^a_{\mu\nu}\tilde{G}^{a\mu\nu}\frac{a}{f_a}\,, \tag{3.56}$$

$$\mathbf{O}_{a\Phi} = i(\Phi^\dagger \overleftrightarrow{D}_\mu \Phi)\frac{\partial^\mu a}{f_a}\,, \tag{3.57}$$

and $\tilde{X}^{\mu\nu} \equiv \frac{1}{2}\epsilon^{\mu\nu\rho\sigma}X_{\rho\sigma}$. The action of the shift symmetry on the first three operators, $a \to a + \alpha$, with α constant, yields

$$\text{Tr}[X_{\mu\nu}\tilde{X}^{\mu\nu}]\frac{a}{f_a} \equiv \partial_\mu K_X^\mu \frac{a}{f_a} \to \partial_\mu K_X^\mu \frac{a+\alpha}{f_a} = -K_X^\mu \partial_\mu \frac{a}{f_a} + \frac{\alpha}{f_a}\partial_\mu K_X^\mu\,, \tag{3.58}$$

and thus the corresponding associated current is anomalous as $\delta\mathcal{L} = \frac{\alpha}{f_a}\partial_\mu K_X^\mu$. Even if this correction is a total derivative, in the case of $\mathcal{A}_{\tilde{G}}$ the existence of instantonic configurations in the QCD Lagrangian implies that the action is modified because the integral of $\partial_\mu K_G^\mu$ does not vanish (although a discrete version of the shift symmetry is preserved); it is nevertheless often added to the Lagrangian given its relevance for the case of the true QCD axion and the solution of the strong CP problem. [4]

After electroweak symmetry breaking, $\mathbf{O}_{a\Phi}$ induces a two-point function contribution, tantamount to a acting as an additional contribution to the longitudinal component of the electroweak gauge fields. An easy way of determining its impact on observables is to trade it for a fermionic vertex [16], either chirality conserving or chirality flipping, or a combination of them. For instance, the Higgs field redefinition

$$\Phi \to e^{ic_\Phi\, a/f_a}\Phi \tag{3.59}$$

applied to the bosonic Lagrangian Eq. (3.52), induces a correction stemming from the Higgs kinetic energy term (see Eq.(3.50)) which cancels exactly $\mathbf{O}_{a\Phi}$ up to $\mathcal{O}(a/f_a)$, while the

4 In any case, $\mathcal{A}_{\tilde{G}}$ will play no role whatsoever in the analysis to be performed in this thesis.

Yukawa terms in that equation induce a new Yukawa-axion coupling for which $\mathbf{O}_{a\Phi}$ can be entirely traded (see App. A.4 for details and a general discussion of possible field redefinitions). The overall effect is thus the replacement in Eq. (3.53)

$$\mathbf{O}_{a\Phi} \longrightarrow \mathbf{O}^{\psi}_{a\Phi}\,, \tag{3.60}$$

where

$$\mathbf{O}^{\psi}_{a\Phi} \equiv i\left(\bar{Q}_L\,\mathbf{Y}_U\,\tilde{\Phi}u_R - \bar{Q}_L\,\mathbf{Y}_D\,\Phi d_R - \bar{L}_L\,\mathbf{Y}_E\,\Phi e_R\right)\frac{a}{f_a} + \text{h.c.}\,, \tag{3.61}$$

which exhibits a relative minus sign between the Yukawa-ALP type of interaction for up and down fermions. This coupling can then be written in a more compact way as

$$\mathbf{O}^{\psi}_{a\Phi} = i\,\frac{a}{f_a}\sum_{\psi=Q,\,L}\left(\bar{\psi}_L\mathbf{Y}_\psi\check{}\,\sigma_3\psi_R\right) + \text{h.c.}\,, \tag{3.62}$$

where $Q_R \equiv \{u_R, d_R\}$ ($L_R \equiv \{0, e_R\}$) –with σ_3 acting on weak isospin space– and where the block matrices $\mathbf{Y}_\psi$ and $\check{}$ are defined by

$$\mathbf{Y}_Q \equiv \text{diag}\,(\mathbf{Y}_U\,,\mathbf{Y}_D)\,, \qquad \mathbf{Y}_L \equiv \text{diag}\,(0\,,\mathbf{Y}_E)\,, \qquad \check{} = \text{diag}(\tilde{\Phi}\,,\Phi)\,. \tag{3.63}$$

Alternatively, using the equations of motion of $\mathcal{L}^{\text{LO}}$, $\mathbf{O}_{a\Phi}$ could be entirely traded by a flavour-blind and chirality-conserving fermionic operator,

$$\mathbf{O}_{a\Phi} \longrightarrow -\frac{1}{2}\,\frac{\partial_\mu a}{f_a}\sum_{\psi=Q,\,L}\left(\bar{\psi}\gamma_\mu\gamma_5\sigma_3\psi\right) + \text{h.c.}\,, \tag{3.64}$$

where again terms with more than one axion insertion have been neglected. In this thesis we choose to use the chirality-flipping version of the fermionic couplings, though. In summary, the expression for $\delta\mathcal{L}^{\text{lin.}}_a$ to be used below reads

$$\delta\mathcal{L}^{\text{lin.}}_a = c_{\tilde{W}}\mathcal{A}_{\tilde{W}} + c_{\tilde{B}}\mathcal{A}_{\tilde{B}} + c_{\tilde{G}}\mathcal{A}_{\tilde{G}} + c_{a\Phi}\mathbf{O}^{\psi}_{a\Phi}\,, \tag{3.65}$$

with $\mathbf{O}^{\psi}_{a\Phi}$ as defined in Eq. (3.62).

For completion, it is worth mentioning that when the complete NLO Lagrangian is considered in the linear case, additional fermionic operators are present. In fact the most general NLO ALP Lagrangian is given by [16, 142, 160]

$$\delta\mathcal{L}^{\text{lin.-tot.}}_a = c_{\tilde{W}}\mathcal{A}_{\tilde{W}} + c_{\tilde{B}}\mathcal{A}_{\tilde{B}} + c_{\tilde{G}}\mathcal{A}_{\tilde{G}} + \frac{\partial_\mu a}{f_a}\sum_{\substack{\psi=Q_L,\,Q_R,\\ L_L,\,L_R}}\bar{\psi}\gamma_\mu X_\psi\psi\,, \tag{3.66}$$

where X_ψ are 3×3 hermitian matrices in flavour space. The chirality-conserving operator in the last term of this equation could alternatively be traded using the equations of motion (EOM) by a chirality-flipping coupling:

$$\frac{\partial_\mu a}{f_a}\sum_{\substack{\psi=Q_L,\,Q_R,\\ L_L,\,L_R}}\bar{\psi}\gamma_\mu X_\psi\psi \longrightarrow \frac{ia}{f_a}\sum_{\psi=Q,L}\bar{\psi}_L\check{}\left(X_{\psi_L}\mathbf{Y}_\psi - \mathbf{Y}_\psi X_{\psi_R}\right)\psi_R + \text{h.c.}\,. \tag{3.67}$$

In this equation, the products $X_{\psi_L}\mathbf{Y}_\psi$ and $\mathbf{Y}_\psi X_{\psi_R}$ are completely generic matrices and in consequence, in the complete linear basis, operators of the type $a\,\bar{\psi}_L\check{}\,\psi_R$ are not Yukawa

suppressed. Note as well that it would be redundant to consider simultaneously a bosonic coupling such as $\mathbf{O}_{a\Phi}$ in Eq. (3.57) and the general fermionic couplings in Eq. (3.66) or (3.67), as the effects of the former are already included in the flavour blind components of the X_ψ matrices, see Eq. (3.64). This thesis focuses on the thorough exploration of observables induced by the purely bosonic ALP couplings as expressed in Eq. (3.65), for the case of linear EWSB realizations.

3.3 EXPERIMENTAL CONSTRAINTS ON AXIONS AND AXION-LIKE PARTICLES

The search for axions has mainly been driven by invisible axion models, all characterised by the relationship between m_a and f_a given in Eq. (3.6), and they are mostly based on axion couplings to photons, electrons and nucleons. A summary of these constraints, which will be described in detail in this section, is presented as a function of one single parameter $f_a \sim 1/m_a$ in Fig. 3.2. Although there is no single measurement that gives an absolute lower (upper) bound for f_a (m_a) because some of these searches are rather model-dependent, a rough value of

$$f_a \gtrsim 10^8 - 10^9\,\text{GeV} \quad \text{and} \quad m_a \lesssim \mathcal{O}(10\,\text{meV}) \tag{3.68}$$

can be extracted in general for axions. The bound on the mass is given for invisible axion models, *i.e.* assuming that the relationship in Eq. (3.6) holds. We anticipate here a result that will be explained in better detail in Chapter 4 which is that, while astrophysics gives a lower bound for the invisible axion scale, cosmology gives an upper bound. Axions produced non-thermally in the early universe provide, as we will discuss later in Sect. 4.4, an explanation for dark matter. Requiring that the relic density does not overcome the measured value requires (depending on the assumptions about inflation)

$$f_a \lesssim 10^{11} - 10^{12}\,\text{GeV} \quad \text{and} \quad m_a \gtrsim \mathcal{O}(10\,\mu\text{eV})\,, \tag{3.69}$$

a bound that can be also seen in Fig. 3.2 for the invisible QCD axion.

On the other hand, the search for ALPs is very much related to the axion one for two reasons.

- *Axion searches may find ALPs:* In the context of axion searches, regions of parameter space not specific to invisible axions are also covered, and thus axion searches also test for axion-like particles that arise in other BSM theories (see Fig. 3.1).
- *ALP searches may find axions:* There exist proposals of "heavy axions" –for instance those in Refs. [134, 135]– which *do* solve the strong CP problem but whose mass and scale do not satisfy Eq. (3.5) (see beginning of Sect. 3.1). In consequence, searches beyond the strict relationship of invisible axions may well find particles solving the strong CP problem. However, unless otherwise specified, we will focus here on invisible axions.

Amongst the bounds presented in this section, those for $m_a \lesssim \mathcal{O}(10\,\text{meV})$ can be interpreted in terms of both invisible axions and other ALPs (except when specified otherwise), while those for higher masses than this should be interpreted as bounds on ALPs.

Many of the bounds will be presented in Figs. 3.1, 3.2 and 3.4. For this reason we prefer to clarify in advance the relationship between these figures

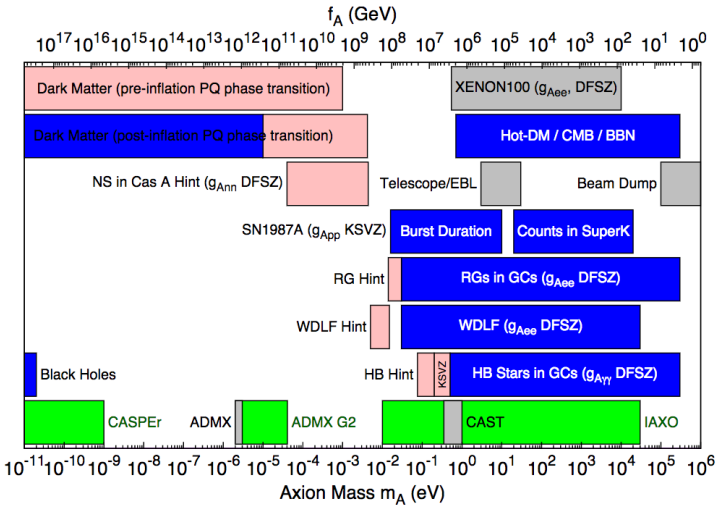

Figure 3.2: Exclusion ranges as described in the text. The intervals in the bottom row are the approximate ADMX, CASPEr, CAST, and IAXO search ranges, with green regions indicating the projected reach. Limits on coupling strengths are translated into limits on $m_A = m_a$ and $f_A = f_a$ using $z = 0.56$ and the $E/N = 0$ values for the coupling strengths, if not indicated otherwise. The"Beam Dump" bar is a rough representation of the exclusion range for standard or variant axions. The limits for the axion-electron coupling are determined for the DFSZ model with an axion-electron coupling corresponding to $x = \frac{v_d}{v_u} = 1$. Figure and caption adapted from Ref. [109].

1. The first, Fig. 3.1, presents the part of the $(m_a, g_{a\gamma\gamma})$ parameter space which is of interest to invisible axions. The coloured diagonal bands show the *phenomenologically preferred* axion bands computed under different assumptions [140], delimited by maximum and minimum values of E/N, the model-dependent quantity that fixes the relationship between m_a and $g_{a\gamma\gamma}$ defined in Eq. (3.3). The minimal band which represents the prediction for both DFSZ and KSVZ (with only one exotic fermion included) shown in green. It is apparent that in reaching this invisible axion band, the experimental constraints test larger regions in parameter space. It is rather a plot of ALP-photon interactions that includes axions.

2. On the other hand, Fig. 3.2 concentrates specifically on the invisible axion band, and fixes $E/N = 0$ so the bounds can be interpreted in terms of a single parameter (either f_a *or* m_a). It incorporates bounds from electron and nucleon couplings to axions, as well as those obtained by the assumption that axions are Dark Matter (a possibiliy which will be explored in Chapter 4 below). Some of these bounds are rather model dependent (as specified by the labels on the plot).

3. Finally, Fig. 3.4 presents searches for ALPs. It is again the $(m_a, g_{a\gamma\gamma})$ parameter space, now including masses as large as $\mathcal{O}$(TeV), and removing the representation of the invisible axion band. Some of the bounds presented here are the same as those in Fig. 3.1, but a number of new searches are shown, especially in the high-mass region.

Figure 3.3: Primakoff effect which explains the conversion of axions to photons and viceversa in presence of an external magnetic field. Fig.**(a)** shows the vertex involved in axion production while Fig.**(b)** the vertex involved in axion detection.

3.3.1 *Axion-photon interactions for axions and ALPs*

Axion couplings to photons, encoded in the Lagrangian $\mathcal{L}_{a\gamma\gamma} = \frac{g_{a\gamma\gamma}}{4} F_{\mu\nu}\tilde{F}^{\mu\nu}\frac{a}{f_a}$, can be expressed in terms of the parameters in the Lagrangian of Eq. (3.2) as,

$$g_{a\gamma\gamma} = \frac{\alpha_{em}}{2\pi f_a}\left[\frac{E}{N} - \frac{2}{3}\frac{4m_d + m_u}{m_d + m_u}\right], \tag{3.70}$$

or of the parameters in Eq. (3.66) for ALPs as

$$g_{a\gamma\gamma} = -\frac{4}{f_a}(c_{\tilde{B}}c_\theta^2 + c_{\tilde{W}}s_\theta^2), \tag{3.71}$$

where c_θ (s_θ) denotes the cosinus (sinus) of the Weinberg angle.

Many searches for $g_{a\gamma\gamma}$ interactions are based on axion-photon conversion, a process known as the Primakoff conversion. It refers to the conversion of axions to photons or viceversa in presence of an external magnetic field, through the axion's two-photon interaction $\sim g_{a\gamma\gamma}\mathbf{E}\cdot\mathbf{B}a$, see Fig. 3.3. It may be responsible for axion production for instance in the Sun, or in light-shining through a wall experiments. Conversely, the same vertex is often used to detect axions, by applying a magnetic field that would convert them back to photons, for instance in solar axion telescopes described below.

For very light axions or ALPs which can be emitted in the range of astrophysical energies, astrophysical constraints are very valuable. Low mass weakly interacting particles are produced in hot astrophysical plasmas and can thus transport energy out of stars [161]. The coupling strength of these particles with standard matter and radiation is bounded by the constraint that stellar lifetimes of energy loss rates do not enter in conflict with observations. In the case of axions and light ALPs, this emission can take place through the Primakoff conversion. A strong bound to this process can be derived from globular-cluster (GC) stars [162]. GCs are homogeneous gravitationally bound systems of stars. The stars in a GC were all formed around the same time and for detailed tests of stellar-evolution theory. In particular, number counts of Horizontal Branch (HB) stars –whose lifetime is expected to be affected by Primakoff axion losses– are compared with the number of red giants (RGs) –that are not much affected– giving: $g_{a\gamma\gamma} \lesssim 10^{-10}\text{GeV}^{-1}$, for $m_a \lesssim \mathcal{O}(30\,\text{keV})$. An even more stringent bound resulting from an updated analysis of 39 Galactic Globular Clusters has been reported [154], setting the limit

$$g_{a\gamma\gamma} \lesssim 0.66\times 10^{-10}\text{GeV}^{-1} \quad (95\%\text{C.L.}) \quad \text{for} \quad m_a \lesssim \mathcal{O}(10\,\text{keV}), \tag{3.72}$$

which is plotted in Figs. 3.1, 3.2 and 3.4.

Experiments based on searching for axion fluxes from astrophysics and cosmology conversely use the Primakoff conversion to detect them. Axion fluxes coming from the Sun are searched for in helioscopes. Several are running at this time, amongst which CAST (CERN Axion Solar Telescope) is the most powerful. It uses a decomissioned LHC magnet on a tracking mount oriented towards the Sun, which converts hypothetical axions to photons which are searched for at the detector. CAST has been able to reach similar levels to the most restrictive astrophysical bounds:

$$g_{a\gamma\gamma} < 0.66 \times 10^{-10}\,\mathrm{GeV}^{-1} \quad (95\%\mathrm{C.L.}) \quad \text{for} \quad m_a < 0.02\,\mathrm{eV} \tag{3.73}$$

and slightly weaker values for axions up to $\mathcal{O}(1\,\mathrm{eV})$ [147]. The future generation of helioscopes includes IAXO which expects to improve these bounds in more than an order of magnitude [149, 156]. These bounds and prospects are also represented in Figs. 3.1, 3.2 and 3.4. Since the constraints in Eqs. (3.72) and (3.73) only rely on the presence of an axion-photon interaction, they apply to axion-like particles in general.

Axions can also constitute dark matter (DM), as will be explained in Chapter 4 below, and thus axion fluxes may also come from galactic halos, in which case they are searched for by haloscopes (again through the Primakoff effect). In a broad range of the plausible m_a range for DM, galactic halo axions may be detected by their resonant conversion into a quasi-monochromatic microwave signal in an electromagnetic cavity permeated by a strong static **B** field in Fabry-Perot optical cavities. The cavity frequency is tunable, and a resonance at a certain frequency would identify the axion mass. The latest experiment of this type is Axion Dark Matter eXperiment (ADMX), which is testing axions in the $1-100\,\mu\mathrm{eV}$ mass range [157], of which we can see some of the latest results are shown in Figs. 3.1 and 3.2. MADMAX (Magnetized Disc and Mirror Axion Experiment) will be using resonant regeneration to search for axions with $40-400\,\mu\mathrm{eV}$ of mass [158]. The main caveat of these searches is that they are obtained under the assumption that axions constitute the whole DM density. These constraints may not apply to other types of ALPs because they rely on the presence of axion DM, whose production in the early universe relies on specific characteristics of the QCD axion (see Chap 4).

An experiment also uses axion-photon conversion in axion production and detection, both processes taking place in the laboratory. These are called light shining through a wall (LSW) experiments. An incoming photon is converted into an axion or ALP, which traverses an opaque wall, to then be reconverted into a photon on the other side. Since the process is suppressed by two powers of f_a instead of only one, the bounds from LSW are weaker than those from astrophysics, helioscopes and haloscopes. They are plotted in Figs. 3.1 and 3.4.

Finally, the recent years have seen a proliferation of searches for axions or ALPs at past, present and future colliders. These have managed to explore the high-mass region of parameter space beyond the invisible axion constraint, see Fig. 3.4. Bounds from LEP data based on the axion-photon coupling include searches for $e^+e^- \to \gamma \to \gamma a$ leading to mono-γ plus missing energy if the ALP is long-lived or tri-γ if it decays to two photons [163]. Di-γ searches allowed to test tri-γ production in the MeV region where two photons are collimated and detected as one [18]. LHC searches have also been used to constrain the $150-2000$ GeV mass region, in particular through searches for photon fusion ($pp \to jj + \gamma\gamma$) [164]. The projection of these bounds in the $(m_a, g_{a\gamma\gamma})$ plane add up in excluding ALPs with couplings above

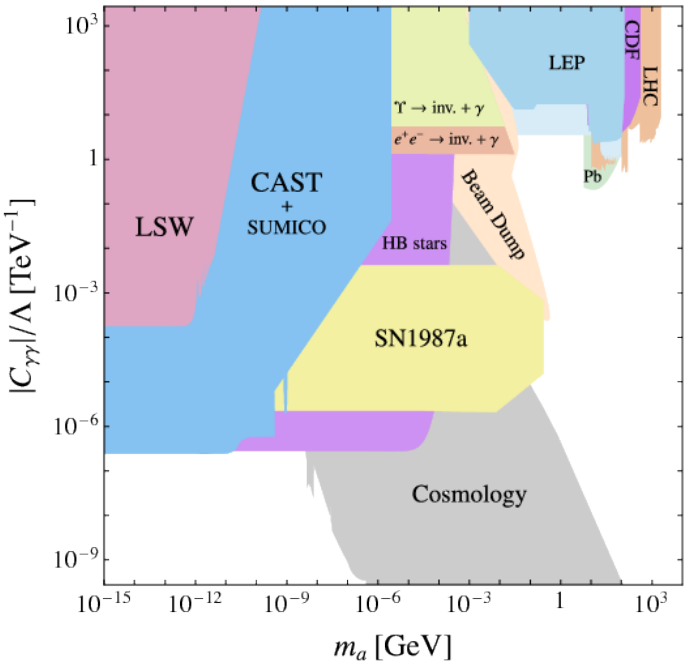

Figure 3.4: Existing constraints on the ALP-photon coupling derived from a variety of particle physics, astro-particle physics and cosmological observations. Contents described in the text. Several of these bounds are model dependent. Figure from Ref. [165].

$g_{a\gamma\gamma} \sim 0.5 - 1\text{TeV}^{-1}$ and masses between the MeV and a few TeV, as can be seen in the top right corner of Fig. 3.4.

3.3.2 *Axion and ALP coupling to gluons*

In turn, the effective ALP-gluon g_{agg} coupling is analogously defined by

$$\mathcal{L}_{agg} \supset -\frac{1}{4} g_{agg}\, a\, G^a_{\mu\nu} \tilde{G}^{a\mu\nu}\,, \tag{3.74}$$

It can be expressed for the case of axions by relating Eq. (3.74) to Eq. (3.2). Also, in terms of the linear ALP effective Lagrangian as a function of the NLO effective operator $\mathcal{A}_{\tilde{G}}$ in Eq. (3.56):

$$g_{agg} = \frac{4}{f_a} c_{\tilde{G}} \tag{3.75}$$

The coupling g_{agg} can be directly constrained at energies above the QCD scale Λ_{QCD} via axion-pion mixing effects, and also via mono-jet searches at hadron colliders.

Bounds on $\text{Br}(K^+ \to \pi^+ + \text{nothing})$ [166] can be used to constrain the process $K^+ \to \pi^+ \pi^0\, (\pi^0 \to a)$, where the pion-axion mixing arises through the anomalous coupling of mesons and of the axion to gluons [142, 167]. These bounds have been used to constrain f_a in contexts where the coupling of the ALP to gluons is only present due to the anomaly, *i.e.*

where $\mathcal{L} \supset \frac{\alpha_s}{8\pi}\frac{a}{f_a} G\tilde{G}$ (see, for example, Ref. [168]). They can be reinterpreted in terms of the generic ALP-gluon coupling, Eq.(3.74), yielding

$$g_{agg} \lesssim 1.1 \cdot 10^{-5}\,\text{GeV}^{-1} \quad (90\%\ \text{C.L.}) \quad \text{for} \quad m_a \lesssim 60\,\text{MeV}\,. \tag{3.76}$$

Slightly higher ALP masses have been considered at colliders, assuming only the coupling in Eq. (3.74). Limits of order

$$g_{agg} \lesssim 10^{-4}\,\text{GeV}^{-1} \quad (95\%\ \text{C.L.}) \quad \text{for} \quad m_a \lesssim 0.1\,\text{GeV}\,, \tag{3.77}$$

were obtained [163] by recasting 8 TeV LHC analyses [169, 170].

3.3.3 *Axion and ALP coupling to fermions*

▷ *Definitions*

Axion and ALP couplings to electrons and nucleons have also been tested. Phenomenological studies generally present their searches in terms of the axial coupling:

$$\mathcal{L}_{a\psi\psi} = \sum_{\psi=u,d,e} -iC_\psi m_\psi \bar{\psi}\gamma^5\psi\,\frac{a}{f_a} = \sum_{\psi=u,d,e} \frac{C_\psi}{2}\bar{\psi}\gamma^\mu\gamma^5\psi\,\frac{\partial_\mu a}{f_a}\,, \tag{3.78}$$

where the constants C_ψ can be related to the PQ charges of the fermions in PQWW and DFSZ axions by comparing Eq. (3.78) to Eqs. (3.24) and (3.35) respectively (also subject to the definition of the axion scale in relation to the PQ-breaking scale given in Eqs. (3.33) and (3.46)). In the case of ALPs, the scale f_a should be interpreted as a general new physics scale, unrelated to the Peccei-Quinn mechanism. As with the case of the photon coupling, they are also related to the parameters in the effective Lagrangian in Eq. (3.66) trivially by $C_\psi/2 = X_{\psi R} - X_{\psi L}$, since the vectorial part cancels due to the conservation of the vector current.

A similar definition for the axion coupling to nucleons reads:

$$\mathcal{L}_{aNN} = \frac{1}{2}\bar{N}\begin{pmatrix} C_p & \\ & C_n \end{pmatrix}\gamma^\mu\gamma^5 N\,\frac{\partial_\mu a}{f_a}\,, \tag{3.79}$$

with $N = (p,\, n)^T$ the nucleon doublet. If the particle $a(x)$ is a true QCD axion, the coefficients C_p and C_n can be computed as a function of the quark couplings in Eq. (3.78), and also receive a model-indepentent contribution directly from the necessary $aG\cdot\tilde{G}$ coupling due to non-perturbative effects [141]:

$$C_p = -0.47(3) + \sum_{\substack{i=u,c,t\\ d,s,b}} x_i^{(p)} C_i^0 \tag{3.80}$$

$$C_n = -0.02(3) + \sum_{\substack{i=u,c,t\\ d,s,b}} x_i^{(n)} C_i^0 \tag{3.81}$$

where C_i^0 are the couplings defined at the scale $f_a = 10^{12}\,\text{GeV}$ and $x_i^{(p)}$ and $x_i^{(n)}$ are computed numerically in chiral perturbation theory using results from Lattice QCD [141].

▷ *Axion-nucleon coupling*

As with the case of photons, astrophysical sources serve to test axion couplings to matter: axion-nucleon interactions are constrained by the requirement that the neutrino signal of the supernova SN 1987A is not excessively shortened by axion losses [162, 171]. Axion couplings to hadrons are particularly relevant in hadronic axion models where axions are not expected to couple to leptons. An upper limit on the energy-loss rate interpreted in the context of hadronic axion models where $C_i^0 = 0$ and in the limit $|C_p| > |C_n| \approx 0$ (see Eq. (3.80)) yields [162]

$$C_p^2 \left(\frac{\text{GeV}}{f_a}\right) < 1.3 \times 10^{-18} \quad \xrightarrow{|C_p| \approx 0.47} \quad f_a \gtrsim 4 \times 10^8\,\text{GeV} \tag{3.82}$$

and through Eq. (3.6) this can be translated to $m_a < 14\,\text{meV}$. This constraint, which is plotted in Fig. 3.2 holds for all hadronic axion models, since it is simply a consequence of the necessary $aG\cdot\tilde{G}$ coupling. However for DFSZ axions, cancellations amongst the C_i^0 contributions to C_n and C_p might weaken this bounds, and for the case of ALPs it can simply be interpreted in terms of C_N/f_a, and the relation to the more fundamental quark-axion couplings is then model-dependent. In any case, the SN 1987A limit involves many uncertainties which are not easy to quantify [162].

▷ *Axion and ALP electron coupling*

Axions and ALPs can also be tested through their coupling to electrons, defined in Eq. (3.78), both in astrophysical processes and in laboratory experiments. The severity of the constraints on $g_{a\psi}$ depends on the ALP mass range considered.

The strongest bounds are those used to constrain DFSZ axions and apply to very low ALP masses. White-dwarf cooling due to axion losses, bound axion-electron coupling to $C_e/f_a \lesssim 10^{-11}\,\text{GeV}^{-1}$ for $m_a \lesssim 9\,\text{meV}$ [162, 172]. However, this observable has recently become a hint for axion detection, allegedly having a best fit of $C_e/f_a \approx 4.4 \times 10^{-10}\,\text{GeV}^{-1}$ [173]. An independent bound is inferred from high-precision photometry of the red giant branch of the color-magnitude diagram for globular clusters [174]. Measurements of axionic recombination and de-excitation, Compton scattering and axion-bremsstrahlung set very strong bounds again on the coupling to electrons:

$$C_e/f_a < 8.6 \cdot 10^{-10}\,\text{GeV}^{-1} \quad (95\%\ \text{C.L.}) \quad \text{for} \quad m_a \lesssim \text{eV}\,. \tag{3.83}$$

These constraints are represented on the invisible axion band in Fig. 3.2.

Heavier axions and ALPs have been tested in axion searches in Xenon100 [175] through the axio-electric effect in liquid xenon (analogue of the photo-electric process with the absorption of an axion instead of a photon), bounding ALP couplings to electrons:

$$C_e/f_a < 1.5 \cdot 10^{-8}\,\text{GeV}^{-1} \quad (90\%\ \text{C.L.}) \quad \text{for} \quad m_a < 1\,\text{keV}\,. \tag{3.84}$$

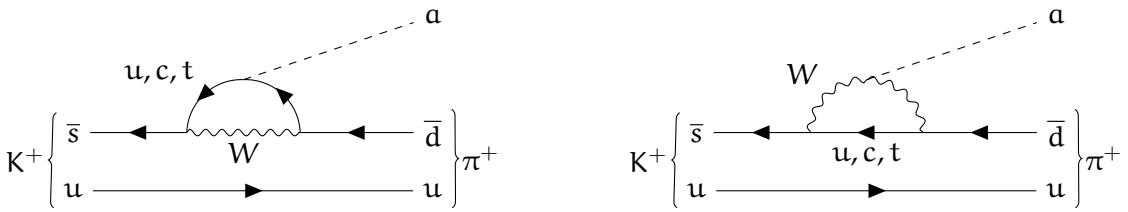

(a) Interaction through flavour diagonal axion-fermion interaction used to test for C_ψ as described in Sect. 3.3.3.

(b) Interaction through $aW\cdot\tilde{W}$ coupling used to test for $c_{\tilde{W}}$ as described in Sect. 3.3.4.

Figure 3.5: Axion contributions to rare meson decays, in particular to $K^+ \to \pi^+ a$. The axion or ALP in the final state may be considered stable in the form of an invisible product or decaying to two photons.

This constraint is also shown in the invisible axion band in Fig. 3.2. The least constrained is the high-mass region, and can thus be rather interpreted for ALPs. It is tested through rare meson decays (see Fig. 3.5a) and in DM direct detection searches (the latter being very model-dependent) [176]. The former provide bounds on ALP-fermion couplings below 10 GeV and in particular Beam Dump experiments (CHARM) constraints read [177, 178]:

$$C_\psi/f_a < \left(3.4\cdot 10^{-8} - 2.9\cdot 10^{-6}\right)\ \text{GeV}^{-1} \quad (90\%\ \text{C.L.}) \quad \text{for} \quad 1\,\text{MeV} \lesssim m_a \lesssim 3\,\text{GeV} \tag{3.85}$$

if considered flavor-universal.

The above set of fermionic bounds could suggest to infer new limits on the coefficient of the linear bosonic operator $\mathbf{O}_{a\Phi}$ of the bosonic linear ALP basis, Eq. (3.57), if considered by itself, via the equivalence discussed in Eqs. (3.59)-(3.62). This bound would depend on the ALP mass, and would be conservatively summarized in

$$|c_{a\Phi}|/f_a < \left(3.4\cdot 10^{-8} - 2.9\cdot 10^{-6}\right)\ \text{GeV}^{-1} \quad (90\%\ \text{C.L.}) \quad \text{for} \quad m_a \lesssim 3\,\text{GeV}\,, \tag{3.86}$$

except for ALPs with masses in the $1\,\text{keV} - 1\,\text{MeV}$ range, where the bounds from rare meson decay and DM searches are much weaker. Nevertheless, more than one effective operator can contribute to the rare processes under discussion and, in consequence, strictly speaking a bound can only be set on the corresponding combination of operators, see further below, in the same spirit that the bounds on $a\gamma\gamma$ decay do not nullify simultaneously the two couplings in the set $\{a_{\tilde{W}}, a_{\tilde{B}}\}$, but only a combination of them, see Eq. (6.19). For the time being, the value of $c_{a\Phi}$ will be thus left free for further exploration below.

3.3.4 *ALP interactions with massive vector bosons*

In contrast to the present constraints discussed above, the couplings of ALPs to the heavy SM bosons have been largely disregarded although they appear at NLO of the linear expansion, that is, at the same order as the pure photonic, gluonic and fermionic ALP couplings. The associated signals stemming from the linear $\delta\mathcal{L}_a^{\text{lin.}}$ in Eq. (3.65) are illustrated in the column on the right hand side of the Feynman rules detailed in App. A.2; they include in particular interaction vertices of the ALP with electroweak gauge bosons such as: $a\gamma Z$, aZZ, aW^+W^-,

$a\gamma W^+W^-$ and aZW^+W^-. Besides the collider signatures that will be presented in the phenomenological sections of this chapter, rare decays provide an additional handle on the ALP couplings to massive vector bosons.

Two types of signals are aiming at neutral and charged gauge boson couplings to heavy ($m_a \gtrsim$ MeV) ALPs; namely collider searches for γ and Z-mediated processes for the former and rare meson decays involving axion emission through WWa interactions.

The ALP coupling to the hypercharge vector boson $g_{a\gamma\gamma}\, aB\cdot\tilde{B}$ instead of $g_{a\gamma\gamma}\, aF\cdot\tilde{F}$ was considered in Ref. [18]. The authors found that interpreting tri-γ and di-γ LEP searches in this setup, the constraints on $g_{a\gamma\gamma}$ were substancially improved *w.r.t.* those on $g_{a\gamma\gamma}$ because on-shell Z mediated production is enhanced *w.r.t.* the highly off-shell γ mediated $a\gamma$ production. EW precision observables have also been used to test for ALPs: one-loop corrections to the oblique parameters and to $\alpha(M_Z)$ have allowed to derive bounds on the Wilson coefficients from the global electroweak fit, although they are rather weak, $c_{\tilde{X}}/f_a \lesssim \mathcal{O}(\text{a few TeV}^{-1})$ [165].

Furthermore, a recent study [165] has considered the NLO analysis of the complete ALP effective Lagrangian in a large number of collider observables. Amongst the most relevant findings is the large sensitivity that LHC will have in its high-luminosity phase to ALPs from Z-pole production. Assuming that $g_{\gamma Z}$ (defined analogously to $g_{a\gamma\gamma}$ in Eq. (3.9)) is of order $1/(4\text{TeV})$, the reach of $300\,\text{fb}^{-1}$ of LHC data will overcome the present ones in up to five orders of magnitude in the 100 GeV−100 MeV mass range.

A new class of observables at LHC are able to test both $aZZ/aZ\gamma$ and $aWW(\gamma)$: mono-Z, mono-W and $aW\gamma$ production. They are proposed and explored in depth, in Chapter 6, at present and future LHC. We postpone a detailed discussion of these results to but anticipate the main results: mono-Z gives the best constraints amongst these signatures, setting $|f_a/c_{\tilde{W}}| > 3.8\,\text{TeV}$ with present data, and up to $\mathcal{O}(20\,\text{TeV})$ will be tested with $3\,\text{ab}^{-1}$ of data for sub-MeV ALPs.

ALP couplings to charged gauge bosons have also been tested in rare meson decays, since the ALP-W^+W^- interaction defined by

$$\delta\mathcal{L}_a \supset -\frac{1}{4} g_{aWW}\, a\, W_{\mu\nu}\tilde{W}^{\mu\nu}\,, \tag{3.87}$$

may induce flavour changing rare meson decays via W exchange at one loop, and an ALP radiated from the W boson, see Fig. 3.5b. This coupling may be related to $c_{\tilde{W}}$ in Eq. (3.66) through $g_{aWW} = 4c_{\tilde{W}}/f_a$. Upon considering the action of $aW\cdot\tilde{W}$ by itself, the same coupling induces the subsequent ALP decay into two photons. NA48/2, NA62 and Beam Dump experiments have been analysed in this context in Ref. [17], resulting in

$$f_a/c_{\tilde{W}} \gtrsim 4 - 8000\,\text{TeV}\,, \quad \text{for} \quad m_a < 500\,\text{MeV}\,. \tag{3.88}$$

Other limits have been obtained from the bounds on rare meson decays into invisible products, $B \to K + a$ and $K \to \pi + a$ with $a \to$ inv.. This is nevertheless at the price of assuming, in addition to $aW\cdot\tilde{W}$, the existence of some supplementary ALP decay channel into invisible sectors that furthermore is required to be largely dominant [17].

Notice that these bounds are obtained from the same observable as those in Eqs. (3.85)-(3.83): more than one effective operator can contribute to the rare processes under discussion and, in consequence, strictly speaking a bound can only be set on the corresponding combination of operators, in the same spirit that the bounds on $a\gamma\gamma$ decay do not nullify simultaneously the two couplings in the set $\{c_{\tilde{W}}, c_{\tilde{B}}\}$, but only a combination of them, see Eq. (3.71). In

particular, the bounds from rare meson decays are being used to test independently $c_{\tilde{W}}$ and C_ψ, and even $c_{a\Phi}$ from Eq. (3.66) (whose physical effect is equivalent to an axion-fermion interaction). The approach of testing one operator at a time is a valid one, but this consideration should be kept in mind in the EFT approach, and a comprehensive analysis taking into accout all operators remains to be done.

In Chapter 6 we will explore the complementary information that the LHC can provide in various tree-level channels, e.g. mono-W, which are insensitive to the presence of the operator coefficient $c_{a\Phi}$ but share with the rare-decay analyses the dependence on the linear operator coefficient $c_{\tilde{W}}$. This complementarity is also manifest as the LHC has access to a larger kinematic range. Hence the breakdown of the ALP Effective Theory, and possible discovery of new physics, may be possible at the LHC but be hidden in physics at B-factories. For these reasons, in the phenomenological sections of Chapter 6 we will obtain LHC bounds on operators involved in tree-level ALP-W couplings (among others) and without the prejudice from rare-decays. The combined impact at LHC of $c_{\tilde{W}}$ and $c_{a\Phi}$ plus general ALP-fermion couplings, as well as the impact of non-linear operators on rare decays is a subject for future work.

3.3.5 *ALP-Higgs interactions*

Finally, a novel path in relation to ALP-higgs interactions is beginning to be explored. Although there are no $a-h$ interactions in the $d=5$ Lagrangian, aZh arises at loop level, or as we will see in the work presented in Chapter 6 of this thesis, it may appear amongst the leading order interactions in the EW chiral Lagrangian. Additionally haa interactions also arise in the $d=6$ Lagrangian if the ALP is allowed to have a mass. These would open new channels of ALP production from Higgs decays which have also been explored in Ref. [165]. They offer complementary information to ALP production from EW gauge bosons. For instance, in scenarios where the only tree-level ALP couplings to SM fields are flavour-universal couplings to the up-type quarks, ALP production from Z bosons is highly suppressed, $\mathrm{Br}(Z\to\gamma a)=4.8\times10^{-9}$ *w.r.t.* ALP production in Higgs decays, $\mathrm{Br}(h\to Za)=2.5\times10^{-4}$ or $\mathrm{Br}(h\to aa)=8.5\times10^{-3}$. However, the bounds and prospects which have been explored in this context rely on a large number of assumptions.

This points precisely at one of the difficulties that ALP phenomenology is facing at present time: the fact that many of these observables depend on more than one coupling at a time requires to make assumptions on some parameters to test for others. A considerable number of independent observables are being collected in the different mass ranges, which may be enough for a global fit of parameters soon.

4

SPIN ZERO CANDIDATES FOR DARK MATTER

4.1 EVIDENCE FOR DARK MATTER

The problem of dark matter is one of the most pressing experimental evidence for new physics. Starting almost 100 years ago, a large variety of observations –at very different time and energy scales– point to the presence of a significant amount of a new type of matter in the Universe. We here review the pieces of evidence that have played a role in strongly establishing the existence of what has come to be known as dark matter (DM).

4.1.1 *Galaxy clusters*

In the 1930's Fritz Zwicky measured the speed of galaxy clusters by analysing data of their red-shifts [179]. The Coma Cluster was found to have a particularly large velocity dispersion: 1000 km/s. The viral theorem, borrowed from thermodynamics, applied to a gravitationally bound system reads

$$\langle E_{kin} \rangle = -\frac{1}{2} \langle E_{pot} \rangle \,, \tag{4.1}$$

where $\langle E_{kin} \rangle = \frac{1}{2} m \langle v^2 \rangle$ is the average kinetic energy of one of the bound objects of mass m and $\langle E_{pot} \rangle = m G_N \langle M/r \rangle$ is the average gravitational potential caused by the other bodies, G_N being the gravitational constant. The average potential energy of the system was estimated by Zwicky approximating the total mass as the product of the number of observed galaxies, 800, and the average mass of a galaxy, which he took to be $10^9 M_\odot$. He took the physical size of the system to be around 10^6 light-years. Using the viral theorem, this gives an expected velocity dispersion of 80 km/s. In a later work [180], he reversed the argument: the measured velocity dispersion could be used to compute the mass of the clusters. In that case he found the Coma Cluster to have a mass-to-light ratio of around 500 (although it was computed with an incorrect value of the Hubble parameter, and when rescaled with the correct oner yields a mass-to-light ratio of ~ 8.3 [181]). He used these observations of the Coma Cluster to conclude that it contained a large amount of invisible matter: dark matter.

Although modern X-ray observations showed that the Coma Cluster contains a halo of hot gas, which constitutes about five times the mass which is visible in form of stars [182], invalidating the quantitative estimation by Zwicky, the qualitative conclusion remains unchanged. The existence of dark matter in galaxy clusters is now supported by modern observational methods applied to several other clusters [183].

4.1.2 *Galaxy rotation curves*

The presence of DM at the scale of a single galaxy is also solidly established by the measurement of galactic rotation curves, $v(r)$. Using Newton's laws for a narrow spherically

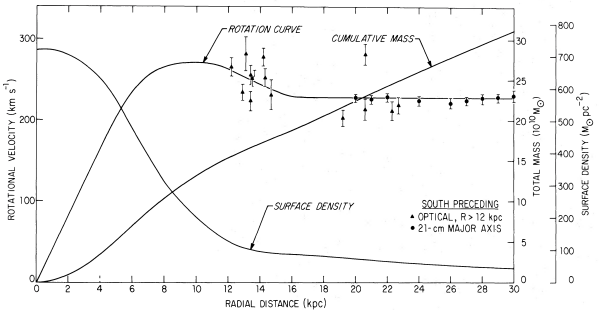

(a) The rotation curve of M31 by Roberts and Whitehurst [185]. The filled triangles show the optical data from Ref. [184], the filled circles show the 21-cm measurements made with the 300-ft radio telescope.

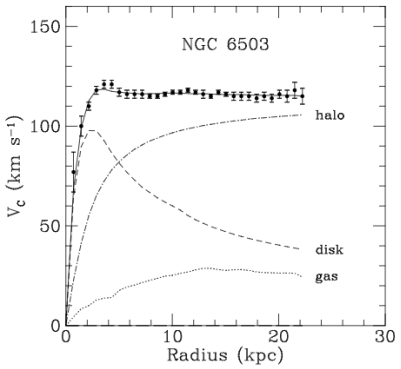

(b) Rotation curve measurement of the galaxy NGC 6503, together with the contributions attributed to the galactic disk, the interstellar gas, as well as the halo of dark matter. Figure originally published in Ref. [186].

Figure 4.1: Galactic rotation curves illustrating the presence of dark matter. See Sect. 4.1.2 for an explanation.

symmetric mass distribution, the velocity at a distance r from the center of the galaxy is given by

$$v(r) = \sqrt{\frac{GM(r)}{r}}, \tag{4.2}$$

where $M(r)$ is the mass enclosed within the radius r. When applied to the luminous matter distributions of galaxies, in which the bulk of the mass is in the center of the galaxy and $M(r)$ remains approximately constant beyond some point, the velocity is expected to fall as $1/\sqrt{r}$.

These predictions were contrasted with spectroscopic observations of various galaxies, pioneered by Vera Rubin [184] which found a striking result. The velocity grew initially with the radius as expected, but then remained approximately flat instead of falling, see Fig. 4.1a. To this date, this same result has been reproduced with a large number of galaxies amongst which the phenomenon is very clearly seen in barred spiral galaxies. These observations suggest a significant amount of non-luminous matter on galactic scales, giving rise to $M(r) \sim r$ at large r, and hence explaining the observed flat rotation curves. The observations are compared to the expected contributions from the visible galactic disk and from interstellar gas, inferring contribution from a dark matter halo, see Fig. 4.1b for an example.

4.1.3 *Gravitational lensing*

The trajectory of light rays may be modified by gravitational effects, as was correctly predicted in 1915 by Einstein. When a large mass is placed between a source of light and an observer, luminous "arcs" or "rings" emerge surrounding the massive object in front, see Fig. 4.2. This phenomenon is known as gravitational lensing, and the rings are known as

Einstein rings. In observations of distant bright objects such as galaxies or quasars, as the result of intervening matter, the light from these distant objects is bent towards the regions of large mass. A large ring shows up if the the light source and the mass are completely aligned with the observer, but small "arclets" can be used to reconstruct the gravitational potential between a set of objects, and this "weak lensing effect" is used in particular to derive mass distributions of galaxy clusters. Again, these mass distributions measure much more than the luminous matter observed, adding to measurements obtained using the viral theorem in supporting the existence of dark matter.

4.1.4 *Power spectrum of perturbations in the CMB*

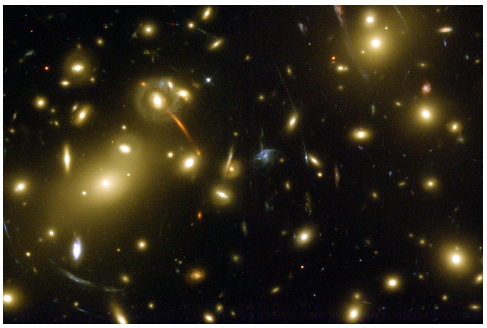

Figure 4.2: Gravitational lensing in Abell 2218 cluster. Picture taken with the Wide Field Planetary Camera 2 on board the Hubble Space Telescope.

In the early universe protons are coupled to photons in a photon-baryon plasma. This fluid is rather homogeneous, except for small acoustic oscillations: the radiation pressure prevents the formation of large overdensities since the baryons are interacting with the photons. However, a form of matter that did not interact with the photons *is* able to form clumps, which will be the seeds of the structure that we see today in the Universe. When the photons decoupled from the primordial plasma and expanded across the Universe they followed the density profiles that the DM had at that point. The image of these photons that we can measure nowadays it is named the *Cosmic Microwave Background (CMB)*. The relative size of the different peaks in the CMB power spectrum is related to the density of baryonic and dark in the universe, as the former are subject to both gravitational and electromagnetic interactions, while the (uncharged) dark matter component only feels the gravitational force. The last measurement of the CMB by Plank is fit to the ΛCDM cosmological model [187]–which includes the presence of a cosmological constant Λ and cold dark matter (CDM)– yielding very precise measurements of of the baryonic and DM densities,

$$\Omega_{DM}h^2 = 0.1198 \pm 0.0015 \quad \text{and} \quad \Omega_b h^2 = 0.02225 \pm 0.00016 \qquad 95\%\text{C.L.}\,, \tag{4.3}$$

where $h = 0.6727 \pm 0.0066$ is the Hubble constant expressed in units of $100\,\mathrm{km\,s^{-1}\,Mpc^{-1}}$ as determined also by Planck [187]. These quantities are interpreted as $\Omega_X = \rho_X/\rho_c$ where $\rho_c = 3H_0^2/8\pi G$ is the critical density of the universe, while ρ_X is the density of the contribution X. Eq. (4.3) implies that 84.3% of the matter content of the universe is in the form of a non-baryonic dark matter, in agreement with estimates of dark matter content gravitational effects described in the previous sections.

Consistent, although less precise, measurements of Ω_{DM} are obtained from constraints on Big Bang Nucleosynthesis (BBN), which is sensitive to the relative density of baryonic matter, confirming that dark matter is non-baryonic. And the presence of dark matter is also required to explain the formation and evolution of the observed large scale structure. In particular the latter observable requires dark matter to be *cold*, i.e. non-relativistic at the

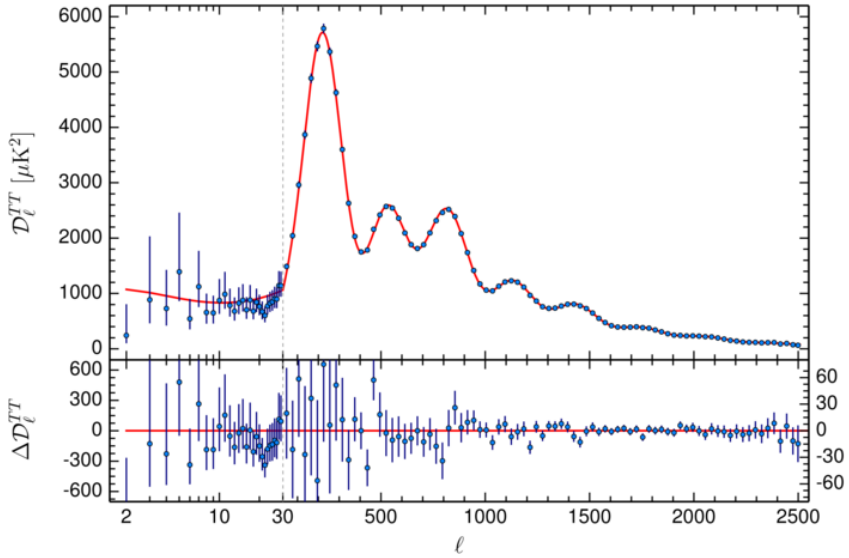

Figure 4.3: Planck 2015 temperature power spectrum $\mathcal{D}_l = l(l+1)C_l/2\pi$ as a function of the multipole l. The x-axis is logarithmic up to $l = 30$ and linear at higher l. The red line is the Planck best-fit primordial power spectrum [187]. Residuals with respect to this model are shown in the lower panel. The error bars show $\pm 1\sigma$ uncertainties. Figure and description adapted from Ref. [187].

time most relevant for structure formation, since hot dark matter would have washed out the initial overdensities.

4.2 DARK MATTER CANDIDATES

Dark matter refers, then, to the problem that our present knowledge is faced with in light of the evidence reviewed in the section above. And the question that follows is: *What is dark matter?*

Before opening the door to the particle dark matter zoo, there is still a possibility that Newton's laws do not apply at galactic scales. Amongst the proposals for modified gravity, Modified Newtonian Dynamics (MOND) proposes that Newton's laws stop working at small velocities as those relevant in galaxy rotation curves. Although it is still an option to the date, it faces uncomfortable issues, for instance, in the measurements of galaxy clusters that still observe a deficit of matter even when using MONDs. Another step that comes before the realm of BSM dark matter is to consider that DM is made of known matter, in the form of massive astronomical compact halo objects (MACHO). This option has been explored through microlensing measurements, finding that they cannot make up a significant fraction of DM [188], and BBN measurements limits the presence of baryonic matter, supporting the hypothesis of DM in the form of a new particle. There exists another form of baryonic dark matter which could avoid the BBN bound: these are primordial black holes [189]. These objects may have formed before nucleosynthesis (e.g., at the quark-hadron phase transition), in which case they would not have a noticeable effect on the light element abundances. Finally, the SM offers a "perfect" candidate for dark matter in its weakly-interacting neutral parti-

cle: neutrinos [190]. However, being relativistic collisionless particles (whose masses are constrained to $m_\nu < 2.05\,\text{eV}$ (95%C.L.) [191]) they would erase fluctuations in the background density, requiring complicated setups to explain present observations. Additionally, these bounds on neutrino masses together with measurements of the solar and atmospheric mass differences translate to an upper bound on neutrino density, $\Omega_\nu h^2 \lesssim 0.07$ (see Ref. [192]) which means that neutrinos are simply not abundant enough to be the dominant component of dark matter.

All of this points dark matter being a new particle (or particles) not yet discovered, a possibility that opens the door to a huge number of candidates. The different pieces of evidence described in Sect. 4.1 lead to a list of characteristics which any dark matter candidate must fulfil. Dark matter is

ELECTRICALLY NEUTRAL: Electric charge would imply it has electromagnetic interactions, making it visible. The strongest constraint comes from the CMB, since charged DM would couple to the photon bath and show up in the CMB power spectrum. [1]

NON-BARYONIC: The shape of the multipole expanded CMB power spectrum and the therein fitted ΛCDM parameters finds that the dominant part of matter in the Universe is non-baryonic dark matter, see Eq. (4.3).

COLD OR WARM: Successful structure formation requires dark matter to be cold, i.e. non-relativistic at the time when structures in the Universe start to form.

STABLE: The fact that galaxies and clusters remain confined states means that DM must be stable on time scales of galactic and cluster ages $\mathcal{O}(10^{17}\,\text{s})$.

Particle DM candidates run over an impressively large range of masses and characteristic couplings to SM particles, as can be observed in Fig. 4.4. Amongst the most explored candidates a generic type are *weakly interacting massive particles* (WIMP). These are a form of cold dark matter, with masses in the GeV-TeV range, and as the name implies they interact with the SM with a coupling strength similar to that of the weak interactions. It is easy to show that the WIMP thermal relic density matches the DM cosmological abundance today. In the early Universe, when the temperature is much higher than the WIMP rest mass, it is in thermal equilibrium with the SM through creation and annihilation of particle pairs and scattering. As the Universe expands and cools down, particles find it harder to interact, and when their scattering rate becomes smaller than Hubble expansion rate, the WIMPs are said to chemically decouple or freeze out. [2] A rough estimate, of the relic density of a certain dark matter candidate, χ as a function of the annihilation cross-section, $\sigma(\chi\chi \to \text{SM})$, results from the condition that decoupling occurs at $n_\chi \langle\sigma v\rangle \sim H$:

$$\Omega_\chi h^2 \approx \frac{3 \times 10^{-27}\,\text{cm}^3\,\text{s}^{-1}}{\langle\sigma v\rangle}\,. \tag{4.4}$$

1 Candidates as milicharged dark matter have been considered, CMB measurements [193] and galaxy clusters [194] constrain this scenario strongly: $|q_{DM}| \lesssim 10^{-14}|e|(m_{DM}/\text{GeV})$.

2 This phenomenon occurs with many particles in the evolution of the early Universe. Indeed, amongst others, photon freeze-out at around $T \sim 0.4\,\text{eV}$ gives rise to the CMB and a similar process for neutrinos at around $T \sim 1\,\text{MeV}$ creates a neutrino background.

Obtaining $\Omega_\chi h^2 \approx \Omega_{DM} h^2 \sim 0.12$ requires a self-annihilation cross-section of $\langle \sigma v \rangle \sim 3 \times 10^{-27}\,\mathrm{cm}^3\,\mathrm{s}^{-1}$, which is roughly what is expected for a new particle in the 100 GeV mass range that interacts at a scale similar to the weak interactions. This reasoning, called the WIMP miracle, has served as a strong motivation for DM candidates such as neutralinos (the lightest –neutral– particle in the standard supersymmetry spectrum), although they are very much constrained by the non-observation at direct detection experiments and at LHC, amongst other experimental probes. Another WIMP candidate, although somewhat ad hoc from a particle physics perspective, is a scalar dark matter particle [196]. The theoretical framework and experimental status of this possibility will be presented in Sect. 4.3 in the standard scenario, and Chapter 7 will additionally explore extensions of this scenario in the context of non-linear physics behind the EW sector of the SM.

Other candidates are considered for various different reasons, and DM may behave in very different ways. For instance Kaluza-Klein excitations appearing in models of universal extra dimensions [197] are also a WIMP candidate arising from a top-bottom approach. And, as seen in Chaps. 2 and 3, the strong CP problem may call for a new pGB, the axion which can be non-thermally produced via what is known as *the misalignment mechanism* (a scenario which will be presented in Sect. 4.4 below). Even lighter candidates exist, for instance in the form of Fuzzy CDM which are scalars with masses in the order of 10^{-22} eV and whose wave behaviour on astrophysical scales would explain the DM halos. As represented in Fig. 4.4 the candidate zoo is extremely diverse as a large number of very creative solutions are being continuously put forth (see Refs. [181, 198, 199] for a further review).

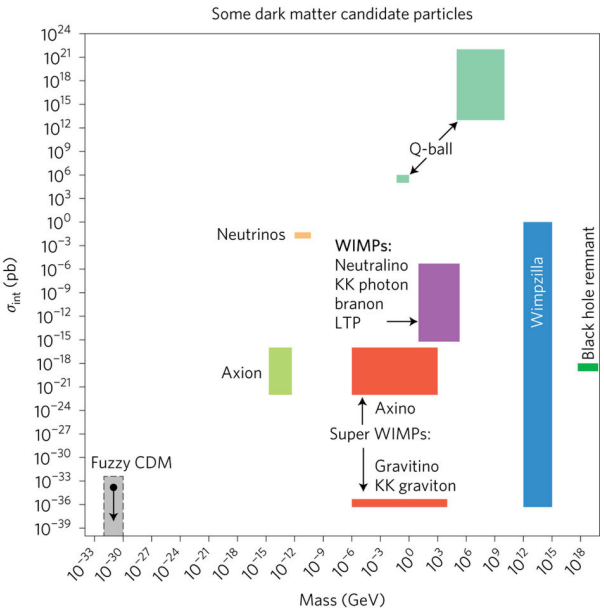

Figure 4.4: The Landscape of dark matter candidates: DM mass and cross section to SM particles for a set of DM candidates. KK stands for Kaluza-Klein, LTP refers to lightest time-parity odd particle, WIMP is weakly interacting massive particle and CDM is cold dark matter. Figure from Ref. [195].

4.3 SCALAR DARK MATTER: THE HIGGS PORTAL

Three types of renormalisable (marginal or relevant, i.e. dimension $d \leqslant 4$) interactions between the SM fields and DM are possible: i) Higgs-scalar DM; ii) hypercharge field strength-vector DM; iii) Yukawa type couplings to fermionic DM. Being the lowest dimension couplings of the ordinary world to DM, they are excellent candidates - beyond gravitational interactions - to provide the first incursions into DM, i.e. to be the experimental “portals" into DM. The scalar-Higgs portal, which we concentrate on in this thesis stands out as one

of the most economical explanation for DM, but is extremely constrained in its minimal realisation.

Assuming as customary a discrete Z_2 symmetry [202, 203] – under which the DM singlet scalar candidate S is odd and the SM fields are even to ensure DM stability – the Higgs-DM portal takes the form

$$\begin{aligned}\mathcal{L}_{SHP} &= \frac{1}{2}\partial_\mu S \partial^\mu S - \frac{m_0^2}{2}S^2 - \lambda_S S^2 \Phi^\dagger \Phi \qquad (4.5)\\ &= \frac{1}{2}\partial_\mu S \partial^\mu S - \frac{m_S^2}{2}S^2 - \lambda_S S^2 (2v h + h^2)\end{aligned}$$

where Φ denotes the $SU(2)_L$ Higgs field doublet, h the observed Higgs particle and λ_S is the Higgs portal coupling. m_S is redefined to include the contribution from the portal term.

The SM Higgs-DM portal in Eq. (7.1) (or *standard* portal) has been extensively explored in the literature [19, 204–221], and is almost completely excluded. Due do the simplicity of the model, its main phenomenological consequences can be reviewed very briefly. There are only two free parameters m_S and λ_S, and the results from the different observables can be plotted on a two-dimensional parameter space, in Fig. 4.5.

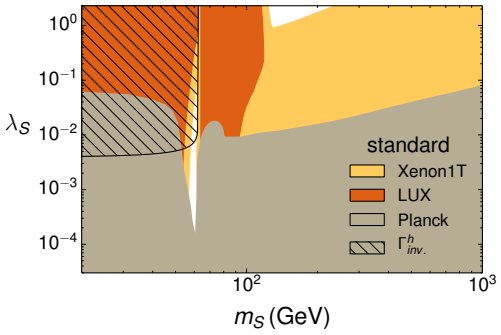

Figure 4.5: Excluded regions on the parameter space of the scalar Higgs portal model including current bounds from Planck [187], LUX [200], XENON1T [201] and from invisible Higgs width data. Figure taken from Ref. [1].

RELIC DENSITY The DM production mechanism of the scalar portal is that of thermal production (as opposed to the non-thermal case of axions that we will see below). Assuming that the S particles are in thermal equilibrium in the early universe, the relic density is determined by their annihilation rate into SM particles, in this case to one and two Higgses: $SS \to h \to WW/ZZ/hh$ and $SS \to hh$. Requiring the abundance not to exceed the observed value in Eq. (4.3), assuming S may either be the sole DM particle or a member of a larger DM sector, $\Omega_S h^2 \leqslant \Omega_{DM} h^2 \simeq 0.12$ excludes the region in grey in Fig. 4.5.

DIRECT DETECION DM-nucleon interactions occur in our scenario via Higgs exchange. The strongest bounds constrain the spin-independent cross section σ_{SI} for S on nucleons N. Again, S may be a member of a larger DM sector, in which case direct detecion bounds are to be rescaled: $\sigma_{SI}(S\,N \to S\,N) \times (\Omega_S/\Omega_{DM}) \leqslant \sigma^{lim}_{exp.}$. The current [200], and projected [201] direct detecion exclusion regions are shown in Fig. 4.5 for the standard Higgs portal scenario.

INVISIBLE HIGGS DECAY The decay channel $h \to SS$ is open for $m_S < m_h/2$, contributing to the Higgs invisible width Γ_{inv} at the LHC. Requiring $BR_{inv} = \Gamma_{inv}/(\Gamma_{inv} + \Gamma_{SM}) < 0.23$ [222], the excluded region is shown in hatched in Fig. 4.5.

INDIRECT SEARCHES DM can annihilate into two photons via a h particle, a process which is constrained by indirect dark matter searches from gamma-ray searches in dwarf

spheroidal galaxies (for the continuum spectrum) and the galactic centre (for gamma ray lines and spectral features), both searched for in the Fermi LAT [223, 224]. In the minimal scenario their impact is almost negligible with respect to the previous probes (see for instance Refs. [225] and [226]).

Fig. 4.5 thus illustrates quite clearly that this simple renormalisable DM proposal is almost completely excluded. However, there exist minimal extensions of the scalar portal which are still viable. For instance a recent work [226] proposed an extended scalar portal with two real scalar fields instead of one. They found that new annihilation and/or coannihilation channels involving the extra singlet allow to reproduce the correct DM relic abundance while avoiding the bounds from direct and indirect searches for any DM mass above 50 GeV, and thus "saving" the portal. Another scenario exists where the portal is saved or "reopened" which is the *non-linear HIggs portal*, which is a reformulation of the leading order interactions of a real scalar DM particle with the SM in the context of non-linearly realised EWSB, *i.e.* using the tool of chiral Lagrangians. The theory and phenomenology of this setup will be explored in Chapter 7.

4.4 AXIONIC DARK MATTER: THE MISALIGNMENT MECHANISM

Axions are one of the dark matter candidates which are strongly motivated by SM problems, in particular as they arise as a very elegant solution to the strong CP problem. As described in detail in Chapter 3, the Peccei-Quinn mechanism solves the strong CP problem via a global chiral $U(1)_{PQ}$, which is exact at the classical level and broken explicitly by anomalies. It is also broken spontaneously, and the associated pseudoGB is the axion. After the spontaneous breaking of the PQ symmetry the axion lives in a $U(1)$-symmetric vacuum manifold.

At the QCD phase transition, non-perturbative effects generate a potential for the axion. This potential, computed analytically through the dilute gas approximation [97] reads

$$V(a,T) = m_a^2(T) f_a^2 \left(1 - \cos\left(\frac{a}{f_a}\right)\right) . \tag{4.6}$$

[3] The PQ mechanism which takes a to its minimum, however, is not an instantaneous process and the axion field oscillates from a random initial value to its final value, zero. The oscillations around its minimum produce a coherent state of zero mode axions, i.e. a Bose-Einstein condensate [227]. This is known as the misalignment mechanism [228–230]. [4]

The energy density contained in axion oscillations is proportional to the initial value of the axion field $a(t_0) = \theta_0 f_a$ where $-\pi \leqslant \theta_0 \leqslant \pi$ is the initial vacuum misalignment angle, and its contribution to the relic density reads [232]

$$\Omega_a h^2 \approx 0.7 \left(\frac{f_a}{10^{12}\,\text{GeV}}\right)^{7/6} \left(\frac{\theta_i}{\pi}\right)^2 . \tag{4.7}$$

3 A recent precise calculation of this potential can be found in Ref. [141] and the authors show that there are up to $\mathcal{O}(1)$ differences with respect to the single cosine potential in Eq. (4.6). However, the behaviour around the minimum of both potentials is very similar (the largest differences being in around the maximums –see Ref. [141] for details–), and the present study of non-thermal production of axion dark matter can be tackled with the semi-classical approximation in Eq. (4.6).

4 Axion dark matter can also be produced thermally [231], see Ref. [232] for a pedagogical review in the case of hadronic axion.

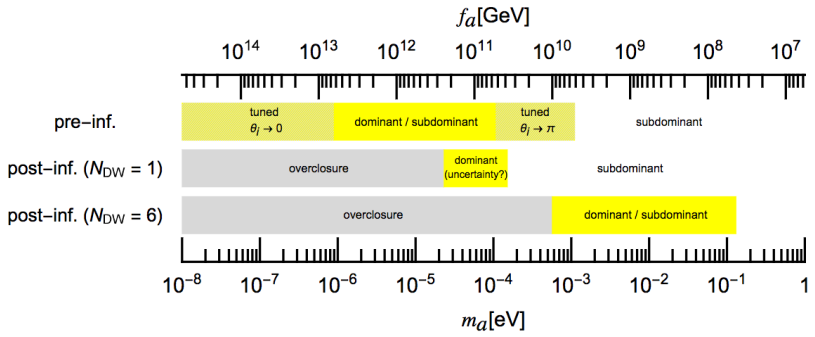

Figure 4.6: Predictions for the axion dark matter mass m_a for the decay constant f_a in the pre-inflationary PQ symmetry breaking scenario (first line), the post-inflation PQ symmetry breaking scenario with $N_{DW} = 1$ (second line), and that with $N_{DW} = 6$ (third line). The yellow regions correspond to the mass ranges in which the axion can be the main constituent of dark matter. The gray regions are excluded since the relicaxion abundance exceeds the observed dark matter abundance. The gray hatched regions correspond to the mass ranges in which more than 10% tuning of θ_i is required in order to explain the observed dark matter abundance. Figure and description adapted from Ref. [241].

If PQ symmetry breaking takes place after inflation θ_i will take on different values in different patches of the universe. The average contribution is [233]

$$\Omega_a h^2 \approx 0.3 \left(\frac{f_a}{10^{12}\,\mathrm{GeV}} \right)^{7/6} . \tag{4.8}$$

Comparing with the measured cold dark matter density $\Omega_{DM} h^2 \approx 0.12$ in Eq. (4.3) implies that axions with $f_a \approx 4.5 \times 10^{11}\,\mathrm{GeV}$ ($m_a \approx 2\,\mu\mathrm{eV}$) provide dark matter, whereas larger scales and smaller masses are excluded. Remarkably, cosmology gives a lower bound on the axion mass (and an upper bound on f_a) [234–236], thus defining the axion window which was depicted in Fig. 3.2 from Chapter 3. However, in this scenario where the axion field takes different values in different spatial regions, this gives rise to topological defects such as domain walls and strings, which also store energy that can behave as dark matter as they decay. The precise computation being more involved and model-dependent, as the result also depends on the domain wall number N_{DW}, see Fig. 4.6, it is important to note that they can be of the same order as the contribution from the misalignment mechanism. The topic is still open to discussion as simulations are finding axion dark matter for different values in the $(1 - 150)\,\mu\mathrm{eV}$ range [237–240].

PQ symmetry breaking may, however, take place before inflation, in which case a region in which the axion field takes a certain value $a(t_0)$ is rapidly expanded during the inflationary epoch. As a consequence, the misalignment angle has a single uniform initial value θ_i within the observable universe. The relic abundance in the regime $|\theta_i| \ll \pi$ is given by [242]

$$\Omega_a h^2 \approx 0.35 \left(\frac{\theta_i}{0.001} \right)^2 \times \begin{cases} \left(\frac{f_a}{3\times 10^{17}\,\mathrm{GeV}} \right)^{1.17} & \text{for} \quad f_a \lesssim 3 \times 10^{17}\,\mathrm{GeV} \\ \left(\frac{f_a}{3\times 10^{17}\,\mathrm{GeV}} \right)^{1.54} & \text{for} \quad f_a \gtrsim 3 \times 10^{17}\,\mathrm{GeV} \end{cases} . \tag{4.9}$$

The relic abundance depends not only on f_a but also on the initial misalignment angle θ_i, hence there is a larger freedom in the value of f_a, but large values can only be implemented at the cost of a tuning in θ_i, which must not be very large in order not to overpopulate the Universe. Apart from computations of the relic abundance, axion DM is being searched for by haloscopes, as it was described in Sect. 3.3.1. The results from these searches are typically plotted in the $(m_a, g_{a\gamma\gamma})$ parameter space plots, such as Fig. 3.1 and they are quite striking in their extremely large sensitivity, although they have the drawback that they rely on axions constituting the whole of dark matter.

Part III

SPIN ZERO WINDOWS TO NEW PHYSICS

5 THE AXION AND THE GOLDSTONE HIGGS

5.1 TWO FINE-TUNING PROBLEMS CONSIDERED AT ONCE: MOTIVATIONS AND SETUP

The standard dynamical solution to the strong CP problem, which was presented at the end of Chapter 2 and thoroughly explored in Chapter 3, is based on extending the SM with a spontaneously broken global axial "Peccei-Quinn" symmetry, $U(1)_{PQ}$, whose associated NGB is the "axion" $a(x)$ [7, 128, 129]. In its most economic and traditional realization, which is the one to be considered here, the matter sector of the SM needs to be extended, but not its gauge group. As a consequence, independently of the model details, the product of the axion mass m_a and scale f_a obeys then the relation of Eq. (3.5), as the mass of the axion arises from non-perturbative QCD effects that break the global PQ symmetry. The couplings to of these axions to ordinary matter are proportional to $1/f_a$, constituting the downside of these models, as phenomenological and astrophysical constraints [154, 243] tend to require then extreme values for f_a, typically : $10^9 < f_a < 10^{14}$ GeV, that is, $10^{-7} < m_a < 10^{-2}$ eV, as concluded in Sect. 3.3. Both paradigmatic examples of invisible axion theories, presented in Sects. 3.1.2 and 3.1.3 require to add to the SM spectrum a scalar singlet S whose vacuum expectation value breaks PQ and sets the scale f_a, the KSVZ model [9, 10] additionally requiring extra vectorial fermions. They guide the current very intense experimental search which was reviewed in Sect. 3.3.

One major drawback of extensions of the Standard Model which embed an invisible axion is that they are strongly fine-tuned in their scalar potential, as f_a is in general many orders of magnitude larger than the observed electroweak scale. Indeed, the Higgs and axion sectors are not watertight but communicate through the scalar potential, which includes S-Higgs interactions which would pull the Higgs mass towards the high scale. The range of f_a mentioned above may be loosened in invisible axion models by assuming several exotic matter representations with ad-hoc cancellations of their contributions to the axion-photon-photon couplings [140, 244], avoiding then some of the most stringent astrophysical constraints. Nevertheless, purely hadronic bounds still hold even in this case, which still imply a few orders of magnitude difference between the value of f_a and the electroweak scale [168], see Sect. 3.3. A coherent picture of the solution to the strong CP problem is thus missing. [1]

It is obviously possible to implement the (high-scale) invisible axion solution to the strong CP problem, without the Higgs mass suffering from the electroweak hierarchy problem, though, assuming that the Higgs mass is protected by some symmetry: supersymmetric models at the electroweak scale and the so-called "composite Higgs models" are examples of it. The latter are within the class of models in which the Higgs particle is protected from putative higher scales via a pseudo-Nambu-Goldstone boson ancestry [8, 245, 246], which were presented in Sect. 1.3, and we focus in this chapter on this avenue (named in what follows

1 In addition, quantum gravitational effects violate global symmetries such as the PQ symmetry, and Planck-suppressed higher dimension operators are a threat unless the f_a scale is small. This aspect of invisible axion models with very large f_a is not addressed here.

"Goldstone Higgs" for brevity). In their most economical realization, the gauge group is just the SM one while both the Higgs and the longitudinal degrees of freedom of the electroweak bosons originate as the GBs from a global $SO(5)$ symmetry [54, 56] spontaneously broken to $SO(4)$ at some high scale Λ_s.

It would be straightforward and trivial to extend such theories so as to implement on them a PQ solution, by simply adding at a higher scale supplementary matter fields specifically for that purpose. Here, instead, we focus on the minimal possible extension. That is, we explore within $SO(5)/SO(4)$ whether the minimal exotic fermionic setup of partial compositeness suffices to the purpose. Indeed, a recurrent characteristic in Goldstone Higgs models is the implementation of partial compositeness via exotic fermion representations which are vectorial with respect to the SM gauge group $SU(2)_L$, in the sense that the left and right-handed components are in equal representations of $SU(2)_L$, much as in KSVZ invisible axion theories. We will take advantage of this fact in this chapter, and it will be shown that a minimal scalar extension is enough to make the models PQ invariant.

In partial compositeness, the global symmetry and spectra forbid tree-level Yukawa couplings and the SM masses are mediated instead by the exotic vectorial fermions. This imposes stringent relations among the parameters and couplings of that exotic fermion sector, which will be shown to point to a reduced phenomenological parameter space when a Peccei-Quinn symmetry is implemented using those same fermions.

The question will first be formulated using the complete renormalizable model [59] presented in Sect. 1.3.3, which in its scalar part is a linear sigma model including a new scalar particle, σ, singlet under the gauge group: the linear σ model for the composite Higgs. The model can be considered either as an ultimate theory describing elementary fields (instead of composite ones), or as a renormalizable version of a deeper dynamics, much as the linear σ model is to QCD; in the limit of very heavy σ mass, the non-linear regime is reached. A clear advantage of using first a complete renormalizable model for a Higgs with GB ancestry is that it allows to gauge how costly the implementation of the PQ symmetry for composite Higgs constructions is, in terms of extending its spectrum and in particular its scalar sector, a task not feasible or at least very obscure in non-renormalizable formulations. Moreover, the need in invisible axion constructions to strongly raise f_a above the electroweak scale suggests its pairing with the limit of a very heavy σ particle, as the mass of the latter is not protected and a light σ could raise issues of fine-tuning. The energy scales involved are those involved in GB Higgs models: the electroweak scale, v, the Goldstone-boson scale f, the scale of the global symmetry breaking Λ_s –all of which were presented in the overview of scales at the end of Sect. 1.3.2– plus two more:

- The axion scale f_a, which is many orders of magnitude larger than any of the above, given the experimental and observational constraints subject to Eq. (3.5). Such a large value is naturally accommodated when it corresponds to the vev of a scalar S which is a singlet of both the SM and $SO(5)$.

- The σ mass, which can range from few hundred of GeV to infinitely heavy in the strong interacting regime. The latter avoids fine-tuning issues by construction. This mass scale is absent in non-linear realizations, which are akin to a very heavy σ decoupled from the spectrum, much as the chiral Lagrangian for QCD with a light pion decay constant f_π corresponds to the infinite mass limit of the renormalizable linear sigma model for

QCD. Alternatively, when the σ particle is present in the spectrum, the scalar potential may tend to homogenize the size of all singlet parameters, e.g. the σ mass and f_a. Note that when minimally extending the renormalizable model to encompass an axion solution to the strong CP problem, the scalar σ cannot be charged under the PQ symmetry as it belongs to a real scalar five-plet of $SO(5)$; S and σ are thus independent fields.

By construction, *the mass of the Goldstone Higgs will not be destabilized by the high scale* f_a *as far as the model preserves the approximate* $SO(5)/SO(4)$ *symmetry pattern*. Nevertheless, the simultaneous presence of the very high scale f_a and the lower scales immediately raises the question of whether some of the axion-related parameters of the Lagrangian may have to be fine-tuned, e.g. in the scalar potential. In particular, the exotic vectorial fermion masses in traditional invisible axion models "à la KSVZ" stem from the vev of S, $\langle S \rangle \sim f_a$, a fact that could be in tension with the requirement of much lighter fermionic states in composite Higgs models. This issue will be addressed discussing the technical naturalness of (dimensionless) mass parameters in the exotic fermion sector.

A precision is pertinent on the size of the exotic fermion masses, though. The comment above expecting them to be of order Λ_s –that is, not very far from the TeV region– is the natural expectation if no higher scales were present in Nature to which the system is sensitive. Here instead, in particular with a renormalizable model which is in itself ultraviolet complete, one cannot exclude that some $SO(5)$-invariant mass parameters may be of the order of the highest scale in the theory, the f_a scale, as quantum corrections may equalize all singlet scales, depending in particular on the couplings in the scalar potential. For instance, fermionic masses of $\mathcal{O}(f_a)$ could be possible for singlet fermions. In fact these contributions are not expected to destabilize the relative size of the Higgs mass, as the latter must be proportional to symmetry-breaking parameters. However, it remains to be verified, with a complete one-loop study of the scalar potential, whether the overall scale f would be pushed to large values in the presence of very heavy fermion singlets. In Ref. [247] it was shown that some of the exotic fermion masses could indeed be larger than the overall TeV scale and still comply with the Higgs and fermion masses, as far as other fermions were lighter than that scale. For the sake of completeness, such particular cases will be included in the discussion below, although in most of our study we will take the most conservative option of assuming implicitly "light" exotic fermion masses $\sim \Lambda_s$, unless otherwise stated. In any case, the phenomenological predictions for axion-photon couplings will be independent of those fermion mass values.

5.2 A RENORMALIZABLE MODEL: THE LINEAR SIGMA MODEL

Following Ref. [59], consider the minimal SO(5) linear σ-model, with the symmetry softly broken to SO(4) and fermionic content given by:

$$\begin{aligned}\mathcal{L}_{ferm} = \Big\{ & \bar{q}_L i\not{D} q_L + \bar{t}_R i\not{D} t_R + \bar{\psi}^{(5)} i\not{D} \psi^{(5)} + \bar{\psi}^{(1)} i\not{D} \psi^{(1)} \\ & - \Big[\bar{\psi}^{(5)}_L M_5 \psi^{(5)}_R + \bar{\psi}^{(1)}_L M_1 \psi^{(1)}_R + y_1\, \bar{\psi}^{(5)}_L \phi\, \psi^{(1)}_R + y_2\, \bar{\psi}^{(5)}_R \phi\, \psi^{(1)}_L \\ & + \Lambda_1\, (\bar{q}_L \Gamma_{2\times 5})\, \psi^{(5)}_R + \Lambda_2\, \bar{\psi}^{(5)}_L\, (\Gamma_{5\times 1} t_R) + \Lambda_3\, \bar{\psi}^{(1)}_L t_R + h.c. \Big] \Big\} \\ + & \left\{ \psi \to \psi', \quad t_R \to b_R, \quad (M, \Lambda, y)_i \to (M', \Lambda', y')_i \right\}, \end{aligned} \tag{5.1}$$

where q_L, t_R and b_R denote respectively the SM doublet and singlet fermions of the third generation, and ϕ is a SO(5) scalar five-plet which contains the Higgs field. $\psi^{(5)}$ and $\psi^{(1)}$ denote exotic fermions in the fundamental and singlet representations of SO(5), respectively.[2] The ensemble of exotic fields can be decomposed in terms of $SU(2)_L$ eigenstates as:

$$\begin{gathered} \psi^{(5)} \sim (X^{(5)}, Q^{(5)}, T^{(5)}) \quad , \quad \psi'^{(5)} \sim (Q^{(5)\prime}, X^{(5)\prime}, B^{(5)}) \,, \\ \psi^{(1)} \sim T^{(1)} \quad , \quad \psi'^{(1)} \sim B^{(1)} \,, \\ \phi = \left(H^T, \tilde{H}^T, \sigma\right)^T \,, \end{gathered} \tag{5.2}$$

where T, B and σ are singlets under $SU(2)_L$, while all other fields are $SU(2)_L$ doublets. Tab. 5.1 shows the SM charges for these fields, as well as for other fermion representations to be considered later on. It shows as well the charges of various SO(5) representations under the global group $U(1)_X$, which is customarily added to the global symmetry group to ensure correct hypercharge assignments for the SM fermions, with the pattern of spontaneous symmetry breaking given by

$$SO(5) \times U(1)_X \to SO(4) \times U(1)_X \approx SU(2)_L \times SU(2)_R \times U(1)_X \,. \tag{5.3}$$

The hypercharge Y corresponds then to a combination of the $U(1)_X$ and $SU(2)_R$ generators (denoted respectively by X and $\Sigma^{(3)}_R$) given by

$$Y = \Sigma^{(3)}_R + X \,. \tag{5.4}$$

Two $U(1)_X$ charge values turn out to be compatible with SM hypercharge assignments: $2/3$ and $-1/3$.

The heavy -exotic- mass eigenstates result from diagonalizing the mass terms containing $\psi^{(5)}$ and $\psi^{(1)}$, shown in the 2nd and 3rd lines in Eq. (5.1). The latter describe the most general SO(5)-invariant mass terms, but for two of them which break SO(5) explicitly and softly: those proportional to Λ_1, Λ_2 (plus their primed counterparts for the bottom sector). Γ_i

2 This model will be denoted $MCHM_{5-1-1}$ (minimal composite Higgs model $5-1-1$) in a notation that keeps track of the SO(5) representation in which the exotic partners of the SM quark doublet, top and bottom are embedded, see Sect. 5.4.

are dimensionless matricial coefficients. The quantities $(\Lambda_1\Gamma_{2\times5})$ and $(\Lambda_2\Gamma_{5\times1})$ act like spurions breaking the global SO(5) symmetry; they are expected to be small compared to the overall SO(5) scale Λ_s and thus to the overall scale of the exotic fermion masses M_i. They induce electroweak symmetry breaking through their one-loop contribution to the Coleman-Weinberg potential: they generate the electroweak scale v and provide a mass for the Higgs particle which is small compared to Λ_s; they are thus expected to be in general about one or two orders of magnitude smaller than Λ_s, e.g. in the hundreds of GeV-TeV range. The Λ_i terms are also essential in generating light fermion masses. Indeed, in the partial compositeness paradigm the direct SM Yukawa coupling is forbidden by the global symmetry, and a chain of interactions mediated by heavier fields is required in a seesaw-like structure. For instance, in the renormalizable model at hand the dominant contribution to the $\bar{t}_L t_R$ mass term corresponds schematically to[3]

$$q_L \xrightarrow[\Lambda_1]{} Q_R \xrightarrow[M_5]{} Q_L \xrightarrow[y_1\langle\tilde{H}\rangle]{} T_R^{(1)} \xrightarrow[M_1]{} T_L^{(1)} \xrightarrow[\Lambda_3]{} t_R\,, \tag{5.5}$$

and analogously for the bottom mass, leading to

$$m_t \sim y_1 \frac{\Lambda_1\Lambda_3}{M_1M_5}\,v\,, \qquad\qquad m_b \sim y_1' \frac{\Lambda_1'\Lambda_3'}{M_1'M_5'}\,v\,. \tag{5.6}$$

It is easy to verify that the renormalizable Lagrangian in Eq. (5.1) is *not* PQ invariant. Note nevertheless that –as customary in most partial compositeness realizations– exotic vectorial fermions are by construction present, which suggests the possibility of a PQ-invariant extension "à la KSVZ". The novel ingredient inbuilt in partial compositeness scenario is precisely the chain of interactions needed to generate fermion masses via Yukawa couplings with exotic heavy fermions. This constraint will strongly reduce the freedom in the relative choice of PQ charges for the exotic fermions, and increase predictivity. We explore next the possible minimal PQ invariant extensions of the linear SO(5)/SO(4) sigma model [59] with its original fermion content as shown in Eq. (5.1), enlarging only its scalar sector.

The need of a PQ scale much higher than the overall SO(5) scale Λ_s suggests to introduce it through the vev of a scalar field (or fields) S (S_i), singlet under the SM and under the global SO(5) symmetry and charged under PQ, e.g.,

$$S(x) = \frac{f_a + \rho(x) + i a(x)}{\sqrt{2}}\,, \tag{5.7}$$

where f_a sets the PQ scale as the vacuum expectation value (vev) of S, $\langle S\rangle \sim f_a$, the real field $\rho(x)$ is expected to be heavy [4] and the imaginary part is to be identified with the axion $a(x)$, which is massless at the classical level.

With only one five-plet scalar in the spectrum of the model, it is not possible to give PQ charge to this field, as an even number of components is needed for it to be charged.[5] The

3 There are subleading contributions to the light fermion masses which do not depend on Λ_3, see Ref. [59]. They could lead to PQ solutions other than those considered below, which focus on the leading option shown in Eq. (5.6).

4 Of $\mathcal{O}(f_a)$. Its dynamics is thus not relevant at low energies; in particular, $\rho(x)$ can be considered integrated out of the spectrum for some cases discussed below with very high f_a scale.

5 A ten-component SO(5) multiplet must be built (e.g. out of two scalar five-plets), in order for it to be PQ charged and still contain all four components of the Higgs doublet: H and its conjugate $\tilde{H}$. We defer this alternative extension path to a future exploration.

fermions instead can easily acquire PQ charges. There are many options for selecting which fermionic mass parameters in the Lagrangian are promoted to dynamical fields so as to implement the PQ symmetry. We will first derive general constraints which are valid for the case in which either just one or more than one scalar singlet would be added.

Extending the model spectrum by only singlet scalars S_i, the most general renormalizable model would correspond to promoting to independent dynamical fields *all* M_i and Λ_i (that is, M_1, M_5 and $\Lambda_{1,2,3}$) parameters in the Lagrangian in Eq. (5.1),

$$M_i \to \kappa_i S_{Mi}\,, \tag{5.8}$$

$$\Lambda_i \to \lambda_i S_{\Lambda i}\,, \tag{5.9}$$

where κ_i and λ_i are constants and S_i are independent fields with generically $\langle S_i\rangle \sim f_a$. κ_i and λ_i are necessarily small if the physical value of the exotic fermion masses is $\sim \Lambda_s$. This is technically natural in the 't Hooft sense if the small κ_i and λ_i values are protected by a symmetry: we find that indeed all models explored with $\mathcal{O}(\Lambda_s)$ fermion masses are protected by chiral symmetries under which the fermions transform but not the scalars. Alternative setups with κ_i and λ_i of $\mathcal{O}(1)$ are possible a priori by allowing some of the M_i and Λ_i values to be of $\mathcal{O}(f_a)$, so as to cancel the f_a dependence between the numerator and denominator in Eq. (5.6); this may be a safe option from the point of view of naturalness and stability of the scalar potential only if the Λ_i parameters involved do not correspond to terms breaking the global symmetry and if the choice is protected at the quantum level, which in practice points to promoting singlet fields, see further below. Nevertheless, although the contributions of heavy $SO(5)$ singlet fermions will not destabilize the Higgs mass, it could affect and destabilize the value of the overall scale f itself: this issue cannot be settled without a specific one-loop analysis of the potential which is beyond the scope of this chapter. In the absence of such analysis, we choose not to discard this type of solutions below. For the results in the rest of this section, all κ_i and λ_i will be general arbitrary parameters.

As previously done for fermions, see Eq. (**??**), we refer to the PQ charges of scalars as $\beta(\phi)$, where ϕ is a generic scalar. For instance, $\beta(S_{Mi})$ and $\beta(S_{\Lambda i})$ will denote the PQ charges of the fields resulting from promoting to dynamical variables the fermionic mass parameters, as indicated in Eqs. (5.8) and (5.9). The following general set of constraints follows for the top sector[6] in order to achieve PQ invariance:

$$\beta(\psi_R^{(5)}) = \beta(q_L) - \beta(S_{\Lambda 1})\,, \tag{5.10}$$

$$\beta(\psi_L^{(5)}) = \beta(q_L) - \beta(S_{\Lambda 1}) + \beta(S_{M5})\,, \tag{5.11}$$

$$\beta(\psi_R^{(1)}) = \beta(q_L) - \beta(S_{\Lambda 1}) + \beta(S_{M5})\,, \tag{5.12}$$

$$\beta(\psi_L^{(1)}) = \beta(q_L) - \beta(S_{\Lambda 1}) + \beta(S_{M5}) + \beta(S_{M1})\,, \tag{5.13}$$

$$\beta(t_R) = \beta(q_L) - \beta(S_{\Lambda 1}) - \beta(S_{\Lambda 3}) + \beta(S_{M5}) + \beta(S_{M1})\,, \tag{5.14}$$

$$\beta(S_{\Lambda 2}) = \beta(S_{\Lambda 3}) - \beta(S_{M1})\,, \tag{5.15}$$

$$0 = \beta(S_{M1}) + \beta(S_{M5})\,. \tag{5.16}$$

6 We allow here top and bottom quarks charged under PQ. Alternatively, it would be possible to charge any of the other two light quark generations. If mixings among light families are taken into account, the generalization to three families may imply charging under PQ all three fermion generations, depending on the model.

The last two constraints, Eqs. (5.15) and (5.16), are respectively those stemming from the Lagrangian terms proportional to Λ_2 and y_2. They are special in the sense that the presence in the Lagrangian of the parameters Λ_2, Λ_2', y_2, y_2' is not strictly necessary, as they only induce subleading contributions to the top and bottom masses [59]. The absence of some or all of them may be protected from radiative instability by symmetries; furthermore, the PQ symmetry itself can guarantee their absence at all orders depending on its implementation, as illustrated further below. Would they be absent in a given model, the number of constraints implied by PQ charge conservation would correspondingly decrease and the parameter space would be enlarged in consequence.

The set of Eqs. (5.10)-(5.16) is accompanied by the analogous constraints stemming from the bottom sector, obtained from the above via the replacement

$$\left\{\psi \to \psi', \quad t_R \to b_R, \quad (M, \Lambda)_i \to (M', \Lambda')_i\right\}. \tag{5.17}$$

They amount in total to 14 equations with 21 free parameters, which leaves much freedom in the choice of dynamical parameters and PQ charges. The individual PQ charges of left-handed and right-handed fields are not physical *per se*: the only quantities relevant for the computation of the color and electric anomalies are the chiral differences,

$$\Delta\Psi \equiv \beta(\Psi_L) - \beta(\Psi_R), \tag{5.18}$$

where Ψ denotes generically a fermion. Here and in what follows *we will refer to fermions with a non-vanishing* $\Delta\Psi$ *as having a chiral PQ charge.* While this definition for the vectorial fermions $\psi^{(1)}$ and $\psi^{(5)}$ and their primed counterparts is straightforward, the chiral PQ charges of the SM top and bottom fields (whose left and right components are not directly coupled in the Lagrangian Eq. (5.1)) will be defined as

$$\Delta t \equiv \beta(q_L) - \beta(t_R), \qquad \Delta b \equiv \beta(q_L) - \beta(b_R). \tag{5.19}$$

Note that charging q_L under PQ implies charging both the top and bottom left-handed quarks, but this does not necessarily imply $\Delta t \neq 0$ and/or $\Delta b \neq 0$. *As for fermions only the chiral PQ differences are physical,* Δt *and* Δb *will be retained as the physically relevant quantities to analyze the top and bottom sectors.*

The fermionic PQ chiral charges can be expressed in terms of the PQ charges of the scalar fields:

$$\begin{aligned} &\Delta\psi^{(5)} = \beta(S_{M5}), \qquad \Delta\psi^{(1)} = \beta(S_{M1}), \\ &\Delta t = \beta(S_{\Lambda 1}) + \beta(S_{\Lambda 3}) - \beta(S_{M1}) - \beta(S_{M5}), \end{aligned} \tag{5.20}$$

plus those for the bottom sector obtained via the replacement in Eq. (5.17). The quantities E and N can then be expressed as general functions of the fermionic PQ chiral charges, resulting in

$$E = \frac{1}{3}\left[38\Delta\psi^{(5)} + 23\Delta\psi'^{(5)} + 4\Delta\psi^{(1)} + \Delta\psi'^{(1)} + 4\Delta t + \Delta b\right], \tag{5.21}$$

$$N = \frac{1}{2}\left[5\,\Delta\psi^{(5)} + 5\,\Delta\psi'^{(5)} + \Delta\psi^{(1)} + \Delta\psi'^{(1)} + \Delta t + \Delta b\right]. \tag{5.22}$$

Using Eq. (5.20), these equations allow to express the ratio E/N in terms of the PQ charges of the scalar fields,

$$\frac{E}{N} = \frac{2}{3}\frac{34\beta(S_{M5}) + 22\beta(S_{M5'}) + 4\beta(S_{\Lambda 1}) + 4\beta(S_{\Lambda 3}) + \beta(S_{\Lambda 1'}) + \beta(S_{\Lambda 3'})}{4\beta(S_{M5}) + 4\beta(S_{M5'}) + \beta(S_{\Lambda 1}) + \beta(S_{\Lambda 3}) + \beta(S_{\Lambda 1'}) + \beta(S_{\Lambda 3'})}\,. \tag{5.23}$$

The number of possible PQ invariant setups reduces if some of the dimensionful parameters are not promoted to dynamical fields, or if several singlet scalar fields are identified among themselves. In fact, when more than one extra scalar singlet is present, relations among their charges may need to be established (for instance through couplings in the scalar potential) if we would only wish to implement one PQ symmetry, and thus a single axion, instead of a plethora of axial $U(1)$ symmetries with their corresponding GBs. As stated, from now on we focus on analyzing the minimal addition of a single scalar singlet S. Note that in this case each charge $\beta(S_i)$ is either 0 or $\pm\beta(S)$, depending on whether a coupling is promoted to S or $S^\dagger$.

5.3 EXTENSION BY ONLY ONE SCALAR SINGLET S: THE RENORMALIZABLE MODEL

In order to gain perspective, two extreme setups with only one extra scalar singlet S will be explored in detail for the renormalizable model presented in the previous section: i) the case in which only one fermion is chirally charged under PQ, and ii) the option in which all fields and couplings are allowed to be freely and arbitrarily charged. For both cases, the values of E/N corresponding to the maximum and minimum $|g_{a\gamma\gamma}|$ attainable will be evaluated. This will allow a comparison with the predictions of recent updated analysis of the standard KSVZ and DFSZ theories. We will first develop the discussion assuming implicitly that all the exotic fermion sector has masses of $\mathcal{O}(\Lambda_s)$, to discuss next which ones among the solutions could *a priori* allow instead $\mathcal{O}(f_a)$ fermion mass parameters.

5.3.1 *Only one exotic fermion representation chirally charged under PQ*

The rationale for considering first only one exotic fermion charged is simplicity to illustrate the procedure, and also to allow an easy comparison with recent updated analyses of the standard KSVZ and DFSZ theories [140, 244], which start by extending the SM fermionic sector by only one exotic fermion. There is otherwise no special advantage or economy in preventing more than one fermion (among those *required* by the composite Higgs model) to be chirally charged under PQ, and this general option will be explored later on.

All PQ-invariant solutions of the composite Higgs model that assume only one heavy exotic fermion charged under PQ require either $y_2 = 0$ or $y_2' = 0$ in order to implement PQ invariance, as otherwise the PQ charges of both exotic fermions are linked, see Eq. (5.16). Tab. 5.2 displays different examples of this kind, together with their corresponding phenomenological predictions for axion-photon interactions.

A simple example is to charge under PQ only S and the $SO(5)$ fermion singlet $\psi_L^{(1)}$, by promoting the mass M_1 and Λ_3 to dynamical variables:

$$\begin{aligned} M_1 &\to \kappa_1 S\,, \\ \Lambda_3 &\to \lambda_3 S\,. \end{aligned} \tag{5.24}$$

$M_1 = \kappa_1 f_a$ is thus generated dynamically, together with the coupling responsible for the decay of the exotic quarks into SM quarks $\Lambda_3 = \lambda_3 f_a$. The application of this prescription to Eq. (5.1) renders a PQ symmetric Lagrangian, with $\psi_L^{(1)}$ charged under PQ and $\psi_R^{(1)}$ uncharged.[7] Furthermore, the condition $y_2 = 0$ is protected from quantum instabilities by the PQ symmetry itself. In turn, the very small values required for the parameters κ_1 and λ_3 (assuming M_i masses not higher than 10 or 100 TeV as usual in composite Higgs models) are natural in 't Hooft sense [6]. Indeed, they are protected by a chiral symmetry: that in which only $\psi_L^{(1)}$ transforms, and neither S nor any other field does. This is a pattern which will hold for basically all cases to follow: as the Lagrangian parameters which are being promoted to dynamical fields are fermionic mass parameters, their absence should be expected to be related to new chiral symmetries, rendering technically natural the choice of small values for the κ_i and λ_i parameters.

An alternative simple solution also with only one exotic heavy field charged under PQ is given by promoting to dynamical fields the parameters relevant for the five-plet fermionic field $\psi^{(5)}$,

$$\begin{aligned} M_5 &\to \kappa_5 S\,, \\ \Lambda_1 &\to \lambda_1 S\,. \end{aligned} \tag{5.25}$$

This solution can be realized charging under PQ only $\psi_R^{(5)}$ and S, which requires $y_2 = 0$. Again, the small values phenomenologically required in this case for κ_5 and λ_1 are technically natural, as in their absence the Lagrangian acquires a chiral symmetry under which only $\psi_R^{(5)}$ would transform. The main contrast with the previous example is that here a parameter associated to a symmetry-breaking term, Λ_1, has been promoted to dynamical field. Intuitively, it is expected that its value should be smaller than those corresponding to $SO(5)$ invariant terms, such as the M_i diagonal mass terms or the Λ_3 coupling. In other words, a dynamically promoted Λ_1 requires a slightly stronger adjustment for the λ_1 parameter than in the previous example (e.g. by one or two orders of magnitude). For this reason it may be preferred to avoid solutions which promote Λ_1 or Λ_2 to dynamical fields, although strictly speaking they are still technically natural solutions and thus valid ones. All options in which M_5 is promoted to a dynamical field require Λ_1 or Λ_2 to be also dynamical, except if a SM quark is simultaneously allowed to acquire a chiral PQ charge,[8] see Tab. 5.2; this case belongs then to the class of solutions with more than one PQ-charged fermion to be discussed later on.

5.3.1.1 *One exotic fermion charged, with mass parameters of* $\mathcal{O}(f_a)$

While the bulk of the solutions is that discussed above with all fermion masses around the TeV range, we consider here a few particular additional solutions: those with still only one fermion chirally charged, although assuming now that it is a very heavy exotic one (and all SM fields uncharged). This option is appealing in the sense that, if such a large scale exists in

7 An analogously economical and natural model consists in charging instead $\psi^{(1)\prime}$, with M_1' and Λ_3' becoming dynamical.

8 Analogous putative solutions with only a singlet exotic fermion (M_1) plus a SM fermion chirally charged under PQ, and no dynamical Λ_i, are not possible because the contribution to the color anomaly cancels in that case, leaving the strong CP problem unsolved.

Nature, dimensionful dynamical parameters of the complete Lagrangian may tend to be of that order, if they correspond to terms invariant under the lower energy symmetries (the SM gauge group and the global $SO(5)$ symmetry in the case under discussion). In our Lagrangian Eq. (5.1) M_1, M_5 and Λ_3 are of this kind, while only the terms proportional to Λ_1 and Λ_2 break $SO(5)$ (and analogously for the primed counterparts of the bottom sector). Intuitively, the dimensionful couplings that involve only singlet fields, and are therefore insensitive to the $SO(5)$ structure, are expected to be of the order of the largest scale in Nature to which they can connect. If that sector is decoupled from the non-singlet one, small parameters will not be required elsewhere either. This point of view would select M_1 and Λ_3 as putative scales of $\mathcal{O}(f_a)$. Indeed, among the solutions of the Lagrangian Eq. (5.1) gathered in Tab. 5.2:

- The solution in Eq. (5.24) with M_1 and Λ_3 dynamical (and/or its primed counterpart) does not require any tuning of the parameters κ_3 and λ_1. That is, both of them can be in this case of $\mathcal{O}(1)$, see nevertheless the caveats regarding the stability of the scale f after Eq. (5.9). The singlet and non-singlet sectors are disconnected, as the PQ symmetry itself forbids the presence of y_2 (or y_2'). The f_a dependence cleanly cancels in the SM mass expressions in Eq. (5.6); the Yukawa coupling y_1 (or y_1') does not requires fine-tuning either. These models are depicted by blue lines in Fig.5.1a: $E/N = 8/3$ for the solution in the top sector (lower line), and $2/3$ for that in the bottom sector (upper line).

- In contrast, the algebraic solution in which M_5 is the only mass parameter which becomes dynamical (and large, with $\kappa_5 \sim \mathcal{O}(1)$), with $\psi_R^{(5)}$ and the SM fermion q_L charged under PQ, would be possible only at the unacceptable price of a very large Yukawa coupling $y_1 \sim f_a M_1/(\Lambda_1\Lambda_3) \gg 4\pi$, well outside its perturbative range. This is because in the expression for the light fermion masses, Eq. (5.6), no other mass parameter is large enough so as to compensate the $M_5 \sim f_a$ dependence of the denominator.

- The solutions in which either Λ_1 or Λ_2 would be of $\mathcal{O}(f_a)$ (that is, λ_1 or λ_2 of $\mathcal{O}(1)$) seem also unacceptable, for the naturalness reasons explained. From the sole point of view of the SM fermion masses in Eq. (5.6) they could be acceptable, in particular those in which the f_a dependence cancels between numerator and denominator. The question that would need clarification, though, is whether a large Λ_1 and/or Λ_2 would induce inordinately large $SO(5)$-breaking terms in the effective potential, rendering it unstable and spoiling the GB character of the Higgs field. Note that the electroweak scale v and the Higgs mass must be ultimately proportional to the only $SO(5)$-breaking parameters of the model, $\Lambda_{1,2}$, unless ad-hoc fine-tunings are implemented in the scalar potential. In the absence of a satisfactory justification, it is safer to disregard these solutions with $\Lambda_{1,2} \sim \mathcal{O}(f_a)$ (in contrast to the case in which they are much smaller, as discussed in the previous subsection).

A general question raised by very heavy fermions is their compatibility with the phenomenological constraints on the S, T and U parameters and other electroweak precision tests. Perfect vector-like fermions (with identical masses) do not contribute to S, T and U and a large overall scale is not an issue then. Their contributions when non-degenerate are suppressed by the vector-like masses M_i, but enhanced by the Λ_i parameters. What really matters then is the mixing, which is again set by Λ_i/M_i ratios. It follows that the preferred solution identified in

the case of fermion masses of $\mathcal{O}(f_a)$, which involves only the singlet SO(5) fermion, Eq. (5.24), could be both natural and not subject to extra phenomenological tensions, up to the question of whether the scale f may be destabilized in this scenario.

All the above considerations about $\mathcal{O}(f_a)$ exotic fermion mass parameters will apply as well to the various different composite Higgs models discussed further below. In any case, the numerical predictions for the E/N factor which determine the strength of axion-photon-photon couplings are independent of the values of the exotic heavy fermion mass parameters; the sole criteria to discriminate among models with different fermionic scales is the conceptual one discussed here.

5.3.2 *Only one SM fermion chirally charged under PQ*

In the case of traditional KSVZ invisible axion models, the options with just one fermion charged under PQ necessarily imply that the fermion is an exotic one, because in these models the SM fermions cannot acquire PQ charges, a fact that follows from the SM Yukawa couplings, which induce the same constraint on fermion couplings as that required by gauge hypercharge anomaly cancellation. For the partial fermion compositeness paradigm instead, as there are no Yukawa couplings linking the left and right components of SM fermions but only Yukawa couplings involving the exotic heavy fermions, SM fermions can be chirally charged under PQ. This can be easily understood from the chain of couplings required to generate fermion masses, Eq. (5.5): by promoting to dynamical fields some of the exotic mass parameters Λ_i, the PQ charge of the left and right components of a given SM fermion do not need to coincide.

PQ-invariant solutions of the composite Higgs model in which the only PQ-charged fermion is a SM one are also shown in Tab. 5.2. They correspond to either $\Delta t \neq 0$ or $\Delta b \neq 0$. These solutions do not require y_2 or y_2' to vanish to enforce PQ invariance. Note that because of the chiral character of SM fermions, the illustration would be slightly different if the analysis was developed in terms of "only one fermion representation", as in that case charging for instance q_L would give additional results, but this would correspond to considering *two* chiral differences, $\Delta t \neq 0$ *and* $\Delta b \neq 0$. [9]

In Fig. 5.1a we project the values of E/N obtained in Tab. 5.2 on the $|g_{a\gamma\gamma}|$ versus m_a parameter space (see Eq. (**??**)), depicting as a yellow band the region allowed when only one fermion representation of the composite Higgs model is allowed to be charged under PQ. This region is delimited by $E/N = (8/3, 76/15)$. This is also the range if only the solutions with one exotic fermion chirally charged are taken into account, as depicted by the orange hatched region superimposed. Would, instead, only solutions with one SM fermion chirally charged be considered, the region allowed would be smaller, corresponding to limiting values of E/N $(8/3, 2/3)$. For comparison, the grey band shows the expectations of the traditional KSVZ invisible axion models with only one exotic fermion charged under PQ, as updated recently in Ref. [244] corresponding to values of $|g_{a\gamma\gamma}|$ delimited by $E/N = (5/3, 44/3)$.

The figure illustrates that, when only one fermion representation is charged under PQ, the region allowed by the renormalizable Goldstone Higgs model with minimal exotic fermion

9 This requires to charge as well Λ_1 and Λ_1', resulting $\Delta t = \Delta b = \pm\beta(S)$ and $E/N = 5/3$. All cases are anyway included further below when allowing all fermions to get simultaneously arbitrary PQ charges.

spectra *à la partial compositeness* discussed in this section is much narrower than that for KSVZ scenarios, a fact that should be relevant for experimental searches. The reason is that in the former models the charges of the exotic fermions are constrained via their essential participation in generating the light fermion masses, while in traditional KSVZ scenarios those charges are free, as light fermion masses result from the SM Yukawa couplings, which do not participate in the PQ mechanism. We will further deepen below on the underlying rationale, when letting all fermions be arbitrarily charged under PQ.

	$SO(5) \times U(1)_X$	$SU(3)_C \times SU(2)_L \times U(1)_Y$	q_{EM}
$\psi'^{(1)}$	$(1, -1/3)$	$B^{(1)} = (3, 1, -1/3)$	$-1/3$
$\psi^{(1)}$	$(1, 2/3)$	$T^{(1)} = (3, 1, 2/3)$	$2/3$
$\psi'^{(5)}$	$(5, -1/3)$	$Q^{(5)} = (3, 2, 1/6)$	$-1/3, 2/3$
		$X^{(5)} = (3, 2, -5/6)$	$-1/3, -4/3$
		$B^{(5)} = (3, 1, -1/3)$	$-1/3$
$\psi^{(5)}$	$(5, 2/3)$	$Q^{(5)} = (3, 2, 1/6)$	$-1/3, 2/3$
		$X^{(5)} = (3, 2, 7/6)$	$2/3, 5/3$
		$T^{(5)} = (3, 1, 2/3)$	$2/3$
$\psi^{(10)}$	$(10, 2/3)$	$Q^{(10)} = (3, 2, 1/6)$	$-1/3, 2/3$
		$X^{(10)} = (3, 2, 7/6)$	$2/3, 5/3$
		$V^{(10)} = (3, 3, 2/3)$	$-1/3, 2/3, 5/3$
		$W^{(10)} = (3, 1, 5/3)$	$5/3$
		$B^{(10)} = (3, 1, -1/3)$	$-1/3$
		$T^{(10)} = (3, 1, 2/3)$	$2/3$
$\psi^{(14)}$	$(14, 2/3)$	$Q^{(14)} = (3, 2, 1/6)$	$-1/3, 2/3$
		$X^{(14)} = (3, 2, 7/6)$	$2/3, 5/3$
		$V_1^{(14)} = (3, 3, 5/3)$	$2/3, 5/3, 8/3$
		$V_1^{(14)} = (3, 3, 2/3)$	$-1/3, 2/3, 5/3$
		$V_3^{(14)} = (3, 3, -1/3)$	$-4/3, -1/3, 2/3$
		$T^{(14)} = (3, 1, 2/3)$	$2/3$

Table 5.1: $SO(5)$ fermion representation content in terms of SM quantum numbers. The last column shows the $U(1)_{EM}$ electromagnetic charges, used to compute the electromagnetic anomaly E.

Exotic fermion charged	Couplings promoted	SM fermions charged	E/N_{top} (E/N_{bottom})
$\Delta\psi^{(1)} = \beta(S)$	$\Lambda_3 \to \lambda_3 S$	–	$\frac{8}{3}$ $\left(\frac{2}{3}\right)$
$M_1 \to \kappa_1 S$	$\Lambda_1 \to \lambda_1 S$ $\Lambda_2 \to \lambda_2 S^\dagger$	–	
	$\Lambda_{1,3} \to \lambda_{1,3} S$	$\Delta t = \beta(S)$	
	$\Lambda_{1,2} \to \lambda_{1,2} S^\dagger$	$\Delta t = -2\beta(S)$	
$\Delta\psi^{(5)} = \beta(S)$ $M_5 \to \kappa_5 S$	$\Lambda_1 \to \lambda_1 S$	–	$\frac{76}{15}$ $\left(\frac{46}{15}\right)$
	$\Lambda_{2,3} \to \lambda_{2,3} S$	–	
	$\Lambda_{1,2,3} \to \lambda_{1,2,3} S$	$\Delta t = \beta(S)$	$\frac{14}{3}$ $\left(\frac{8}{3}\right)$
	–	$\Delta t = -\beta(S)$	$\frac{17}{3}$ $\left(\frac{11}{3}\right)$
	$\Lambda_1 \to \lambda_1 S^\dagger$ $(\lambda_1 S)$ $\Lambda_{2,3} \to \lambda_{2,3} S$ $(\lambda_{2,3} S^\dagger)$	$\Delta t = -\beta(S)$	
	$\Lambda_1 \to \lambda_1 S^\dagger$	$\Delta t = -2\beta(S)$	$\frac{20}{3}$ $\left(\frac{14}{3}\right)$
	$\Lambda_{2,3} \to \lambda_{2,3} S^\dagger$	$\Delta t = -2\beta(S)$	
	$\Lambda_{1,2,3} \to \lambda_{1,2,3} S^\dagger$	$\Delta t = -3\beta(S)$	$\frac{26}{3}$ $\left(\frac{20}{3}\right)$
None	$\Lambda_1 \to \lambda_1 S$	$\Delta t = \beta(S)$	$\frac{8}{3}$ $\left(\frac{2}{3}\right)$
	$\Lambda_{2,3} \to \lambda_{2,3} S$	$\Delta t = \beta(S)$	
	$\Lambda_{1,2,3} \to \lambda_{1,2,3} S$	$\Delta t = 2\beta(S)$	

Table 5.2: Possible setups extending the spectrum of the renormalizable composite Higgs model by one singlet scalar S and allowing one or none of the exotic fermions to acquire chiral PQ charges. Either the top or the bottom sector are considered at a time; the top sector is explicitly illustrated, while for the bottom sector ($M_i \to M_i'$, $\Lambda_i \to \Lambda_i'$ with $\Lambda_i = 0$) the E/N values are shown within brackets.

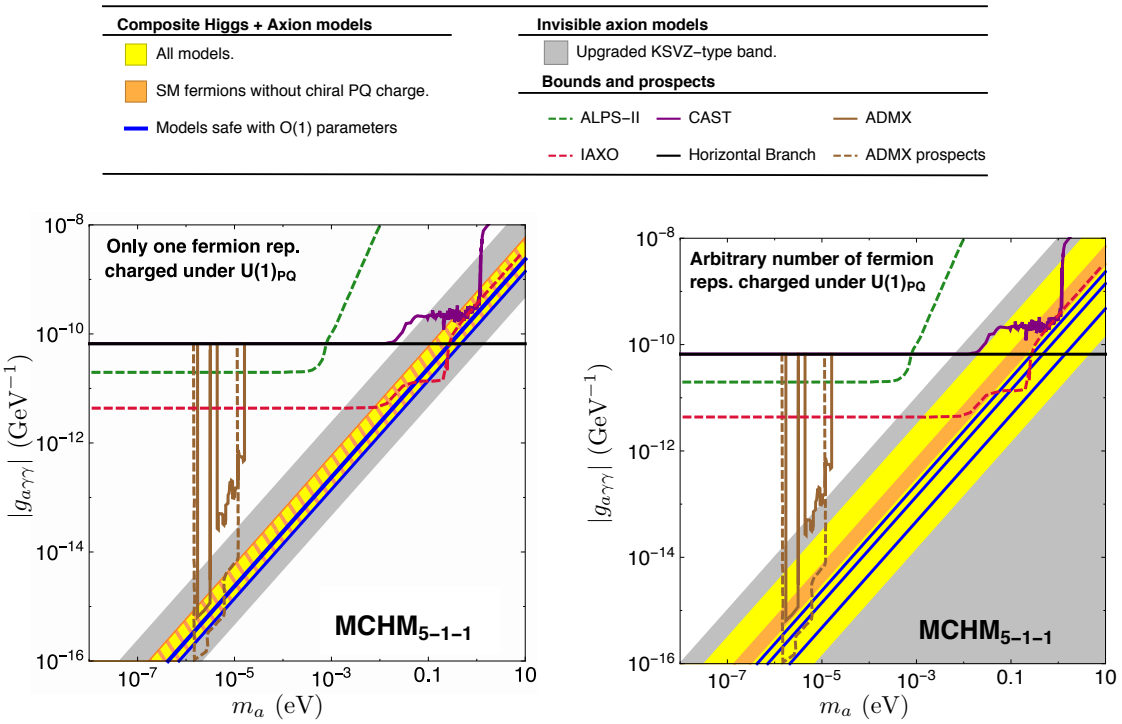

(a) In yellow, $|g_{a\gamma\gamma}|$ values allowed when only one fermion representation is chirally charged amongst the ensemble of those for exotic and SM fermions, in the renormalizable composite Higgs model. The subset of models in which only the exotic fermions are PQ-chirally charged (orange hatched) spans the same maximal region in this case. The grey area corresponds to the updated [244] standard KSVZ prediction.

(b) The yellow band indicates the allowed values of $|g_{a\gamma\gamma}|$ when more than one fermion is allowed to be charged under $U(1)_{PQ}$. The subset of models in which the SM fermions are not chirally charged under PQ is indicated by an orange band. The grey band corresponds to the upgraded [244] KSVZ prediction.

Figure 5.1: Expected $g_{a\gamma\gamma}$ for KSVZ-type axionic extensions of the $SO(5)/SO(4)$ renormalizable Goldstone Higgs model described in Sect. 5.3. The blue lines correspond to solutions in which the only PQ-chirally charged fermion(s) are $SO(5)$ singlet(s), e.g. Eq. (5.24), *and* which allow $\mathcal{O}(f_a)$ fermion mass and $\mathcal{O}(1)$ couplings: amongst the two uppermost lines, the upper (lower) one is the bottom (top) sector solution, while the extra one in Fig. 5.1b corresponds to charging both sectors. Current limits from CAST [147], ADMX [148–152] and and horizontal branch (HB) stars [154] are delimited by solid lines, while projected sensitivities for ALPS-II [155], IAXO [**Carosi:2013rla** , 156] and ADMX [157] are dashed.

5.3.3 *Arbitrary number of fermions charged*

Charging more than one fermion expands logically the range of possible E/N values. As an example, $E/N = 5/3$ when $\psi_L^{(1)}$, $\psi_L^{(1)\prime}$, Λ_3 and Λ_3' are charged under $U(1)_{PQ}$ (and still $y_2 = y_2' = 0$ required by PQ invariance). We consider next the general case in which fields and couplings are allowed to take arbitrary PQ charges simultaneously (always as a function of just one field, the singlet S or $S^\dagger$). The aim is to determine the maximum and minimum possible values of $|g_{a\gamma\gamma}|$. Note that the condition $y_2 = y_2' = 0$ is no more necessary in the general case to obtain a PQ invariant setup involving the minimal set of exotic fermions responsible for light fermion masses, as Eq. (5.20) can be fulfilled then even in the presence of only one scalar singlet. For instance, with chirally charged exotic fermions it allows

$$\pm\,\beta(S) \equiv \beta(S_{M5}) = -\beta(S_{M1}) \quad \Longrightarrow \Delta\psi^{(5)} = -\Delta\psi^{(1)}\,, \tag{5.26}$$

suggesting a dynamical origin for both M_1 and M_5,[10] e.g.

$$M_5 \longrightarrow \kappa_5\, S\,, \qquad M_1 \longrightarrow \kappa_1\, S^\dagger\,. \tag{5.27}$$

The ensemble of solutions allowed by Eq. (5.20) include as well those in which *none* of the exotic fermions have PQ-chiral charges, that is, those in which the only fermions involved in the PQ mechanism are the SM ones. As previously stated, this interesting possibility exists for composite Higgs models while it is absent in KSVZ standard invisible axion models, and constitutes a distinctive feature.

Fig. 5.1b depicts in yellow the generic band in parameter space allowed for arbitrary number of fermions chirally charged under PQ and arbitrary values of y_2 and y_2', whose limits correspond to $E/N = (2, 56/3)$. A narrower orange band ($E/N = (11/3, 17/3)$) has been superimposed, in order to indicate the smaller parameter space of the solutions in which only exotic heavy fermions acquire chiral PQ charges. For comparison, the grey region ($E/N < 170/3$) is that for standard invisible axion models when they allow the simultaneous presence of several exotic fermions charged under the PQ symmetry, as recently predicted [244]. This comparison reveals a striking fact: *while in the standard constructions it may be possible to make the strength of the axion-photon-photon coupling arbitrarily small, this is not possible in the wide range of Goldstone Higgs setups with fermionic partial compositeness reviewed here*. The generic origin of the narrower parameter space for composite Higgs models can be understood from Fig. 5.1b as the net effect of two characteristics competing in opposite directions, see Eqs. (5.5) and (5.6):

- Light fermion masses are directly mediated by the exotic fermions (while there are no SM Yukawa couplings), implying strong constraints on the possible PQ charges of the exotic dynamical mass parameters. They induce the very narrow orange band in Fig. 5.1b.
- The fact that SM fermions can now acquire PQ chiral charges (unlike in traditional KSVZ models) somewhat relaxes the allowed parameter space. This explains the pas-

10 Charging under PQ both $\psi^{(1)}$ and $\psi^{(5)}$ does not allow a natural solution with exotic fermion masses of $\mathcal{O}(f_a)$, because of the constraints imposed by the top mass discussed earlier. The solution with small values for κ_1 and κ_5 is technically natural, though.

sage from the orange band to the wider yellow one in Fig. 5.1b, in the most general case.

Overall, the comparison illustrates that, in the axion solutions of the renormalizable Goldstone Higgs models based on $SO(5)/SO(4)$ with minimal exotic fermion spectrum, the viable phenomenological parameter space is much restricted with respect to that for the standard invisible axion setups. We will see that this result holds as well for the many other Goldstone Higgs models in the literature to be discussed next.

5.4 EXTENSION BY ONLY ONE SCALAR SINGLET: NON-LINEAR SETUPS

In its strong coupling limit, the renormalizable model discussed in the previous section (corresponding to a large mass for the SM scalar singlet σ contained in its $SO(5)$ scalar five-plet) acquires a non-linear formulation in terms of effective couplings, which is the usual approach for instance in composite Higgs models. In this non-linear context, several very different fermionic UV contents have been considered in the literature. This section will be entirely devoted to these effective non-renormalizable formulations. From the point of view of the effective field theory formulation, the implicit assumption is that the σ particle of a putative renormalizable ultraviolet completion of composite Higgs models has been integrated out.

The notation MCHM_{A-B-C} is often used to indicate the fermionic spectrum of composite Higgs models, with A, B, C indicating the $SO(5)$ representation which contains the heavy partner of the SM doublet q_L, up-type right-handed and down-type right-handed fermions, respectively.[11] The heavy partner of a given SM quark is understood here as the SM multiplet contained in the $SO(5)$ exotic representation which is dominant in the generation of the SM quark mass, through a soft mixing Λ_i. For example, the model described in the previous section can be tagged in its fermionic content as MCHM_{5-1-1} since the partners of the q_L are found inside a five-plet of $SO(5)$ and those of t_R and b_R correspond to $SO(5)$ singlets; these partners were called Q, Q', T and B respectively and contained in $SO(5)$ five-plet and singlet representations, see Eq. (5.2) and Tab. 5.1.

We extend now the study performed in the previous sections to a plethora of fermionic spectra used usually in composite Higgs models [248], which are typically non-linear effective realizations. Details of the specific fermion representations involved are given in Tab. 5.1, and the models are summarized in Tabs. 5.3 and 5.4.[12] For all models, the generation of the light quark masses results from a seesaw-like chain of interactions of the form

$$q_L \xrightarrow[\Lambda_q]{} Q_R \xrightarrow[M_Q]{} Q_L \xrightarrow[y_1^t]{} T_L \xrightarrow[M_T]{} T_L \xrightarrow[\Lambda_t]{} t_R\,, \tag{5.28}$$

where Λ_i and y_i generalize the MCHM_{5-1-1} couplings in Eqs. (5.1) and (5.5), upon the replacement $\{M_5 \to M_Q, M_1 \to M_T, \Lambda_1 \to \Lambda_q, \Lambda_3 \to \Lambda_t, \text{and}\, y_1 \to y_1^t\}$. An analogous chain holds for the bottom mass, with $\{Q \to Q', T \to B, \Lambda_q \to \Lambda_q', \Lambda_t \to \Lambda_b\,, y_1^t \to y_1^b\}$. The Yukawa-like couplings of exotic fermions to the Higgs particle, y_t^1 and y_b^1 (equivalent to y_1 and y_1' in the notation used for the renormalizable model), correspond to operators whose mass dimension is model dependent, as shown in Tabs. 5.3 and 5.4.

11 Sometimes, when only one subindex appears as in MCHM_A it is understood to be of the type MCHM_{A-A-A}.

12 Models with spinorial $SO(5)$ embeddings, e.g. MCHM_4 [54], are phenomenologically excluded in particular in view of $Z \to b\bar{b}$ data.[56]

We denote by Ψ^i the SO(5) representation which contains the heavy partner $i = Q, Q', T, B$, which in this study will be either a fermionic singlet, a five-plet, a ten-plet or a fourteen-plet, as shown in Tab. 5.1.[13] In MCHM_{5-1-1} each of the four heavy partners (Q, Q′, T, B) was contained in a different SO(5) representation, so four exotic SO(5) fermions were to be added, but this is not always needed as can be seen in Tab. 5.1. For example, MCHM_{5-5-5} requires only two SO(5) representations: the $(5, 2/3)$ representation $\psi^{(5)}$ contains both Q and T, while the $(5, -1/3)$ representation $\psi^{(5)\prime}$ contains both Q′ and B. Indeed, in this model the SM-exotic fermion mixings are given by

$$\bar{q}_L Q_R \supset \bar{q}_L \Gamma_q \Psi^Q_R = \bar{q}_L \Gamma_{2\times5} \psi^{(5)}_R , \tag{5.29}$$

$$\bar{q}_L Q'_R \supset \bar{q}_L \Gamma'_q \Psi^{Q'}_R = \bar{q}_L \Gamma_{2\times5} \psi^{(5)\prime}_R , \tag{5.30}$$

$$\bar{T}_L t_R \supset \bar{\Psi}^T_L \Gamma_t t_R = \bar{\psi}^{(5)}_L \Gamma_{1\times5} t_R , \tag{5.31}$$

$$\bar{B}_L b_R \supset \bar{\Psi}^B_L \Gamma_b b_R = \bar{\psi}^{(5)\prime}_L \Gamma_{1\times5} b_R , \tag{5.32}$$

where again by Γ we denote dimensionless couplings, whose SO(5) matrix dimension has been made explicit on the right-hand side for clarity. In summary, $\Psi^Q = \Psi^T$ and $\Psi^{Q'} = \Psi^B$ in the MCHM_{5-5-5} model. Yet other models shown in Tabs. 5.3 and 5.4 do not distinguish between Q and Q′ and thus $\Psi^Q = \Psi^{Q'}$, further reducing the number of exotic fermion representations required.

Generalizing the definitions above, the Lagrangian can be written as:

$$\mathcal{L}_{ferm} = \bar{q}_L i\not{D} q_L + \bar{t}_R i\not{D} t_R + \bar{b}_R i\not{D} b_R + \sum_{i=Q,\,Q',\,T,\,B} \left\{ \bar{\Psi}^i i\not{D} \Psi^i - \left[\bar{\Psi}^i_L M_i \Psi^i_R + \text{h.c.} \right] \right\} \tag{5.33}$$

$$-\mathcal{L}_{\text{Yuk.}} - \left[\Lambda_q \, \bar{q}_L \, \Gamma_q \, \Psi^Q_R + \Lambda'_q \, \bar{q}_L \, \Gamma'_q \, \Psi^{Q'}_R + \Lambda_t \, \bar{\Psi}^T_L \, \Gamma_t \, t_R + \Lambda_b \, \bar{\Psi}^B_L \, \Gamma_b \, b_R + \mathcal{L}_{\text{subdom.}} + \text{h.c.} \right] ,$$

where the sum on the mass and kinetic terms runs over as many different fermion representations as needed, as discussed above. The dimensions of the Γ coupling matrices are model-dependent.

$\mathcal{L}_{\text{Yuk.}}$ contains the low-energy effective fermion-Higgs operators of mass dimension $d \geqslant 4$ –this depends on the model– which can be schematically written as

$$\mathcal{L}_{\text{Yuk}} \sim \frac{y^t_1}{f^{n-1}} \bar{\Psi}^Q_L [\phi^n] \Psi^T_R + \frac{y^b_1}{f^{n-1}} \bar{\Psi}^{Q'}_L [\phi^n] \Psi^B_R + \frac{y^t_2}{f^{n-1}} \bar{\Psi}^Q_R [\phi^n] \Psi^T_L + \frac{y^b_2}{f^{n-1}} \bar{\Psi}^{Q'}_r [\phi^n] \Psi^B_L + \text{h.c.} , \tag{5.34}$$

where ϕ denotes here a five-component SO(5) matrix with only four independent degrees of freedom, as its fifth component is fixed in the non-linear regime to be $\sigma \to f^2 - 2|H|^2$, instead of the dynamical field σ of the previous renormalizable model Eq. (5.2). The precise form of the $[\phi^n]$ insertions for each model considered can be read in Tabs. 5.3 and 5.4 for illustration. This Lagrangian generalizes the Yukawa couplings of the renormalizable model in Eq. (5.1), with the correspondence $\{y_1, y'_1, y_2, y'_2\} \to \{y^t_1, y'^b_1, y^t_2, y'^b_2\}$. Those models in Tabs. 5.3 and 5.4 with Yukawa structures of mass dimension four can be easily rewritten as renormalizable ones by simply replacing the non-linear constraint mentioned above by a dynamical σ field and adding a scalar potential, along the lines of the renormalizable model

13 The Q, T, B representation superscript (1), (5) (10) or (14) shown in Tab. 5.1 are left implicit here for simplicity.

discussed in detail in Sect. 5.2; this is the case for instance of $\mathrm{MCHM}_{5-10-10}$, MCHM_{5-1-10} and $\mathrm{MCHM}_{5-14-10}$, while an UV completion for models with higher-dimension Yukawa structures would require to consider extra mediator fields. In any case, note that the precise form of the Yukawa structures is irrelevant for the E/N values predicted, as the $SO(5)$ five-plet scalars ϕ are not PQ charged and in consequence that ratio only depends on the relative PQ chiral charges of fermions.[14]

The last line in Eq. (5.33) contains the mixings between SM and exotic fermions. Its first four terms are those participating in the chain in Eq. (5.28), which gives the dominant contributions to the light fermion masses (the different content and $SO(5)$ matrix size of the Γ couplings are model-dependent and have been left implicit here for notational simplicity). $\mathcal{L}_{\text{subdom.}}$ includes other fermion mixing terms which give subdominant contributions to the light fermion masses;[15] they are the equivalent of the Λ_2 and Λ_2' couplings in the renormalizable model Eq. (5.1) discussed in Sect. 5.3. They are couplings of the type $\bar{q}_L Q_R$, $\bar{T}_L t_R$ or $\bar{B}_L b_R$. As an illustration, model $\mathrm{MCHM}_{5-10-10}$ allows subdominant contributions of the form $\bar{q}_L \psi^{(10)}_R$ and $\bar{\psi}^{(5)}_L t_R$ in addition to the dominant mixings $\bar{q}_L \psi^{(5)}_R$, $\bar{\psi}^{(10)}_L t_R$ and $\bar{\psi}^{(10)}_L b_R$, see Tabs. 5.3 and 5.4; using the Ψ notation, they read

$$\mathcal{L}^{5-10-10}_{\text{subdom.}} = \tilde{\Lambda}_q \bar{q}_L \Gamma \Psi^T_R + \tilde{\Lambda}_t \bar{\Psi}^Q_L \Gamma t_R \,. \tag{5.35}$$

We have identified and shown in Tabs. 5.3 and 5.4 the set of subdominant $\tilde{\Lambda}_i$ terms for each of the models considered. These terms further constrain significantly the phenomenological axion-photon analysis below.

A $U(1)_{PQ}$-invariant formulation of the effective Lagrangian in Eq. (5.33) can be achieved along the same lines as for the renormalizable model in Sect. 5.3. Scalar fields singlet under both $SO(5)$ and the SM gauge group and whose vev sets the size of the PQ scale f_a as in Eq. (5.7) are introduced, combined with the promotion to dynamical fields of some of the mass parameters described above, i.e.

$$M_i \to \kappa_i S_{Mi} \,, \qquad \text{and / or} \qquad \Lambda_i \to \lambda_i S_{\Lambda i} \,. \tag{5.36}$$

Again, the small κ_i and λ_i values, which may be required in order to get a spectrum of exotic fermion masses in the TeV range, are protected by $U(1)$ chiral symmetries under which only the fermions transform. In some cases, $\mathcal{O}(1)$ parameters may be safely allowed as previously discussed in Sect. 5.3. [16] Alike to Eq. (5.20), the PQ chiral charge differences are then given by

$$\begin{aligned} \Delta\Psi^i &= \beta(S_{Mi}) \,, \\ \Delta t &= \beta(S_{\Lambda q}) + \beta(S_{\Lambda t}) - \beta(S_{MQ}) - \beta(S_{MT}) \,, \end{aligned} \tag{5.37}$$

14 For some models involving 10-plets or 14-plets of $SO(5)$ [248], the compact Lagrangian in Eq. (5.34) includes additional Yukawa structures with respect to those shown in Tabs. 5.3 and 5.4. They do not make a difference for the E/N values predicted.

15 These were not made explicit in the summary of models in Ref. [248] which focused on the issue of mass, but here their presence/absence does influence the size of the axion-$\gamma\gamma$ parameter space and we thus include them.

16 As this case corresponds to singlet fermion masses much higher than the Λ_s scale, the effective Lagrangian formulation in Eq. (5.34) should have to be replaced then by one in which the heavy singlet fermion fields are not present. Their effect will be included in higher dimension operators resulting from the integration of those fermions. For the practical analysis here there is no need of expliciting these steps. Additionally, the caveats discussed in the introduction and after Eq. (5.9) as to the stability of the f scale for these solutions are also pertinent here.

and analogously for the bottom sector. In the minimal extension scenario of enlarging the spectrum by only one singlet scalar S, the Yukawa couplings may force some of the scalar PQ charges $\beta(S_{Mi})$ to vanish, see Tabs. 5.3 and 5.4.

A clarification is pertinent from the point of view of the effective field theory. Although Eq. (5.36) is written in terms of a scalar singlet under the SM and $SO(5)$, this is only for bookkeeping and easy comparison with the renormalizable model in the previous section. The full S dynamics is not playing a role in the phenomenological analysis, or the maybe more complex UV completion for that matter. The only ingredient used is the promotion of dimensional parameters to dynamical ones, endowing them with PQ charges as in Eq. (5.37), and the only field retained is the light axion stemming from them. In other words, the analysis is independent of the physics of the real components of S.

The ensuing general expression for the ratio of electromagnetic and color anomalies E/N reads now

$$\frac{E}{N} = \frac{2}{3}\frac{182\,\Delta\psi^{(14)} + 94\,\Delta\psi^{(10)} + 38\Delta\psi^{(5)} + 23\Delta\psi'^{(5)} + 4\Delta\psi^{(1)} + \Delta\psi'^{(1)} + 4\Delta t + \Delta b}{14\Delta\psi^{(14)} + 10\Delta\psi^{(10)} + 5\Delta\psi^{(5)} + 5\Delta\psi'^{(5)} + \Delta\psi^{(1)} + \Delta\psi'^{(1)} + \Delta t + \Delta b}\,. \quad (5.38)$$

which generalizes Eq. (5.23) derived for the $MCHM_{5-1-1}$ model.

Using the results above, we have identified the E/N values that correspond to the maximum and minimum possible values of $|g_{a\gamma\gamma}|$, for the different minimal (in fermion content) models in Tabs. 5.3 and 5.4, within the minimal extension of the spectrum by just one scalar singlet and allowing all fermions to take arbitrary PQ charges. The results are shown on the last column of the table, and the corresponding allowed area of the $(m_a,\, g_{a\gamma\gamma})$ plane is depicted for the different models by yellow bands in Figs. 5.1b and 5.2.[17]

The allowed yellow regions tend to be wider for the models which involve a number of different exotic fermion representations, as otherwise the constraints implied by their Yukawa couplings reduce strongly the parameter space of PQ-invariant formulations. The extreme case is that in which only one exotic $SO(5)$ representation is involved, as the Yukawa coupling forces then its chiral PQ charge to vanish (alike to the constraint imposed in traditional KSVZ theories by the SM Yukawa couplings) and the remaining allowed parameter space is entirely due to PQ-charged SM fermions. Again, the overall pattern is that the parameter space corresponding to PQ chirally charged exotic fermions is strongly constrained, while the presence of PQ chirally charged SM fermions relaxes that constraint to some extent. A narrower orange band has been superimposed over the yellow ones in Figs. 5.1b and 5.2 for illustration, indicating the smaller parameter space that would remain if only the exotic fermions would be allowed to acquire chiral PQ charges: the figure shows that $MCHM_{5-5-5}$, $MCHM_{10-10-10}$, $MCHM_{10-5-10}$, $MCHM_{5-5-10}$, $MCHM_{10-14-10}$ and $MCHM_{14-14-10}$ would not be then compatible with a minimal PQ invariant formulation. There is no good reason for such restriction to non PQ chirally charged SM fermions within composite Higgs models, though, so those models are also good candidates for an axion solution in the framework of a pGB nature for the Higgs boson.

17 The results are independent of the linear or non-linear formulation of the models, assuming that no scalar acquires is PQ-charged other than the added singlet S .

MCHM	ψ^{Q} $\psi^{Q'}$	ψ^{T} ψ^{B}	$\mathcal{L}_{Yuk.}$	$\mathcal{L}_{subdominant}$	$\left[\frac{E}{N}\Big\vert_{\lvert g_{a\gamma\gamma}\rvert\,min.}, \frac{E}{N}\Big\vert_{\lvert g_{a\gamma\gamma}\rvert\,max.}\right]$
$5-1-1$	$(5,2/3)$ $(5,-1/3)$	$(1,2/3)$ $(1,-1/3)$	$\bar{\psi}_L^{(5)}\phi\,\psi_R^{(1)}$ $\bar{\psi}_L^{\prime(5)}\phi\,\psi_R^{\prime(1)}$	$\bar{\psi}_L^{(5)}(\Gamma_{5\times1}t_R)$ $\bar{\psi}_L^{\prime(5)}(\Gamma_{5\times1}b_R)$	$[2,56/3]$
$5-5-5$	$(5,2/3)$ $(5,-1/3)$	$(5,2/3)$ $(5,-1/3)$	$\bar{\psi}_L^{(5)}\phi\phi^\dagger\psi_R^{(5)}$ $\bar{\psi}_L^{\prime(5)}\phi\phi^\dagger\psi_R^{\prime(5)}$	–	$[2,-4/3]$
$5-10-10$	$(5,2/3)$	$(10,2/3)$	$\bar{\psi}_L^{(5)}\phi\,\psi_R^{(10)}$	$(\bar{q}_L\Gamma_{2\times10})\psi_R^{(10)}$ $\bar{\psi}_L^{(5)}(\Gamma_{5\times1}t_R)$	$[2,50/3]$
$10-10-10$	$(10,2/3)$	$(10,2/3)$	$\phi^\dagger\bar{\psi}_L^{(10)}\psi_R^{(10)}\phi$	–	$[2,2/3]$
$10-5-10$	$(10,2/3)$	$(5,2/3)$ $(10,2/3)$	$\bar{\psi}_L^{(10)}\phi\,\psi_R^{(5)}$ $\phi^\dagger\bar{\psi}_L^{(10)}\psi_R^{(10)}\phi$	$(\bar{q}_L\Gamma_{2\times5})\psi_R^{(5)}$ $\bar{\psi}_L^{(10)}(\Gamma_{10\times1}t_R)$	$[2,2/3]$
$5-5-10$	$(5,2/3)$	$(5,2/3)$ $(10,2/3)$	$\bar{\psi}_L^{(5)}\phi\phi^\dagger\psi_R^{(5)}$ $\bar{\psi}_L^{(5)}\phi\,\psi_R^{(10)}$	$(\bar{q}_L\Gamma_{2\times10})\psi_R^{(10)}$ $\bar{\psi}_L^{(10)}(\Gamma_{10\times1}t_R)$	$[2,2/3]$
$5-1-10$	$(5,2/3)$	$(1,2/3)$ $(10,2/3)$	$\bar{\psi}_L^{(5)}\phi\,\psi_R^{(1)}$ $\bar{\psi}_L^{(5)}\phi\,\psi_R^{(10)}$	$(\bar{q}_L\Gamma_{2\times10})\psi_R^{(10)}$ $\bar{\psi}_L^{(5)}(\Gamma_{5\times1}t_R)$ $\bar{\psi}_L^{(10)}(\Gamma_{10\times1}t_R)$	$[2,12]$

Table 5.3: Summary of the non-renormalizable MCHMs in the literature which involve only fermionic five-plets and/or ten-plets and/or singlets. The second and third columns specify the particle content of each model; the fourth contains the $SO(5)$−invariant Yukawa interactions (the first row inside each column is proportional to y_1^t and the second to y_1^b, except when they coincide). The fifth column specifies subdominant mixing terms. The last column gives the ranges of E/N that define the phenomenological band in the $|g_{a\gamma\gamma}|$ versus m_a parameter space.

Figs. 5.1b and 5.2 also depict in grey the area allowed by the recent updated predictions of the traditional KSVZ invisible axion model. Overall, the comparison shows that the phenomenological region allowed by general Goldstone Higgs realizations with minimal fermion

content *à la partial compositeness* is much more restrictive, and thus predictive, than for traditional KSVZ constructions, confirming the pattern already identified for the renormalizable model in the previous section.

Finally, the very few particular cases with $\mathcal{O}(1)$ κ_i or λ_i parameters are indicated in Figs. 5.1b and 5.2 by blue lines superimposed over the bulk of the solutions. Only MCHM_{5-1-1}, MCHM_{5-1-10} and $\text{MCHM}_{14-1-10}$ allow this possibility, being the only ones containing at least one heavy partner in a singlet representation of $SO(5)$. This is needed for the mixings between light and heavy fermions to be exclusively $SO(5)$-invariant, e.g. $\psi^{(1)}t_R$ or $\psi^{(1)}b_R$, allowing the singlet $\psi^{(1)}$ to be charged under PQ and its mass term promoted to a dynamical field, without promoting to scalar fields any of the soft-breaking couplings. It could be a natural possibility that the fermionic fields which are singlets of $SO(5)$ acquire a mass much larger than that of the $SO(5)$ group whenever a new higher physics scale is present, as for instance f_a in the framework of a $U(1)_{PQ}$ solution to the strong CP problem.

The model which overall allows for a larger variety of implementations is MCHM_{5-1-1}, see Fig. 5.1b, because it has the largest number of different fermionic representations, which translates into a sizable fraction of models with only exotic fermions charged (orange band) and three solutions with $\mathcal{O}(f_a)$ exotic fermion masses.

MCHM	ψ^{Q} $\psi^{Q'}$	ψ^{T} ψ^{B}	$\mathcal{L}_{Yuk.}$	$\mathcal{L}_{subdominant}$	$\left[\frac{E}{N}\Big\vert_{\lvert g_{a\gamma\gamma}\rvert min.}, \frac{E}{N}\Big\vert_{\lvert g_{a\gamma\gamma}\rvert max.}\right]$
$14-1-10$	$(14,2/3)$	$(1,\,2/3)$ $(10,\,2/3)$	$\phi^\dagger\bar{\psi}_L^{(14)}\psi_R^{(1)}\phi$ $\phi^\dagger\bar{\psi}_L^{(14)}\psi_R^{(10)}\phi$	$(\bar{q}_L\Gamma_{2\times10})\psi_R^{(10)}$ $\bar{\psi}_L^{(10)}(\Gamma_{10\times1}t_R)$ $\bar{\psi}_L^{(14)}(\Gamma_{14\times1}t_R)$	$[2, 158/3]$
$14-5-10$	$(14,2/3)$	$(5,2/3)$ $(10,2/3)$	$\bar{\psi}_L^{(14)}\phi\,\psi_R^{(5)}$ $\phi^\dagger\bar{\psi}_L^{(14)}\psi_R^{(10)}\phi$	$(\bar{q}_L\Gamma_{2\times5})\psi_R^{(5)}$ $(\bar{q}_L\Gamma_{2\times10})\psi_R^{(10)}$ $\bar{\psi}_L^{(14)}(\Gamma_{14\times1}t_R)$ $\bar{\psi}_L^{(10)}(\Gamma_{10\times1}t_R)$	$[2, -100/3]$
$5-14-10$	$(5,2/3)$	$(14,2/3)$ $(10,2/3)$	$\bar{\psi}_L^{(5)}\phi\,\psi_R^{(14)}$ $\bar{\psi}_L^{(5)}\phi\,\psi_R^{(10)}$	$(\bar{q}_L\Gamma_{2\times14})\psi_R^{(14)}$ $(\bar{q}_L\Gamma_{2\times10})\psi_R^{(10)}$ $\bar{\psi}_L^{(5)}(\Gamma_{5\times1}t_R)$ $\bar{\psi}_L^{(10)}(\Gamma_{10\times1}t_R)$	$[2, 29/3]$
$10-14-10$	$(10,2/3)$	$(14,\,2/3)$ $(10,\,2/3)$	$\phi^\dagger\bar{\psi}_L^{(10)}\psi_R^{(14)}\phi$ $\phi^\dagger\bar{\psi}_L^{(10)}\psi_R^{(10)}\phi$	$(\bar{q}_L\Gamma_{2\times14})\psi_R^{(14)}$ $\bar{\psi}_L^{(10)}(\Gamma_{10\times1}t_R)$	$[2, 2/3]$
$14-10-10$	$(14,2/3)$	$(10,\,2/3)$	$\phi^\dagger\bar{\psi}_L^{(14)}\psi_R^{(10)}\phi$	$(\bar{q}_L\Gamma_{2\times10})\psi_R^{(10)}$ $\bar{\psi}_L^{(14)}(\Gamma_{14\times1}t_R)$	$[2, 83/3]$
$14-14-10$	$(14,2/3)$	$(14,\,2/3)$ $(10,\,2/3)$	$\phi^\dagger\bar{\psi}_L^{(14)}\psi_R^{(14)}\phi$ $\phi^\dagger\bar{\psi}_L^{(14)}\psi_R^{(10)}\phi$	$(\bar{q}_L\Gamma_{2\times10})\psi_R^{(10)}$ $\bar{\psi}_L^{(10)}(\Gamma_{10\times1}t_R)$	$[2, 2/3]$

Table 5.4: Summary of the non-renormalizable MCHMs in the literature that include fermions in the 14-plet representation of SO(5). The second and third columns specify the particle content of each model; the fourth contains the SO(5)−invariant Yukawa interactions (the first row inside each column is proportional to y_1^t and the second to y_1^b, except when they coincide). The fifth column specifies subdominant mixing terms. The last column gives the ranges of E/N that define the phenomenological band in the $|g_{a\gamma\gamma}|$ versus m_a parameter space.

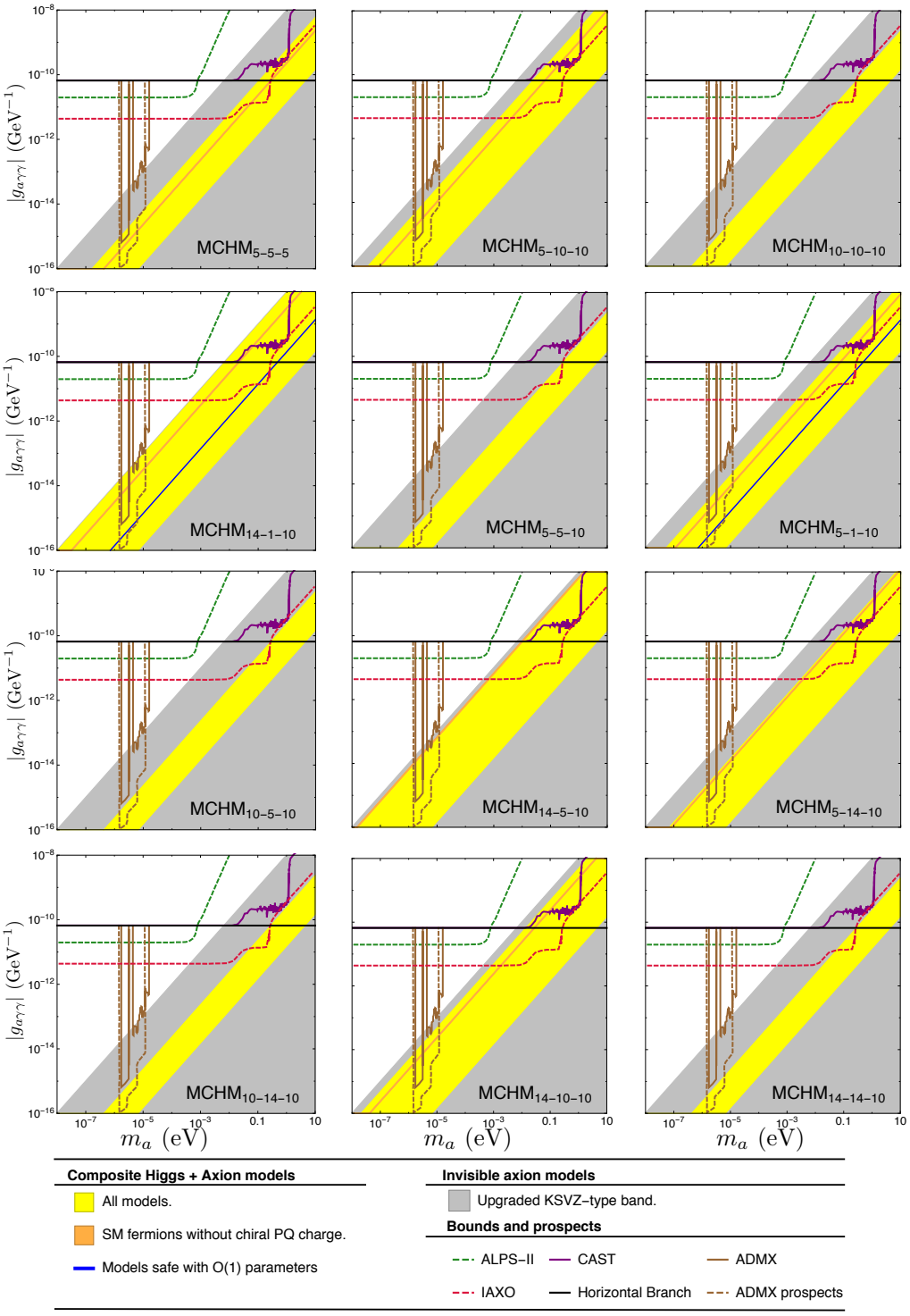

Figure 5.2: Yellow bands: expected $g_{a\gamma\gamma}$ for various MCHMs when extending the spectrum by only one singlet scalar field PQ charged. Both dominant and subdominant heavy-SM fermion mixings are included, see Eq. (5.33). The subset of solutions in which only exotic fermions are charged is depicted by orange bands/lines. The blue lines correspond to solutions with only $SO(5)$-singlet fermions charged, for which masses $\mathcal{O}(f_a)$ and couplings of $\mathcal{O}(1)$ could be allowed. For comparison, the predictions of the updated [244] standard KSVZ invisible axion scenarios are depicted as a grey region. The plot for the case MCHM_{5-1-1} is not shown here because it is exactly the same as that shown in Fig. 5.1b.

5.5 SUMMARY

An important problem of current dynamical solutions to the strong CP problem, assuming only the SM gauge symmetries, is that they are strongly fine-tuned, as the axion scale f_a is phenomenologically required to be many orders of magnitude above the electroweak scale, while the scalar sector of the models communicates both scales and tends to homogenize their values. This problem hinders all invisible axion constructions.

With this perspective, we have explored the implementation of the Peccei-Quinn axial symmetry $U(1)_{PQ}$ in models in which the Higgs particle has a pseudo-Nambu-Goldstone boson nature. In them, that Higgs ancestry results from some global symmetry spontaneously broken at high-energy, protecting the Higgs mass from electroweak hierarchy issues, as it can only become massive after some small and explicit symmetry breaking. Furthermore, the global symmetry forbids direct SM Yukawa couplings. The light observed fermion masses are then generated via "partial compositeness": a seesaw-like pattern mediated by heavy exotic fermion partners of the SM fermions; Yukawa couplings are allowed by the global symmetry only for the partners. In general, these exotic fermions appear in vectorial representations of the SM gauge group. This means that, by construction, Goldstone Higgs models come with a heavy spectrum alike to that of the hadronic invisible axion model KSVZ. We have discussed possible extensions of their spectra so as to make those models $U(1)_{PQ}$ invariant, with the minimality criterion of not extending their fermionic sector, and focusing on the simplest case of $SO(5)$ global symmetry.

We have shown that the minimal extension consisting in the addition of a single $SO(5)$ *scalar singlet to the spectrum and no additional heavy fermions suffices to implement the PQ symmetry in those models*, although the constraints for extensions with more than one singlet scalar have also been determined. In a first step, a renormalizable sigma model with $MCHM_{5-1-1}$ fermionic content has been thoroughly explored, which allowed a precise identification of model building constraints. From the point of view of naturalness, the Peccei-Quinn scale f_a may be expected to be close to the mass of the sigma particle (as neither is protected by the symmetries of the problem and the scalar potential may connect them), which when taken very massive results in the customary low-energy effective non-linear formulation typical of effective Goldstone Higgs constructions. The pGB character of the Higgs protects its mass from large corrections even in the presence of these scalars. In a second step, a plethora of fermionic setups used in non-renormalizable formulations existing in the literature has been considered. The latter differ by the type of exotic heavy fermions and Yukawa couplings, and we have discussed how to formulate them as renormalizable sigma models and how to extend them minimally (only by scalar singlets) so as to acquire a Peccei-Quinn invariant formulation.

The issue of naturalness for the solutions found has been discussed in detail and used as a discriminating tool. Although the Higgs mass is protected from the electroweak hierarchy problem by construction, the question is pertinent with respect to the other scales of the theories, given the large value of f_a. When all heavy exotic fermion mass eigenstates are assumed to remain at most of the order of the composite scale ($\sim 1 - 100$ TeV), we have found that all axion solutions are technically natural as they are protected by a chiral symmetry under which some fermions transform but not the scalars. An appealing and different possibility has been also identified, though, for a very small subset of the solutions found: that

in which the $SO(5)$ singlet fermion representations –often used in the literature in Goldstone Higgs models– may be the only ones with Peccei-Quinn charges and having masses of order f_a. Only three of the many fermionic setups considered satisfy this more restrictive criteria: $MCHM_{5-1-1}$, $MCHM_{5-1-10}$ and $MCHM_{14-1-10}$, and for each of them some solution(s) could accommodate very heavy fermions. Such options would not necessarily require small dimensionless parameters among the axionic couplings discussed here; this would be a natural solution in the sense that the mass parameters for $SO(5)$ singlets are not protected by any low-energy symmetry. Although the value of the Higgs mass itself cannot be destabilized by large contributions induced by the heavy $SO(5)$ singlet fermions, it remains to be clarified, though, whether such heavy singlet fields may destabilize instead the value of the f scale itself or not, and whether a fine tuning of other parameters in the model (e.g. in the scalar potential) would be required to compensate for this effect. Anyway, the bulk of the solutions found do not assume such high scales though.

The phenomenological predictions for the axion-photon-photon coupling (actively searched for at present by many experiments all over the world) have been next determined for all models explored. We have demonstrated that *the region in the* $(m_a, g_{a\gamma\gamma})$ *parameter space allowed for Goldstone Higgs models on which the PQ symmetry is implemented without enlarging their original fermionic sector is much more restrictive than that for standard invisible axion formulations*. The reason is that, while in the latter scenarios the SM fermion masses are unrelated to the vectorial exotic sector, in Goldstone Higgs scenarios the generation of SM masses via partial compositeness imposes stringent relations among the parameters and couplings of the exotic fermions that mediate them. For instance, within the fermionic spectra of existing Goldstone Higgs models, that is, assuming as fermionic content exclusively their inherent minimal spectrum, it is not possible to obtain an arbitrarily small axion-photon-photon coupling for any given m_a. The latter would require instead to add extra fermions to the spectrum with the specific purpose of implementing the axion solution via the couplings of those extra fermions. This restricted parameter space for the minimal fermionic setup holds in spite of the complex spectrum of fermionic spectra in Goldstone Higgs models, which in general requires several distinct fermion representations, in contrast to recent finds for standard invisible axion models [140, 244].

It is remarkable that the plethora of existing Goldstone Higgs models exhibit by construction a KSVZ-like structure simply with their inherent minimal fermionic sector, a suggestive fact explored here. Although the precise phenomenological analysis has been done for the case of only adding to the spectrum a single scalar singlet field,, the underlying reason for the restricted parameter space is generic and should hold with more extended scalar spectra. This enhanced predictivity of the minimal Goldstone Higgs setups explored has a relevant impact on the planned experimental searches, and may also serve as discriminating tool in case of future axion and/or Goldstone Higgs signals.

6

ALPS EFFECTIVE FIELD THEORY AND COLLIDER SIGNATURES

This chapter explores the physics of an extra singlet scalar which is a CP-odd (pseudo)Nambu-Goldstone boson. We will formulate in all generality its leading CP-invariant effective couplings to SM fields using the tool of effective field theories, presented in Sect. 1.4. In order to construct the bases of effective operators, only the low-energy fields will be used: the ALP and the fields of the SM. On the ALP side, it is just required that its couplings are derivative and suppressed by the new physics scale f_a, a characteristic feature of GBs. On the SM side the are two possible ways to implement the EFT: a linear Lagrangian which is typically used to describe scenarios where the BSM physics is weakly interacting, defined in Sect. 1.4.1, and a chiral (non-linear) Lagrangian for the cases of strongly-interacting NP, defined in 1.4.2. While the former had been derived long ago for the case of axions and ALPs, and is reported in Sect. 3.2, the latter has been derived for the first time in the context of this thesis.

We will first concentrate on determining a complete basis of CP-even bosonic operators containing one ALP insertion; nevertheless, the fermionic operators are also derived in this thesis (they are presented in App. A.1), building a complete and non-redundant chiral set. The relation and differences between the dominant operators in both expansions –linear and chiral– will be subsequently discussed. It is interesting to note that all results to be obtained below apply as well to a different case: the complete basis of CP-odd derivative couplings of an hypothetical CP-even scalar (see also Chapter 7 for a generic CP-even scalar).

Up to now, most phenomenological ALP analyses concentrated on their couplings to photons, gluons and/or quarks, as they dominate at low energies and determine astrophysical and cosmological constraints for very light ALPs. Nevertheless, ALPs may well show up first at colliders [18, 163, 249] or in rare mesonic decays [17, 178], and the $SU(2)_L \times U(1)_Y$ invariant formulation of their interactions developed here provides new beautiful channels involving the electroweak gauge bosons and the Higgs particle. The status of ALP physics from the point of view of experiment has been throughly reviewed in Sect. 3.3. In this section re have additionally reinterpreted preixisting contraints in terms of the complete set of operators in the linear basis. For instance, rare meson decays have been used in the past to constrain axion-fermion and aW^+W^- couplings, and we have shown that for the bosonic basis $c_{a\Phi}$ defined in Eq. (3.50) can also be tested. In the second –phenomenological– part of this chapter (Sects. 6.4 and 6.5), new phenomenological signals will be presented and analysed for the first time. Some signals will be shown to be sensitive to both operators which are expected both in the linear and in the non-linear setups. Moreover, we will identify signatures which would only be expected in the non-linear case.

6.1 THE BOSONIC CHIRAL ALP LAGRANGIAN

This section explores the leading effective couplings between an ALP and the SM fields, in the general framework of a non-linear (often referred to as chiral or HEFT) realization of EWSB. The complete set of LO and NLO bosonic CP-even couplings involving one ALP will be determined (they could also be read as the complete bosonic set of derivative CP-odd couplings involving a CP-even singlet scalar). It will be assumed that the characteristic scale f_a associated to the Nambu-Goldstone boson origin of the ALP is at least of the same order of magnitude or larger than the cut-off of the BSM electroweak theory Λ. The ALP scale and the electroweak BSM scale Λ will nevertheless be treated here as independent.

Although the HEFT formalism was explained in detail in Sect. 1.4.2, we here shortly remind its main characteristic. In the chiral EW Lagrangian –HEFT– the four degrees of freedom which compose the Higgs doublet in the SM –the three longitudinal components of the $W^\pm$ and the Z bosons and the Higgs particle– are no longer introduced in the Lagrangian in the form of the doublet in Eq. (1.22). Instead, two building blocks are used:

- A unitary matrix $\mathbf{U}$, defined in Eq. (1.52) describes the EW would-be-Goldstone bosons. It is in fact introduced in the Lagrangian via two $SU(2)_L$ covariant objects, $\mathbf{T}$ and $\mathbf{V}_\mu$ defined in Eq. (1.53).
- Polynomial functions of the Higgs field $\mathcal{F}_i(h/v)$, defined in Eq. (1.56), allow to reproduce the more general Higgs dependence that arises in specific models described at low-energy by the HEFT Lagrangian. For instance, for the case of composite Higgs models, sinusoidal functions of the scalar field often replace the typical SM dependence as $(v+h)^n$.

The task now consists in the generalization of the HEFT Lagrangian to include insertions of derivatives of a/f_a. This could be approached via the insertion in that Lagrangian of general polynomial functions of the SM singlet scalar a, $\mathcal{F}_i(a/f_a)$, in analogy with the treatment given to the scalar h in the HEFT Lagrangian. After all, the $\mathcal{F}_i(h/v)$ polynomials are reminiscent of the deformed exponential Nambu-Goldstone nature of the Higgs particle in some non-linear EWSB realizations, such as "composite Higgs" models [8, 86, 87]. From this point of view, to restrict below to terms with a single $a(x)/f_a$ insertion is consistent with the assumption $f_a \geqslant \Lambda$. In summary, the effective Lagrangian can be written as

$$\mathcal{L}_{\text{eff}}^{\text{chiral}} = \mathcal{L}^{\text{LO}} + \delta\mathcal{L}_a^{\text{chiral}}\,, \tag{6.1}$$

As it was also explained in Sect. 1.4.2, the counting of dimensions also changes in the HEFT with respect to the SMEFT formulation. In this setup, the leading order is composed out of operators with two derivatives, in which case amongst the LO operators there are now two terms which are two-derivative couplings:

$$\mathcal{L}^{\text{LO}} = \mathcal{L}_{\text{HEFT}}^{\text{LO}} + \mathcal{L}_a^{\text{LO}}\,. \tag{6.2}$$

The Lagrangian $\mathcal{L}_{\text{HEFT}}^{\text{LO}}$ is the generalisation of the SM Lagrangian in terms of the HEFT formulation, defined in Eq. (1.57). The ALP leading order Lagrangian reads

$$\mathcal{L}_a^{\text{LO}} = \frac{1}{2}(\partial_\mu a)(\partial^\mu a) + c_{2D}\mathcal{A}_{2D}(h)\,, \tag{6.3}$$

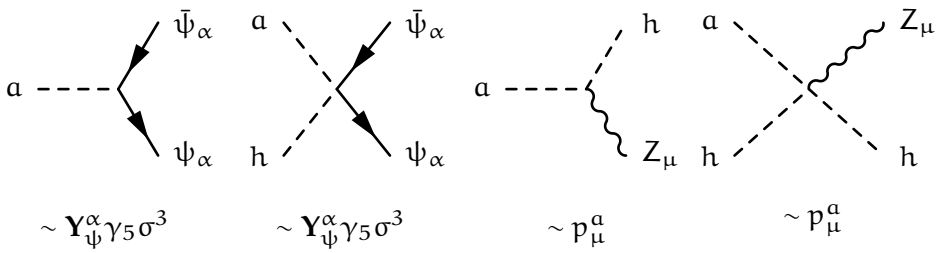

Linear @ NLO ($d = 5$)	$\mathbf{O}_{a\Phi}$	$\mathbf{O}_{a\Phi}$	–	–
Chiral @ LO (2∂)	$\mathcal{A}_{2D}$	$\mathcal{A}_{2D}$	$\mathcal{A}_{2D}$	$\mathcal{A}_{2D}$

Table 6.1: Couplings resulting from the bosonic axion NLO linear coupling $\mathbf{O}_{a\Phi}$ and from its LO chiral sibling $\mathcal{A}_{2D}$, as formulated in the Lagrangians Eqs. (3.65) and (6.12), respectively. Only fermionic vertices survive as physical impact from $\mathbf{O}_{a\Phi}$, as in the linear expansion higher orders ($d \geqslant 7$) are required for aZh^n ($n \neq 1$) couplings, while the latter are present in the chiral case at LO. For the complete Feynman rules see App. A.2.

where $\mathcal{A}_{2D}(h)$ is a custodial breaking two-derivative operator with mass dimension three,

$$\mathcal{A}_{2D}(h) = iv^2 \mathrm{Tr}[\mathbf{T}\mathbf{V}_\mu]\partial^\mu \frac{a}{f_a}\mathcal{F}_{2D}(h)\,. \tag{6.4}$$

This operator appears then singled out at the LO in the chiral expansion, unlike the case of the linear expansion in which the only LO ALP term was the a kinetic energy, see Eq. (3.52) and Table 6.1. In other words, if the EWSB is non-linearly realised $\mathcal{A}_{2D}(h)$ may well provide the dominant and distinctive signals. It induces a two-point function of the form $Z^\mu \partial^\mu a$ which contributes to the longitudinal component of the Z boson together with the usual would-be Nambu-Goldstone boson of the SM, and thus to the Z mass. Its impact is in this respect analogous to that of the two-point function stemming from the $d = 5$ NLO linear operator $\mathbf{O}_{a\Phi}$, see Sect. 3.2 and Eq. (3.57). Nevertheless, it will be shown in Sects. 6.1.2 and 6.2 that $\mathcal{A}_{2D}$ has additional physical consequences distinct from those induced by $\mathbf{O}_{a\Phi}$, as illustrated in Table 6.1.

A discussion of scales

The normalization of the operators in Eqs. (1.57) and (6.4), and in the NLO chiral corrections to be discussed below follows the Naive Dimensional Analysis (NDA) master formula for the HEFT Lagrangian as discussed in Refs. [57, 82–84]. With this convention the gauge boson kinetic terms appear canonically normalised. In addition, the strongly interacting regime would correspond to operator coefficients of $\sim \mathcal{O}(1)$.

Furthermore, the mass parameter in front of several operators in Eqs. (1.57) and in Eq. (6.4) should be a generic scale f, which in specific models is that associated to a Nambu-Goldstone ancestry for the Higgs resonance (alike to f_π for QCD pions), such that $\Lambda \leqslant 4\pi f$ [57]. Instead,

v –the electroweak scale– is shown as explicit mass parameter for bosons and fermions in Eqs. (1.57) and (6.4), with $v < f$: this inequality is the well-known fine-tuning of the chiral electroweak Lagrangian, necessary to recover the correct scale of the gauge boson masses. It reflects as well the fine-tuning problems of specific "composite Higgs" scenarios. For consistency v has been then chosen as weight in all mass-related terms in those equations; for instance a factor of f^2/v^2 is thus implicitly embedded in the definition of the coefficient c_{2D} in Eq. (6.3).

The same fine-tuning is at the origin of the $\mathcal{F}_i(h)$ functions being customarily written as generic polynomials in h/v instead of h/f, see Eq. (1.56). It can be considered that in this parametrization factors of v/f have been reabsorbed in the free parameters a_i, b_i, etc. in Eq. (1.56). Note as well that, in principle, a function $\mathcal{F}_i(h)$ can be attached to any of the operators in (6.3). However, as it was done for the $\mathcal{F}_i(h)$ functions in $\mathcal{L}^{\rm LO}_{\rm HEFT}$ [85] (see discussion below Eq. (1.57)) they can be redefined away at the price of redefining $\mathcal{F}_{2D}(h)$. Moreover, much as the $\mathcal{F}_i(h)$ insertions in the gauge bosons kinetic terms can from $\mathcal{L}^{\rm LO}_{\rm HEFT}$ can be avoided assuming that the transverse components of the gauge fields do not couple at tree level to the Higgs sector, as it has been explicitly shown in Refs. [74, 75] for composite Higgs models [8, 86, 87], a similar assumption on the ALP sector prevents from writing terms of the type $aX_{\mu\nu}\tilde{X}^{\mu\nu}$ at LO.

6.1.1 *The NLO ALP Operators*

The complete list of HEFT CP-even bosonic operators at NLO is known [14, 70, 73] and will not be further discussed. We address here the NLO bosonic chiral interactions involving one insertion of a/f_a, encoded in $\delta\mathcal{L}^{\rm chiral}_a$ in Eq. (6.1). The additional inclusion of fermionic couplings and the construction of a complete and non-redundant CP-even basis, which will turn out to be composed of a total of 32 – bosonic and fermionic – operator structures (including the LO axionic operator $\mathcal{A}_{2D}$ and assuming one flavour), is deferred to App. A.1. The NLO Lagrangian $\delta\mathcal{L}^{\rm chiral}_a$ consists instead of 20 independent bosonic operator structures (disregarding in the counting the different coefficients inside the $\mathcal{F}_i(h)$ functions),

$$\delta\mathcal{L}^{\rm chiral}_a = \sum_{X=\tilde{B},\tilde{W},\tilde{G}} c_X \mathcal{A}_X + \sum_{i=1}^{17} c_i \mathcal{A}_i(h)\,, \tag{6.5}$$

where

$$\left.\begin{aligned}
\mathcal{A}_{\tilde{B}} &= -B_{\mu\nu}\tilde{B}^{\mu\nu}\frac{a}{f_a}\\
\mathcal{A}_{\tilde{W}} &= -W^a_{\mu\nu}\tilde{W}^{a\mu\nu}\frac{a}{f_a}\\
\mathcal{A}_{\tilde{G}} &= -G^a_{\mu\nu}\tilde{G}^{a\mu\nu}\frac{a}{f_a}\\
\mathcal{A}_1(h) &= \frac{i}{4\pi}\tilde{B}_{\mu\nu}\mathrm{Tr}[\mathbf{T}\mathbf{V}^\mu]\partial^\nu\frac{a}{f_a}\mathcal{F}_1(h)\\
\mathcal{A}_2(h) &= \frac{i}{4\pi}\mathrm{Tr}[\tilde{W}_{\mu\nu}\mathbf{V}^\mu]\partial^\nu\frac{a}{f_a}\mathcal{F}_2(h)\\
\mathcal{A}_3(h) &= \frac{1}{4\pi}B_{\mu\nu}\partial^\mu\frac{a}{f_a}\partial^\nu\mathcal{F}_3(h)
\end{aligned}\right\}\text{Custodial symmetry preserving}$$

$$\begin{aligned}
\mathcal{A}_4(h) &= \frac{i}{(4\pi)^2}\mathrm{Tr}[\mathbf{V}_\mu\mathbf{V}_\nu]\mathrm{Tr}[\mathbf{T}\mathbf{V}^\mu]\partial^\nu\frac{a}{f_a}\mathcal{F}_4(h)\\
\mathcal{A}_5(h) &= \frac{i}{(4\pi)^2}\mathrm{Tr}[\mathbf{V}_\mu\mathbf{V}^\mu]\mathrm{Tr}[\mathbf{T}\mathbf{V}^\nu]\partial_\nu\frac{a}{f_a}\mathcal{F}_5(h)\\
\mathcal{A}_6(h) &= \frac{1}{4\pi}\mathrm{Tr}[\mathbf{T}[W_{\mu\nu},\mathbf{V}^\mu]]\partial^\nu\frac{a}{f_a}\mathcal{F}_6(h)\\
\mathcal{A}_7(h) &= \frac{i}{4\pi}\mathrm{Tr}[\mathbf{T}\tilde{W}_{\mu\nu}]\mathrm{Tr}[\mathbf{T}\mathbf{V}^\mu]\partial^\nu\frac{a}{f_a}\mathcal{F}_7(h)\\
\mathcal{A}_8(h) &= \frac{i}{(4\pi)^2}\mathrm{Tr}[[\mathbf{V}_\nu,\mathbf{T}]\mathcal{D}_\mu\mathbf{V}^\mu]\partial^\nu\frac{a}{f_a}\mathcal{F}_8(h)\\
\mathcal{A}_9(h) &= \frac{i}{(4\pi)^2}\mathrm{Tr}[\mathbf{T}\mathbf{V}_\mu]\mathrm{Tr}[\mathbf{T}\mathbf{V}^\mu]\mathrm{Tr}[\mathbf{T}\mathbf{V}_\nu]\partial^\nu\frac{a}{f_a}\mathcal{F}_9(h)\\
\mathcal{A}_{10}(h) &= \frac{1}{4\pi}\mathrm{Tr}[\mathbf{T}W_{\mu\nu}]\partial^\mu\frac{a}{f_a}\partial^\nu\mathcal{F}_{10}(h)\\
\mathcal{A}_{11}(h) &= \frac{i}{(4\pi)^2}\mathrm{Tr}[\mathbf{T}\mathbf{V}_\mu]\Box\frac{a}{f_a}\partial^\mu\mathcal{F}_{11}(h)\\
\mathcal{A}_{12}(h) &= \frac{i}{(4\pi)^2}\mathrm{Tr}[\mathbf{T}\mathbf{V}_\mu]\partial^\mu\partial^\nu\frac{a}{f_a}\partial_\nu\mathcal{F}_{12}(h)\\
\mathcal{A}_{13}(h) &= \frac{i}{(4\pi)^2}\mathrm{Tr}[\mathbf{T}\mathbf{V}_\mu]\partial^\mu\frac{a}{f_a}\Box\mathcal{F}_{13}(h)\\
\mathcal{A}_{14}(h) &= \frac{i}{(4\pi)^2}\mathrm{Tr}[\mathbf{T}\mathbf{V}_\mu]\partial_\nu\frac{a}{f_a}\partial^\mu\partial^\nu\mathcal{F}_{14}(h)\\
\mathcal{A}_{15}(h) &= \frac{i}{(4\pi)^2}\mathrm{Tr}[\mathbf{T}\mathbf{V}_\mu]\partial^\mu\frac{a}{f_a}\partial_\nu\mathcal{F}_{15}(h)\partial^\nu\mathcal{F}'_{15}(h)\\
\mathcal{A}_{16}(h) &= \frac{i}{(4\pi)^2}\mathrm{Tr}[\mathbf{T}\mathbf{V}_\mu]\partial_\nu\frac{a}{f_a}\partial^\mu\mathcal{F}_{16}(h)\partial^\nu\mathcal{F}'_{16}(h)\\
\mathcal{A}_{17}(h) &= \frac{i}{(4\pi)^2}\mathrm{Tr}[\mathbf{T}\mathbf{V}_\mu]\partial^\mu\frac{\Box a}{f_a}\mathcal{F}_{17}(h)\,.
\end{aligned}\tag{6.6}$$

The requirement that all ALP couplings respect a (continuous or discrete) shift symmetry prevents the insertion of $\mathcal{F}_i(h)$ functions in the three first couplings in this list. The first block

of six operators are those invariant under custodial symmetry, assuming as customary no sources of custodial symmetry breaking other than those present in the SM.

The "penalization" of the operator coefficients by inverse powers of 4π is a most conservative choice of their possible value, which reflects the NDA normalization of the chiral sector [57, 82–84] in which $\mathcal{O}(1)$ operator coefficients indicate the strong regime. A particular case is that of vertices involving one Higgs leg, for which the overall amplitude will be proportional in practice to the product

$$\tilde{a}_i \equiv c_i \, a_i \,, \tag{6.7}$$

see Eq. (1.56). Given the f/v factor absorbed in the definition of a_i, in the strong coupling limit $\tilde{a}_i$ is expected to be somewhat smaller than 1 for all $i \neq 2D$. Conversely, $\tilde{a}_{2D}$ as defined here is expected to be larger than 1 by a factor $\mathcal{O}(f/v)$ in that limit, see the discussion at the end of Sect. 6.1. Analogous reasoning applies to vertices with more than one Higgs leg.

6.1.2 *Two-point functions*

The last NLO operator in Eq. (6.6), $\mathcal{A}_{17}(h)$, introduces a Z-a two-point function alike to that from the LO coupling $\mathcal{A}_{2D}(h)$, albeit with a higher momentum dependence. That is, both operators feed derivatives of the ALP field into the longitudinal components of the Z boson, in addition to the usual derivative of the SM would-be Nambu-Goldstone neutral field:

$$\begin{aligned}
&c_{2D}\mathcal{A}_{2D}(h) + c_{17}\mathcal{A}_{17}(h) \supset \\
&\supset -\frac{i}{f_a}\,\mathrm{Tr}\left(\mathbf{T}\,(\partial_\mu \partial^\mu \mathbf{U})\,\mathbf{U}^\dagger\right)\,\left(c_{2D}\,v^2\,a + \frac{c_{17}}{16\pi^2}\,\Box a\right) + \\
&\quad + \frac{i}{2}\,g'\,B^\mu\left\{v^2 \mathrm{Tr}\left(\,(\partial_\mu \mathbf{U})\,\tau_3\,\mathbf{U}^\dagger - \mathbf{U}\,\tau_3\,\left(\partial_\mu \mathbf{U}^\dagger\right)\right) - \frac{2i}{f_a}\left[c_{2D}\,v^2\,\partial_\mu a + \frac{c_{17}}{16\pi^2}\,\partial_\mu\,(\Box a)\right]\right\} \\
&\quad + \frac{i}{2}\,g\,W^i_\mu\left\{v^2 \mathrm{Tr}\left(\,\left(\partial^\mu \mathbf{U}^\dagger\right)\tau^i \mathbf{U} - \mathbf{U}^\dagger \tau^i\,(\partial^\mu \mathbf{U})\right) + \frac{i}{f_a}\left[c_{2D}\,v^2\,\partial_\mu a + \frac{c_{17}}{16\pi^2}\,\partial_\mu\,(\Box a)\right]\mathrm{Tr}\left(\mathbf{T}\,\tau^i\right)\right\}\,.
\end{aligned} \tag{6.8}$$

The physical impact can be illustrated best via a field redefinition which trades completely this combination of two-point functions by interaction vertices, alike to the procedure applied to the linear operator $\mathbf{O}_{a\Phi}$ in Sect. 3.2,

$$\mathbf{U}(x) \to \mathbf{U}(x)\,\exp\left\{\frac{2i}{f_a}\left(c_{2D}\,a(x) + c_{17}\frac{1}{16\pi^2 v^2}\,\Box a(x)\right)\sigma^3\right\}\,, \tag{6.9}$$

which translates also in contributions to the definition of the gauge fixing terms, the mass term for the gauge bosons and the Yukawa couplings (see also Chapter 7 for a similar discussion in the context of CP-odd effective operators within non-linearly realised EWSB). The net physical impact is:

- The introduction of new fermionic couplings, alike to those fully equivalent in the linear case to the bosonic operator $\mathbf{O}_{a\Phi}$, see Eqs. (3.59)-(3.65).
- The presence in addition of aZh and other vertices of the form $(Z_\mu \partial^\mu a)h^n$, $n \geqslant 1$, which are *not* redefined away in the non-linear case. The reason is that the functional dependence on h of $\mathcal{F}_i(h)$ differs generically from that characteristic of the linear regime (in powers of $(v+h)^2$).

The purely bosonic couplings cannot be thus completely traded by fermionic ones in the generic case of non-linear EWSB. This is remarkable, as it implies that aZh couplings could be then expected among the dominant signals of ALPs, at variance with linear realizations in which they are only expected at NNLO (as argued in Sect. 6.2 below). This comparison is illustrated in Table 6.1.

The fermionic couplings, stemming from $\mathcal{A}_{2D}(h)$ and $\mathcal{A}_{17}(h)$ after the field redefinition discussed, will be denoted by $\mathcal{A}^{\psi}_{2D}$ and $\mathcal{A}^{\psi}_{17}$ and defined as:

$$\begin{aligned}\mathcal{A}^{\psi}_{2D} &= -i\sqrt{2}v\,\frac{a}{f_a}\sum_{\psi=Q,L}\left(\bar{\psi}_L Y_\psi(h)\mathbf{U}\sigma^3\psi_R\right)+\text{h.c.}\,,\\ \mathcal{A}^{\psi}_{17} &= -\frac{i\sqrt{2}v}{16\pi^2}\,\frac{\Box a}{v^2 f_a}\sum_{\psi=Q,L}\left(\bar{\psi}_L Y_\psi(h)\mathbf{U}\sigma^3\psi_R\right)+\text{h.c.}\,,\end{aligned} \tag{6.10}$$

see Eq. (1.58) and App. A.4 for details. These expressions are the non-linear equivalent of the linear interaction $\mathbf{O}^{\psi}_{a\Phi}$ in Eq. (3.62). Alternatively, the part of $\mathcal{A}_{2D}$ and $\mathcal{A}_{17}$ that can be traded by fermionic couplings could be written as chirality-conserving transitions, e.g.

$$\begin{aligned}\mathcal{A}^{\psi}_{2D} &\to \frac{\partial_\mu a}{f_a}\sum_{\psi=Q,\,L}\left(\bar{\psi}\gamma^\mu\gamma_5\sigma^3\psi\right)\mathcal{F}_\psi(h)\,,\\ \mathcal{A}^{\psi}_{17} &\to \frac{1}{16\pi^2v^2}\left(\frac{\partial_\mu\Box a}{f_a}\right)\sum_{\psi=Q,\,L}\left(\bar{\psi}\gamma^\mu\gamma_5\sigma^3\psi\right)\mathcal{F}_\psi(h)\,,\end{aligned} \tag{6.11}$$

which are the chiral equivalent of Eq. (3.64). In this chapter, when analyzing the non-linear EWSB scenario we will use the formulation of chirality-flipping fermionic couplings in Eq. (6.10).[1]

6.1.3 *The bosonic chiral ALP basis*

In summary, the resulting bosonic ALP Lagrangian up to NLO couplings can be written, after the redefinition in Eq. (6.9), as the sum of 23 terms, besides the kinetic term:

$$\mathcal{L}^{\text{chiral}}_a = \frac{1}{2}(\partial_\mu a)(\partial^\mu a)+c_{2D}\mathcal{A}'_{2D}(h)+\sum_{X=\tilde{B},\tilde{W},\tilde{G}}c_X\mathcal{A}_X+\sum_{i=1}^{16}c_i\mathcal{A}_i+c_{17}\mathcal{A}'_{17}(h)+\sum_{i=2D,17}c_i\mathcal{A}^{\psi}_i\,, \tag{6.12}$$

where $\mathcal{A}'_{2D}(h)$ and $\mathcal{A}'_{17}(h)$ are defined as the operators $\mathcal{A}_{2D}(h)$ and $\mathcal{A}_{17}(h)$ without their h-independent terms, which have been traded instead by the fermionic $\mathcal{A}^{\psi}_i$ couplings as defined in Eq. (6.10). The rest of the operators have been defined in Eq. (6.6). All Feynman rules stemming from $\mathcal{L}^{\text{chiral}}_a$ can be found in App. A.2, up to four-leg interactions.

$\mathcal{A}_{\tilde{B}}$, $\mathcal{A}_{\tilde{W}}$, $\mathcal{A}_{\tilde{G}}$ and $\mathcal{A}^{\psi}_{2D}$ are identical to the operators found in the framework of the linear EWSB Lagrangian. In consequence, the bounds on ALP-photon and ALP-gluon vertices in Eqs. (6.18) and (6.17) apply. This would also hold, restricted to the indicated mass ranges, for the aW^+W^- coupling in Eq. (3.88), if $\mathcal{A}_{\tilde{W}}$ was considered just by itself. Nevertheless, the

1 The Feynman rules for all bosonic and fermionic vertices stemming from $\mathcal{A}_{2D}(h)$ and $\mathcal{A}_{17}(h)$, up to four-field couplings, can be found in FR.7 - FR.22 and FR.18 - FR.19 of App. A.2, respectively.

caveats to that approach discussed in the linear case are even stronger here in the sense that the aW^+W^- couplings may receive contributions in the non-linear case from the set (see FR.4)

$$\{c_{\tilde{W}}, c_2, c_6, c_8\}\,. \tag{6.13}$$

Analogously, the ALP-fermion vertices in Eqs. (3.85)-(3.86) would constrain the magnitude of $\mathcal{A}_{2D}$, if the latter is taken just by itself, to

$$|c_{2D}|/f_a \,<\, \left(1.7\cdot 10^{-8} - 1.4\cdot 10^{-6}\right)\ \text{GeV}^{-1} \quad (90\%\ \text{C.L.}) \quad \text{for} \quad m_a \lesssim 3\,\text{GeV}\,. \tag{6.14}$$

Again, in the non-linear EWSB setup many other couplings may contribute in addition to rare meson decay processes than in the linear case, see FR.17-FR.19, to wit

$$\{c_{2D}, c_{\tilde{W}}, c_2, c_6, c_8, c_{17}, \{c_{\mathcal{P}_i^q}\}\}\,, \tag{6.15}$$

In this ensemble, the subset $\{c_{\mathcal{P}_i^q}\}$ of operator coefficients refers to the flavour-changing operators of the general ALP-fermion couplings $\mathcal{P}_i^q$ in the complete Lagrangian, see Eq. (A.1), which can contribute either at tree-level or at one loop via W, Z or h exchange, and thus on the same footing than for instance $c_{\tilde{W}}$ or c_2, c_6, c_8 and c_{17}. Even if the data analysis was restricted for simplicity to bosonic couplings (the focus of this chapter), a six-dimensional parameter space would still remain, which means that a large freedom remains for the possible value of one given coupling. In consequence, consistently with the complementarity perspective, in the second -phenomenological- part of this chapter we will explore the independent impact that the bosonic non-linear operator coefficients in Eq. (6.15) may have on LHC signals, which they impact via a different combination than in rare decays. Those couplings will be thus considered there first one at a time and occasionally in some combinations.

6.2 LINEAR VS NON-LINEAR EXPANSIONS

The results in the previous sections on bosonic ALP-SM interactions uncovered a plethora of effective couplings in the bosonic sector of the chiral expansion, in contrast with the mere four operator structures of the linear one shown in Eq. (3.66), when both Lagrangians are considered up to NLO. All ALP couplings are NLO ones in the linear case, while one of the chiral set ($\mathcal{A}_{2D}$) stands out at LO.

Three operators are exactly the same in both expansions. They are those with an "anomalous-type" structure of the form $aX_{\mu\nu}\tilde{X}^{\mu\nu}$, where $X_{\mu\nu}$ stands for a SM field strength: $\mathcal{A}_{\tilde{B}}$, $\mathcal{A}_{\tilde{W}}$ and $\mathcal{A}_{\tilde{G}}$. The total number of independent interactions has to be equal in both expansions when all orders are considered, though. It is thus pertinent to identify which are the effective operators of the linear expansion that lead to the same interaction vertices than the chiral (up to) NLO couplings. This is accomplished in App. A.3, which identifies the linear siblings with mass dimension:

- $d = 5$, corresponding to $\mathcal{A}_{\tilde{B}}, \mathcal{A}_{\tilde{W}}$ and $\mathcal{A}_{\tilde{G}}$ and to the fermionic couplings induced by $\mathcal{A}_{2D}$ with no attached Higgs leg (these are identical in both expansions), as well as other fermionic vertices.

- $d = 7$, corresponding to $\mathcal{A}_1$-$\mathcal{A}_6$, $\mathcal{A}_8$, $\mathcal{A}_{10}$-$\mathcal{A}_{12}$ and $\mathcal{A}_{15}$-$\mathcal{A}_{17}$.

- $d = 9$, corresponding to $\mathcal{A}_7$, $\mathcal{A}_{13}$ and $\mathcal{A}_{14}$.
- $d = 11$, corresponding to $\mathcal{A}_9$.

Furthermore, the siblings of the vertices induced by $\mathcal{A}_{2D}$ with one or more Higgs legs are linear effective operators with dimension $d = 7$ [250] or higher, depending on their Lorentz structure.

Common/distinctive phenomenological signals

Interaction vertices predicted by both expansions include the well-known ALP-photon and ALP-gluon couplings, and in addition the yet mainly unexplored $a\gamma Z$, aZZ, aW^+W^-, $a\gamma W^+W^-$ and aZW^+W^- signals.

Distinctive signals are those only present in the chiral EWSB Lagrangian at the order considered, which are: i) an extra ALP-gauge boson vertex, $aZZZ$, and new Lorentz structures in others such as aZZ, aW^+W^-, $a\gamma W^+W^-$ and aZW^+W^- ; ii) ALP-Higgs interactions stemming from $\mathcal{A}_{2D}$, which include $a\gamma h$, aZh, $a\gamma Zh$, $aZZh$, aW^+W^-h, $a\gamma hh$ and $aZhh$ interactions, among others. All these signals are thus putatively important pointers of non-linear realizations of EWSB.

A natural question about the bosonic ALP-Higgs interactions is how come those $(Z_\mu \partial^\mu a)h^n$ couplings with $n \geqslant 1$ appear at LO in the non-linear expansion while they are instead very suppressed in the linear one, as after all the latter is a limit of the former. The gist lies in the generality of the $\mathcal{F}_i(h)$ functions, and more specifically in the difference between $\mathcal{F}_C(h)$ and $\mathcal{F}_{2D}(h)$, see Eqs. (1.56), (1.57) and (6.4). Would those two functions be equal, as it happens in the linear expansion, all bosonic ALP vertices involving the Higgs would also be redefined away completely in the chiral expansion at LO and NLO. Furthermore, even if the difference between the a_i, b_i etc. coefficients for those two $\mathcal{F}_i(h)$ functions was considered to be qualitatively a NLO effect, all $(Z_\mu \partial^\mu a)h^n$, $n \geqslant 1$ couplings would still be phenomenologically considered NLO effects, which means in any case higher strength expected than in linear realizations of EWSB (where they start to appear only at NNLO).

The phenomenology of the ALP couplings to heavy SM bosons will be explored in Sects. 6.4 and 6.5 below.

6.3 ANALYSIS ASSUMPTIONS AND VALIDITY OF THE EFT

The theoretical results in the previous sections focused on a generic Nambu-Goldstone boson, singlet under the SM, identifying all bosonic derivative couplings at LO in the linear and chiral expansions (a complete set including fermionic ones was also derived and for the chiral case they can be found in App. A.1). They hold independently of whether the –unknown– underlying global symmetry is exact or slightly and explicitly broken, that is of whether the ALP is indeed exactly massless or not, as far as its mass is negligible compared to the typical momenta considered. A few considerations are nevertheless in order before moving to the phenomenological analysis of ALPs signatures at colliders.

6.3.1 *Axion-photon decoupling*

Both $\mathcal{A}_{\tilde{B}}$ and $\mathcal{A}_{\tilde{W}}$ –in Eqs. (3.54) and (3.55) for the linear Lagrangian and Eq. (6.6) for the non-linear– contribute to the interaction of the ALP with two photons, defined again as

$$g_{a\gamma\gamma} = \frac{4}{f_a}(c_{\tilde{B}} c_\theta^2 + c_{\tilde{W}} s_\theta^2)\,. \tag{6.16}$$

This coupling is being used for ALP exploration for a very large range of ALP masses via a diversity of experimental approaches ranging from low-energy astrophysical and laboratory probes to high-energy searches at LHC. These probes were reviewed in Sect. 3.3.1, where a summary of the experimental status of ALP-photon interactions was presented in Fig. 3.4. No positive detection has been found in these probes up to the date, and as a result the coupling $g_{a\gamma\gamma}$ is extremely constrained, especially when compared to other phenomenological couplings which are also being presently searched for.

For substantially low ALP masses astrophysical constraints may apply, e.g. for $m_a = 1\,\text{keV}$ the combination of helioseismology, solar neutrino data observations [243] and Horizontal Branch stars data [154, 162, 251] results in $g_{a\gamma\gamma} \lesssim 10^{-10}\,\text{GeV}^{-1}$, that is,

$$|c_{\tilde{B}} c_\theta^2 + c_{\tilde{W}} s_\theta^2| \lesssim 2.5 \cdot 10^{-8} \left(\frac{f_a}{1\,\text{TeV}}\right) \quad \text{for} \quad m_a \leqslant 1\,\text{keV}\,. \tag{6.17}$$

For higher masses, a small window remains in the MeV ALP range which makes this bound looser. Indeed, for $m_a \simeq 1\,\text{MeV}$ the best present constraint is set by Beam Dump experiments, $g_{a\gamma\gamma} \lesssim 10^{-5}\,\text{GeV}^{-1}$[163, 252] [2], that is

$$|c_{\tilde{B}} c_\theta^2 + c_{\tilde{W}} s_\theta^2| \lesssim 0.0025 \left(\frac{f_a}{1\,\text{TeV}}\right) \quad (90\%\ \text{C.L.}) \quad \text{for} \quad m_a \leqslant 1\,\text{MeV}\,. \tag{6.18}$$

All in all, they enforce the combination $|c_\theta^2 c_{\tilde{B}} + s_\theta^2 c_{\tilde{W}}|/f_a$ to cancel to one part in 10^3 (10^8) for $m_a = 1\,\text{MeV}\,(\text{keV})$. These strong constraints on $g_{a\gamma\gamma}$ could suggest that each of the two coefficients involved, $c_{\tilde{B}}$ and $c_{\tilde{W}}$, may be individually subject to bounds of the same order of magnitude. Nevertheless, often symmetry reasons force a given theory to produce couplings to photons much suppressed with respect to Z couplings. In any case, from the point of view of effective theory they are two independent degrees of freedom: the combination orthogonal to that in $|c_\theta^2 c_{\tilde{B}} + s_\theta^2 c_{\tilde{W}}|$ should be probed and bounded independently. In practice, in most of the phenomenological analysis to be developed in this chapter the constraint

$$c_{\tilde{B}} = -t_\theta^2 c_{\tilde{W}} \tag{6.19}$$

will be systematically enforced.

2 There are in fact stronger bounds on g for $m_a = 1\,\text{MeV}$ from SN1987a measurements, which rule out the range $10^{-9}\,\text{GeV}^{-1} < g_{a\gamma\gamma} < 10^{-6}\,\text{GeV}^{-1}$ (see e.g. Ref. [163]). The one given here is describing a window that remained untested for $m_a \sim 1\,\text{MeV}$ and $g_{a\gamma\gamma} \sim 10^{-5}\,\text{GeV}^{-1}$. This window may be excluded through the model-dependent constraints in Ref. [253], in which case the bound for 1 MeV axions would be $g_{a\gamma\gamma} \ll 10^{-12}\,\text{GeV}^{-1}$

6.3.2 *Validity of the EFT*

For the effective Lagrangian description to be valid, the relevant suppression scale, in this case f_a, must be significantly larger than the typical energy scale of the process under study. In order to strictly ensure the validity of the EFT, one should require $\sqrt{\hat{s}} < f_a$ for each event ($\sqrt{\hat{s}}$ corresponding to the invariant mass of the event). However, $\sqrt{\hat{s}}$ is not experimentally observable in processes with invisible particles in the final state. In this case, the comparison to f_a may be naively performed using either the missing transverse energy of a given event $\not{E}_T$ or the transverse mass m_T, defined as (in events characterised by the presence of a lepton and significant $\not{E}_T$)

$$m_T^2 = 2p_T^\ell \not{E}_T (1 - \cos\phi), \tag{6.20}$$

where p_T^ℓ is the transverse momentum of the lepton and ϕ is the azimuthal angle between the lepton and the missing transverse momentum vector $\vec{\not{E}}_T$ (note that m_T encompasses contributions from both the visible and invisible parts of the final state). We use these two variables in the analysis below, depending on the process, and require that the maximum values allowed for those variables obey

- $m_T^{max} < f_a$ for mono-W analyses (see Sect. 6.4.3), as the ATLAS search we reinterpret uses m_T as discriminating variable. m_T^{max} corresponds to the highest m_T data bin in a given analysis, for each value of f_a considered.
- $2\not{E}_T^{max} < f_a$ for all other processes analyzed. $\not{E}_T^{max}$ is the highest $\not{E}_T$ data bin in a given analysis for each value of f_a considered.

The effect of imposing the strict validity criterium $\sqrt{\hat{s}} < f_a$ can be assessed through the correlation between $\not{E}_T$, m_T and $\sqrt{\hat{s}}$ for each analyzed signal, obtained from Monte Carlo. For binned analyses, the signal event fraction for which $\sqrt{\hat{s}} > m_T^{max}$, $\not{E}_T^{max}$ in different bins may then be discarded. We will explicitly use this procedure for the mono-W and mono-Z analyses in Sects. 6.4.3 and 6.5.1, and discuss the impact of the strict validity criterium on the bounds/sensitivities on f_a/c_i obtained from the rest of analyses. [3]

On a different note, we stress that as the chiral expansion has an implicit BSM electroweak scale $\Lambda \leqslant 4\pi f$, there is an underlying assumption that $f_a \geqslant \Lambda$. This Λ/f_a hierarchy sustains the choice of restraining the analysis to vertices involving only one ALP.

6.3.3 *ALP stability at the LHC and its mass*

In the LHC phenomenological exploration to follow, it will be assumed that the ALP is stable on collider scales, thus escaping the detector as missing transverse energy $\not{E}_T$. This further restricts the range of values of m_a, f_a, appropiate for the concrete numerical analysis below, given the various interactions of a that could allow its decay – see Eqs. (FR.1) - (FR.7) and (FR.17) - (FR.19) in App. A.2. The valid m_a range should be specified for a correct interpretation of the collider results: because of the assumed stability, all phenomenological results to be obtained below hold for ALP masses $m_a \leqslant 1$ MeV, without any additional

3 See also Ref. [254], where a similar method has been applied to DM searches with the added feature of marginalizing over the unknown contribution of new physics beyond the cutoff.

assumption about which channels may be open. The ratio between the ALP mass m_a and f_a is then safely small, $m_a/f_a \leqslant \text{MeV/TeV}$, for characteristic f_a scales of at least a few TeV.

For ALP masses above the MeV, the signals to be studied below may also be present even if the pattern is altered, accompanied by new ones which can be used to precisely test the couplings through which the ALP may decay within the detector (e.g. leptonic couplings). [4] This would require an extended dedicated study.

In this chapter, an ALP mass $m_a \sim 1\,\text{MeV}$ is used in the numerical simulations, light enough to avoid altogether $a \to \ell^+\ell^-$ and $a \to \nu\bar{\nu}\ell^+\ell^-$ decays. The decay channels which then remain *a priori* available are:

– $\underline{a \to \nu\bar{\nu}\nu\bar{\nu}}$ As neutrinos are undetectable at the LHC, this decay doesn't have any impact on our phenomenological analysis. It would simply become part of the $\not{E}_T$ contributions.

– $\underline{a \to \gamma\gamma}$ This decay is constrained by astrophysical observations, as detailed in Sect. 3.3. The distance d covered in the laboratory frame by an ALP before decaying can be estimated as

$$d = \tau\beta c = \frac{\hbar}{\Gamma(a)}\frac{|\vec{p}_a|}{m_a}c\,, \tag{6.21}$$

where τ, $\Gamma(a)$ and $\vec{p}_a$ are, respectively, the proper lifetime, width and three-momentum of the a particle, and c denotes the speed of light. Restricting the width to $\Gamma(a \to \gamma\gamma)$ and using the coupling strength $g_{a\gamma\gamma}$ as defined in Eq. (**??**), it follows that

$$d = \frac{16\pi\hbar c}{m_a^4}\frac{1}{g_{a\gamma\gamma}^2}|\vec{p}_a|\,, \tag{6.22}$$

which can be rewritten as

$$d \simeq 10^8 \left(\frac{\text{MeV}}{m_a}\right)^4 \left(\frac{10^{-5}\,\text{GeV}^{-1}}{g_{a\gamma\gamma}}\right)^2 \left(\frac{|p_a|}{\text{GeV}}\right) \text{m}. \tag{6.23}$$

For $m_a = 1\,\text{MeV}$, given the experimental constraint (see Eqs. (6.16)-(6.18)), it results

$$d > 4\cdot 10^8\,\text{m} \times \left(\frac{|\vec{p}_a|}{\text{GeV}}\right)\,. \tag{6.24}$$

The ALP momentum $|\vec{p}_a|$ is typically of the order of the missing energy of the candidate signals, selected imposing a minimum $\not{E}_T$ cut, which for instance using ATLAS and CMS data is $\gtrsim \mathcal{O}(100)$ GeV. Thus, within the allowed range for $g_{a\gamma\gamma}$ and $\not{E}_T$, the ALP always covers an enormous distance – many orders of magnitude larger than the LHC detectors size ($\sim 10\,\text{m}$) – before decaying into two photons. For lighter ALPs, the situation is even safer given the inverse quartic dependence of d with m_a. ALP masses above the MeV range and up to hundreds of MeV could be considered without risking two-photon ALP decay in the data analyzed [5] by raising the minimum $\not{E}_T$ cut imposed on data, but this would open the $e^+\,e^-$ leptonic decay channels.

4 As an example, the decay channel $a \to e^+e^-$ can produce collimated signals of e^+e^- signals; we thank Jos Vermaseren for this comment.

5 Near the GeV range and further up there are barely any constraints [163] on the value of $g_{a\gamma\gamma}$. A more elaborate study of the ALP signals involving SM gauge bosons could be pertinent for that scenario, allowing for the corresponding decay channels to be taken into account. This is beyond the scope of this chapter.

– $\underline{a \to \gamma\nu\bar{\nu}}$ Analogously, this process does not affect the stability of the ALP particle at the LHC. It could be mediated by the ALP-Z-γ interaction parametrised by $g_{aZ\gamma}$,

$$\delta\mathcal{L}_a \supset -\frac{1}{4} g_{aZ\gamma}\, a\, F_{\mu\nu}\tilde{Z}^{\mu\nu}\,, \tag{6.25}$$

where $Z^{\mu\nu}$ denotes the Z-boson field strength. The decay width shows a very strong dependence on the mass of the ALP, due to a peculiar cancellation occurring in the phase space integration. In the limit $m_a \ll m_Z$ (and neglecting the Z boson width for simplicity) we find

$$\Gamma(a \to \gamma\nu\bar{\nu}) = \frac{g^2\, g_{aZ\gamma}^2\, m_Z^3}{1024\,(2\pi)^3\, c_\theta^2} \times \left(\frac{13}{20}\frac{m_a^7}{m_Z^7} + \mathcal{O}(m_a^9/m_Z^9)\right)\,. \tag{6.26}$$

For $m_a = 1\,\text{MeV}$, this corresponds to a distance covered by the ALP before decaying

$$d \simeq 10^{22}\,\text{m} \times \left(\frac{|\vec{p}_a|/g_{aZ\gamma}^2}{\text{GeV}^3}\right) > 3.3\cdot 10^{27}\,\text{m} \times \left(\frac{|\vec{p}_a|}{\text{GeV}}\right)\,, \tag{6.27}$$

where on the last inequality the constraint on $g_{aZ\gamma}$ derived further below has been used (see Eq. (6.31)).

6.4 PHENOMENOLOGICAL ANALYSIS I: NEW BOUNDS

In this section we derive new constraints on the operator coefficients using LEP and LHC Run I and II data. Table 7.1 summarizes the observables/processes which are sensitive to the various effective operator coefficients, to be considered in this and the next section.

Unless otherwise specified, we will consider the effect of one operator at a time. Note that the dependence of the signal cross section σ or partial width Γ on an operator coefficient c_i is $(c_i/f_a)^2$, hence the ratio c_i/f_a is the relevant combination of parameters throughout the analysis.

For the operator coefficients we will use the notation of the chiral expansion, as its couplings outnumber and include those of the linear expansion – see Sect. 6.1. Whenever pertinent, the applicability of a given bound or a sensitivity prospect to both expansions will be specified. Special attention will be paid overall to the comparison between the expectations based on the linear and non-linear effective Lagrangians.

6.4.1 *ALP coupling to Z-photon*

In the non-linear expansion, the effective $aZ\gamma$ coupling

$$\delta\mathcal{L}_a \supset -\frac{1}{4} g_{aZ\gamma}\, a\, Z_{\mu\nu}\tilde{F}^{\mu\nu} \tag{6.28}$$

takes the form:

$$g_{aZ\gamma} = f_a^{-1}\left[4 s_{2\theta}(c_{\tilde{W}} - c_{\tilde{B}}) + \frac{g}{4\pi}\,(2c_1 + t_\theta(c_2 + 2c_7))\right]\,, \tag{6.29}$$

with the custodial-preserving limit recovered for $c_7 = 0$ and the linear limit at NLO recovered for $c_1 = c_2 = c_7 = 0$. This interaction can be constrained from various sets of experimental data:

	Observables/Processes		Parameters contributing	
			Linear	**Non-Linear**
	Astrophysical obs.	$g_{a\gamma\gamma}$	$\mathbf{c_{\tilde{W}}}$ $\mathbf{c_{\tilde{B}}}$	$\mathbf{c_{\tilde{W}}}$ $\mathbf{c_{\tilde{B}}}$
	Rare meson decays		$\mathbf{c_{\tilde{W}}}$ $\mathbf{c_{a^\vee}}$	$\mathbf{c_{\tilde{W}}}$ $\mathbf{c_{2D}}$ c_2 c_6 c_8 c_{17}
New constraints	**LEP data**			
	BSM Z width	$\Gamma(Z \to a\gamma)$	$\mathbf{c_{\tilde{W}}}$ $\mathbf{c_{\tilde{B}}}$	$\mathbf{c_{\tilde{W}}}$ $\mathbf{c_{\tilde{B}}}$ c_1 c_2 c_7
	LHC processes			
	Non-standard h decays	$\Gamma(h \to aZ)$		$\mathbf{\tilde{a}_{2D}}$ $\tilde{a}_3$ $\tilde{a}_{10}$ $\tilde{a}_{11-14}$ $\tilde{a}_{17}$
	Mono-Z prod.	$pp \to a\,Z$	$\mathbf{c_{\tilde{W}}}$ $\mathbf{c_{\tilde{B}}}$ $c_{a\Phi}$	$\mathbf{c_{\tilde{W}}}$ $\mathbf{c_{\tilde{B}}}$ c_{2D} c_1 c_2 c_3 c_7 c_{10} c_{11-14} c_{17}
	Mono-W prod.	$pp \to a\,W^\pm$	$\mathbf{c_{\tilde{W}}}$ $c_{\tilde{B}}$ $c_{a\Phi}$	$\mathbf{c_{\tilde{W}}}$ $c_{\tilde{B}}$ c_{2D} c_2 $\mathbf{c_6}$ c_8 c_{10}
Prospects	Associated prod.	$pp \to aW^\pm\gamma$	$\mathbf{c_{\tilde{W}}}$ $c_{\tilde{B}}$ $c_{a\Phi}$	$\mathbf{c_{\tilde{W}}}$ $c_{\tilde{B}}$ c_{2D} c_1 c_2 $\mathbf{c_6}$ c_7 c_8
	VBF prod.	$pp \to ajj(\gamma)$	$c_{\tilde{W}}$ $c_{\tilde{B}}$ $c_{a\Phi}$	$c_{\tilde{W}}$ $c_{\tilde{B}}$ c_{2D} c_1 c_2 c_6 c_7 c_8
	Mono-h prod.	$pp \to h\,a$		$\mathbf{\tilde{a}_{2D}}$ $\mathbf{\tilde{a}_3}$ $\mathbf{\tilde{a}_{10}}$ $\tilde{a}_{11-14}$ $\tilde{a}_{17}$
	$at\bar{t}$ prod.	$pp \to at\bar{t}$	$\mathbf{c_{a^\vee}}$	$\mathbf{c_{2D}}$

Table 6.2: Couplings contributing to the observables considered here, stemming from the purely bosonic operators in the linear and non-linear scenarios. The block of new constraints explores the sensitivity of LEP and present LHC data to different operators, see Sect. 6.4. The last block corresponds instead to the sensitivity analysis from Sect. 6.5, which assumes both LHC prospects with 300 fb^{-1} of data and projections to the HL-LHC phase with 3000 fb^{-1} of data. The operator coefficients to which present or expected measurements are found to be sensitive appear in bold.

- The uncertainty on the Z boson width [109], $\Gamma(Z \to \text{BSM}) \lesssim 2\,\text{MeV}$ at 95% C.L., allows to set a conservative bound on the process $Z \to a\gamma$. The latter would contribute to the Z width as

$$\Gamma(Z \to a\gamma) = \frac{M_Z^3}{384\pi}\, g_{aZ\gamma}^2 \left(1 - \frac{m_a^2}{M_Z^2}\right)^3 . \tag{6.30}$$

  In consequence, we use for the first time the Z boson width to obtain a bound on this coupling, constraining the combination of coefficients in Eq. (6.29) within the limit (with basically no dependence on m_a for $m_a \lesssim 1\,\text{GeV}$)

$$|g_{aZ\gamma}| < 1.8\,\text{TeV}^{-1} \quad (95\%\ \text{C.L.})\,. \tag{6.31}$$

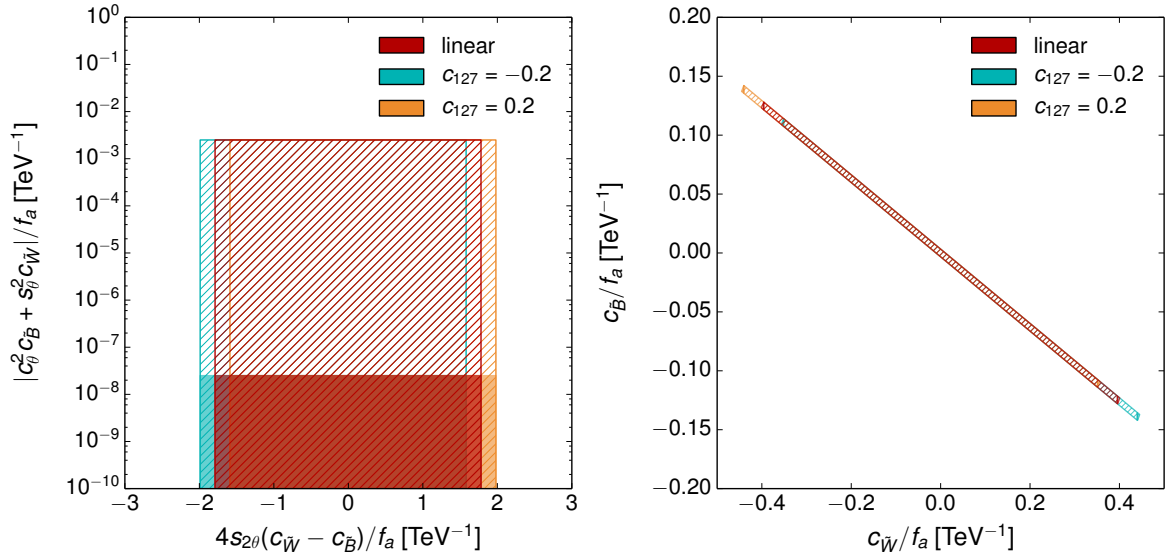

Figure 6.1: Left: Constraints on the parameters $c_{\tilde{B}}/f_a$ and $c_{\tilde{W}}/f_a$ derived from the tree-level bounds on the combinations $g_{a\gamma\gamma}$ (y-axis) and $g_{aZ\gamma}$ (x-axis) defined in Eqs. (6.16) and (6.29). The hatched (solid) region is obtained with the benchmark mass $m_a \simeq 1\,\text{MeV}\,(\text{keV})$. The different colours show how the allowed region is shifted in the non-linear setup, depending on the parameter $c_{127} = \frac{g}{4\pi}(2c_1 + t_\theta(c_2 + 2c_7))$. The value $c_{127} = 0.2$ is about maximal, as it is obtained fixing $c_1 = c_2 = c_7 = 1$ typical of the strongly interacting regime. The linear case corresponds to $c_{127} = 0$. Right: the rotated figure shows only the region allowed for $m_a = 1\,\text{MeV}$.

- LEP limits on $Z \to 3\gamma$ [18] constrain the product $g_{a\gamma\gamma}\, g_{aZ\gamma}$. However, given the bounds on $g_{a\gamma\gamma}$ reported in Sect. 3.3, the inferred bound on $g_{aZ\gamma}$ is weaker than that in Eq. (6.31).

As illustrated in Fig. 6.1, the Z boson width is able to probe regions in the parameter space orthogonal to those tested by $g_{a\gamma\gamma}$. In the linear EWSB setup, those two bounds constrain $c_{\tilde{B}}/f_a$ and $c_{\tilde{W}}/f_a$ to take values within a limited area: imposing Eq. (6.19) leads to $|c_{\tilde{W}}/f_a| < 0.42\,\text{TeV}^{-1}$. In the non-linear EWSB case, that region can be shifted depending on the value taken by the combination $c_{127} \equiv \frac{g}{4\pi}(2c_1 + t_\theta(c_2 + 2c_7))$, as shown in Fig. 6.1. Overall, the constraints on the quantities c_i/f_a are of order TeV^{-1} and thus correspond to a loose $\mathcal{O}(1)$ bound on the coefficients c_i for $f_a = 1\,\text{TeV}$.

6.4.2 *ALP coupling to Z-Higgs: Non-standard Higgs decays*

As shown in Sect. 6.1.2 and App. A.4, the presence of the coupling aZh is a characteristic feature of the non-linear effective Lagrangian, as in the linear expansion it would only be expected at NNLO. We propose here for the first time to use non-standard Higgs channels to bind couplings of the ALP to the Higgs particle. Consider a range of ALP masses such that it allows the Higgs particle to decay into Za. The presence of non-standard decay modes of the Higgs is constrained by ATLAS and CMS global fits to Higgs signal strengths. Current

constraints on the Higgs non-standard branching fraction $\mathrm{Br}(h \to \mathrm{BSM})$ from LHC 7 and 8 TeV data yield [255]

$$\mathrm{Br}(h \to \mathrm{BSM}) = \frac{\Gamma_{\mathrm{BSM}}}{\Gamma_{\mathrm{BSM}} + \Gamma_{\mathrm{SM}}} \leqslant 0.34 \quad (95\%\ \mathrm{C.L.})\,, \tag{6.32}$$

where the SM Higgs width is $\Gamma_{\mathrm{SM}} = (4.07 \pm 0.16)\,\mathrm{MeV}$ [256] and Γ_{BSM} denotes the non-standard Higgs partial width stemming in this case from the presence of the ALP,

$$\Gamma_{\mathrm{BSM}} \;=\; \Gamma_{h\to aZ} + \Gamma_{h\to aZ\gamma} + \Gamma_{h\to a f\bar{f}}\,. \tag{6.33}$$

The interaction vertices contributing to $\Gamma_{h\to aZ}$, $\Gamma_{h\to a f\bar{f}}$ and $\Gamma_{h\to aZ\gamma}$ are shown in FR.7, FR.20 - FR.22 and FR.14 in App. A.2, respectively. The last two terms are three-body phase-space suppressed and yield negligible contributions to the Higgs total width; [6] they will be then discarded in what follows. Using then $\Gamma_{\mathrm{BSM}} \simeq \Gamma_{h\to aZ}$ in Eq. (6.32) yields the present bound

$$\Gamma_{h\to aZ} < 2.1\,\mathrm{MeV} \quad (95\%\ \mathrm{C.L.})\,. \tag{6.34}$$

$\Gamma_{h\to aZ}$ receives contributions from the chiral LO operator $\mathcal{A}_{2D}$, Eq. (6.4), and from several NLO ones in Eq. (6.6),

$$\begin{aligned}\Gamma_{h\to aZ} &= \frac{m_h^7}{1024\pi^5 v^4 f_a^2}\left(\left(1-\frac{m_a^2}{m_h^2}-\frac{m_Z^2}{m_h^2}\right)^2-\frac{4m_a^2m_Z^2}{m_h^4}\right)^{3/2}\left(\kappa_h+\kappa_Z\frac{m_Z^2}{m_h^2}+\kappa_a\frac{m_a^2}{m_h^2}\right)^2 \\ &\simeq \frac{m_h^7}{1024\pi^5 v^4 f_a^2}\left(1-\frac{m_Z^2}{m_h^2}\right)^3\left(\kappa_h+\kappa_Z\frac{m_Z^2}{m_h^2}\right)^2+\mathcal{O}(m_a/m_h)\,,\end{aligned} \tag{6.35}$$

with

$$\begin{aligned}\kappa_h &= \tilde{a}_{13}+\frac{1}{2}(\tilde{a}_{12}-\tilde{a}_{14})-\frac{2\pi s_{2\theta}}{e}(\tilde{a}_3 s_\theta-\tilde{a}_{10}c_\theta)-16\pi^2\tilde{a}_{2D}\frac{v^2}{m_h^2}\,,\\ \kappa_Z &= -\frac{1}{2}(\tilde{a}_{12}-\tilde{a}_{14})\,,\\ \kappa_a &= \tilde{a}_{17}-\tilde{a}_{11}+\frac{1}{2}(\tilde{a}_{12}-\tilde{a}_{14})+\frac{2\pi s_{2\theta}}{e}(\tilde{a}_3 s_\theta-\tilde{a}_{10}c_\theta)\,,\end{aligned} \tag{6.36}$$

and where the coefficients $\tilde{a}_i$ for the couplings involving one Higgs leg have been defined in Eq. (6.7). The bound in Eq. (6.34) translates into the constraint

$$\frac{1}{f_a}\left|\kappa_h+\frac{m_Z^2}{m_h^2}\kappa_Z+\frac{m_a^2}{m_h^2}\kappa_a\right| \lesssim 0.22\,\mathrm{GeV}^{-1} \longrightarrow \frac{f_a}{\tilde{a}_{2D}} \gtrsim 2.78\,\mathrm{TeV} \quad \text{for} \quad m_a \lesssim 34\,\mathrm{GeV}\,, \tag{6.37}$$

where we use the fact that the inequality on the left is generically dominated by the $\tilde{a}_{2D}$ contribution, as it enters weighted by a large factor. If the constraint in Eq. (6.14) is considered, the impact of $\mathcal{A}_{2D}$ on $h \to aZ$ decay is negligible for ALP masses below 3 GeV, and in consequence the bound in Eq. (6.34) would apply to the combination of $\tilde{a}_3$ and $\tilde{a}_{10}$. However, present LHC sensitivity does not allow to constrain these operators.

6 $\Gamma_{h\to a f\bar{f}}$ is further suppressed by factors of $(m_f/v)^2 \ll 1$, while the interaction $ahZ\gamma$ is linked to the $aZ\gamma$ vertex (see FR.14 and FR.3 in App. A.2), whose strength is bounded from the Z width (see Sect. 6.4.1).

The above limits are expected to improve significantly at the high luminosity phase of LHC (HL-LHC). For example, Ref. [257] estimates that a bound

$$\mathrm{Br}(h \to \mathrm{BSM}) \leqslant 0.1 \quad (95\%\ \mathrm{C.L.})\,, \tag{6.38}$$

will be reached for 3000 fb^{-1} of data at $\sqrt{s} = 14$ TeV (neglecting here theoretical uncertainties). This would roughly translate into a sensitivity $\Gamma^{3\,\mathrm{ab}^{-1}}_{h\to aZ} \lesssim 0.45$ MeV ($f_a/\tilde{a}_{2D} \gtrsim 6$ TeV for the case in Eq. (6.37)).

An alternative approach to tackle $\Gamma_{h\to aZ}$ is to use the constraints from direct searches for invisible Higgs decays, since $h \to aZ$ yields an invisible Higgs decay for $Z \to \nu\bar{\nu}$. Current experimental searches by ATLAS [222, 258] and CMS [259] constrain the branching ratio for Higgs decay into invisible states $\mathrm{Br}(h \to \mathrm{inv})$ to [222]

$$\mathrm{Br}(h \to \mathrm{inv}) < 0.23 \quad (95\%\ \mathrm{C.L.})\,. \tag{6.39}$$

Nevertheless, no constraint on $\Gamma_{h\to aZ}$ follows from this present bound, since $\mathrm{Br}(Z \to \nu\bar{\nu}) = 0.2 \pm 0.006$ [153]. In the future, given the improvement on the sensitivity to $\mathrm{Br}(h \to \mathrm{inv})$ foreseen at HL-LHC with 3000 fb^{-1} of data at $\sqrt{s} = 14$ TeV [260],

$$\mathrm{Br}(h \to \mathrm{inv}) < 0.08 \quad (95\%\ \mathrm{C.L.})\,, \tag{6.40}$$

direct searches of the invisible decays of the Higgs resonance may be sensitive to $\Gamma_{h\to aZ}$. Indeed, in the ALP scenarios under discussion

$$\mathrm{Br}(h \to \mathrm{inv}) \simeq \frac{\Gamma_{h\to aZ} \times \mathrm{Br}(Z \to \nu\bar{\nu})}{\Gamma_{h\to aZ} + \Gamma_{\mathrm{SM}}}\,, \tag{6.41}$$

and in consequence, barring a positive signal in future data, Eq. (6.40) may translate into $\Gamma^{3\,\mathrm{ab}^{-1}}_{h\to aZ} \lesssim 2.71$ MeV, setting new limits on the operator coefficients participating in this decay. This expected sensitivity is however weaker than the present bound obtained from global fits to Higgs signal strengths in Eq. (6.36), and the latter will be used in the remainder of the chapter.

6.4.3 *Mono-W and mono-Z searches at* $\sqrt{s} = 13$ TeV

We now study the production of a in association with a W and a Z boson, as illustrated in Fig. 6.2. Since the ALP escapes the LHC detectors as missing transverse energy $\not{E}_T$, this yields respectively "mono-W" [261] and "mono-Z" [262–266] signatures. Both channels are being currently searched for by the ATLAS and CMS experimental collaborations. In this section we use their studies from public Run II data to set limits on the presence of different ALP effective operators that contribute to these signals.

Analysis tools

All signals and backgrounds to be discussed below in this and the next section will be generated using `MadGraph5_aMC@NLO` [267]. For this section it is enough to consider a parton-level analysis as the final states considered involve only leptons in addition to the ALP.

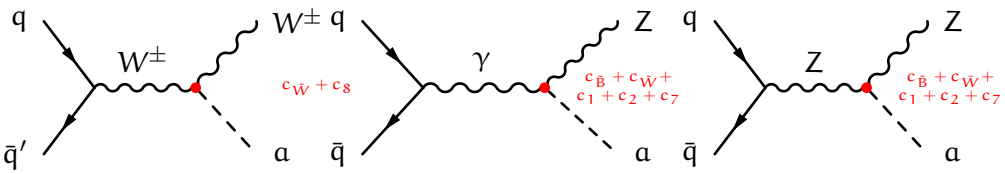

Figure 6.2: Feynman diagrams contributing to mono-W and mono-Z production.

Statistical tools

In order to set limits on c_i/f_a for each effective operator, a binned likelihood analysis will be performed. The likelihood function for a given lepton flavour in the final state $\ell = e, \mu$, is built as a product of bin Poisson probabilities

$$L^{\ell}(\mu_i) = \prod_k e^{-(\mu_i s_k^i + b_k)} \frac{(\mu_i s_k^i + b_k)^{n_k}}{n_k!}, \tag{6.42}$$

where

$$\mu_i \equiv (c_i/f_a)^2 \tag{6.43}$$

and b_k and s_k^i are respectively the background prediction and the signal prediction for $c_i = 1$ and $f_a = 1$ TeV in a given bin k. The significance is estimated via the test statistic $Q^{\ell}_{\mu_i}$,

$$Q^{\ell}_{\mu_i} \equiv -2\,\mathrm{Log}\left[\frac{L^{\ell}(\mu_i)}{L^{\ell}(\hat{\mu}_i)}\right], \tag{6.44}$$

with $\hat{\mu}_i$ being the value of μ_i which maximizes $L^{\ell}(\mu_i)$. Alternatively, we may include the effect of systematic uncertainties on the background prediction (which for the mono-W searches can be obtained from Refs. [268, 269] and for the mono-Z searches from Ref. [270]) by convoluting each bin Poisson probability with a Gaussian prior,[7] such that the likelihood function is given by

$$L^{\ell}_S(\mu_i) = \prod_k \int_0^{\infty} dr\, \frac{e^{\frac{-(r-1)^2}{2\sigma_k^2}}}{\sqrt{2\pi}\sigma_k} e^{-(\mu_i s_k^i + r\, b_k)} \frac{(\mu_i s_k^i + r\, b_k)^{n_k}}{n_k!}, \tag{6.45}$$

with σ_k being the background systematic uncertainty in each bin k. Our test statistic accounting for background systematic uncertainties $Q^{\ell}_{S\,\mu_i}$ is then defined as

$$Q^{\ell}_{S\,\mu_i} = -2\,\mathrm{Log}\left[\frac{L^{\ell}_S(\mu_i)}{L^{\ell}_S(\hat{\mu}_i)}\right]. \tag{6.46}$$

The value of μ_i that can be excluded at 95% C.L. corresponds to $Q^{\ell}_{\mu_i} = 3.84$ ($Q^{\ell}_{S\,\mu_i} = 3.84$) if background systematic uncertainties are not (are) included.

7 The Gaussian normalization in Eq. (6.45) is consistent as long as $\sigma_i \ll 1$, which is the case in our present analysis.

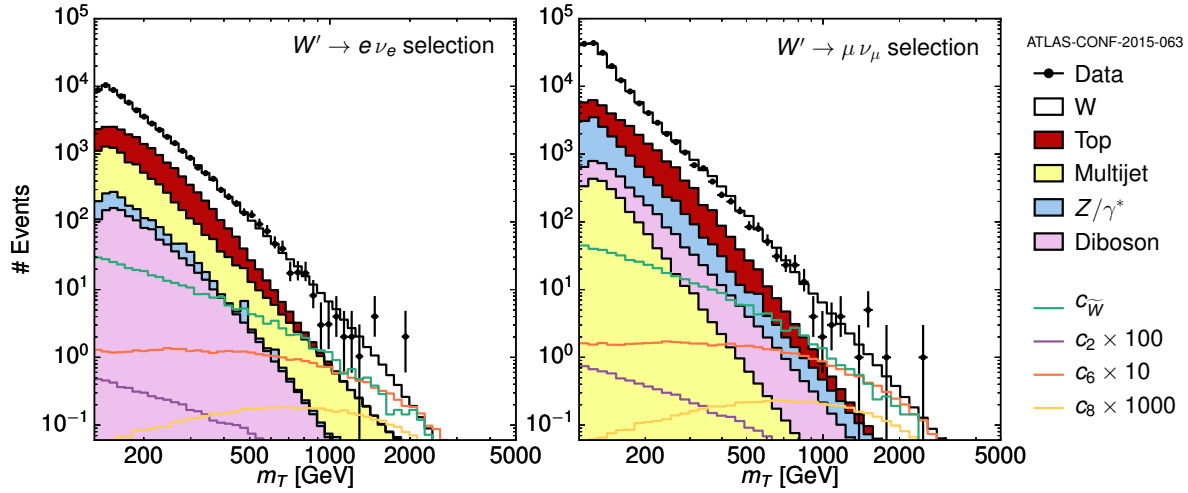

Figure 6.3: Transverse mass m_T distribution for $a\,W^\pm$ ($W^\pm \to \ell^\pm \nu_\ell$) production in the $e + \not{E}_T$ final state (Left) and $\mu + \not{E}_T$ final state (Right), generated from $\mathcal{A}_{\widetilde{W}}$ (green), $\mathcal{A}_2$ (purple), $\mathcal{A}_6$ (orange) and $\mathcal{A}_8$ (yellow). Also shown are the binned experimental data and dominant backgrounds from the 13 TeV ($3.3\,\text{fb}^{-1}$) ATLAS analysis [268].

Mono-W signatures: $pp \to a\,W^\pm$

We are targeting in this chapter bosonic couplings of the ALP particle, and here in particular ALP couplings to electroweak gauge bosons, as illustrated in Fig. 6.2. Let us first concentrate on the ALP production in association with a W boson, as illustrated in Fig. 6.2 (left). It is possible to derive limits on the coefficient of each effective operator contributing to this process from LHC Run II data at $\sqrt{s} = 13\,\text{TeV}$, by reinterpreting the ATLAS search for W' decaying to $\ell + \not{E}_T$ final states with $3.3\,\text{fb}^{-1}$ of integrated luminosity [268] (with $\ell = e, \mu$). The backgrounds will be taken from Ref. [268], considering independently the electron and muon samples and selecting events with transverse momentum $p_T > 65$ GeV (55 GeV) as well as $\not{E}_T > 65$ GeV (55 GeV) and transverse mass $m_T > 130$ GeV (110 GeV) in events with electrons (muons).

The couplings that may contribute to this process are the custodial-invariant $\mathcal{A}_{\widetilde{W}}$ and $\mathcal{A}_2$ operators, and the custodial-breaking ones $\mathcal{A}_6$ and $\mathcal{A}_8$ in Eq. (6.6), as illustrated in Fig. 6.2 and shown in the Feynman rules FR.5. Fig. 6.3 depicts the m_T spectrum of the SM background contributions, as well as the various signals corresponding to the c_2, c_6, c_8, $c_{\widetilde{W}}$ Wilson coefficients, for $f_a = 1$ TeV and $c_i = 1$ (with $c_{\tilde{B}}$ obeying Eq. (6.19)). The bins used in this figure are those for which there is experimental information on the background [268], corresponding to $m_T < m_T^{\text{max}} = 2.6$ TeV for electrons and $m_T < m_T^{\text{max}} = 3$ TeV for muons. As discussed in Sect. 6.3, the strict EFT validity condition $\sqrt{\hat{s}} < f_a$ can be imposed by computing the fraction of events in each bin for which $\sqrt{\hat{s}} > m_T^{\text{max}}$, and discarding it. In Fig. 6.4 (left) we show the correlation between m_T and $\sqrt{\hat{s}}$ for mono-W through a double-differential Monte Carlo distribution for the $\mathcal{A}_{\widetilde{W}}$ signal. We also show the normalised m_T distribution (again, for the $\mathcal{A}_{\widetilde{W}}$ signal) before/after discarding the events for which $\sqrt{\hat{s}} > m_T^{\text{max}}$.

	$c_{\tilde{W}}$ (mono-W)		$c_{\tilde{W}}$ (mono-Z)	
ℓ	e	μ	e	μ
$(f_a/c_{\tilde{W}})_{min}$ [TeV]	0.94	1.63	3.77	2.54
$(f_a/c_{\tilde{W}})_{min}$ [TeV] [No Syst.]	1.62	2.44	3.79	2.54

Table 6.3: Present 95% C.L. $f_a/c_{\tilde{W}}$ exclusion limits for the effective operator $\mathcal{A}_{\tilde{W}}$ from mono-W (left), inferred from the search presented in Ref, [268] as detailed in Sect. 6.4.3 and mono-Z (right) inferred from the search presented in Ref. [270] as detailed in Sect. 6.5.1. Values obtained without including background systematics are labeled [No Syst.].

We note that although the c_6 and c_8 signatures in Fig. 6.3 exhibit a kinematical shape *a priori* much more favorable to be distinguished from background than those proportional to $c_{\tilde{W}}$ and c_2, at the end the most prominent impact on this purely LHC analysis is that of $c_{\tilde{W}}$ (followed by that of c_6) due to suppression factors in the cross sections.[8] Mono-W signatures from the operators $\mathcal{A}_6$, $\mathcal{A}_8$ and $\mathcal{A}_2$ are buried in the backgrounds of present LHC data, and they will remain out of reach with future HL-LHC data, except for $\mathcal{A}_6$, see Sect. 6.5 below.

The loop-level bound obtained in Eq. (3.88) would imply (if taken at face value) that $\mathcal{A}_{\tilde{W}}$ is out of reach of foreseen LHC prospects, for light enough ALPs; however, as previously discussed, because more than one operator contributes to those rare process –see Eq. (6.15)– the data only constrain a combination of operator coefficients which differs from that in LHC signals, see Eq. (6.13); it is thus pertinent to analyze the impact of $\mathcal{A}_{\tilde{W}}$ on LHC independently.

The results obtained, for which the LHC sensitivity in $f_a/c_{\tilde{W}}$ extends up to significant values, are listed in Table 6.3. They show an important impact of the systematic uncertainties on the background and also indicate that present LHC Run II limits on $f_a/c_{\tilde{W}}$ from mono-W signals would *a priori* be sensitive to $c_{\tilde{W}}$ only in the region of strong coupling $c_{\tilde{W}} \gtrsim 1$ (possible in non-linear EWSB constructions), for values of f_a compatible with the validity of the EFT. These bounds have been computed in compliance with the strict validity criterium ($\sqrt{\hat{s}} < f_a$) by discarding the fraction of events in each bin for which $\sqrt{\hat{s}} > m_T^{max}$ (recall the discussion in Sect. 6.3). We note that here the effect of considering a strict validity criterium instead of the milder $f_a > m_T^{max}$ one is of the order of the few percent on the numbers in Table 6.3. The bound which suffers the most from applying the strict validity criterium is the present constraint from the $W \to e\nu$ final state, where applying the naive validity criterium would imply overestimating the bound in $\sim 20\%$. However, this is not a problem since it is the muon channel with yields a more constraining result.

8 The impact of $\mathcal{A}_8$ is suppressed with respect to that from $\mathcal{A}_6$ well beyond what suggests the $\sim (g/4\pi)^2$ factor in the Feynman rule FR.5, as the squared matrix element of its contribution $q\bar{q}' \to W^{\pm}a$ vanishes with the quark mass as $\sim m_q^2/m_W^2$ ($\sim 2 \times 10^{-4}$ for the charm quark).

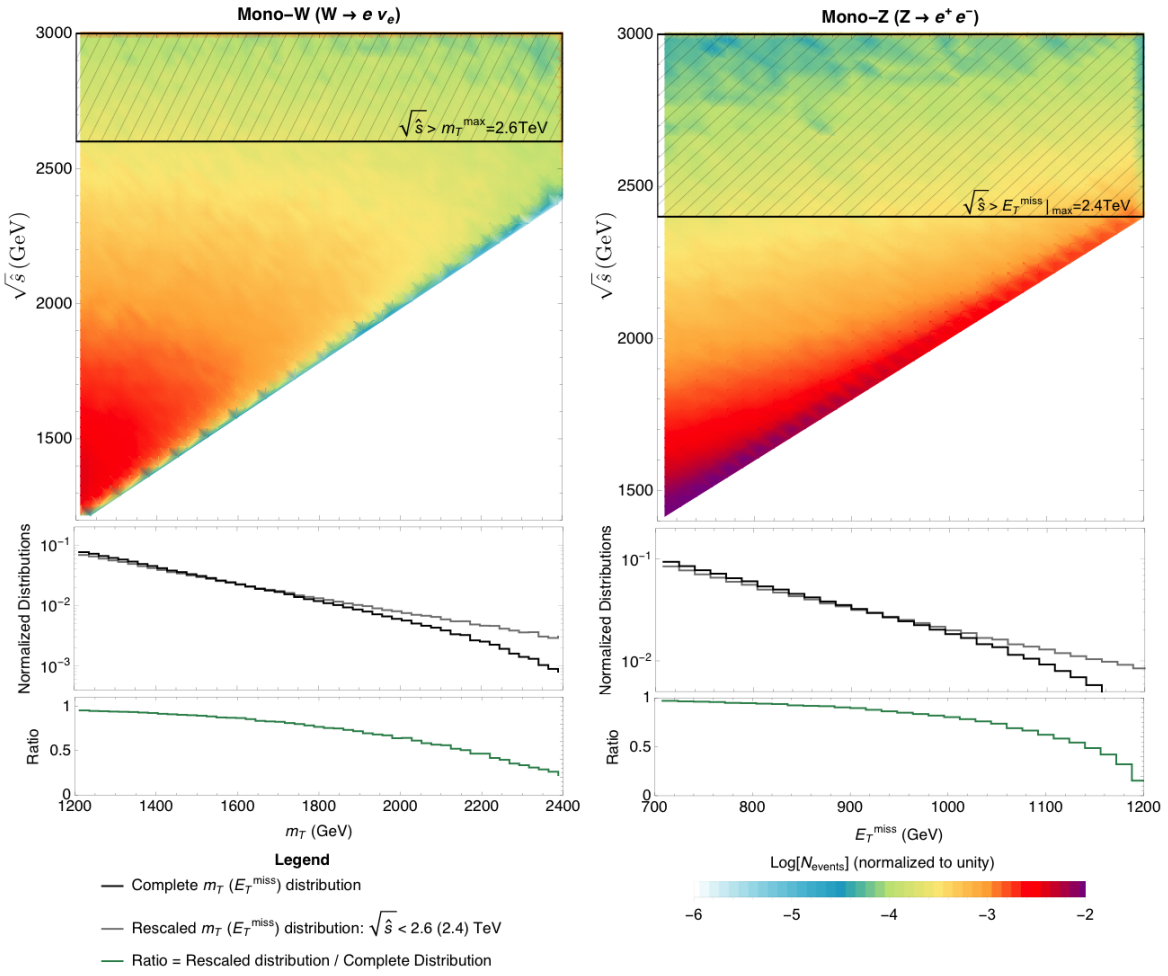

Figure 6.4: The left (right) top panel shows the correlation between m_T ($\not{E}_T$) and $\sqrt{\hat{s}}$ for mono-W (mono-Z) through a double-differential Monte Carlo distribution for the $\mathcal{A}_{\tilde{W}}$ signal. The centre plots show the normalised m_T ($\not{E}_T$) distribution before/after discarding the events for which $\sqrt{\hat{s}} > m_T^{max}$ ($2\,\not{E}_T^{max}$) (grey/black). The bottom panel displays the ratio between the two distributions above.

*Mono-*Z *signatures:* $pp \to a\,Z$

Consider now ALP production in association with a Z boson, in hadronic collisions, as illustrated in Fig. 6.2 (center and right). The recent CMS $Z + \not{E}_T$ search [270] with $\sqrt{s} = 13\,\text{TeV}$ and integrated luminosity $2.3\,\text{fb}^{-1}$ will be used to estimate present sensitivities to various Wilson coefficients. Table 7.1 summarizes the couplings which may *a priori* contribute to a mono-Z signal among those in the chiral basis, Eqs. (6.4) and (6.6). It will be argued next that only $c_{\tilde{W}}$ may be expected to be seriously tested by this signal.

The $\not{E}_T$ distribution for signal and background will be used as kinematic discriminator, applying the same tools and procedure described at the beginning of Sect. 6.4.3. In order to optimize the search, the following preselection and selection cuts are applied: $p_T^\ell > 20$ GeV, $|\eta_\ell| < 2.5$, $p_T^{\ell\ell} > 50$ GeV, $m_{\ell\ell} \in [80, 100]$ GeV, $\not{E}_T > 80$ GeV, $\left|\not{E}_T - p_T^{\ell\ell}\right| / p_T^{\ell\ell} < 0.2$, $\Delta\phi_{\ell\ell,\vec{\not{E}}_T} > 2.7$ (rad), an furthermore 3rd-lepton and extra high-p_T jets vetoes are implemented. The cut

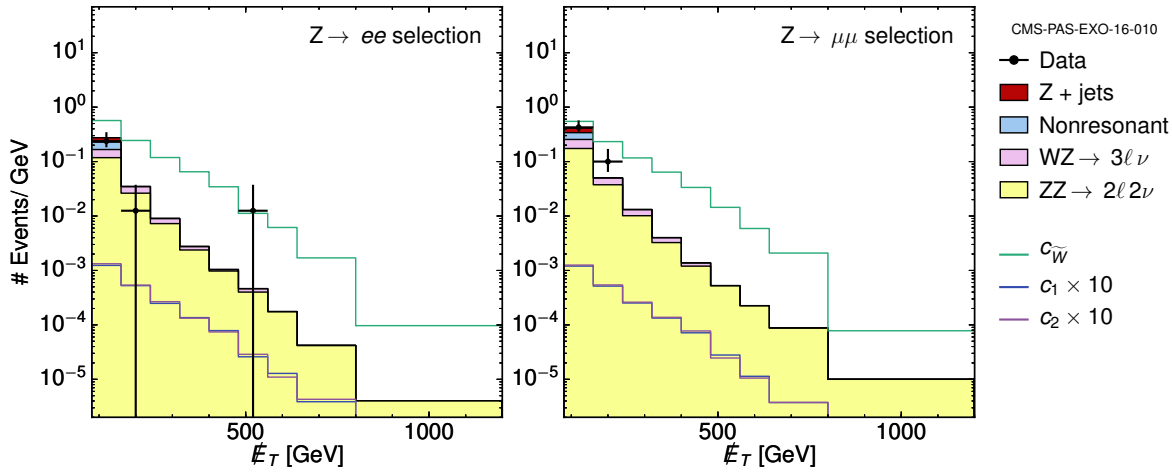

Figure 6.5: $\not{E}_T$ distribution for a Z ($Z \to \ell^+\ell^-$) production in the $ee + \not{E}_T$ final state (Left) and $\mu\mu + \not{E}_T$ final state (Right), generated from $\mathcal{A}_{\tilde{W}}$ (green), $\mathcal{A}_1$ (blue), and $\mathcal{A}_2$ (purple). Also shown are the binned experimental data and dominant backgrounds from the 13 TeV (2.3 fb^{-1}) CMS analysis [270].

$\not{E}_T > 80$ GeV ensures that a contamination from the gluon-fusion initiated signal leading to s-channel Higgs mediation can be safely neglected: for an on-shell Higgs the maximum $\not{E}_T$ is ~ 30 GeV. Furthermore, for a higher $\not{E}_T$ cut the fraction of the cross section contributed by this channel may be estimated as the integral of the Breit-Wigner distribution of the Higgs resonance for $\hat{s} > m_Z^2 + 2\not{E}_T^2[1 + (1 + m_Z^2/\not{E}_T^2)^{1/2}]$, which for $\not{E}_T > 80$ GeV gives a suppression factor of 5×10^{-6}. Given that the on-shell Higgs production via gluon-fusion is $\sigma(gg \to h) = 48.6\,\text{pb}$ [271], the Higgs-mediated contribution is completely negligible. Similarly, contributions involving a quark in the t-channel are not relevant in the kinematic region considered. In summary, with present data the signal cross-sections for $pp \to Za$ have a negligible dependence on the Wilson coefficients parameterizing the qqa and hZa vertices, *i.e.* $c_{a\Phi}$ in the linear case and c_{2D}, c_3, c_{10-14}, c_{17} in the non-linear one (see App. A.2).

The remaining ALP-gauge boson interactions which may induce a mono-Z signal are the custodial invariant operators $\mathcal{A}_{\tilde{W}}$, $\mathcal{A}_{\tilde{B}}$, $\mathcal{A}_1$ and $\mathcal{A}_2$, and the custodial-breaking coupling $\mathcal{A}_7$, see Fig. 6.2 (center and right). $\mathcal{A}_{\tilde{B}}$ will not be considered independently all through the rest of this chapter, given the constraint in Eq. (6.19). The contribution from $\mathcal{A}_7$ does not need to be considered separately either, as c_7 enters exclusively through the combination $c_2 + 2c_7$, see the Feynman rules FR.3 and FR.2. The analysis focuses thus on $c_{\tilde{W}}$, c_1 and c_2.

The comparison of signals and background $\not{E}_T$ distributions for $\ell = e, \mu$ is shown in Fig. 6.5. The highest-energy bin considered is $\not{E}_T^{\text{max}} = 1.2$ TeV. In analogy with the previous mono-W analysis, the EFT validity condition $\sqrt{\hat{s}} < f_a$ is implemented by discarding the fraction of events in each bin for which $\sqrt{\hat{s}} > 2\not{E}_T^{\text{max}}$ (see Sect. 6.3). The correlation between $\sqrt{\hat{s}}$ and $\not{E}_T$ is shown in Fig. 6.4 (right), as well as the normalised $\not{E}_T$ distributions before/after discarding the invalid event fraction in each bin.

The results obtained for $\mathcal{A}_{\tilde{W}}$ are listed in Table 6.3: the present mono-Z search turns out to be significantly more powerful in constraining $c_{\tilde{W}}/f_a$ than the ATLAS mono-W search previously analyzed. Furthermore, the impact of systematic errors is negligible in this case.

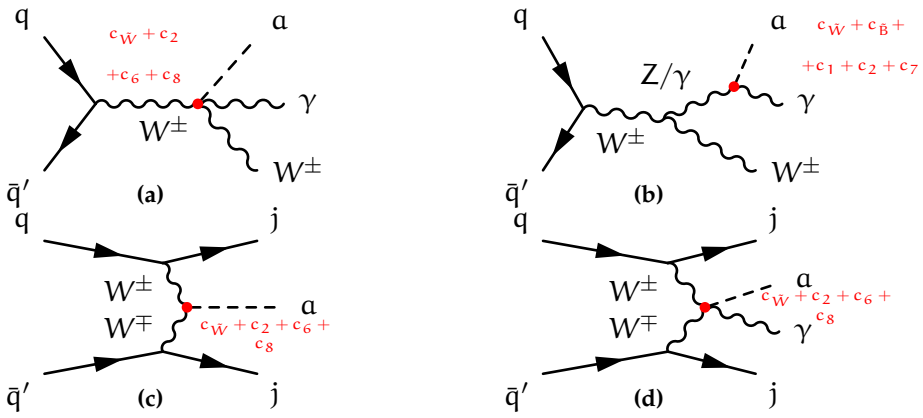

Figure 6.6: Main diagrams contributing to the processes analysed in Sect. 6.5.2. Upper line (**(a)** and **(b)**): $a\gamma W$ associated production. Lower line: VBF-type interaction producing ajj **(c)** and $ajj\gamma$ **(d)**. The proportionality of each diagram to the non-linear parameters is indicated in the figure (overall factors and relative coefficients are not displayed).

An interesting fact is the different discriminating power of electrons and muons in mono-Z signals induced by ALP emission with respect to the coupling strength: while present muon data data could *a priori* be sensitive to $c_{\tilde{W}}$ only in the region of strong coupling $c_{\tilde{W}} \geqslant 1$, a signal in electron data would be compatible as well with $c_{\tilde{W}}$ values in the perturbative regime, $c_{\tilde{W}} \leqslant 1$. It is relevant to point out that these results, obtained imposing $\sqrt{\hat{s}} < m_T^{max} < f_a$, are equal up to the permille level to the ones which are obtained if the naive validity criterium (only $m_T^{max} < f_a$) is used instead.

The contributions to mono-Z signals from $\mathcal{A}_{1,2}$ are shown in Fig. 6.5 for illustration only, as the corresponding values for $c_{1,2}$ would lie outside the region of validity of the EFT in present data and also if assuming the 3000 fb^{-1} integrated luminosity foreseeable at HL-LHC, see next section. The mono-Z analysis with present and projected data is thus only sensitive to the $\mathcal{A}_{\tilde{W}}$ operator, which is common to the NLO of the linear and of the non-linear expansion. It follows that mono-Z searches alone are not sensitive to a possible non-linear component in the nature of EWSB, unlike mono-W future searches at HL-LHC.

6.5 PHENOMENOLOGICAL ANALYSIS II: $\sqrt{s} = 13$ TeV LHC PROSPECTS

This section explores the sensitivity prospects for constraining the effective ALP couplings to SM bosons at the HL-LHC, as well as the analysis strategy sensitive to the linear/non-linear character of the underlying EWSB mechanism. Assuming thus proton-proton collisions at c.o.m. energy $\sqrt{s} = 13$ TeV and successive integrated luminosities of 300 fb^{-1} and 3000 fb^{-1}, the following channels will be analyzed:

- Mono-W and mono-Z signatures, see Fig. 6.2, projecting the analysis in Sect. 6.4 onto future data. A qualitative discussion of their ratio as a probe of non-linear character will be added.
- $Wa\gamma$ associated production, see Fig. 6.6.

- Mono-Higgs signatures, see Fig. 6.10.

Table 7.1 summarizes the set of operator coefficients that could contribute to these signals and be tested in LHC prospects, among those defined in the Lagrangians Eqs. (3.54)-(3.57) and (6.4)-(6.5). The corresponding Feynman rules are shown in App. A.2.

Mono-W and $W\alpha\gamma$ associated production, together with $\alpha jj(\gamma)$ production through vector boson fusion (VBF) – also shown in Fig. 6.6 – are intimately related processes, as they probe the same limited set of effective operator coefficients [9] $c_{\tilde{W}}$, $c_{\tilde{B}}$, c_1, c_2, c_6, c_7 and c_8.

A special role is played by the Higgs-ALP couplings associated to c_{2D} which, barring extreme fine-tunings, may be only expected among the leading signals if the underlying EWSB enjoys a non-linear character, and within a certain ALP mass range, as previously discussed. This coupling will be shown to be *a priori* testable through mono-Higgs searches at HL-LHC, that exhibit a sensitivity reach well beyond the bounds obtained in Sect. 6.4.2 from the limits on the non-standard Higgs decay width.

Relevant information about the structure of the ALP couplings can be inferred both by analyzing the different signatures independently and by studying their interplay. As some effective operators contribute to several processes, a combined analysis may be necessary in order to access the individual Wilson coefficients. Furthermore, the study of (de)correlations between the various putative signals serves as a good probe of the degree of EWSB non-linearity.

6.5.1 *Mono-W and mono-Z signatures*

The result of extending the analysis in Sect. 6.4.3 to the projected sensitivity in $(c_i/f_a)^2$ for LHC 13 TeV with 300 fb^{-1} and 3000 fb^{-1} is summarised in Table 6.4 (for mono-Z) and Table 6.5 (for mono-W), considering electrons and/or muons in the final state.

They show that mono-Z searches will be stronger than mono-W ones in probing at LHC the effective operator $\mathcal{A}_{\tilde{W}}$. Both electron and muon channels will access the perturbative regime $c_{\tilde{W}} < 1$. Mono-Z searches would reach ALP scales up to $f_a \sim 20$ TeV (for $c_{\tilde{W}} = 1$) with 3000 fb^{-1} disregarding background systematics – see Table 6.4. Assuming instead future background systematics as (1/2 of) the present ones, the mono-Z reach is somewhat milder, up to $f_a \sim 15$ TeV (~ 18 TeV). Table 6.5 shows that instead the limits on $c_{\tilde{W}}/f_a$ from LHC mono-W searches are systematics dominated.[10]

Future mono-W searches appear instead of special interest in order to uncover the $\mathcal{A}_6$ coupling, which is a signal of non-linearity up to NLO. Table 6.5 shows that with 300 fb^{-1} and 3000 fb^{-1} it is possible to either discover it or derive a consistent projected limit. The sensitivity to c_6 turns out to be mainly limited by statistical uncertainties, being less dependent than $\mathcal{A}_{\tilde{W}}$ on SM background systematics. Nevertheless a significant reduction of the latter is shown to have a significant impact also on tackling $\mathcal{A}_6$, particularly with 3000 fb^{-1}: scales up to $f_a/c_6 \leqslant 3.44$ TeV (4.68 TeV) would be then attainable if systematic errors were reduced

9 c_{2D} –or its linear sibling $c_{a\Phi}$– is also mentioned in Table 7.1 in connection to these channels, contributing through the fermionic vertices that it induces. Nevertheless, this contribution is in any case much suppressed by ratios of quark mass over momentum.

10 The mono-W results are shown for electrons in the final state. Muon final states display similar sensitivities.

	$c_{\tilde{W}}$ (mono-Z)			
ℓ	e		μ	
Luminosity [fb^{-1}]	300	3000	300	3000
$f_a/c_{\tilde{W}}$ [TeV]	10.47	15.81	9.79	14.33
$f_a/c_{\tilde{W}}$ [TeV] [Syst.×1/2]	11.10	18.40	10.39	16.67
$f_a/c_{\tilde{W}}$ [TeV] [No Syst.]	11.64	21.47	10.91	19.64

Table 6.4: Projected 95% C.L. f_a/c_i reach at LHC, with $\mathcal{L} = 300$ fb^{-1} and $\mathcal{L} = 3000$ fb^{-1} for $\mu_{\tilde{W}} = (c_{\tilde{W}}/f_a)^2$ from mono-Z production, as detailed in Sect. 6.4.3. Top row: Assuming future systematic uncertainties on the background scale as present ones. Middle row: Assuming systematic uncertainties are reduced by a factor 2 w.r.t. present ones. Bottom row: Assuming no background systematic uncertainties.

	c_6 (mono-W)		$c_{\tilde{W}}$ (mono-W)	
Luminosity [fb^{-1}]	300	3000	300	3000
f_a/c_i [TeV]	2.00	2.53	1.83	2.20
f_a/c_i [TeV] [Syst.×1/2]	2.24	3.25	2.23	2.90
f_a/c_i [TeV] [No Syst.]	2.51	4.51	3.40	6.05

Table 6.5: Projected 95% C.L. f_a/c_i LHC reach for $\ell = e$ final states, with $\mathcal{L} = 300$ fb^{-1} and $\mathcal{L} = 3000$ fb^{-1} for the effective operators relevant to mono-W production, as detailed in Sect. 6.4.3. Top row: Assuming future systematic uncertainties on the background scale as present ones. Middle row: Assuming systematic uncertainties are reduced by a factor 2 w.r.t. present ones. Bottom row: Assuming no background systematic uncertainties.

by 1/2 (completely) with respect to their present value (see Table 6.5), leading to c_6 being testable within the perturbative region.

Finally, mono-W and mono-Z signals may turn out to be especially prominent as phenomenological signals of the complete NLO ALP basis, in particular of ALP-fermion couplings in the chiral EWSB case. For instance, the $aZ\bar{\psi}\psi$ couplings $\mathcal{P}_3^q$, $\mathcal{P}_4^q$, $\mathcal{P}_6^q$, $\mathcal{P}_7^q$, $\mathcal{P}_8^q$ and $\mathcal{P}_{10}^q$ in Eq. (A.1) may have a large impact on the very sensitive mono-Z channel, while the $aW\bar{\psi}\psi$ vertices in $\mathcal{P}_3^q$, $\mathcal{P}_5^q$, $\mathcal{P}_6^q$, $\mathcal{P}_7^q$, $\mathcal{P}_9^q$ and $\mathcal{P}_{10}^q$ may induce mono-W signals; these couplings are not Yukawa suppressed and will be explored in a future study.

Strategy for a combined analysis

As is apparent from the discussion above, the interplay between mono-Z and mono-W signatures may be relevant as a way of disentangling the presence of non linearity in the Higgs sector. Up to NLO in both expansions and barring extreme fine-tunings of operator coefficients, the cross sections for those two processes are:

- Strongly correlated in the linear case, being both controlled by the coefficient $c_{\tilde{W}}$ ($c_{\tilde{B}}$ is not independent, see Eq. (6.19)).
- Less correlated in the non-linear case, as operators other than $\mathcal{A}_{\tilde{W}}$ and $\mathcal{A}_{\tilde{B}}$ are expected to contribute to those mono-signals. For instance the purely chiral $\mathcal{A}_6$ operator may contribute visibly to mono-W production within the projected HL-LHC prospects, as shown above.

A combined analysis of mono-Z and mono-W appears thus to be a valid method to shed light on the nature of the EWSB dynamics, once a positive detection occurs. Here we illustrate the (de)correlations of those signals in a purely qualitative way. The cross-sections for $pp \to Z\alpha$ and $pp \to W^{\pm}\alpha$ at a c.o.m. energy $\sqrt{s} = 13$ TeV are computed using `MadGraph5_aMC@NLO`, and subject to no other constraint than Eqs. (6.18) and (6.31) and a kinematical cut $\not{E}_T > 200$ GeV. A random scan of Wilson coefficients $c_i \in [-1, 1]$ has been performed, along three scenarios: i) the *linear* setup, which in practice reduces to the custodial-preserving $\mathcal{A}_{\tilde{W}}$ and $\mathcal{A}_{\tilde{B}}$ operators, see Eq.(3.54) and Eq. (3.55); ii) the *non-linear custodial* case, involving operators $\mathcal{A}_{\tilde{W}}$, $\mathcal{A}_{\tilde{B}}$, $\mathcal{A}_1$ and $\mathcal{A}_2$; iii) the non-linear case including both custodial preserving and non-custodially invariant couplings, here denominated *non-linear* for short, which adds to the previous set $\mathcal{A}_6$ and $\mathcal{A}_7$, see Eq. (6.5).

The results for the cross-sections are summarised in Fig. 6.7 (top) in the $\sigma(pp \to W^{\pm}\alpha)$, $\sigma(pp \to Z\alpha)$ plane, for linear (orange), cyan (non-linear custodial) and dark blue (non-linear), for $f_\alpha = 1$ TeV. The strong correlation characteristic of the EWSB linear scenario is clearly seen. In contrast, in the non-linear setup deviations from the sharp linear pattern emerge as expected as they stem from the non-linear operators $\mathcal{A}_{1,2,6,7}$. Those deviations are necessarily small, though, as the contribution from any of the coefficients $c_{1,2,6,7}$ is suppressed by a factor $g/(16\pi)$ – see Feynman rules in App. A.2 – compared to that of $c_{\tilde{W}}$, $c_{\tilde{B}}$ (this conclusion may however be somewhat modified if a harder $\not{E}_T$ cut is imposed on the signal). In any case, in the event of a mono-W and/or mono-Z excess in future data, the ratio

$$R_{ZW} = \frac{\sigma(pp \to Z\alpha)}{\sigma(pp \to W^{\pm}\alpha)} \tag{6.47}$$

may be used to discern among possible physical explanations. This observable has the advantage of being in principle independent of the scale f_α as well as of the ALP mass m_α (provided that $m_\alpha \ll m_Z$, as is the case assumed in this analysis for ALP stability reasons). Fig. 6.7 (bottom) shows, for the three sets of operators considered, the R_{ZW} distributions obtained letting the coefficients of each operator considered assume random values in the interval [-1,1]. Note that neither the slope in the upper plot in Fig. 6.7, nor the numerical values in the other plots in this figure, are meaningful *per se*, but rather strongly dependent on the specifics of the analysis (e.g. on the kinematical cuts applied, here $\not{E}_T > 200$ GeV). Therefore, the strategy to follow in a realistic experimental analysis would be to look for

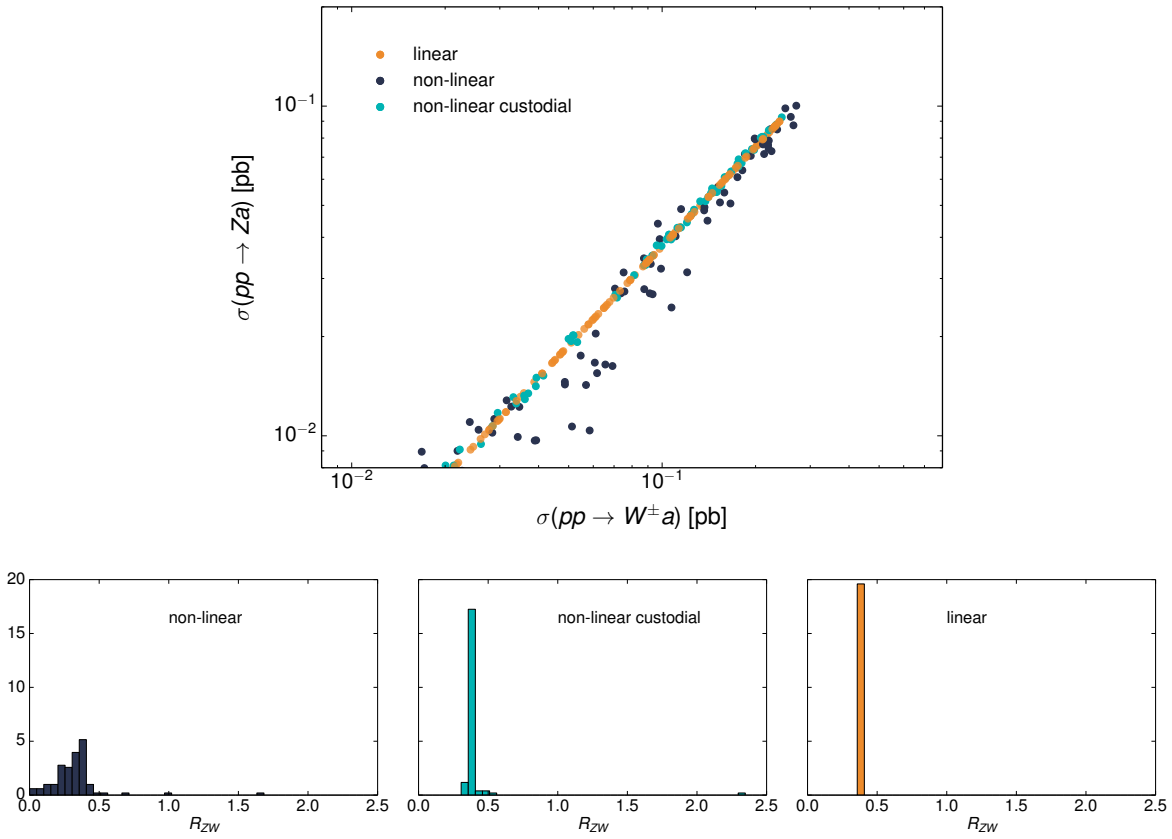

Figure 6.7: Top: Cross sections for $pp \to Za$ and $pp \to W^{\pm}a$ at $\sqrt{s} = 13\,\text{TeV}$ with $\not{E}_T \geqslant 200\,\text{GeV}$, computed with `Madgraph5_aMC@NLO` for a random scan of Wilson coefficients $c_i \in [-1, 1]$ (see text for details) within the region allowed by Eq. (6.18) and (6.31), and using $m_a = 1\,\text{MeV}$ and $f_a = 1\,\text{TeV}$ for illustration. Bottom: Distribution of the ratio R_{ZW} defined in Eq. (6.47), with the area of the histograms normalised to 1. In both cases, orange, cyan and dark blue correspond respectively to linear, non-linear custodial and non-linear non-custodial setups.

a coincidence/tension between the expected value of R_{ZW} in the linear scenario and the measured one which, if detected, could indicate the presence of non-linearity in the Higgs sector.

We stress that the considerations in this subsection are aimed at discussing the expected relative strength of the mono-W and mono-Z observables in a purely qualitative way, having in mind future hadronic machines in general. Indeed, besides the strong dependence of the results on the kinematical cuts chosen, no consideration of backgrounds has been taken into account here. This is in contrast to the detailed phenomenological analysis at the beginning of the subsection, where it was shown that only the deviations stemming from $\mathcal{A}_6$ have a chance of being visible within the foreseen HL-LHC prospects.

6.5.2 *Associated production:* $pp \to aW^{\pm}\gamma$

Consider next ALP production in association with both a W boson and a photon, as illustrated in Fig. 6.6 i) and ii). Examining the interactions in the chiral effective Lagrangian Eq. (6.6), it is easy to see that those couplings exhibit a particularly interesting combined potential for disentangling the presence of different effective operators:

$$\begin{aligned} a\,W^+W^- &\to \frac{g}{4\pi f_a}\left[c_6\, g^{\mu\nu}(p_+^2 - p_-^2) + \left(\frac{g}{4\pi}c_8 - c_6\right)(p_+^\mu p_+^\nu - p_-^\nu p_-^\nu)\right] + \\ &\quad -\frac{4i}{f_a}\left(c_{\tilde{W}} + \frac{g}{16\pi}c_2\right) p_{+\alpha} p_{-\beta}\,\varepsilon^{\mu\nu\alpha\beta}\,, \\ a\,W^+W^-\gamma &\to \frac{ge}{4\pi f_a}\left[\left(\frac{g}{4\pi}c_8 - c_6\right)(g^{\mu\rho}p_a^\nu + g^{\nu\rho}p_a^\mu) + 2c_6 g^{\mu\nu}p_a^\rho\right] - \frac{4ig}{f_a}\left(c_{\tilde{W}} + \frac{g}{16\pi}c_2\right)\varepsilon^{\mu\nu\rho\alpha}p_{a\alpha}\,, \end{aligned} \tag{6.48}$$

as illustrated respectively in FR.4 and FR.11 of App. A.2 and summarised in Table 7.1. Both processes are thus *a priori* sensitive [11] to $\mathcal{A}_6$, $\mathcal{A}_8$, and to a fixed combination of $\mathcal{A}_{\tilde{W}}$ and $\mathcal{A}_2$ which therefore singles out a flat direction. In contrast, in the linear scenario only the Wilson coefficient $c_{\tilde{W}}$ contributes significantly to both interaction vertices.

The first process in Eq. (6.48) leads to the striking mono-W signal being already searched by LHC collaborations and whose physics impact has been explored in Sects. 6.4.3 and 6.5.1. The second process leads to $aW^{\pm}\gamma$ associated production, a search not being yet performed by the ATLAS and CMS collaborations. We will explore its prospects next, focusing on final states characterised by leptonic W decays. It is necessary to take into account, though, that the $pp \to aW^{\pm}\gamma$ channel may be induced also by $a\,Z\gamma$-mediated contributions, to which the set $\{\mathcal{A}_{\tilde{W}}, \mathcal{A}_{\tilde{B}}, \mathcal{A}_1, \mathcal{A}_2, \mathcal{A}_7\}$ may contribute as illustrated in Fig. 6.6 (ii),[12]

$$a\,Z\gamma \to \frac{i}{f_a} p_{Z\alpha} p_{A\beta}\,\varepsilon^{\mu\nu\alpha\beta}\left(-2t_\theta c_{\tilde{W}} - \frac{g}{8\pi}(2c_1 + t_\theta(c_2 + 2c_7))\right), \tag{6.49}$$

where the constraint in Eq. (6.19) has been applied. The contribution of $\mathcal{A}_7$ is equivalent to that of $\mathcal{A}_1$ and it is not necessary to consider it independently. In summary, the analysis is done on five distinct operators: $\{\mathcal{A}_1, \mathcal{A}_2, \mathcal{A}_6, \mathcal{A}_8\}$ and the combination of $\{\mathcal{A}_{\tilde{W}}, \mathcal{A}_{\tilde{B}}\}$ orthogonal to the $a\gamma\gamma$ coupling. They are studied next, one at a time and keeping our analysis at parton level.[13]

The main irreducible SM background is $pp \to W^{\pm}\gamma$ (with $W^{\pm} \to \ell^{\pm}\nu$), a process which has been measured by ATLAS [272] and CMS [273] during the LHC $\sqrt{s} = 7$ TeV Run. The reducible backgrounds are subdominant with respect to the direct $W^{\pm}\gamma$ production and consist of (i) $W^{\pm}$+jets (with a jet misidentified as a photon), (ii) $Z\ell^+\ell^-$ (with one of the leptons misidentified as a photon or unidentified and the Z decaying into neutrinos), (iii) γ+jets (with a lepton originating from a heavy quark decay) and (iv) $t\bar{t}$ (with a semileptonic decay of the top pair and a misidentification of a field as a photon). Their combined effect is to approximately increase the size of the $W^{\pm}\gamma$ background by 15-25% depending on kinematics

11 The sensitivity to c_{2D} ($c_{a\Phi}$ in the linear expansion) remains in practice negligible even for $\mathcal{L} = 3000\,\text{fb}^{-1}$ for the same reasons explained in Footnote 9.

12 The $a\gamma\gamma$ contribution to $pp \to aW^{\pm}\gamma$ is proportional to $(c_\theta^2 c_{\tilde{B}} + s_\theta^2 c_{\tilde{W}})$ and thus irrelevant, see Eq. (6.19).

13 An analysis of the associated $aW\gamma$ channel including parton shower and a detector simulation is beyond the scope of this chapter and it is left for the future once the viability of the searches proposed is established.

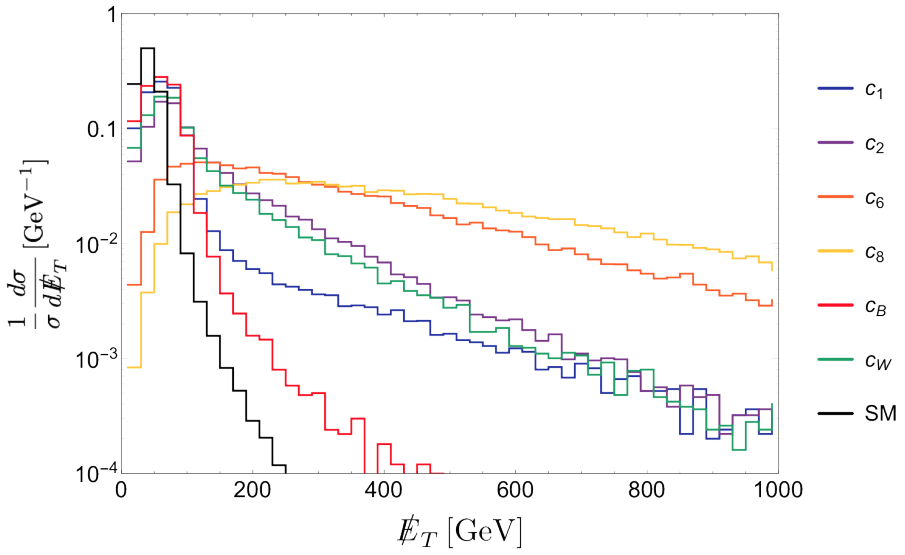

Figure 6.8: Missing transverse energy distributions for $pp \to aW^{\pm}\gamma$ ($W^{\pm} \to \ell^{\pm}\nu$) at $\sqrt{s} = 13$ TeV LHC normalised to unity, for signals generated one by one for operators $\mathcal{A}_1$ (blue), $\mathcal{A}_2$ (violet), $\mathcal{A}_6$ (orange), $\mathcal{A}_8$ (yellow), $\mathcal{A}_{\tilde{W}}$ (green) and $\mathcal{A}_{\tilde{B}}$ (red).

and the flavour of the lepton [272, 273]. For the present analysis, we simply account for this by scaling up our dominant SM $W^{\pm}\gamma$ background by 20%.

The event selection requirements for photons and leptons for both signal and background are $p_T^{\gamma} > 20\,\text{GeV}$, $p_T^{\ell} > 20\,\text{GeV}$, $|\eta^{\gamma}| < 2.5$ and $|\eta^{\ell}| < 2.5$. $\not{E}_T$ will be employed as kinematic variable for distinguishing signal from background, as we find that this variable has significantly more signal discrimination power than the p_T of the lepton, because it receives contributions directly from the ALP in the signal set. The $\not{E}_T$ distributions (normalised to unity) for the various effective operators and the SM background are shown in Fig. 6.8. The harder momentum dependence of the effective couplings explored compared to the SM contribution are illustrated. In practice, we simulate events only up to $\not{E}_T = 1$ TeV, as we find that signal cross sections for $\not{E}_T > 1$ TeV are negligible.

The significance σ_i of a signal associated to one given operator $\mathcal{A}_i$ is defined here as [274]

$$\sigma_i = \sqrt{2\left[(\mu_i s_i + b)\ln\left(1 + \frac{\mu_i s_i}{b}\right) - \mu_i s_i\right]}\,, \tag{6.50}$$

where μ_i was defined in Eq. (6.43), and $\mu_i s_i$ and b denote respectively the number of events in the signal and the background, alike to the definitions used in Eq. (6.42) with, in this case,

$$s_i = L \times \int_{\not{E}_T^{min}}^{\not{E}_T^{max}} \frac{d\sigma_i}{d\not{E}_T} d\not{E}_T \qquad \text{and} \qquad b = L \times \int_{\not{E}_T^{min}}^{\not{E}_T^{max}} \frac{d\sigma_{SM}}{d\not{E}_T} d\not{E}_T\,, \tag{6.51}$$

where L is the integrated luminosity, σ_i stands for the cross-section induced by $\mathcal{A}_i$ and σ_{SM} for the SM one. The kinematical cuts are taken as follows:

- $\not{E}_T^{min} = 200\,\text{GeV}$, as it optimizes the sensitivity by removing most of the background, see Fig. 6.8. Higher $\not{E}_T^{min}$ values do not improve the signal-to-background ratio.

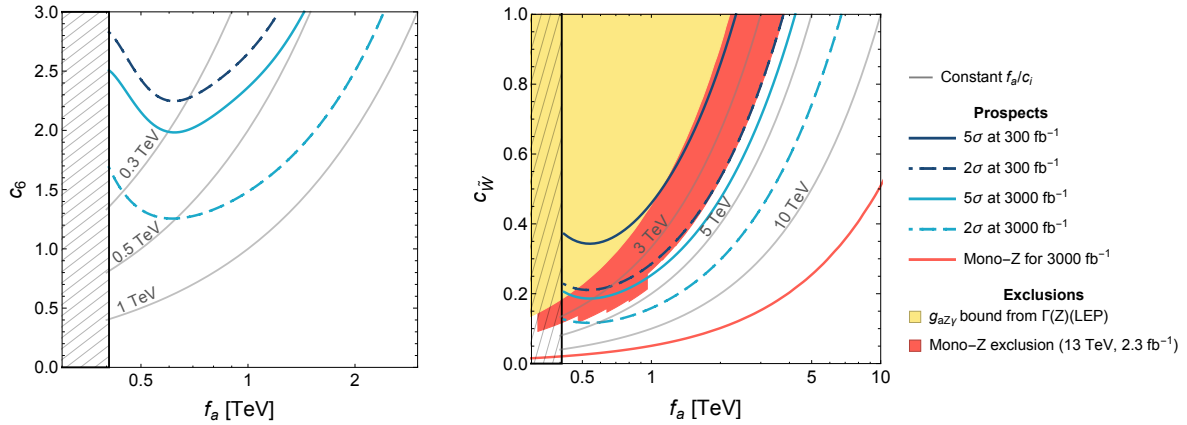

Figure 6.9: Contours for $\varpi = 2$ (dashed) and $\varpi = 5$ (solid) sensitivity to $pp \to aW^{\pm}\gamma$ ($W^{\pm} \to \ell^{\pm}\nu$) signal at the LHC with $\sqrt{s} = 13\,\text{TeV}$ and for an integrated luminosity of $300\,\text{fb}^{-1}$ (dark blue) and $3000\,\text{fb}^{-1}$ (light blue), as a function of $\{f_a, c_i\}$. The left (right) panel shows the results obtained assuming that only the operator $\mathcal{A}_6$ (the combination of operators $(\mathcal{A}_{\tilde{W}} - t_\theta^2 \mathcal{A}_{\tilde{B}})$) is contributing. The hatched region corresponds to $f_a < 2\not{E}_T^{\min}$, and is excluded by the EFT validity. The yellow region is excluded by the bound on $g_{aZ\gamma}$ reported in Eq. (6.31). The mono-Z exclusion region from $\sqrt{s} = 13\,\text{TeV}$ LHC with $2.3\,\text{fb}^{-1}$ of data is depicted by the red region. The gray reference lines correspond to constant values of f_a/c_i. The region explored for $c_{\tilde{W}}$ would be superseeded by the bound from rare decays in Eq. (3.88), within their range of applicability, if the correlation between operators contributing simultaneously was disregarded.

	c_6		$c_{\tilde{W}}$	
Luminosity [fb^{-1}]	300	3000	300	3000
Optimal $\not{E}_T^{\min}$ [GeV]	300	330	220	220
$(f_a/c_i)_{\max}$ [GeV]	470	950	3800	6800

Table 6.6: Optimal missing transverse energy cut $\not{E}_T^{\min}$, and $(f_a/c_i)_{\max}$ 2ϖ projected sensitivity reach for $aW\gamma$ production, for $\sqrt{s} = 13$ TeV and integrated luminosities 300 fb^{-1} and 3000 fb^{-1}.

- $\not{E}_T^{\max} = f_a/2$ for a given f_a value, as required by the EFT validity considerations, see Sect. 6.3.

A very slight improvement in sensitivity to c_6 is found for $\not{E}_T^{\min} = 300\,\text{GeV}$, as illustrated in Table 6.6 where the optimal cuts in $\not{E}_T^{\min}$ and the corresponding sensitivity reach are shown. Nevertheless, for comparison purposes it is more appropiate to use one single cut for all operators, and the value $\not{E}_T^{\min} = 200\,\text{GeV}$ indicated above will be used in the $aW\gamma$ analysis for all operators.

Fig. 6.9 shows the 2ϖ and 5ϖ sensitivity to the Lagrangian terms $c_{\tilde{W}}\left(\mathcal{A}_{\tilde{W}} - t_\theta^2 \mathcal{A}_{\tilde{B}}\right)$ (right) and $c_6\mathcal{A}_6$ (left), depicted in the $\{f_a, c_i\}$ plane and for 300 fb^{-1} and 3000 fb^{-1}. The hatched area is excluded as it would correspond to $f_a \leqslant 2\not{E}_T^{\min}$ (corresponding to all signal events

being outside the range of validity of the EFT). The 2σ exclusion sensitivity reaches $f_a/c_{\tilde{W}} \lesssim 3.8$ TeV (6.8 TeV) and $f_a/c_6 \lesssim 0.4$ TeV (0.8 TeV) for an integrated luminosity of 300 fb^{-1} (3000 fb^{-1}) of data, assuming the naive EFT validity criterium $f_a > 2\not{E}_T^{max}$. [14] We also note that when f_a drops below 2 TeV (twice the energy of the highest bin in the $\not{E}_T$ distribution in Fig. 6.8) the reach in f_a/c_i is diminished: this can be seen from Figure 6.9 comparing the sensitivity curves with the gray reference lines which correspond to constant f_a/c_i. The rightmost parts of the sensitivity curves is "parallel" to the latter lines, signaling that the reach in f_a/c_i is constant in this region. For $f_a \leqslant 2$ TeV instead, the sensitivity lines drift upwards compared to the reference lines, meaning that in that region the analysis is sensitive only to smaller values of f_a/c_i than for the regions to the right. This effect is due to the fact that, as f_a is diminished, the EFT validity gradually excludes the high-energy bins from the analysis, thus losing discrimination power (note also that considering the strict EFT validity criterium $\sqrt{\hat{s}} < f_a$ would amplify this effect).

Alike to the conclusions in Sect. 6.5.1 based on mono-W and mono-Z searches, associated $aW\gamma$ production at the LHC exhibits thus some (weaker but complementary) sensitivity to $c_{\tilde{W}}$ and to c_6 (for large values of the latter), and may potentially reach stronger constraints on $c_{\tilde{W}}$ than those obtained from LEP data, see Sect. 6.4.1, but weaker than the limits from rare-decays– see discussion around Eqs. (3.88). It should be possible to further increase the reach of the analysis by using a sophisticated version of the transverse mass instead of $\not{E}_T$, the so-called m_{T2} variable [275, 276].

Decorrelating power

The vertices in Figs. 6.2 (left) and 6.6 contribute simultaneously to the production of a and $a\gamma$ in association with $W^\pm$, as well as to VBF processes. Eqs. (6.49) and (6.48) show a dependence of these processes on certain combinations of coefficients and thus correlation effects are *a priori* expected. A combined analysis of $a/a\gamma$ production in association with $W^\pm$ and through VBF would enlarge the amount of kinematical information available, helping to disentangle their respective contributions.[15]

We consider for illustration the simultaneous action of c_2 and $c_{\tilde{W}}$ on mono-W signals and on $aW\gamma$ production. Note that it is precisely the contribution to the latter process of the $aZ\gamma$ vertex in Eq. (6.49) which would allow to separate the contributions of those two operator coefficients if data were sensitive to both, while from Eqs. (6.48) alone the two coefficients would have been tied in a blind direction. Similar considerations apply to other combinations of coefficients.

Nevertheless, our results indicate that, within the foreseen experimental prospects, no sensitivity is expected via mono-W and $aW\gamma$ production to couplings other than $c_{\tilde{W}}$ and c_6, that is to $\{\mathcal{A}_1, \mathcal{A}_2, \mathcal{A}_7, \mathcal{A}_8\}$ as these yield very suppressed contributions. The combination of mono-W data and $aW\gamma$ production data will therefore allow to disentangle the measurement/constraint of $c_{\tilde{W}}$ (a custodial-invariant signal common to linear and non-linear EWSB)

14 We warn the reader that, while the sensitivity to $c_{\tilde{W}}$ is expected not to appreciably change if the strict EFT validity criterium $\sqrt{\hat{s}} < f_a$ were required, the sensitivity to c_6 could be significantly modified. We leave a more precise assessment of this effect for future work.

15 The study of $a/a\gamma$ production in VBF is significantly more involved, due to the difficulty in accurately modelling the important multijet background, and is left for the future.

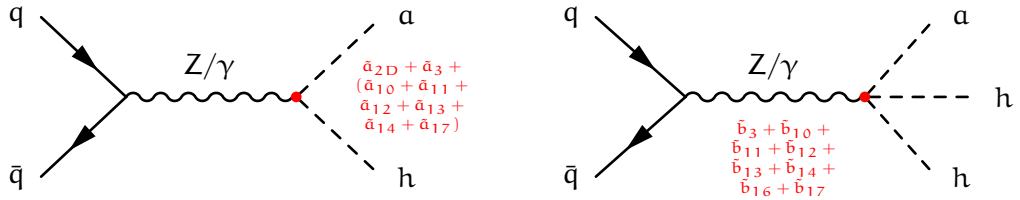

Figure 6.10: Main diagrams contributing to mono-Higgs (left) and di-Higgs (right) production in association with an ALP. The non-linear parameters entering each vertex are reported in the figure. Note that for the case of mono-Higgs, the contributions of $\tilde{a}_{2D}$ and $\tilde{a}_3$ are phenomenologically dominant, as the other coefficients enter the coupling with an extra suppression. The compact notation $\tilde{a}_i \equiv c_i a_i$, $\tilde{b}_i \equiv c_i b_i$ has been adopted.

from that of c_6 (only expected if the EWSB mechanism enjoys non-linear aspects and violates custodial symmetry).

6.5.3 *Higgs signatures*

Bosonic ALP-Higgs couplings are an interesting class of new signals which may be observable only within non-linear realizations of EWSB. Indeed, in the latter case aZh^n vertices with $n \geqslant 1$ are expected at LO, while they do not appear in the linear expansion below NNLO, as discussed in Sects. 6.1.2 and 6.2. They could induce especially interesting ALP signals: non-standard Higgs decay ($h \to aZ$) including invisible Higgs decay ($h \to a\nu\bar{\nu}$), associated ALP-Higgs production yielding an $h + \not{E}_T$ "mono-Higgs" signature at the LHC, or even a $hh + \not{E}_T$ di-Higgs signature, see Fig. 6.10. The possibility that aZh couplings of heavy pseudoscalars with masses in the $0.5 - 2\,\text{TeV}$ range may yield observable signals in $pp \to a \to Zh\,(h \to b\bar{b})$ was recently considered in the context of the linear expansion [250] (while the ALP signatures in Higgs and Z decays are presented in this chapter for the first time), stemming from one loop corrections to the NLO linear Lagrangian and from $d = 7$ operators.

The set of operators in the Lagrangian Eq. (6.5) contributing *a priori* to those signals are $\{\mathcal{A}_{2D}, \mathcal{A}_3, \mathcal{A}_{10}, \mathcal{A}_{11}, \mathcal{A}_{12}, \mathcal{A}_{13}, \mathcal{A}_{14}, \mathcal{A}_{17}\}$, see Table 7.1. Nevertheless, only the first three will be phenomenologically relevant within the LHC prospects, as the contributions from the rest are comparatively much suppressed by extra powers of $1/(4\pi)$ and/or m_a^2/v^2 in the case of $\mathcal{A}_{17}$, see Feynman Rules FR.6 and FR.7. This section focuses thus on the prospects for detecting $\mathcal{A}_{2D}$, $\mathcal{A}_3$ and $\mathcal{A}_{10}$, both taken one by one and in a combined analysis. The vertices relevant to the mono-h signal and the non-standard Higgs decays are

$$\begin{aligned} aZh &\to -\frac{4ev}{s_{2\theta} f_a}\tilde{a}_{2D}\, p_a^\mu + \frac{1}{2\pi v f_a}(\tilde{a}_3 s_\theta - \tilde{a}_{10} c_\theta)(p_Z^\mu p_h \cdot p_Z - p_h^\mu p_Z^2)\,, \\ a\gamma h &\to \frac{1}{2\pi v f_a}(\tilde{a}_3 c_\theta + \tilde{a}_{10} s_\theta)\left(p_A^\mu p_a \cdot p_A - p_A^2 p_a^\mu\right)\,, \end{aligned} \tag{6.52}$$

showing that a_3 and a_{10} enter in two different combinations into the processes considered:

- the mono-h (and di-Higgs) signatures depend on the combination $\tilde{a}_3 s_\theta - \tilde{a}_{10} c_\theta$ via Z exchange, and also on the orthogonal one $\tilde{a}_3 c_\theta + \tilde{a}_{10} s_\theta$ via γ exchange – see Fig. 6.10;
- in contrast, the non-standard Higgs decays depends only on $\tilde{a}_3 s_\theta - \tilde{a}_{10} c_\theta$.

We are thus contemplating three coefficients and two distinct processes. For the range of ALP masses used in the present numerical simulations ($m_a \leqslant 1$ MeV), the fermionic-induced bound on c_{2D} in Eq. (6.14) would lead to disregard the impact of $\mathcal{A}_{2D}$ on LHC data if that coupling were considered by itself. Nevertheless, given that a different combination of couplings is at work in rare decays and in LHC signals, for consistency with the perspective of exploring complementary approaches, and given that for larger ALP masses the LHC signals would still be present in a refined analysis, the contributions of $\mathcal{A}_{2D}$ must be retained in the analysis to follow. With this strategy, the impact of $\mathcal{A}_3$ and $\mathcal{A}_{10}$ on the non-standard Higgs decay width is subdominant with respect to that of $\mathcal{A}_{2D}$, given the different v dependence, see Eq. (6.52). On the contrary, LHC data are instead quite sensitive to c_3 and c_{10}, in addition to c_{2D}, given the stronger momentum dependence of $\mathcal{A}_3$ and $\mathcal{A}_{10}$. This suggests that, in order to disentangle the contributions from $\mathcal{A}_3$ and $\mathcal{A}_{10}$, a detailed study of the kinematic distributions of the mono-Higgs channel would be necessary, together with the combination of these results with those stemming from bounds on $h \to$ BSM from Higgs signal strength measurements. On the other side, a_3 and a_{10} have a similar overall impact on the total mono-h cross section. For the sake of simplicity, we will then consider here only the impact of a_{2D} and a_3, separately and combined, deferring the detailed study of $\mathcal{A}_{10}$ to a future work.

A remark on the range of values of the operator coefficients is pertinent. Generally speaking, large values correspond to strongly interacting regimes, and NDA suggests $c_i \leqslant 1$, with the bound saturated in the strong regime. Nevertheless, as discussed in Sect. 6.1, a factor (f/v) has been implicitly absorbed in the definition of the parameter $\tilde{a}_{2D} = c_{2D} a_{2D}$, where a_{2D} is the coefficient of the one-Higgs contribution in the polynomial $\mathcal{F}_{2D}(h)$. The ratio $\xi \equiv v^2/f^2$ is not a parameter from the effective theory point of view, but it is currently bounded to be $\lesssim 0.2$ in concrete models [271] such as composite Higgs scenarios. Numerically, this would translate into an enhancement of a factor $f/v \gtrsim 2.3$, which implies that the absolute value of the parameter $\tilde{a}_{2D}$ can naturally exceed by at least 2-3 units the bare NDA constraint $\tilde{a}_{2D} \leqslant 1$. In this section we will assume a maximum absolute value $\tilde{a}_{max} = 3$ for both $\tilde{a}_{2D}$ and $\tilde{a}_3$, along the same lines as the analysis presented in Sect. 6.5.2.

Mono-Higgs: $pp \to a\,h$

The process $pp \to ah(h \to 4\ell)$ is considered next at 13 TeV LHC, and it follows the mono-Higgs analysis from the "Les Houches 2015" report [277], considering both 300 fb^{-1} and 3000 fb^{-1} integrated luminosity. Our signal sample is produced with `MadGraph5_aMC@NLO` [267], passed on to `Pythia 8` [278] for showering and hadronization and then to `FastJet` [279] for jet reconstruction. The reconstructed events are finally filtered imposing the selection cuts from Ref. [277], for a consistent comparison with SM backgrounds which are taken precisely from that reference.

The $\not{E}_T$ spectrum can be used to disentangle the new interactions from the SM background. This applies in particular to $\mathcal{A}_3$, which induces a strong momentum dependence through both the aZh and the $a\gamma h$ contributions to the mono-h signal. This is illustrated in Fig. 6.11 for an integrated luminosity of 3000 fb^{-1}. As expected, the $\not{E}_T$ spectrum produced by $\mathcal{A}_3$ (orange line) is harder compared to that produced by $\mathcal{A}_{2D}$ (red line) while, at the same time, the total (no cuts) integrated cross section for the signal generated with $\mathcal{A}_3$ is manifestly lower than the one induced by $\mathcal{A}_{2D}$.

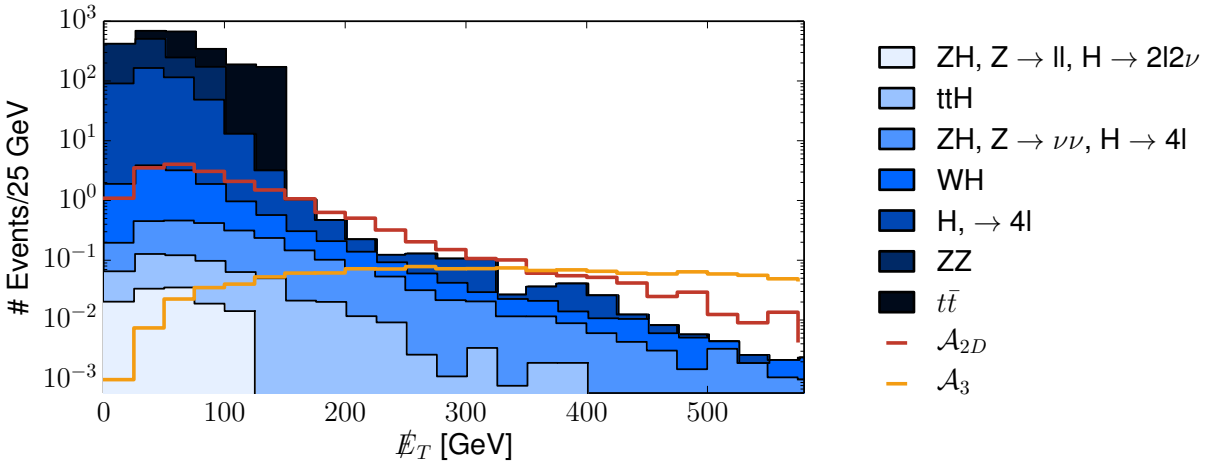

Figure 6.11: $\not{E}_T$ distributions for $4\ell + \not{E}_T$ signal and background for $\sqrt{s} = 13\,\text{TeV}$ and $3000\,\text{fb}^{-1}$ of integrated luminosity, after applying the selection cuts from [277]. SM $\not{E}_T$ background distributions are obtained directly from [277], and the signal $pp \to ah$ ($h \to 4\ell$) $\not{E}_T$ distribution is shown for $\mathcal{A}_{2D}$ (red) and $\mathcal{A}_3$ (orange).

In order to quantify the potential for observing in future LHC data a mono-Higgs signal generated by either of the two operators $\mathcal{A}_{2D}$ and $\mathcal{A}_3$, the analysis is done in two different stages.[16]

One operator at a time

In a first stage, each of the two relevant operators, $\mathcal{A}_{2D}$ and $\mathcal{A}_3$, is considered individually, *i.e.* assuming that only one of the coefficients c_{2D} and c_3 has a non-zero value. With this choice, the procedure already described in Sect. 6.5.2, Eqs. (6.50) and (6.51), is applied. The significance is computed as a function of f_a/c_i, integrating the distributions in Fig. 6.11 from a chosen $\not{E}_T^{\text{min}} = 150\,\text{GeV}$ (which removes most of the background contribution) up to $\not{E}_T^{\text{max}} = f_a/2$, according to the naive validity criterium (recall the discussion in Sect. 6.3).

Fig. 6.12 shows the $\sigma = 2$ and $\sigma = 5$ sensitivity regions obtained for the two coefficients $\tilde{a}_{2D}$ and $\tilde{a}_3$ individually (see Eq. (6.50)), and integrated luminosities of $300\,\text{fb}^{-1}$ and $3000\,\text{fb}^{-1}$. As shown in Fig. 6.12, only a very restricted region of the parameter space for $\mathcal{A}_3$ is accessible within $3000\,\text{fb}^{-1}$ at the LHC, due to its very small cross-section: it results in a 2σ sensitivity to $f_a/\tilde{a}_3 \lesssim 470$ GeV, which is expected to further degrade if the strict EFT validity criterium $\sqrt{\hat{s}} < f_a$ would be considered.

In contrast, Fig. 6.12 illustrates that mono-Higgs signatures in the $h \to 4\ell$ final state at HL-LHC have the potential to explore some region of parameter space for $\mathcal{A}_{2D}$ within the range of EFT validity. The 2σ exclusion sensitivity reaches $f_a/\tilde{a}_{2D} \lesssim 340$ GeV (780 GeV) for an integrated luminosity of 300 fb^{-1} (3000 fb^{-1}) of data. While considering the strict EFT validity criterium would somewhat degrade these limits, we also stress that considering other final states, e.g. $h \to \gamma\gamma$, $h \to b\bar{b}$, would significantly increase the sensitivity of this search, and we leave such a study for the future.

These results can be contrasted with the bounds on $f_a/\tilde{a}_i$, $(i = 2D, 3)$ inferred from the current upper limit on $\text{Br}(h \to \text{BSM})$ in Sect. 6.4.2, which is depicted as a green region in

16 Only tree level insertions of the operators $\mathcal{A}_{2D}$ and $\mathcal{A}_3$ will be considered below.

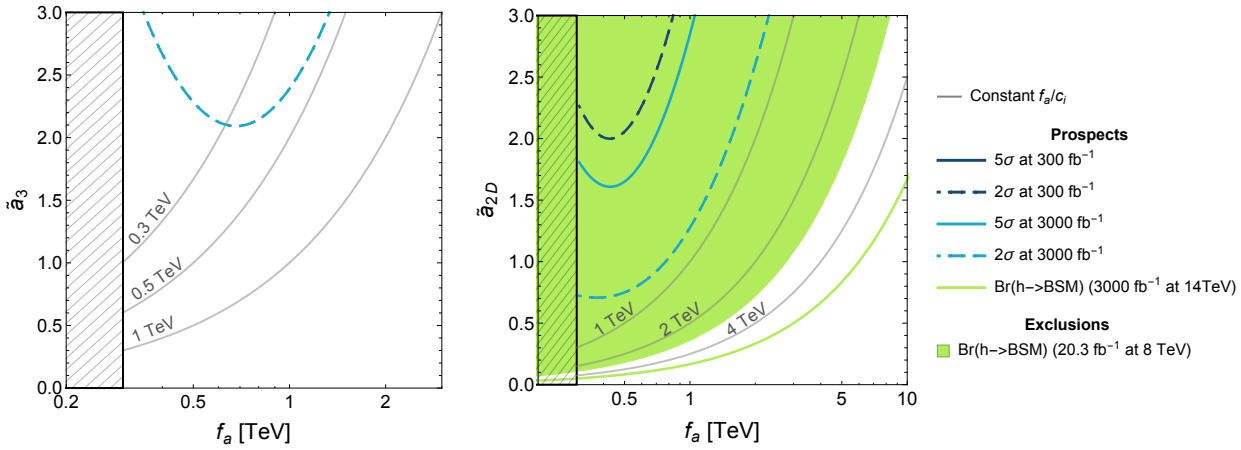

Figure 6.12: Contours for $\varpi = 2$ (dashed) and $\varpi = 5$ (solid) sensitivity to mono-H signal at the LHC with $\sqrt{s} = 13$ TeV and for an integrated luminosity of 300 fb^{-1} (dark blue) and 3000 fb^{-1} (light blue), as a function of $\{f_a, c_i\}$. The left (right) panel shows the results obtained assuming that only the operator $\mathcal{A}_3$ ($\mathcal{A}_{2D}$) is contributing. The hatched region corresponds to $f_a < 2\not{E}_T^{\min}$, and is excluded by the EFT validity, while the green region is excluded by the bound on Br($h \to$ BSM) reported in Eq. (6.37) (for the left-panel, this bound is not visible). The gray reference lines correspond to constant values of f_a/c_i.

Fig. 6.12 (right). If only $\mathcal{A}_{2D}$ is considered, the area of parameter space which is to be probed by LHC with 3000 fb^{-1} is already ruled out by that limit. This is not the case when only $\mathcal{A}_3$ is considered, since its contribution to $h \to$ BSM is very suppressed. Nevertheless, cancellations might exist amongst the contributions of those two operators to non-standard Higgs decays, in regions of the parameter space where a mono-Higgs signal could be expected at a testable level. This is the motivation for the second stage in the analysis: a combined study where both operators are considered simultaneously.

Combination of the two operators $\mathcal{A}_{2D}$ and $\mathcal{A}_3$

In this case of simultaneous consideration, the shape of the $\not{E}_T$ distribution after applying the analysis cuts can be estimated, for an arbitrary choice of f_a, $\tilde{a}_{2D}$ and $\tilde{a}_3$, as

$$(f_a/\text{TeV})^{-1} \left[\tilde{a}_{2D}^2\, x_k + \tilde{a}_3^2\, y_k + \tilde{a}_{2D}\,\tilde{a}_3\,(z_k - x_k - y_k)\right] , \tag{6.53}$$

where the index k runs over the distribution bins, and x_k, y_k, and z_k represent the $\not{E}_T$ prediction in the k-th bin obtained with $f_a = 1$ TeV and for the configurations $(\tilde{a}_{2D} = 1, \tilde{a}_3 = 0)$, $(\tilde{a}_{2D} = 0, \tilde{a}_3 = 1)$ and $(\tilde{a}_{2D} = 1, \tilde{a}_3 = 1)$, respectively. With this estimate of the $\not{E}_T$ distribution one can easily compute the maximal projected sensitivity to mono-Higgs signals, varying the lower cut in missing transverse energy, $\not{E}_T^{\min}$, in order to maximise the sensitivity ϖ at each $\{f_a/\tilde{a}_{2D},\, f_a/\tilde{a}_3\}$ point.

The results are shown in the scatter plot in Fig. 6.13. The yellow (orange) points are those for which there exists a lower $\not{E}_T$ cut within the EFT validity region, that allows to observe a mono-Higgs signature with a significance of least 2 (5) ϖ at the 13 TeV LHC with 3000 fb^{-1}. The left and right panels distinguish the two cases in which $\tilde{a}_{2D}$ and $\tilde{a}_3$ have either opposite or same sign. In both cases, in the limit $f_a/\tilde{a}_{2D} \to \infty$, the 2ϖ and 5ϖ sensitivity curves for

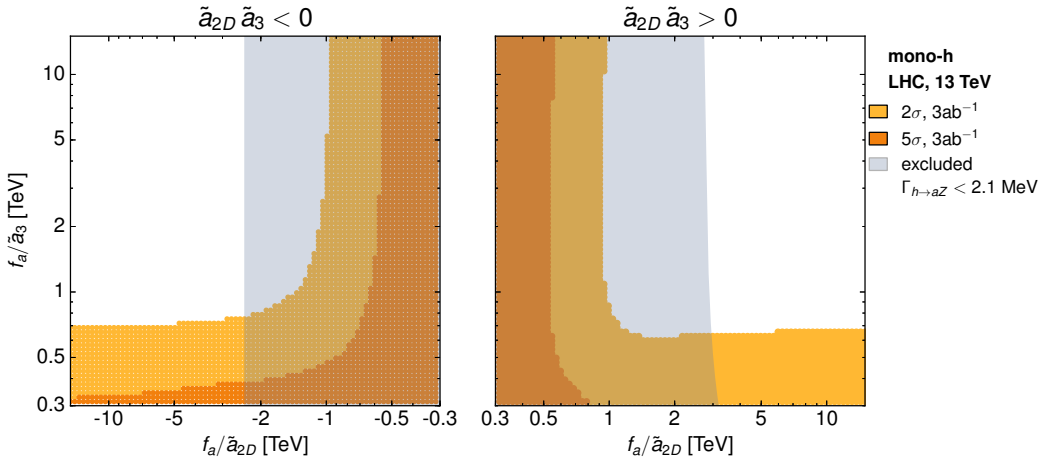

Figure 6.13: Contours for 2σ and 5σ sensitivity to the mono-H signal at the LHC with $\sqrt{s} = 13\,\text{TeV}$ and for an integrated luminosity of $3000\,\text{fb}^{-1}$, for different values of the parameters $(f_a/\tilde{a}_{2D})$ and $(f_a/\tilde{a}_3)$. The left (right) panel shows the result obtained for opposite-sign (same-sign) scaling factors. The gray shaded region is excluded by the bound on $\text{Br}(h \to \text{BSM})$ reported in Eq. (6.37).

$f_a/\tilde{a}_3$ converge towards values close to the optimal ones found in the $\mathcal{A}_3$-only analysis (the discrepancy is due to the different treatment of the $\not{E}_T^{\text{min}}$ cut). An analogous behavior is also observed in the orthogonal direction.

More interesting is the region where $\tilde{a}_{2D}$ and $\tilde{a}_3$ are close in absolute value. In particular, it shows that the contributions to the mono-Higgs process stemming from the two operators produce destructive interference when $\tilde{a}_{2D}$ and $\tilde{a}_3$ have the same sign: for $\tilde{a}_{2D} \simeq \tilde{a}_3$ (right panel) the signal is reduced compared to the case in which one of the two operators dominates, and the sensitivity is therefore lower in this region of the parameter space. On the other hand, for $\tilde{a}_{2D} \simeq -\tilde{a}_3$ (left panel) constructive interference effects enhance mono-Higgs production, so that the LHC would be sensitive to larger values of $f_a/\tilde{a}_i$ than in the one-operator case.

As with the previous study, the results obtained for projected mono-Higgs searches in the $(\tilde{a}_{2D}, \tilde{a}_3)$ plane can be easily contrasted with the bound inferred in Sect. 6.4.2 from the current upper limits on $\text{Br}(h \to \text{BSM})$. This is depicted as a grey-shaded region in Fig. 6.13 and seen to be more stringent for same sign $\tilde{a}_{2D}$ and $\tilde{a}_3$, as no cancellation can then take place in the dominant expression in $\text{Br}(h \to \text{BSM})$, see Eq. (6.36).

As a result of the combination of the existing bound with the projected reach, it appears that mono-Higgs searches may be useful for probing a relevant region of the parameter space, namely that with $300\,\text{GeV} \lesssim |f_a/\tilde{a}_3| \lesssim 700\,\text{GeV}$, where the lower bound is a direct consequence of requiring the EFT validity. In this region, $|f_a/\tilde{a}_{2D}|$ may be no smaller than 2-3 TeV, as lower values are already excluded by the $h \to \text{BSM}$ constraint that we derived from present data in Sect. 6.4.2. Overall, we find that although mono-Higgs searches at the LHC are sensitive to the presence of both operators $\mathcal{A}_{2D}$ and $\mathcal{A}_3$, they are not competitive in constraining $f_a/\tilde{a}_{2D}$ with the $\text{Br}(h \to \text{BSM})$ bound, neither with the fermionic-induced bound in Eq. (6.14) when that coupling is considered just by itself. On the other hand, they are more sensitive to the presence of $\tilde{a}_3$ and therefore they may provide valuable, complementary, information in the study of the ALP's coupling to the Higgs.

In conclusion, if interpreted in terms of the presence of a light pseudo-Goldstone boson, and barring fine-tunings, the observation of a mono-Higgs signature at the LHC represents a smoking gun of non-linearity in the EWSB sector, as couplings such as $aZ(\gamma)h$ are not to be found in the NLO Lagrangian of linear EWSB setups (see FR.1, FR.7). Within the effective Lagrangian in Eq. (6.1), the observation of this signal at foreseen LHC data can only be attributed to the presence of $\mathcal{A}_3$ (or eventually $\mathcal{A}_{10}$), as $\tilde{a}_{2D}$ is out of reach in that data set given the range of values allowed by the current bounds.

A comment on di-Higgs production

The $aZhh$ interaction allows for di-Higgs final state, due to a quark-initiated $hh + \not{E}_T$ production via Drell-Yan (see Fig. 6.10 (right)). This is in contrast to di-Higgs production in the SM, which is exclusively gluon-fusion initiated. Moreover, the presence of $\not{E}_T$ in the final state could serve as an additional handle to suppress SM backgrounds to the di-Higgs process. This discussion highlights that a-h interactions could constitute a very promising avenue for non-linear ALP phenomenology at the LHC, which we intend to explore in the future.

6.5.4 *Coupling to fermions*

In this chapter we have focused on the relation of the ALP with the EWSB sector via bosonic operators, and explored the impact of couplings of the ALP to SM bosons. However, in Sects. 3.2 and 6.1 we noticed that bosonic operators would lead to ALP-fermion couplings via a field redefinition.

Although the bounds we obtained in Eqs. (3.86) for the linear operator $\mathcal{O}_{a\Phi}$ and (6.14) for the non-linear one $\mathcal{A}_{2D}$ when considering operators one at a time are very strong, it is worth exploring complementary searches at the LHC. The structure of these fermionic couplings is very specific, proportional to the Yukawa matrices, see Feynman rules in App. A.2. One would then expect the ALP to couple more strongly to third generation quarks, provided the matrices X_ψ in Eq. (3.67) are generic. We then consider the characteristics of the leading ALP production in association with a $t\bar{t}$ pair at LHC.

For ALPs stable on LHC scales, this final state is similar to searches for supersymmetric scenarios, where two stops are strongly produced and produce a signature of $t\bar{t}$ in association with two neutralinos (Dark Matter candidates). For example, via the LO coupling c_{2D} the production cross section of the final state $t\bar{t}$+ALP, where the ALP is emitted as final state radiation –see FR.17, is given by

$$\sigma(p\,p \to t\,\bar{t}\,a)[\sqrt{s} = 13\ \text{TeV}\ ] = c_{2D}^2 \left(\frac{1\ \text{TeV}}{f_a}\right)^2 (50\ \text{fb}). \tag{6.54}$$

In these searches, final states are selected by requiring a number of jets, b-jets with characteristics matching those of top decays. More importantly, a substantial cut on missing energy is required. For example, in a recent study with 13 TeV data by ATLAS [280], the cut on missing energy for the channel of interest (TT) (topology of two tops) is 400 GeV . In our scenario, with single-production of a light pseudoscalar via strong production of two tops, the distribution of missing energy is not as hard as in scenarios where heavy stops are pair produced and inject a large boost into the neutralino. This is shown in Fig. 6.14, where we

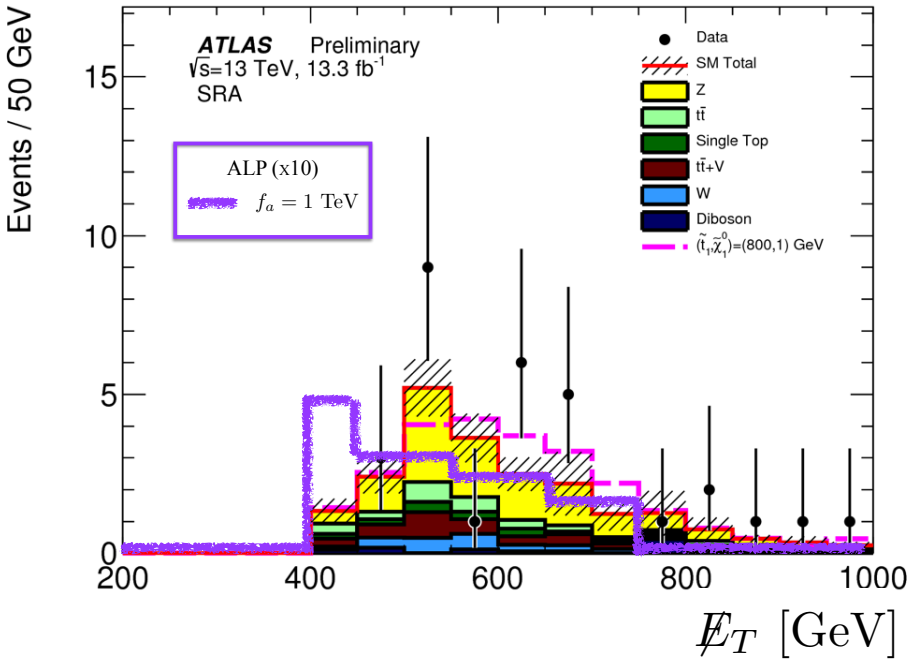

Figure 6.14: Missing energy distribution for the production of an light ALP in association with $t\bar{t}$ for 13.3 fb^{-1} of 13 TeV data. The normalization has been chosen with $f_a = 1$ TeV and then multiplied by a factor 10. We show the corresponding simulation of supersymmetric scenarios by ATLAS, as well as their event count.

compare our results for $f_a = 1$ TeV with the ATLAS data and Monte Carlo simulations for a supersymmetric scenario with 800 GeV stops and a light neutralino.

This type of analysis opens the way to further phenomenological explorations of the fermionic signals associated to ALP production. This is most relevant and promising in order to tackle the ALP-fermionic couplings identified in App. A.1, which are part of the complete NLO basis of operators –bosonic and fermionic– involving one ALP and established in this chapter. See also the phenomenological signals discussed just before Sect. 6.5.1.

6.6 SUMMARY

In this chapter we have developed a systematic approach to describe interactions of an axion or an axion-like particle (ALP), with special attention to the sector responsible for electroweak symmetry breaking (EWSB), obtaining the complete –bosonic and fermionic– NLO Lagrangian in the case that EWSB is non-linearly realised. With this theoretical framework in place, we have then studied new collider and other phenomenological signals associated with ALPs, as well as explored the sensitivity of the LHC in the high-luminosity phase (HL-LHC). Both the approach and the phenomenological results in this chapter are novel, and will hopefully guide new searches at the LHC and the study of complementarity with other experiments at lower energies.

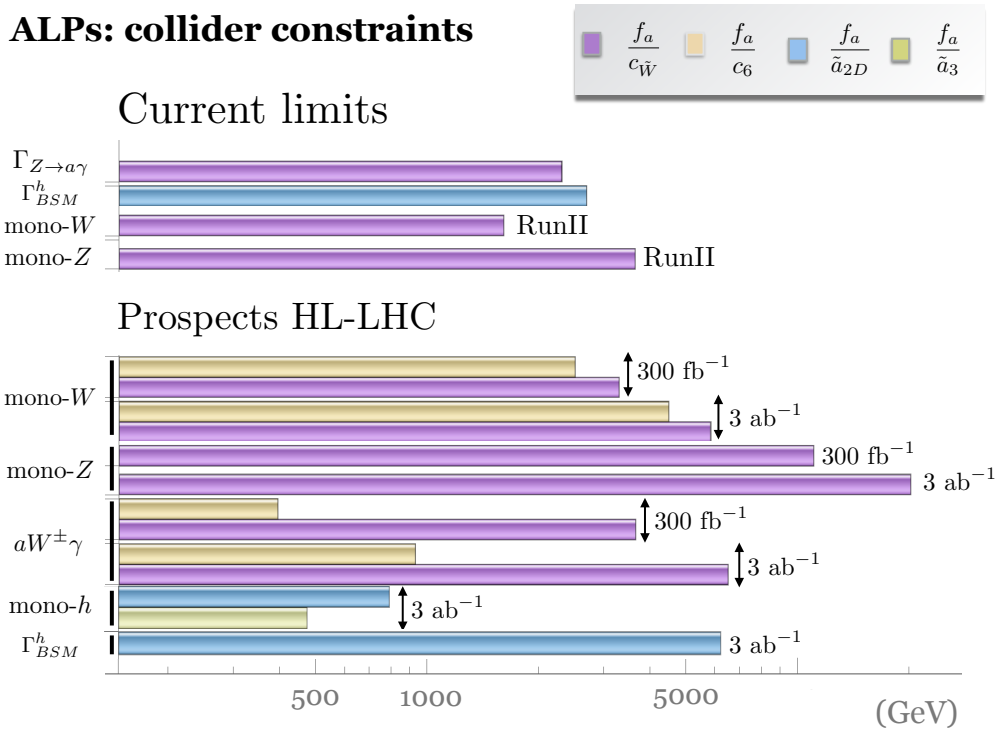

Figure 6.15: Summary of the most significant constraints stemming from the studies on tree-level ALP couplings presented in this chapter, upon the assumption $g_{a\gamma\gamma} = 0$ or equivalently $c_{\tilde{B}} = -t_\theta^2 c_{\tilde{W}}$. The bars for $\Gamma_{Z\to a\gamma}$, Γ^h_{BSM}, mono$-W$ and mono$-Z$ correspond to 95% C.L., both in existing constraints and expected reaches for $\sqrt{s} = 13\,\text{TeV}$, inferred in Sects. 6.4 and 6.5 respectively. The bars for $aW^\pm\gamma$ and mono$-h$, instead, indicate the 2σprojected reach of given searches at the LHC with $\sqrt{s} = 13\,\text{TeV}$, see Sect. 6.5. Systematic uncertainties are taken into account for the present constraints but are neglected in the projected ones.

Theoretical developments

Neglecting ALP masses, we have developed a complete list of bosonic operators under two scenarios, with EWSB linearly and non-linearly realised, valid in all generality for any value of the axionic scale larger than the electroweak scale (and in the non-linear case also larger than its implicit electroweak BSM scale). In the linear case, in which the couplings involving an ALP first appear at $d = 5$, special attention has been paid to recalling the subtle effect of the operator $(\Phi^\dagger \overleftrightarrow{D}_\mu \Phi)\frac{\partial^\mu a}{f_a}$, which induces a contribution to the two-point function involving *longitudinal* gauge bosons, and can be removed via a Higgs field redefinition. This redefinition generates new couplings of the ALP to fermions, with the distinctive feature of being proportional to the Yukawa couplings.

In the non-linear realization, we have employed a systematic approach to classify the new operators order-by-order, and much care has been paid to define the expansion in both its non-linear and ALP sectors. A complete and non-redundant basis of operators involving an ALP has been determined, even though the impact analysis has focused on the bosonic couplings. Several interesting features arise when considering ALPs coupled to a non-linear realization of EWSB, in particular the existence –already at the leading order in the derivative

expansion– of interaction vertices involving the Higgs and gauge bosons with the ALP. This is due to the fact that the two-point function stemming from the operator $\mathcal{A}_{2D}$ cannot be entirely traded by fermionic couplings (in contrast to the analogous operator for the linear case above). Additionally, we find that the non-linear effects induce new Lorentz structures beyond those in the *traditional* (linear) ALPs couplings.

Furthermore, a detailed comparison of the differences and correspondences between the operators in the linear and non-linear setups has been developed, as well as a prospective study on how to disentangle *a priori* both expansions if a signal is found.

For the most part, phenomenological studies on the ALP effective Lagrangians have focused on couplings to photons, gluons and fermions. However, if the ALP couples to photons, SM gauge invariance also implies the existence of similar couplings to the massive gauge bosons, irrespective of whether the mechanism behind EWSB gives rise to a linear or a non-linear expansion. In this chapter we propose for the first time signals in accelerator searches with heavy SM bosons in the final state.

In this chapter we have obtained new constraints on ALP couplings to SM particles, as well as provided a guide for future searches of ALPs and the sensitivity HL-LHC could reach, for ALP scales of $\mathcal{O}$(TeV) or somewhat above. Special attention has been paid to the consistency of the kinematic regions used for each search with the assumption of validity of the ALP expansion in powers of $1/f_a$.

Current constraints

We started by looking at new constraints on (linear) ALP couplings to all EW gauge bosons. In particular, we looked for observables sensitive to the linear combination of $SU(2)_L \times U(1)_Y$ operators $(c_{\tilde{B}}, c_{\tilde{W}})$ orthogonal to the coupling to photons, i.e. orthogonal to $g_{a\gamma\gamma} \sim c_{\tilde{W}} s_\theta^2 + c_{\tilde{B}} c_\theta^2$.

To account for the strong constraints on the value of $g_{a\gamma\gamma}$ we then imposed $c_{\tilde{B}} \simeq -t_\theta^2 c_{\tilde{W}}$ in our analyses, effectively reducing the number of parameters by one. In Fig. 6.15 one can see that LEP constraints on the invisible width of the Z boson, and LHC searches for final states with one massive boson and missing energy (mono-Z and mono-W channels), provide handles to probe the Wilson coefficient $c_{\tilde{W}}$. We find that mono-Z limits impose at present a constraint $f_a/c_{\tilde{W}} \gtrsim 4\,\text{TeV}$.

We also discussed the impact on bounds from rare-decays of mesons into channels with missing energy, and how they provide a complementary approach to accelerator searches. Besides the stringent constraints existing in the literature on $f_a/c_{\tilde{W}}$ from the former searches –which strictly speaking only apply when all other operators are set to zero– a similar new bound on the strength of the linear operator $\mathbf{O}_{a\Phi}$ has been obtained here.

In non-linear realizations of EWSB in particular, many other operators affect LHC physics. For ALP masses under 3 GeV, data on rare meson decays allowed to strongly bound c_{2D} if considered by itself. Furthermore, of particular interest are operators which induce new type of couplings, specifically new couplings of the ALP to Higgs particles, e.g. ALP-Zh or ALP-Zhh, which are dominantly generated by the non-linear operators $\mathcal{A}_{2D}$, $\mathcal{A}_3$ and $\mathcal{A}_{10}$. In the LHC Run-I the coupling ALP-Zh was here probed via non-standard Higgs decays; if the impact of the different operators contributing is considered one at a time, a bound on $f_a/\tilde{a}_{2D}$ of the order of 3 TeV follows for ALP masses in the range 3-34 GeV.

Future sensitivity

We then moved on to examine the capability of the HL-LHC to search for ALPs. Apart from improvements on current channels (non-standard Higgs decays, mono-W and mono-Z), we proposed and evaluated possible new channels at 13 TeV which could dramatically change our understanding of ALPs both in the linear and non-linear realizations.

Future improvements of mono-Z searches with 3 ab^{-1} of data could bring the collider sensitivity to the linear operator coefficient $f_a/c_{\tilde{W}}$ to above 20 TeV. But the most striking signatures stemming from bosonic operators, i.e. mono-Higgs and associated $W^{\pm}\gamma$ production plus missing energy, would access the non-linear operators mentioned before, $\mathcal{A}_3$ and $\mathcal{A}_{2D}$, and a new one, $\mathcal{A}_6$. We also propose the study of different channels, like mono-W in combination with $aW\gamma$ production, to disentangle the presence of two different operators. On the other hand, the very sensitive mono-Z and mono-W signals may play a specially important role in probing fermion-ALP interactions; this will be tackled in a future study.

Besides these signals, we proposed to use the searches on stops in on-shell top final states to look for ALPs, whose couplings to quarks are derived from couplings to the bosonic sector and are proportional to the fermion mass.

This study motivates further work on ALP physics beyond the usual framework of couplings to photons and gluons, and more emphasis was placed on the effects in the sector responsible for electroweak symmetry. Additionally, we propose to perform dedicated experimental analyses in channels like mono-Higgs and new channels involving the ALP and two bosons in the final state, such as $W^{\pm}\gamma$ and missing energy.

Although in this chapter we presented a rather comprehensive analysis of the effective theory for ALPs as well as their phenomenology, there are a number of open issues that deserve further study. To name a few: the extension of the collider analysis to higher ALP mass regions (including signals from ALP decays), the study of vector-boson fusion channels, the analysis of ALP-fermion signals to probe the complete NLO basis of operators –bosonic and fermionic– established in this chapter, the combination of collider constraints with lower-energy experiments (particularly rare decays of mesons), and the evaluation of modifications to the history of the axion in the Early Universe due to the non-linear effects.

7

NON-LINEAR HIGGS PORTAL TO DARK MATTER

In a last step in this thesis, the interactions of a real scalar dark matter candidate will now be considered. There is only one type of renormalisable ($d \leqslant 4$) interaction of a scalar DM particle to the fields of the SM: it is a coupling to the Higgs in the scalar potential which receives the name of the scalar Higgs portal, and was presented in Sect. 4.3. Its simple expression (which assumes a customary Z_2 symmetry [202, 203]) reads off from Eq. (4.5):

$$\lambda_S S^2 \Phi^\dagger \Phi \longrightarrow \lambda_S S^2 (v + h)^2 \longrightarrow \lambda_S S^2 (2vh + h^2)\,, \tag{7.1}$$

where Φ denotes the $SU(2)_L$ Higgs field doublet, h the observed Higgs particle and λ_S is the Higgs portal coupling; the right-hand side of the equation shows the DM-Higgs interaction in unitary gauge. The SM Higgs-DM portal in Eq. (7.1) ("standard" portal all through this chapter) has been extensively explored in the literature [19, 204–221] and very tightly constrained, see Sect. 4.3.

The standard Higgs portal is however only one possibility amongst the BSM formulations of scalar DM interactions: it is constructed in the context of the SMEFT –describing scenarios where EWSB is linearly realised and the BSM physics is weakly interacting–, while there exists another possibility. Models where NP related to the EW sector (for instance to explain the EW hierarchy problem) is strongly interacting and/or EWSB is realised non-linearly can be described instead by the Higgs EFT. These two options were presented in Sect. 1.4. The interactions of a scalar DM particle using the HEFT formalism will be derived for the first time and explored in this chapter. The basis of interactions of the non-linear Higgs portal will be determined at leading order, and the phenomenological consequences will also be studied in detail, including the possibility of distinguishing this scenario from the standard Higgs portal in which the electroweak symmetry breaking is linearly realised.

7.1 THE NON-LINEAR HIGGS-PORTAL

The general features of a scenario in which the lightness of the Higgs particle results from its being a pseudo-Goldstone boson of some global symmetry, spontaneously broken by strong dynamics at a high scale Λ_s, were presented in Sect. 1.3.2. There exist a large number of models for composite of GB Higgs, for which this strongly interacting new-physics is expressed at low-energies by means of a chiral or non-linear Lagrangian. An interesting characteristic of these non-linear scenarios is that the low-energy physical Higgs field turns out not to be an exact electroweak doublet, and can be parametrised in the effective Lagrangian as a generic SM scalar singlet with arbitrary couplings [65, 67, 80, 88]. In other words, the typical SM dependence on $(v + h)$ in Eq. (7.1) is to be replaced by a generic polynomial $\mathcal{F}(h)$, which was defined in Eq. (1.56) implying the substitution of the standard portal in Eq. (7.1) by the functional form

$$\lambda_S S^2 (2vh + b\, h^2)\,, \tag{7.2}$$

where b is an arbitrary, model dependent constant. The hSS and $hhSS$ couplings - whose relative amplitude is fixed in the standard portal - are now decorrelated. This simple fact will be shown to have a deep impact on the estimates of the DM relic abundance, for which the relative strength of the DM coupling to one versus two h particles plays a central role.

A further consequence of h being treated as a generic scalar singlet is that its interactions are not necessarily correlated with those of the longitudinal components of the $W^{\pm}$ and Z gauge bosons, denoted by $\pi(x)$ in the customary $\mathbf{U}(x)$ matrix which was defined in Eq. (1.52). While in linear BSM scenarios, h and $\mathbf{U}(x)$ are components of the same object, i.e. the $SU(2)_L$ Higgs doublet the independence of h and $\mathbf{U}(x)$ in the non-linear Lagrangian induces a different pattern of dominant couplings. It will be shown here that the bosonic couplings of S show this pattern, motivating the consideration of other interactions in addition to those in Eq. (7.2) above. The ensemble will lead to potential smoking guns of the nature of the EWSB mechanism and of the Higgs particle. Distinct signals and (de)correlations in direct and collider DM searches will be discussed.

We restrict the analysis to the purely bosonic sector, except for the fermionic Yukawa-like terms. The relevant effective Lagrangian is derived below: it will be shown that *only v and the fermion and S mass terms will remain as explicit scales*.

This general Lagrangian may describe the leading effects of a plethora of models, for particular values of its coefficients. In those subjacent models, aside from fermion masses, several scales may be involved explicitly and implicitly, typically:

- The electroweak (EW) scale v, at which the effective Lagrangian is defined.
- The Goldstone-boson scale f associated to the physical Higgs h, whose value does not need to coincide with v. Arbitrary functions $\mathcal{F}(h)$ would encode the Higgs dependence as a polynomial expansion in h.
- The scale Λ_s of the high-energy strong dynamics, with $\Lambda_s \leqslant 4\pi f$.
- The new physics scale Λ_{DM} characteristic of the DM interactions with the visible world, that is the effective DM-Higgs portal scale, typically corresponding to the mass of a dark mediator.
- The mass of the scalar DM particle m_S.

In the effective Lagrangian approach v and the natural Goldstone boson scale f are not separate parameters: v is introduced as a fine-tuning requirement [13]. For instance it is customary to trade the $\mathcal{F}(h)$ polynomial dependence in powers of h/f by an expansion in powers of h/v, with the arbitrary expansion coefficients absorbing the v/f tuning, as it was already argued in Sect. 1.4.2. For the heavy scales, would Λ_{DM} coincide with Λ_s or f, it would indicate a common origin for the Higgs and the DM candidate, as it occurs in models where both have their origin as Goldstone bosons of the high-energy strong dynamics [281–283]. Notice that, in such a scenario, the behavior of the S field is expected to follow closely that of the Higgs particle: its dependence should be encoded in generic functions $\mathcal{F}(S)$ invariant under the $\mathbb{Z}_2$ symmetry (*e.g* $\cos(S/f)$). The discussion will be kept here on a more general level and Λ_{DM} will be taken as an independent scale, although assuming $f \ll \Lambda_{DM}$ in addition to plausibly $m_S \ll \Lambda_{DM}$.

Furthermore, only the leading terms weighted down by Λ_{DM} and Λ_s will be kept below, which in practice means no explicit dependence on them. Indeed, at leading order the expansion is tantamount to keeping the leading two-derivative terms of the electroweak chiral expansion [65, 77–79, 284], supplemented by the $\mathcal{F}(h)$ dependences [14, 66, 68–71, 73–75, 89, 90, 285] and the S insertions: at this order the effective Lagrangian depends only on v, the fermion and S mass terms, plus the operator coefficients.

The Lagrangian can be written as the sum of two pieces, with the second one encoding the DM interactions:

$$\mathcal{L} = \mathcal{L}^{LO}_{HEFT} + \mathcal{L}_S\,, \tag{7.3}$$

with $\mathcal{L}^{LO}_{HEFT}$ defined in Eq. (1.57) and the DM Lagrangian $\mathcal{L}_S$ at leading order in the $1/\Lambda_{DM}$ expansion reading

$$\mathcal{L}_S = \frac{1}{2}\partial_\mu S\partial^\mu S - \frac{m_S^2}{2}S^2\mathcal{F}_{S_1}(h) - \lambda S^4\mathcal{F}_{S_2}(h) + \sum_{i=1}^{5} c_i\mathcal{B}_i(h)\,, \tag{7.4}$$

where the $\mathcal{B}_i$ operators form a basis:

$$\left.\begin{aligned}\mathcal{B}_1 &= \mathrm{Tr}(\mathbf{V}_\mu\mathbf{V}^\mu)S^2\mathcal{F}_1(h)\\ \mathcal{B}_2 &= S^2\Box\mathcal{F}_2(h)\end{aligned}\right\}\ \text{Custodial Preserving}$$

$$\left.\begin{aligned}\mathcal{B}_3 &= \mathrm{Tr}(\mathbf{T}\mathbf{V}_\mu)\mathrm{Tr}(\mathbf{T}\mathbf{V}^\mu)S^2\mathcal{F}_3(h)\\ \mathcal{B}_4 &= i\mathrm{Tr}(\mathbf{T}\mathbf{V}_\mu)(\partial^\mu S^2)\mathcal{F}_4(h)\\ \mathcal{B}_5 &= i\mathrm{Tr}(\mathbf{T}\mathbf{V}_\mu)S^2\partial^\mu\mathcal{F}_5(h)\end{aligned}\right\}\ \text{Custodial Violating} \tag{7.5}$$

All $\mathcal{F}_i(h)$ functions in $\mathcal{L}^{LO}_{HEFT}$, (7.4) and (7.5) could be generically parametrised as an expansion in powers of h, as defined in Eq. (1.56) and the scalar and vector fields parametrising the electroweak GBs, respectively $\mathbf{T}(x)$ and $\mathbf{V}(x)$ defined in Eq. (1.53). Finally, it is useful to rewrite $\mathcal{L}_S$ as

$$\mathcal{L}_S = \frac{1}{2}\partial_\mu S\partial^\mu S - \frac{m_S^2}{2}S^2 - \lambda_S S^2\left(2vh + bh^2\right) + \sum_{i=1}^{5} c_i\mathcal{B}_i(h) + \dots \tag{7.6}$$

by redefining the constant parameters in an obvious way, so that the $d \leqslant 4$ pure Higgs-DM non-linear portal takes the form announced in Eq. (7.2). The dots in Eq. (7.6) stand for terms with more than two h bosons and/or more than two S fields, which are not phenomenologically relevant in the analysis below and are henceforth discarded.

A pertinent question is how to complete the basis including fermionic couplings. There are two possible chiral fermionic structures to consider:

$$\bar{Q}_{L_i}\mathbf{U}Q_{R_j}S^2\mathcal{F}(h)\,, \qquad \bar{L}_{L_i}\mathbf{U}L_{R_j}S^2\mathcal{F}(h)\,, \tag{7.7}$$

$$\begin{aligned}&\bar{Q}_{L_i}\gamma_\mu Q_{L_j}\partial^\mu S^2\,\mathcal{F}(h)\,, \qquad &&\bar{L}_{L_i}\gamma_\mu L_{L_j}\partial^\mu S^2\,\mathcal{F}(h)\,,\\ &\bar{Q}_{R_i}\gamma_\mu Q_{R_j}\partial^\mu S^2\,\mathcal{F}(h)\,, \qquad &&\bar{L}_{R_i}\gamma_\mu L_{R_j}\partial^\mu S^2\,\mathcal{F}(h)\,,\end{aligned} \tag{7.8}$$

where i, j are flavour indices. The equations of motion, however, allow to relate a combination of the operators in Eq. (7.7) to the operator $\mathcal{B}_2$, and a combination of the operators in Eq. (7.8) to $\mathcal{B}_4$. In consequence, in order to avoid redundancies, a complete basis can be defined by the ensemble of all bosonic operators in Eq. (7.5) plus those in Eqs. (7.7) and (7.8), except for the two combinations of fermionic operators mentioned. Alternatively, the basis could be defined by all fermionic operators in Eqs. (7.7) and (7.8) plus the bosonic ones in Eq. (7.5), excluding $\mathcal{B}_2$ and $\mathcal{B}_4$. An optimal choice of the basis may depend on the data considered: in this chapter the focus is set on the bosonic sector only, while the effects of introducing the fermionic one deserves a comprehensive future study, where flavour effects will also be taken into account.

In Eq. (7.6), the c_i's ($i = 1...5$) – together with the coefficients inside $\mathcal{F}_i(h)$ – parametrise the contributions of the $\mathcal{B}_i$ operators in the basis of Eq. (7.5). These five effective operators describe interactions between two S particles and either two W bosons, one or two Z or h bosons, or a Z and a h boson (see the Feynman rules in Appendix B.1), inducing interesting phenomenological signatures as shown in the next section. $\mathcal{B}_1$ and $\mathcal{B}_2$ are custodial invariant couplings, in the sense that they do not contain sources of custodial symmetry breaking other than those present in the SM (hypercharge in this case). $\mathcal{B}_3$, $\mathcal{B}_4$ and $\mathcal{B}_5$ provide instead new sources of custodial symmetry violation. Nevertheless, the contribution of $\mathcal{B}_4$ to the Z mass vanishes while that from $\mathcal{B}_5$ arises only at the two loop level (see Appendix B.1), and no significant constraint on their operator coefficient follows the ρ parameter and EW precision data; on the other hand, these observables do receive a one-loop contribution from $\mathcal{B}_3$. The bound on the corresponding coefficient is estimated to be around $c_3 \sim 0.1$. Finally, notice that operators $\mathcal{B}_1$, $\mathcal{B}_2$ and $\mathcal{B}_3$ are CP-even, while $\mathcal{B}_4$ and $\mathcal{B}_5$ are CP-odd.

In summary, the non-linear portal in Eq. (7.6) shows a much richer parameter space than the standard Higgs portal in Eq. (7.1). The relationship between higher-dimension operators in the linear realisation of EWSB and the non-linear DM Higgs portal will be discussed in Sect. 7.3.

7.2 DARK MATTER PHENOMENOLOGY

A wide variety of experimental data constrains the DM parameter space of Higgs portal scenarios described by the Lagrangian (7.6). The precise measurement of the DM density today, $\Omega_{\rm DM}$, performed by Planck [187] provides an upper bound on the relic abundance of S particles, Ω_S. Direct detection experiments set complementary limits on the strength of the DM-nucleon interactions, the current most stringent bounds coming from the Large Underground Xenon (LUX) experiment [200]. Upcoming experiments like XENON1T [201, 286] will further increase the sensitivity in DM direct detection. The couplings of DM to SM particles may be also probed at the LHC, with potential avenues including searches of invisible decay modes of the Higgs boson, and searches for mono-X signatures, namely final states where one physical object X is recoiling against missing transverse energy $\not{E}_T$.

In the following we explore the rich phenomenology of non-linear Higgs portals. We first analyse the current constraints on the properties of DM coming from the DM relic abundance, direct detection limits from LUX and bounds on the invisible decay width of the Higgs boson. We then study the prospects for mono-X signatures, with $X = h, W^\pm, Z$, at the 13

Observable		**Parameters contributing**					
		b	c_1	c_2	c_3	c_4	c_5
Thermal relic density	$\Omega_S h^2$	✓	✓	✓	✓	✓	✓
DM-nucleon scattering in direct detection	σ_{SI}	–	–	✓	–	✓	–
Invisible Higgs width	Γ_{inv}	–	–	✓	–	–	–
Mono-h production at LHC	$\sigma(pp \to hSS)$	✓	–	✓	–	✓	✓
Mono-Z production at LHC	$\sigma(pp \to ZSS)$	–	✓	✓	✓	✓	✓
Mono-W production at LHC	$\sigma(pp \to W^+SS)$	–	✓	✓	–	✓	–

Table 7.1: Non-linear Higgs portal parameters affecting each of the observables considered. The standard Higgs-DM portal $b = 1$ and all c_i=0.

TeV run of the LHC. We also comment on the astrophysical signatures induced by the non-linear realisation, but defer a more detailed study of indirect detection in these models to future work. While our phenomenological study does not intend to exhaustively explore the parameter space of non-linear Higgs portals to DM, we do showcase all salient features of these scenarios and confront them with the standard Higgs portal. A list of the observables affected by each of the new terms in the DM Lagrangian[1] (7.6) is shown in Table 7.1.

The non-linear DM-Higgs portal from Eq. (7.6) is implemented in `FeynRules` [287] and interfaced to `MicrOMEGAs` [288] and `MadGraph5_aMC@NLO` [267] to compute the relevant observables. For the analysis of mono-X signatures at the LHC, we use in addition the 1-loop `FeynRules/NLOCT` implementation of gluon-initiated mono-X signatures via an s-channel mediator from [289], in order to capture the full momentum dependence in the production of mono-X signatures via gluon fusion. In all cases, the standard portal corresponds to the choice $b = 1$, $c_i = 0$, and we compare it with different non-linear portal setups in which one of the parameters of the set $\{b, c_i\}$ is varied at a time. This approach ensures a clear and conservative phenomenological comparison between the standard and the non-linear portal scenarios, allowing to single out the physical impact of each effective operator.

Finally, a comment on the range of validity of the analysis is in order: while the couplings studied do not depend on the actual value of Λ_{DM}, our results should only be taken as indicative when involving scales (m_S or p_T) above 1 TeV, as the heavy scale Λ_{DM} cannot

1 Our analysis has some overlap with the singlet scalar case of [283], which focuses on DM candidates that arise as pseudo-Goldstone bosons in specific composite Higgs models. While it is possible to identify a correspondence between our description and theirs for the case of $\mathcal{B}_1$ and $\mathcal{B}_2$: $\lambda_S \to \bar{\lambda}$, $c_1 \to d_4\,(v/f)^2$, $c_2 \to a_{d_1}\,(v/f)^2$, in the basis of [283] there is no equivalent of the operators $\mathcal{B}_3$, $\mathcal{B}_4$, $\mathcal{B}_5$. Moreover, the $(v/f)^2$ suppression in the analysis of [283] (where $f = 800$ GeV, $f = 2.5$ TeV are considered) leads to a scan over values $|a_{d_1}| \times (v/f)^2 < 0.1$, $|d_4| \times (v/f)^2 < 0.1$, corresponding to a small subset of the parameter space probed in this chapter.

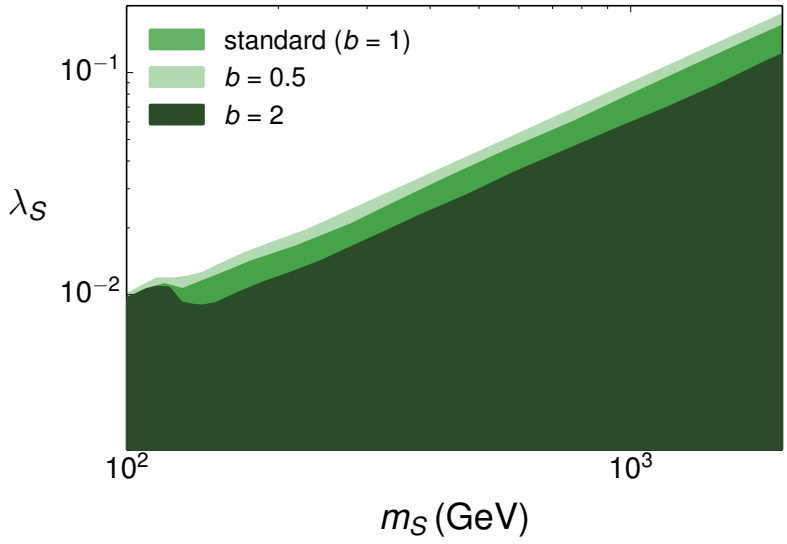

Figure 7.1: Regions excluded by the condition $\Omega_S h^2 \leqslant 0.12$ for DM masses $m_S \geqslant 100\,\text{GeV}$. The medium green region corresponds to the standard Higgs portal case $b = 1$, while the light/dark green regions (superimposed) correspond respectively to $b = 0.5$ and $b = 2$.

plausibly be much larger while still having an impact on the present and foreseen experimental sensitivities.

7.2.1 *Dark Matter relic density*

Assuming that the singlet scalar particle S is a thermal relic, its abundance Ω_S today is determined by the thermally averaged annihilation cross section into SM particles in the early Universe $(\sigma v)_{\text{ann}} = \sigma(SS \to XX)\, v$. For non-relativistic relics, this cross section can be expanded as

$$(\sigma v)_{\text{ann}} = \alpha_s + \alpha_p\, v^2 \tag{7.9}$$

where α_s is the (unsuppressed) s-wave contribution, and the next order in the expansion, α_p, corresponds to the p-wave contribution. Noticing that $\langle v \rangle^2 = 6/x_F$, with x_F given by the freeze-out temperature as $x_F = m_S/T_F \simeq 20$, the relic density is determined by

$$\Omega_S h^2 \simeq \frac{2.09 \times 10^8\,\text{GeV}^{-1}}{M_P \sqrt{g_{*s}(x_F)}\,(\alpha_s/x_F + 3\,\alpha_p/x_F^2)}\,, \tag{7.10}$$

with M_P being the Planck mass and $g_{*s}(x_F)$ the number of relativistic degrees of freedom at a temperature T_F. The s-wave contributions to the DM annihilation cross-section for the

different channels (the corresponding tree-level Feynman diagrams are shown in Appendix B.2) are given by

$$\alpha_s(S\,S \to f\bar{f}) = \frac{6\lambda_S^2}{\pi m_S^2}\frac{r_f^2(1-r_f^2)^{3/2}}{(r^2-4)^2}\left[\left(1+\frac{4c_2a_2}{r_v^2}\right)^2+\frac{c_4^2}{r_v^4}\frac{(r^2-4)^2}{1-r_f^2}\right], \tag{7.11}$$

$$\alpha_s(S\,S \to h\,h) = \frac{\lambda_S^2}{8\pi m_S^2}\frac{\sqrt{1-r^2}\,K_{h_0}^2}{(r^4-6r^2+8)^2}\left[1+\frac{4c_2a_2}{K_{h_0}}\frac{r^2}{r_v^2}\Big(4r_v^2(r^2-4)-3(r^2-2)+\right.$$
$$\left.+2c_2a_2r^2(r^2-4)+\frac{b_2}{a_2}\frac{r^4-6r^2+8}{r^2}\Big)\right]^2, \tag{7.12}$$

$$\alpha_s(S\,S \to Z\,Z) = \frac{\lambda_S^2}{8\pi m_S^2}\frac{\sqrt{1-r_Z^2}}{(r^2-4)^2}K_{Z_0}\left[1+\frac{4c_2a_2}{r_v^2}+(c_1+2c_3)\frac{r^2-4}{r_v^2}\right]^2, \tag{7.13}$$

$$\alpha_s(S\,S \to W^+W^-) = \frac{\lambda_S^2}{4\pi m_S^2}\frac{\sqrt{1-r_W^2}}{(r^2-4)^2}K_{W_0}\left[1+\frac{4c_2a_2}{r_v^2}+c_1\frac{r^2-4}{r_v^2}\right]^2, \tag{7.14}$$

$$\alpha_s(S\,S \to Z\,h) = \frac{\lambda_S^2}{512\pi m_S^2}\frac{\left[(r^2+r_Z^2-4)^2-4r^2r_Z^2\right]^{3/2}}{r_v^4}(2c_4+c_5a_5)^2, \tag{7.15}$$

with $r = m_h/m_S$, $r_f = m_f/m_S$, $r_{Z,W} = m_{Z,W}/m_S$, $r_v = \sqrt{\lambda_S}\,v/m_S$ and K_{h_0}, K_{Z_0}, K_{W_0} defined as

$$K_{h_0} = (b-3)r^4-6(b-1)r^2+8b+8\left(r^2-4\right)r_v^2, \tag{7.16}$$

$$K_{Z_0} = 4(1-r_Z^2)+3r_Z^4, \tag{7.17}$$

$$K_{W_0} = 4(1-r_W^2)+3r_W^4. \tag{7.18}$$

Each annihilation channel contains, in general, new non-linear pieces in addition to the standard contributions, including the decorrelations from b in the $SS \to hh$ channel. The sole exception to this behaviour is the annihilation channel $SS \to Zh$, which receives contributions from the CP-violating operators $\mathcal{B}_{4,5}$ and is absent in the standard case, inducing an s-wave leading term proportional to $c_{4,5}^2$.

In the following we discuss how non-linear contributions change the predictions for the Higgs portal. In a conservative approach, we require the abundance of S particles today not to exceed the total DM density measured by Planck [187], imposing $\Omega_S h^2 \leqslant \Omega_{DM} h^2 \simeq 0.12$ but not requiring S to account for the entire DM relic abundance[2]. Let us start by discussing the non-linear mismatch between the terms which are linear and quadratic in Higgs fields, parametrised by the coefficient b in Eq. (7.6). Values $b \neq 1$ modify the relative strength of the $SShh$ and SSh couplings *w.r.t.* the standard Higgs portal. This mismatch can be observed in the region $m_S > m_h$, where the annihilation into two Higgs bosons is important. As shown in Figure 7.1, for $b > 1$ the annihilation cross section into Higgses increases significantly, thus enlarging the allowed region of parameter space for the non-linear portal.

2 This constitutes another important difference with the analysis of Ref. [283], which requires the scalar singlet S to constitute all the DM. Although a direct comparison of our results with those of Ref. [283] is then difficult due to the different analysis methodology, we can state that our conclusions are compatible with theirs.

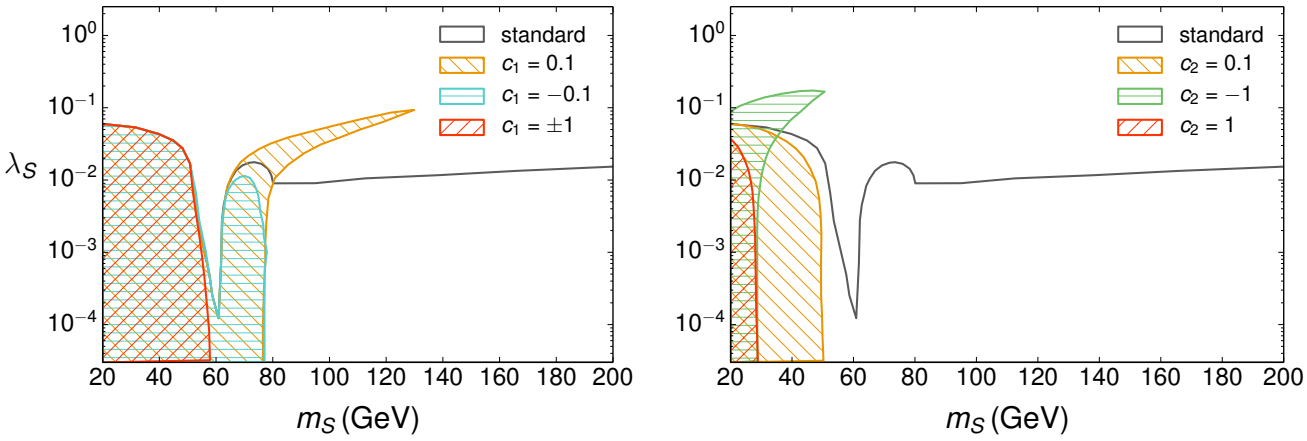

Figure 7.2: Regions in the (m_S, λ_S) plane excluded by the constraint $\Omega_S h^2 \leqslant 0.12$ from Planck [187], in presence of non-linear operators $\mathcal{B}_1$ (Left) and $\mathcal{B}_2$ (Right) with $c_i \neq 0$. The region below the black line is excluded for the standard Higgs portal. Left: excluded regions for $c_1 = 0.1$ (yellow), $c_1 = -0.1$ (light blue), $|c_1| = 1$ (red). Right: excluded regions for $c_2 = 0.1$ (yellow), $c_2 = 1$ (red), $c_2 = -1$ (green).

Consider now the impact of the non-linear $\mathcal{B}_i$ operators on σ_{ann}. Operators $\mathcal{B}_{1-5}$ affect DM annihilations into gauge bosons, Higgses and b-quarks, as shown in Appendix B.2. This modifies the relic density Ω_S both for large and small values of m_S. To illustrate these new effects, we compare in Figure 7.2 the parameter space excluded for the standard Higgs portal (our results for the standard Higgs portal scenario are in agreement with those of Refs. [225, 290–292]) and in the presence of the custodially-preserving and CP-even operators $\mathcal{B}_1$ and $\mathcal{B}_2$, with c_1, c_2 in the range $[-1, 1]$. It shows the drastic increase resulting in the parameter space for DM masses larger than tens of GeV, as compared with the allowed region for the standard portal above the black curve. For simplicity, in this figure the dependence on the Higgs field is fixed to be $\mathcal{F}_1(h) = \mathcal{F}_2(h) = (1 + h/v)^2$, corresponding to $a_1 = b_1 = a_2 = b_2 = 1$; we have checked that varying these values does not change noticeably the impact on the dark matter relic density $\Omega_S h^2$, as expected [3].

In the presence of $\mathcal{B}_1$, DM can directly interact with SM gauge bosons via the vertices SSZZ and SSW^+W^-. The new interactions induced by $\mathcal{B}_1$ do not modify the allowed parameter space for $m_S \lesssim 65$ GeV, where DM annihilates dominantly into $b\bar{b}$, while they have a strong impact on the DM annihilation process into two gauge bosons, which becomes important as m_S grows, as shown in Figure 7.2 (Left). For negative values of c_1, the positive interference with the linear amplitude (see the Feynman rules in Appendix B.1) increases the total annihilation cross-section everywhere and some of the points ruled out in the standard Higgs portal scenario become viable. On the other hand, if $c_1 > 0$ the interference is destructive and spurious cancellations may happen in regions of the parameter space that are allowed for standard Higgs portals, but become now excluded. As an example, the yellow "branch"

3 a_1 (b_1) parametrises vertices SSVVh (SSVVhh), with $V = Z, W^\pm$, whose tree-level contribution to the DM annihilation cross section is very much suppressed due to phase space considerations; a variation of a_2 can be reabsorbed in the normalisation of c_2; finally, b_2 enters the $SS \to hh$ cross-section for masses $m_S > m_h$, but its effect is only significant for unrealistically large values of b_2.

structure in Figure 7.2 (Left) for 60 GeV $\lesssim m_S \lesssim$ 130 GeV is traversed by a curve on which $\alpha_s(SS \to VV) = 0$ for $V = Z, W^{\pm}$.

The impact of the operator $\mathcal{B}_2$, shown in Figure 7.2 (Right), can be understood in an analogous way: the coefficient c_2 enters the couplings SShh and SSh, with the double effect of boosting the $SS \to hh$ process for $c_2 > 0$ and generating local cancellations when $c_2 < 0$ on one side, and also altering the annihilation $SS \to b\bar{b}$ through an s−channel Higgs, which significantly affects the annihilation cross section below $m_S \simeq m_h/2$.

The operator $\mathcal{B}_3$ has a similar phenomenology to that of $\mathcal{B}_1$, although restricted exclusively to DM annihilation into Z bosons (at tree level). However, the presence of $\mathcal{B}_3$ is tightly constrained by EW precision data (see the discussion at the end of Sect. 7.1). As the present bound on c_3 is already below the foreseen experimental sensitivities we will not further analyze it separately.

7.2.2 *Direct detection of Dark Matter*

DM interactions with nucleons are probed at direct detection experiments, which provide upper limits on the spin-independent and spin-dependent cross-sections. The scalar S interacts with fermions via the Higgs and, in the non-linear case, via $W^{\pm}$ and Z exchange. The most important constraints in our scenario come from the stronger spin-independent limits, which give an upper bound on the cross section σ_{SI} for scattering of S on nucleons. S may not be the only DM particle, but a member of a new DM sector, and in this case $\Omega_S < \Omega_{DM}$. When translating bounds on direct detection cross-section one can account for this fact by the following rescaling

$$\sigma_{SI}(S\,N \to S\,N)\,\frac{\Omega_S}{\Omega_{DM}} \leqslant \sigma_{exp}^{lim}\,, \tag{7.19}$$

where σ_{exp}^{lim} is the experimental upper limit on the DM-nucleon scattering cross-section. Here we consider the current most stringent 95% Confidence Level (C.L.) experimental limits by LUX [200], as well as the 95% C.L. projected sensitivity of XENON1T [201].

The white areas in Figure 7.3 and 7.4 summarise the DM parameter space allowed by Planck data and lying below the XENON1T direct detection sensitivity reach, for the standard and non-linear portals respectively. Specifically, the current and projected direct detection exclusion regions in the plane (m_S, λ_S) obtained with `MicrOMEGAs` are shown in Figure 7.3 for the standard Higgs portal scenario, and in Figure 7.4 in the presence of the non-linear operators $\mathcal{B}_1$ or $\mathcal{B}_2$ with a coefficient $c_i = 0.1$, fixing for simplicity $\mathcal{F}_1(h) = \mathcal{F}_2(h) = (1 + h/v)^2$ (see footnote 4). The following discussion will be restricted to these two cases, that exemplify quite exhaustively the main features introduced by non-linearity. For further scenarios corresponding to different choices of the coefficients c_1, c_2 in the range $[-1, 1]$ we defer the reader to Appendix B.3. We stress that, while neither $\mathcal{B}_1$ nor $\mathcal{B}_2$ affect the S-nucleon scattering cross-section to first approximation ($\mathcal{B}_1$ gives SSZZ and SSW^+W^- vertices which do not enter the scattering at tree level, while the contribution of $\mathcal{B}_2$ is proportional to the transferred momentum, and thus highly suppressed at such low energies), the impact of these two operators on the relic abundance Ω_S affects the direct detection exclusion regions, as shown in Figure 7.4. It is also worth noting that, despite providing an independent and complementary bound to that from the Planck Satellite, the direct detection results share some features

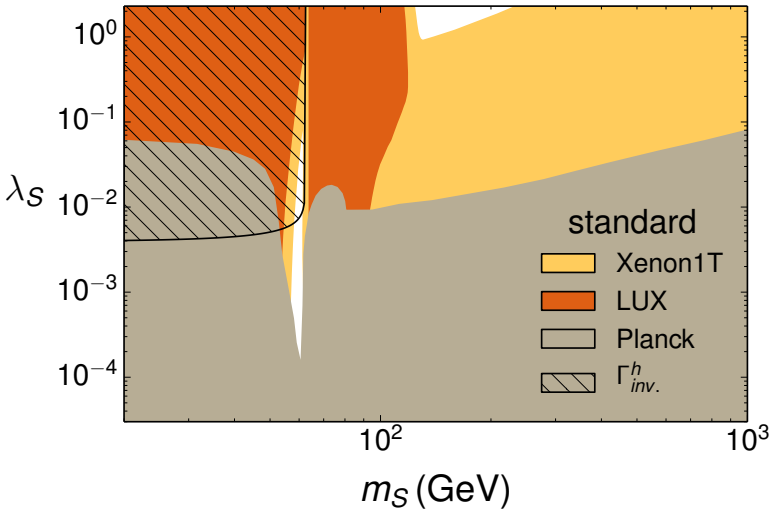

Figure 7.3: Standard Higgs portal (corresponding to the case $c_i \equiv 0$, $b = 1$) in the (m_S, λ_S) plane, for masses m_S up to 1 TeV. The grey region is excluded by current bounds from Planck [187]. The orange region is excluded by LUX [200], while the yellow area is currently allowed but within the reach of XENON1T [201]. The black-hatched region represents the region excluded from the invisible Higgs width data (see Sect. 7.2.3).

with those obtained imposing the constraint by Planck. As discussed in the previous section, the allowed portion of parameter space is generically enlarged for either $c_1 < 0$ or $c_2 > 0$ compared to the standard case (see Figure 7.4b), while for $c_1 > 0$ or $c_2 < 0$ the exclusion region may occasionally stretch further into an area that is allowed in the standard setup, as in Figure 7.4a.

Let us also comment on the impact of the operator $\mathcal{B}_4$ on DM-nucleon scattering: as shown in Appendix B.1, this operator induces an effective vertex SSZ that allows a diagram for the $qS \to qS$ process with a Z boson mediating in t-channel. However, the corresponding contribution to the squared amplitude is proportional to the Mandelstam variable, t:

$$|\mathcal{A}(qS \to qS)|^2 \sim c_4^2 \frac{g^4}{(c_{\theta_W})^4} \frac{m_q^2}{m_Z^4} t \tag{7.20}$$

with c_{θ_W} denoting the cosine of the Weinberg angle. This contribution then vanishes in the limit of zero transferred momentum $t \to 0$. As a result, the coefficient c_4 is not bounded by direct detection experiments, a conclusion that we have independently verified using `MadDM` [293].

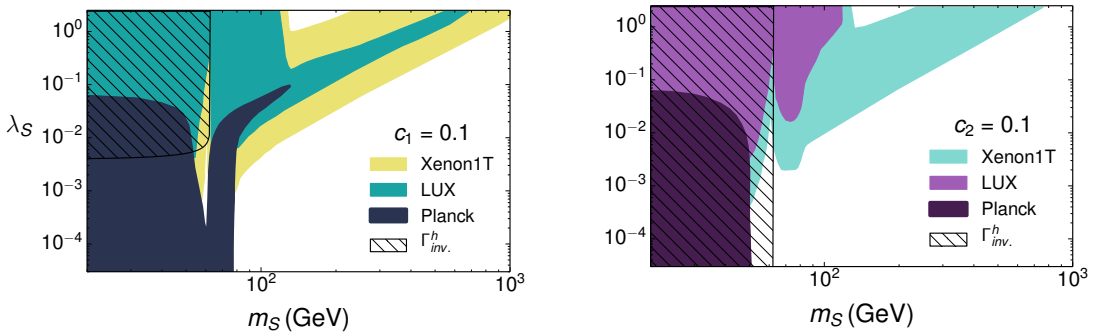

(a) $c_1 = 0.1$ **(b)** $c_2 = 0.1$

Figure 7.4: Non-linear Higgs portals in the (m_S, λ_S) plane, considering the non-linear operators $\mathcal{B}_1$ (Left) and $\mathcal{B}_2$ (Right) with $\mathcal{F}_i(h) = (1 + h/v)^2$ and $c_i = 0.1$. The darkest region is excluded by current bounds from Planck, the green/purple one is excluded by LUX, while the area in yellow/light blue is within the projected reach of XENON1T. The black hatched region represents the bound from the invisible Higgs width (see Sect. 7.2.3).

7.2.3 *Invisible Higgs decay width*

A very powerful probe of Higgs portal DM in the mass region $m_S < m_h/2$ is given by searches for an invisible decay width of the Higgs boson at the LHC. The decay $h \to SS$ is open for $m_S < m_h/2$, and contributes to the Higgs invisible width Γ_{inv} as

$$\Gamma_{inv} = \frac{\lambda_S^2 v^2}{2\pi m_h} \sqrt{1 - \frac{4m_S^2}{m_h^2}} \left(1 + \frac{c_2 a_2 m_h^2}{\lambda_S v^2}\right)^2 . \tag{7.21}$$

As is clear from Eq. (7.21), the presence of $\mathcal{B}_2$ gives a further contribution to Γ_{inv} *w.r.t.* the standard Higgs portal, such that, if $c_2 a_2 \neq 0$, then $\Gamma_{inv} > 0$ even for $\lambda_S \to 0$. Current experimental searches by ATLAS [222, 258] and CMS [259] constrain the $h \to$ *invisible* branching fraction, with the strongest limit requiring [222]

$$BR_{inv} = \frac{\Gamma_{inv}}{\Gamma_{inv} + \Gamma_{SM}} < 0.23 \quad (95\%\,CL) \tag{7.22}$$

where the SM width is $\Gamma_{SM} \simeq 4\,MeV$. Conveniently setting the parameter $a_2 = 1$ (as it can always be reabsorbed in the normalization of c_2), we present the exclusion region obtained from Eqs. (7.21) and (7.22) as a black hatched area in Figures 7.3 and 7.4a for $c_2 = 0$, and Figure 7.4b for $c_2 = 0.1$. For Figure 7.4a the limit coincides with the one derived for the standard Higgs portal plotted also in Figure 7.3 (see e.g. [225, 290–292]), while Figure 7.4b illustrates the effect of $c_2 \neq 0$: even for small values of this coefficient, the bound becomes very stringent, with practically all the region $m_S < m_h/2$ being excluded.

It is important to stress that, even though the non-linear operator $\mathcal{B}_4$ generates a SSZ vertex, the Z invisible width is not affected by it. The would-be contribution from $\mathcal{B}_4$ is CP-odd and also vanishes whenever the Z is on-shell.

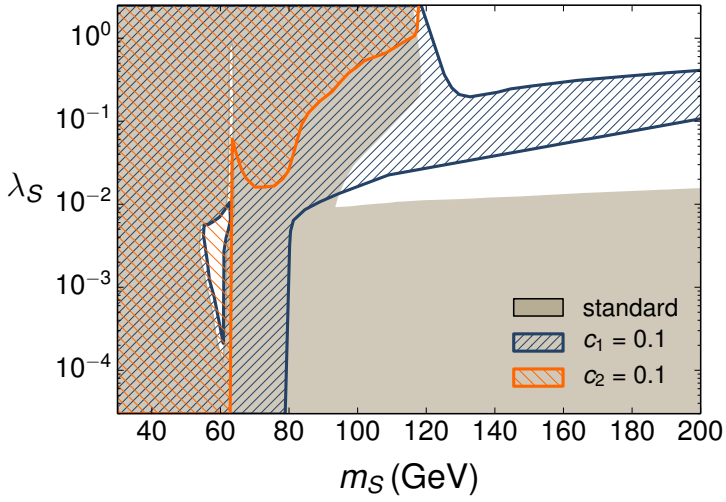

Figure 7.5: Current excluded region in the (m_S, λ_S) plane for the standard Higgs portal (grey) versus the non-linear one for $c_1 = 0.1$ (blue) and $c_2 = 0.1$ (orange), from DM relic abundance, direct detection and invisible decay width of the Higgs.

The impact of non-linear contributions on the parameter space of Higgs portals, combining the information from the DM relic density, direct detection experiments and searches for invisible decay modes of the Higgs boson is exemplified in Figure 7.5, which shows the comparison between the combined excluded region for the standard Higgs portal (grey region) and the combined excluded regions in the presence of $\mathcal{B}_1$ with $c_1 = 0.1$ (hatched-blue region) and in the presence of $\mathcal{B}_2$ with $c_2 = 0.1$ (hatched-orange region).

7.2.4 *Dark Matter at the LHC: Mono-X searches*

As already highlighted in the previous section, the LHC (and collider experiments in general) constitutes a natural place to search for DM interactions with the SM, in particular if such interactions involve the EW sector of the theory. LHC probes of DM provide an independent test of the results from low-energy and astrophysical experiments, while being able to directly explore a new energy regime.

A key probe of DM production at colliders are "mono-X" signatures, *i.e.* the associated production of DM particles with a visible object X, which is seen to recoil against a large amount of missing transverse energy $\not{E}_T$. These signatures are in principle sensitive to relatively large DM masses, but for the standard Higgs portal scenario the relevant cross sections at the LHC drop very quickly for $m_S > m_h/2$, making it challenging to extract information on the DM properties from these searches (see *e.g.* [221]). As we show below, the presence of non-linear Higgs portal interactions $\mathcal{B}_{1-5}$ has a dramatic impact on the LHC potential for probing such mono-X signatures.

We focus our analysis on mono-h, mono-Z and mono-W signatures at the LHC, and present a detailed comparison of the standard and non-linear Higgs portal DM scenarios

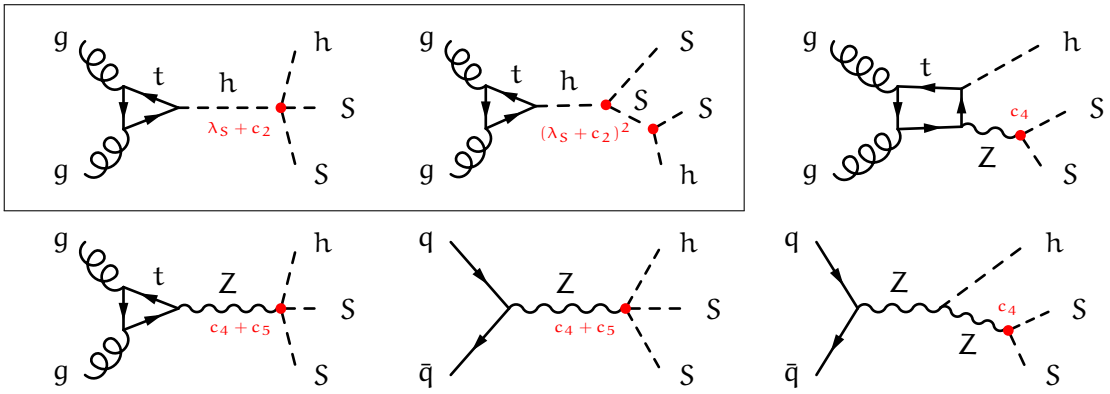

Figure 7.6: Sample of the main Feynman diagrams contributing to mono-h production. In the standard Higgs case only those inside the frame are present: the process is entirely gg-initiated, with contributions proportional to λ_S and to λ_S^2. In the non-linear scenario all the diagrams contribute: both gg- and $\bar{q}q$-initiated processes are included. The proportionality of each diagram to the non-linear parameters is indicated in the figure (overall factors and numerical coefficients are not specified).

in this context. We stress that for the case of mono-h, Z signatures, both $\bar{q}q$ and gluon (gg) -initiated processes are possible. The latter are characterised by loop-induced DM production processes, which we compute using the `FeynRules/NLOCT` framework [294] interfaced to `MadGraph5_aMC@NLO` and `MadLoop` [295, 296], to ensure that the momentum dependence of the loop is accurately described. This particular aspect is crucial for a meaningful comparison between the standard and non-linear Higgs portal scenarios.

7.2.4.1 *Mono-h signatures*

Mono-Higgs searches [265, 297–299] have been proposed recently as a probe of the DM interactions with the SM, particularly in the context of Higgs portal scenarios. This proposal has led the ATLAS experiment to perform a search for mono-h signatures in the $\not{E}_T + \gamma\gamma$ [300] and $\not{E}_T + b\bar{b}$ [301] final states with 20.3 fb^{-1} of LHC 8 TeV data. While the latter channel is not conclusive for the case of scalar Dark Matter, the former yields a 95% C.L. limit on the mono-h fiducial cross section $\sigma^{\gamma\gamma}_{\text{mono-h}} \leqslant 0.7\,\text{fb}$ (with $h \to \gamma\gamma$) after the selection $\not{E}_T > 90$ GeV.

For the standard Higgs portal, mono-h processes are gg-initiated and the amplitude receives contributions from Feynman diagrams scaling as $\sim \lambda_S$ and $\sim \lambda_S^2$, as depicted in Figure 7.6 (within the frame), the latter providing a significant enhancement in the cross section when $\lambda_S \sim 1$. We note however that for $\lambda_S = 1$, satisfying the direct detection bound from LUX requires $m_S > 127$ GeV (see Figure 7.3), and for that range of masses the mono-h cross section gets suppressed due to the intermediate off-shell Higgs state and the steep fall of the gluon PDF at high $\sqrt{\hat{s}}$. Moreover, limits from the invisible decay width of the Higgs require $\lambda_S \lesssim 0.007$ for $m_S < m_h/2$ in this scenario (see Figure 7.3). Overall, the cross section for mono-h in the standard scalar DM Higgs portal is predicted to be very small.

The presence of non-linear Higgs-DM interactions may significantly change the previous picture, as the suppression factors for the standard scenario can be overcome by the appearance of new production channels – *e.g.* direct couplings of DM to Z-bosons which yield

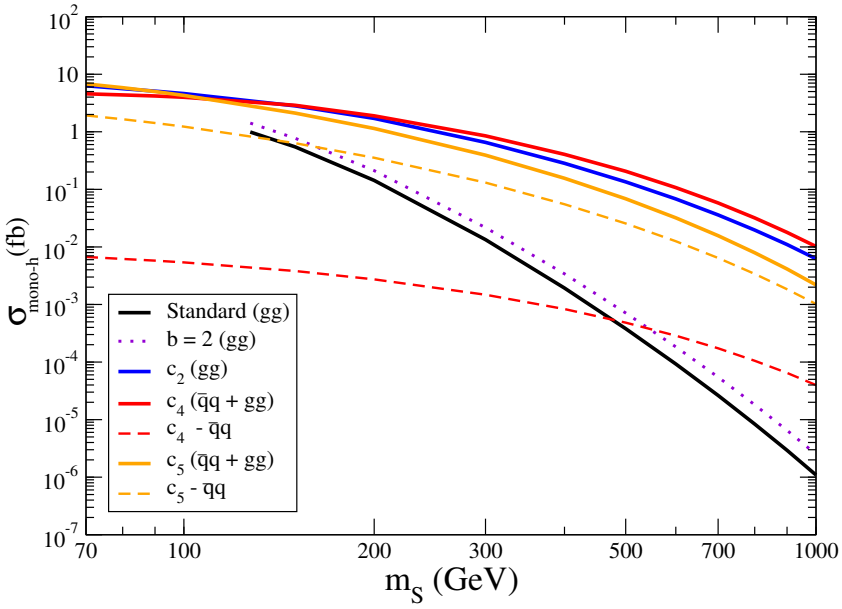

Figure 7.7: Cross section of the process $pp \to h\,SS$ at $\sqrt{s} = 13$ TeV as a function of m_S for the standard Higgs portal with $\lambda_S = 1$ (solid-black line) and different non-linear setups. The dotted-purple line corresponds to the case $\lambda_S = 1$, $b = 2$, $c_i = 0$. The solid-blue, solid-red and solid-orange lines correspond to $\lambda_S = 0$ and $c_2 = 1$, $c_4 = 1$, $c_5 = 1$ respectively. For the latter two cases, the dashed-red and dashed-orange lines show the $\bar{q}q$-initiated contribution from $\mathcal{B}_4$ and $\mathcal{B}_5$. The low mass end-point for the solid-black and dotted-purple lines, given by $m_S = 127$ GeV, corresponds to the mass bound for the standard Higgs portal scenario for $\lambda_S = 1$ (see Figure 7.3).

a $\bar{q}q$-initiated mono-h contribution (case of $\mathcal{B}_4$ and $\mathcal{B}_5$) – and/or by the momentum dependence of the S-h, S-Z and S-h-Z interactions (case of $\mathcal{B}_2$, $\mathcal{B}_4$ and $\mathcal{B}_5$). A sample of the Feynman diagrams contributing to mono-h in this case is shown in Figure 7.6. For $\mathcal{B}_2$, mono-h is gg-initiated, and the amplitude receives contributions from Feynman diagrams scaling as $\sim c_2$ and $\sim c_2^2$. $\mathcal{B}_4$ and $\mathcal{B}_5$ yield gg- and $\bar{q}q$-initiated contributions to the mono-h process, both scaling linearly with $c_{4,5}$. In Figure 7.7 we illustrate the behavior of the cross section $\sigma_{\text{mono}-h} = \sigma(pp \to h\,SS)$ as a function of the DM mass m_S at a centre of mass (*c.o.m.*) energy of $\sqrt{s} = 13$ TeV, for each of the possible non-linear operators $\mathcal{B}_i$ with $c_i = 1$ and $\lambda_S = 0$ compared to the standard Higgs portal with $\lambda_S = 1$ (solid-black line). Let us first note that a non-linear value $b > 1$ (dotted-purple line) enhances several processes $\sim \lambda_S$ *w.r.t.* the standard Higgs portal scenario (which modifies the interference between $\sim \lambda_S$ and $\sim \lambda_S^2$ terms) and yields a somewhat larger mono-h cross section. More importantly, Figure 7.7 shows that the presence of either of $\mathcal{B}_2$ (solid-blue line), $\mathcal{B}_4$ (solid-red line), $\mathcal{B}_5$ (solid-orange line) may lead to a large enhancement in the cross section for DM masses $m_S > 100$ GeV, potentially reaching enhancements of order $10^4 \times c_i^2$ for $m_S \gg v$ (we recall that $\lambda_S = 1$ for the standard Higgs portal scenario is only allowed for $m_S > 127$ GeV, and the same bound applies roughly to the scenario $b \neq 1$, as this only has a significant impact on the value of Ω_S for $m_S > m_h$, as shown in Figure 7.1).

Besides the potentially large increase in the mono-h cross section, in the presence of $\mathcal{B}_{2,4,5}$ the differential distribution of the Higgs boson transverse momentum P_T^h is shifted towards

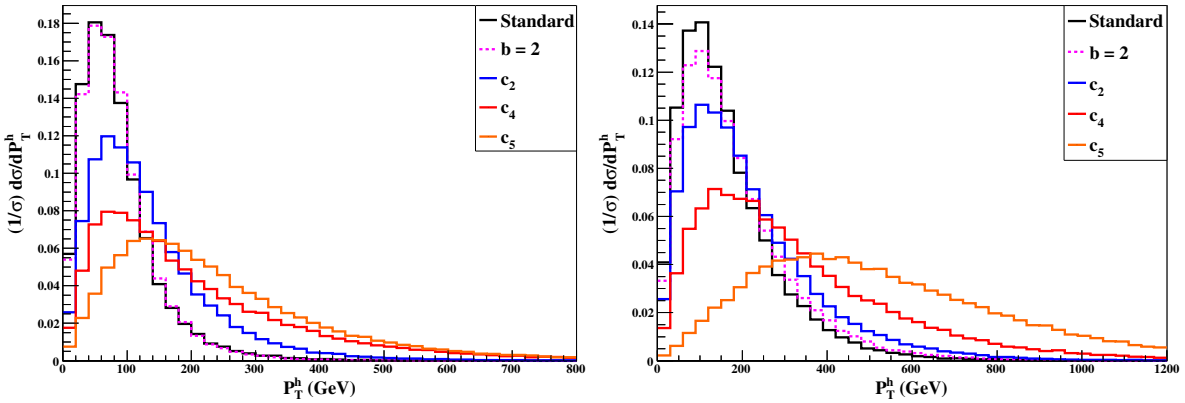

Figure 7.8: Normalised differential P_T^h distribution for the process $pp \to h\,SS$ in the standard Higgs portal with $\lambda_S = 1$ (solid-black line), non-linear Higgs portal with $b = 2$ (dashed-purple line), $\mathcal{B}_2$ with $c_2 = 1$ (solid-blue line), $\mathcal{B}_4$ (solid-red line) and $\mathcal{B}_5$ (solid-orange line), for $m_S = 100$ GeV (Left) and $m_S = 500$ GeV (Right).

larger values, as shown in Figure 7.8 for $m_S = 100$ GeV (Left) and $m_S = 500$ GeV (Right). This much harder mono-h P_T^h spectrum, particularly for the case of $\mathcal{B}_5$, is a landmark signature of non-linear Higgs portals, which also allows for a much better signal extraction from the SM background.

Finally, let us stress that given the 13 TeV results from Figure 7.7 the 8 TeV mono-Higgs searches at the LHC do not put any meaningful constraint on the parameter space under discussion here, since if we assume a SM value for $\text{Br}(h \to \gamma\gamma) \simeq 2 \cdot 10^{-3}$ the ATLAS 95% C.L. limit [300] on the fiducial mono-h cross section is $\sigma_{\text{mono-h}} \leqslant 0.35\,\text{pb}$, two orders of magnitude larger than the (13 TeV) cross sections showed in Figure 7.7.

7.2.4.2 *Mono-Z and mono-W searches*

As a last category of DM observables, we discuss the searches for mono-$W^\pm$ [261] and mono-Z [262–264, 266] signatures at the LHC in the context of Higgs portal scenarios. We first focus on the process $pp \to ZSS$, which receives non-linear contributions from all the effective operators $\mathcal{B}_i$ in Eq. (7.5). Both for the standard Higgs portal scenario and in the presence of $\mathcal{B}_1$, $\mathcal{B}_2$, $\mathcal{B}_3$, $\mathcal{B}_4$ these contributions are both gg- and $\bar{q}q$-initiated, while $\mathcal{B}_5$ only gives rise to gg-initiated contributions to mono-Z. We also note that $\mathcal{B}_1$ and $\mathcal{B}_3$ give exactly the same contribution to the mono-Z process if $c_1 = 2\,c_3$ - see Appendix B.1, and furthermore $c_3 \lesssim 0.1$ is required from EW precision data (recall the discussion at the end of Sect. 7.1), so in the following we do not explicitly discuss the impact of $\mathcal{B}_3$ on mono-Z searches.

In Figure 7.9 (Left) we show the LHC cross sections $\sigma(pp \to ZSS)$ as a function of m_S for a *c.o.m.* energy $\sqrt{s} = 13\,\text{TeV}$. The solid-black line corresponds to the standard Higgs portal scenario with $\lambda_S = 1$ (with $\sigma^{\text{standard}}_{\text{mono}-Z} \sim \lambda_S^2$), which decreases quite fast for increasing m_S. As in the mono-h case (see Sect. 7.2.4.1), the solid-green, solid-blue, solid-red and solid-orange curves respectively correspond to non-linear Higgs portal scenarios with $\lambda_S = 0$ and $\mathcal{B}_1$, $\mathcal{B}_2$, $\mathcal{B}_4$ or $\mathcal{B}_5$ being present with $c_i = 1$. In all the non-linear setups, $\sigma^i_{\text{mono-Z}} \sim c_i^2$, the only exception being $\mathcal{B}_4$, which contributes with diagrams scaling both as c_4 and as c_4^2. As can be

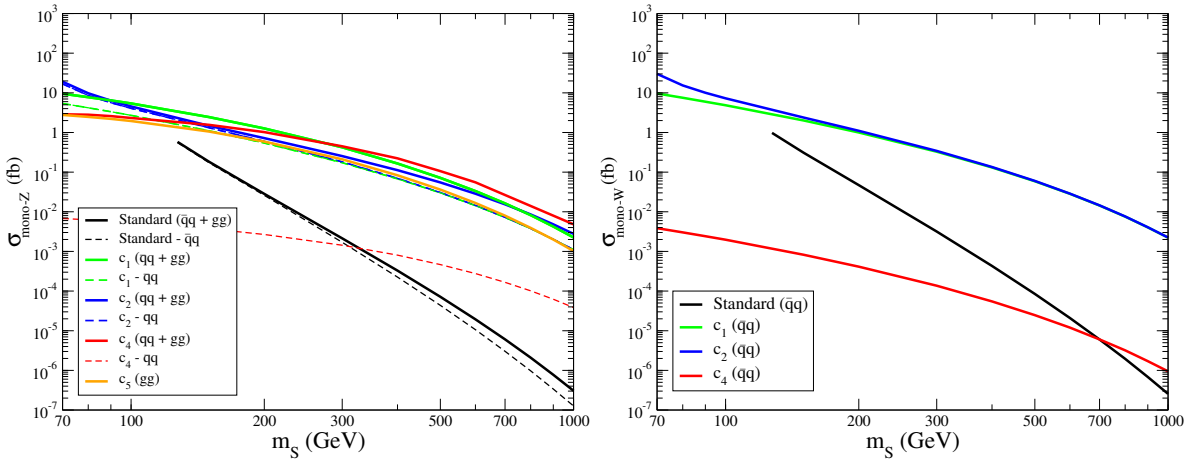

Figure 7.9: Cross section of the process $pp \to Z\,SS$ (Left) and $pp \to W^{\pm}\,SS$ (Right) at $\sqrt{s} = 13\,\text{TeV}$ as a function of m_S for the standard Higgs portal with $\lambda_S = 1$ (solid-black line) and different non-linear setups. The solid-green, solid-blue, solid-red and solid-orange lines correspond to $\lambda_S = 0$ and $c_1 = 1$, $c_2 = 1$, $c_4 = 1$, $c_5 = 1$ respectively. In the Left Figure, the dashed-black, dashed-green, dashed-blue and dashed-red lines respectively show the $\bar{q}q$-initiated contribution to the process $pp \to Z\,SS$ for the standard, $\mathcal{B}_1$, $\mathcal{B}_2$ and $\mathcal{B}_4$ scenarios.

seen from Figure 7.9, these non-linear contributions yield a significantly larger mono-Z cross section as compared to the standard Higgs portal for $m_S \simeq 100$ GeV, leading to very large enhancements for $m_S \gg v$. As with the mono-h signature, the non-linear operators $\mathcal{B}_{1,2,4,5}$ also affect the differential distribution of the Z-boson transverse momentum P_T^Z, yielding a harder mono-Z P_T^Z spectrum, as can be seen from Figure 7.10. This effect is more important for DM masses in the range $100 - 300$ GeV, while for $m_S \gg v$ the standard and non-linear P_T^Z spectra become very similar. Mono-Z signatures therefore constitute a promising probe of non-linear Higgs portals at the 13 TeV run of the LHC for intermediate DM masses ($m_h/2 < m_S \ll 1$ TeV) and sizable values of the coefficients $c_i \lesssim 1$. On the other hand, current 8 TeV mono-Z searches at the LHC are only able to constrain values $c_i \gg 1$: the ATLAS analysis [302], using 20.3 fb^{-1} of LHC 8 TeV data, yields 95% C.L. limits on the mono-Z ($Z \to \ell^+\ell^-$) fiducial cross section $\sigma^{\ell\ell}_{\text{mono-Z}} \leqslant 2.7\,\text{fb}$, 0.57 fb, 0.27 fb, 0.26 fb after a corresponding selection $\not{E}_T > 150$ GeV, 250 GeV, 350 GeV, 450 GeV. Such limits lie well above the (13 TeV) curves in Figure 7.9 (Left), and moreover for fairly light DM ($m_S \lesssim 100$ GeV) the selection criteria from the ATLAS search [302] will discard most of the DM signal, as shown in Figure 7.10.

Turning now to mono-$W^{\pm}$ signatures, these are affected by the non-linear operators $\mathcal{B}_1$, $\mathcal{B}_2$ and $\mathcal{B}_4$. Both for these operators and for the standard Higgs portal, the contributions to mono-$W^{\pm}$ are all $\bar{q}q$-initiated, which as we will see makes an important difference *w.r.t.* the case of mono-Z signatures. In Figure 7.9 (Right) we show the cross section $\sigma(pp \to W^{\pm}SS)$ as a function of m_S for the standard and non-linear Higgs portal scenarios (using the same criteria and colour convention as for the mono-Z analysis). In the presence of $\mathcal{B}_1$ and/or $\mathcal{B}_2$ a significant enhancement in the cross section can occur for large values of m_S, similar to the case of mono-Z and mono-h signatures. However, for the operator $\mathcal{B}_4$ mono-$W^{\pm}$ signatures are very suppressed, as the dominant gg-initiated contribution (compare the solid- and dashed-red lines in Figure 7.9 (Left) for mono-Z) is absent in this case. We find

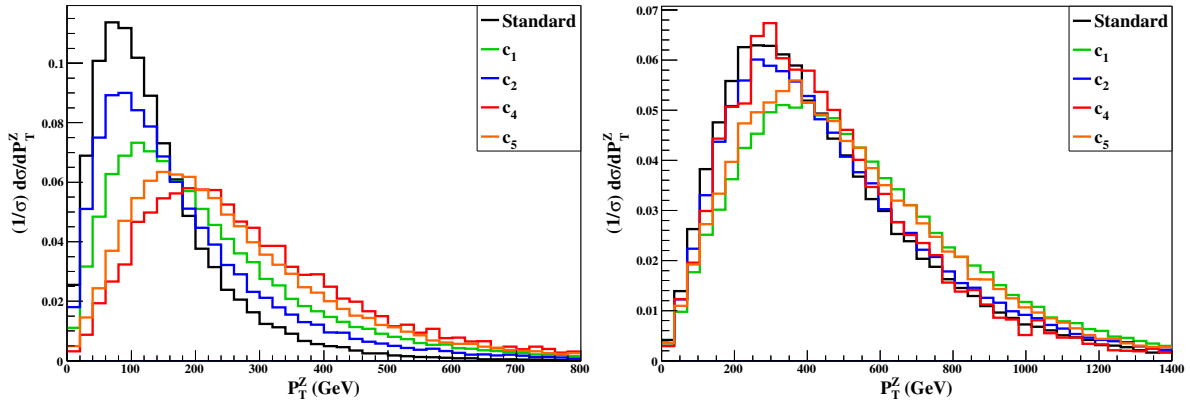

Figure 7.10: Normalised differential P_T^Z distribution for the process $pp \to Z\,SS$ in the standard Higgs portal with $\lambda_S = 1$ (black line), and for non-linear Higgs portal operators $\mathcal{B}_1$ (green line), $\mathcal{B}_2$ (blue line), $\mathcal{B}_4$ (red line) and $\mathcal{B}_5$ (orange line), for $m_S = 100$ GeV (Left) and $m_S = 500$ GeV (Right).

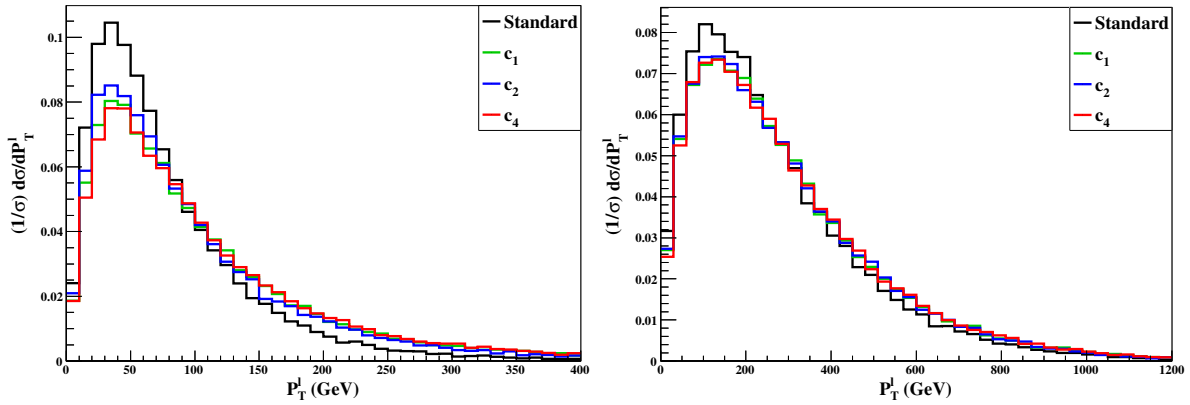

Figure 7.11: Normalised differential P_T^ℓ distribution for the process $pp \to W^\pm SS$ ($W^\pm \to \ell^\pm \nu_\ell$) in the standard Higgs portal (black line), and for non-linear Higgs portal operators $\mathcal{B}_1$ (green line), $\mathcal{B}_2$ (blue line) and $\mathcal{B}_4$ (red line), for $m_S = 100$ GeV (Left) and $m_S = 500$ GeV (Right).

that, contrary to the situation encountered in the mono-h and mono-Z analyses above, for mono-$W^\pm$ signatures with $W^\pm \to \ell^\pm \nu_\ell$ the P_T^ℓ of the final state lepton has a very similar distribution for the standard and non-linear Higgs portal scenarios, both for low and high DM masses, as seen in Figure 7.11.

Finally, we discuss the possibility of using the ratio $R_{WZ} \equiv \sigma(pp \to ZSS)/\sigma(pp \to W^\pm SS)$ as a probe of non-linear Higgs portal scenarios, as shown in Figure 7.12 (Left) as a function of m_S. Remarkably, the impact of each non-linear operator on this ratio is determined only by its gauge and Lorentz structure, independently of the value of the coefficient[4] c_i. Analogously, the dependence on λ_s factors out in the standard case. While the effect of the operator $\mathcal{B}_2$ on this observable cannot be effectively disentangled from that of a standard Higgs portal (as can be seen by comparing the black and blue curves in Figure 7.12 (Left)), the ratio R_{WZ}

4 The line for $\mathcal{B}_4$ is an exception, due to the fact that the amplitude for mono-Z receives contributions scaling both as c_4 and as c_4^2, so that the coefficient does not fact out in R_{WZ}. However, this does not impair the interpretation of the plot in Fig. 7.12.

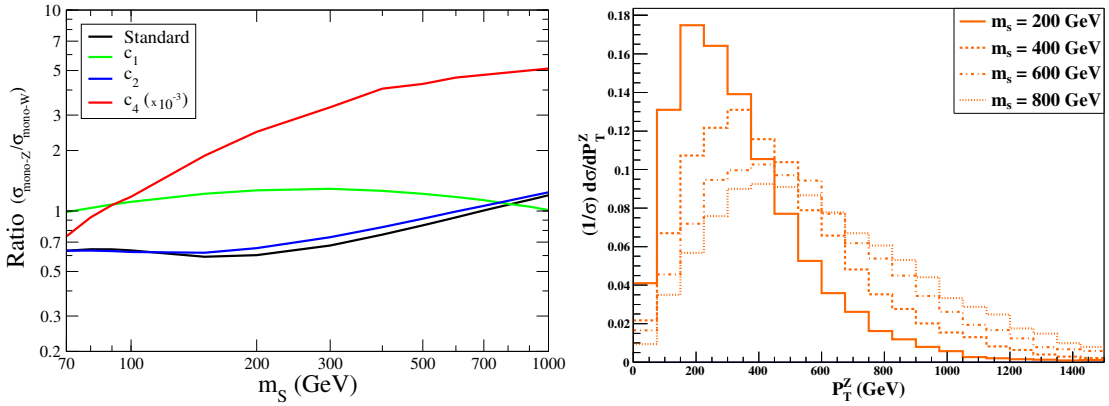

Figure 7.12: Left: Cross section ratio $R_{WZ} \equiv \sigma(pp \to ZSS)/\sigma(pp \to W^{\pm}SS)$ at $\sqrt{s} = 13\,\text{TeV}$ as a function of m_S in the standard Higgs portal scenario (black line) and for the non-linear operators $\mathcal{B}_1$ (green-line), $\mathcal{B}_2$ (blue-line) and $\mathcal{B}_4$ (red-line), the latter ratio having been multiplied by 10^{-3} to be shown in the Figure. Right: Normalised differential P_T^Z distributions for the process $pp \to Z\,SS$ for $\mathcal{B}_5$ and DM masses $m_S = 200$ GeV (solid), 400 GeV (dashed), 600 GeV (dash-dotted) and 800 GeV (dotted).

is a very powerful non-linear discriminator for the cases of $\mathcal{B}_1$ and $\mathcal{B}_4$ (also trivially for $\mathcal{B}_5$, for which the mono-$W^{\pm}$ process is absent and $R_{WZ} \equiv \infty$), corresponding respectively to the green and red curves in Figure 7.12 (Left). Moreover, recalling that the operator $\mathcal{B}_3$ enters the mono-Z process with the corresponding coefficient in the combination $(c_1 + 2c_3)$ (see Appendix B.1), while it does not enter the mono-$W^{\pm}$ process, the green curve in Figure 7.12 (Left) will get rescaled by $(c_1 + 2c_3)^2/c_1^2$ in the presence of $\mathcal{B}_3$. Thus, for $\mathrm{sign}(c_1) = \mathrm{sign}(c_3)$, the green curve actually represents a lower bound on the contribution of $\mathcal{B}_1$ and $\mathcal{B}_3$ to the ratio R_{WZ}.

Importantly, it is in principle possible to infer the DM mass from the mono-Z/mono-$W^{\pm}$ processes through the differential information on the P_T^V ($V = W^{\pm}, Z$) as shown explicitly in Figure 7.12 (right) for the case of $\mathcal{B}_5$ (alternatively, the $\not{E}_T$ distribution may be used). Taking this into account, the hypothetical observation of mono-Z and mono-W signals would allow to extract at the same time a measurement of R_{WZ} and of m_S, *i.e.* to identify a unique point (surrounded by a finite error region) in the parameter space of figure 7.12 (Left). Naively, the further this point lies away from the black line, the more disfavored the standard portal scenario will be. Employing this technique in a more thorough analysis, which would keep all the relevant uncertainties into account, it would be possible to quantify a confidence level for the exclusion of the standard portal. Therefore, the ratio R_{WZ} can be an efficient probe of the nature of the DM portal to the SM. Notice that the non-linear scenario cannot be ruled out by this kind of study, since any point in the (m_S, R_{WZ}) space corresponds to a whole set of combinations of the coefficients c_{1-5}.

7.2.5 *A comment on indirect detection of Dark Matter*

DM annihilation into charged particles (or states further decaying into charged particles), whether $W\pm$ or charged fermions, would result in significant fluxes of gamma-rays, which

can be constrained by astrophysical observations, *e.g.* from the Fermi-LAT Space Telescope. Rather than performing a detailed study of the indirect detection signatures of non-linear Higgs portal DM scenarios (which we defer for the future), we just discuss briefly the impact of such indirect limits on their parameter space, focusing on DM annihilation into W^+W^- and $b\bar{b}$, which receive contributions from $\mathcal{B}_{1,2,4}$ and $\mathcal{B}_{2,4}$ respectively (see Appendix B.2). We consider the limits on such DM annihilation channels from measurements of the gamma-ray flux from the Milky Way galactic center [303], which have been shown to be competitive [304] with those derived from other astrophysical sources, such as dwarf galaxies. Using the limits from [304] on the DM annihilation cross-section $(\sigma v)_{ann}$ into W^+W^- and $b\bar{b}$, given respectively by Eqs. (7.14) and (7.11), we can potentially derive constraints on λ_S and/or c_i as a function of the DM mass m_S. After the appropriate rescaling of the indirect DM signal by $(\Omega_S/\Omega_{DM})^2$, we find that the current limits from [304] do not provide a meaningful constraint on the parameter space under consideration.

7.3 CONNECTION WITH THE LINEAR EFT EXPANSION

In this section the connection between the non-linear scenario analysed in the previous sections and the linear context is discussed. Eq. (7.1) accounts for the only possible renormalisable coupling between the elementary SM Higgs particle and a singlet scalar DM particle (assuming Z_2 symmetry). Nevertheless, scenarios for BSM electroweak physics can - and often do - correspond to linear realisations of the EWSB mechanism, typical of perturbative completions. A model-independent parametrisation of the new physics for the SM degrees of freedom is then given by higher-dimension operators of mass dimension $\geqslant 4$, suppressed by inverse powers of the BSM physics scale $\Lambda \gg v$: a linear operator expansion, in which the h participates via Φ insertions and thus through a $(v+h)$ functional dependence. The question then arises of the extent up to which the signals determined above for the non-linear DM portal could be mimicked by effective couplings of the linear expansion, that is by Eq. (7.1) plus a tower of operators of mass dimension 6, 8 etc.

$d=6$	$d=8$
$b \longrightarrow \mathcal{O}_b \equiv (\Phi^\dagger\Phi)^2 S^2$	$\mathcal{B}_3 \longrightarrow \mathcal{O}_3 \equiv (\Phi^\dagger \overleftrightarrow{D_\mu} \Phi)(\Phi^\dagger \overleftrightarrow{D^\mu} \Phi) S^2$
$\mathcal{B}_1 \longrightarrow \mathcal{O}_1 \equiv D_\mu\Phi^\dagger D^\mu\Phi\, S^2$	$\mathcal{B}_5 \longrightarrow \mathcal{O}_5 \equiv (\Phi^\dagger \overleftrightarrow{D_\mu} \Phi) D^\mu \left(\Phi^\dagger\Phi\right) S^2$
$\mathcal{B}_2 \longrightarrow \mathcal{O}_2 \equiv \Box \left(\Phi^\dagger\Phi\right) S^2$	
$\mathcal{B}_4 \longrightarrow \mathcal{O}_4 \equiv (\Phi^\dagger \overleftrightarrow{D_\mu} \Phi) D^\mu S^2$	

Table 7.2: Linear siblings of the non-linear operators $\mathcal{B}_i$ and of the deviations of the standard Higgs portal coupling.

First of all, the couplings of the non-linear Higgs portal, that is, the deviations from the standard portal given by $b \neq 1$ in Eq. (7.2) as well as the operators $\mathcal{B}_1 - \mathcal{B}_5$, appear among the dominant couplings of that expansion, while their linear counterparts are not found at the renormalisable level but only at higher orders in the expansion. Indeed, the siblings

(lowest dimension operators in the linear expansion which contain at least the same physical couplings) of $\mathcal{B}_1$, $\mathcal{B}_2$, $\mathcal{B}_4$ and the linear operator inducing $b \neq 1$ are linear operators of mass dimension $d = 6$, while the couplings $\mathcal{B}_3$ and $\mathcal{B}_5$ would first appear as $d = 8$ linear operators. The explicit definition of the linear siblings can be found in Table 7.2, providing a one-to-one mapping between the linear and the non-linear operators.

The complete $d = 6$ bosonic linear portal describing the interaction with at most two S fields includes, in addition to $\mathcal{O}_1$, $\mathcal{O}_2$, $\mathcal{O}_4$ and $\mathcal{O}_b$ above, 9 four-derivative couplings [5]:

$$\begin{aligned} &g^2 S^2 W_{\mu\nu} W^{\mu\nu} && g^2 S^2 W_{\mu\nu} \tilde{W}^{\mu\nu} \\ &g'^2 S^2 B_{\mu\nu} B^{\mu\nu} && g'^2 S^2 B_{\mu\nu} \tilde{B}^{\mu\nu} \\ &g g' S^2 B_{\mu\nu} W^{\mu\nu} && g g' S^2 B_{\mu\nu} \tilde{W}^{\mu\nu} \\ &g_s^2 S^2 G_{\mu\nu} G^{\mu\nu} && g_s^2 S^2 G_{\mu\nu} \tilde{G}^{\mu\nu} \\ &\Box S \Box S \end{aligned} \tag{7.23}$$

Being four-derivative couplings, these operators would correspond to sub-dominant operators in the non-linear expansion considered here, which includes at most two-derivative operators; they will thus be disregarded in what follows.

As in the case of non-linear expansion, in order to define a complete basis, fermionic structures should be also considered in addition to those in Eq. (7.8):

$$\bar{Q}_{L_i} \Phi \, d_{R_j} S^2 \,, \qquad \bar{Q}_{L_i} \tilde{\Phi} \, u_{R_j} S^2 \,, \qquad \bar{L}_{L_i} \Phi \, e_{R_j} S^2 \,. \tag{7.24}$$

Again, two flavour blind combinations of the two types of chiral fermion structures (Eq. (7.8) and (7.24)) may be related to the bosonic operators $\mathcal{O}_2$ and $\mathcal{O}_4$, respectively. In order to avoid redundancies either the two combination or the two latter bosonic operators should then be disregarded.

The sector of the linear effective Lagrangian containing the siblings of interest for the comparison is then given by

$$\mathcal{L}_S^{\text{linear portal}} \supset \sum_{i=b,1,2,4} \frac{c_i^L}{\Lambda_{DM}^2} \mathcal{O}_i + \sum_{i=3,5} \frac{c_i^L}{\Lambda_{DM}^4} \mathcal{O}_i \,, \tag{7.25}$$

where c_i^L denote the operator coefficients.

The rationale of the operator expansions calls for their dimensionless parameters to be naturally $\mathcal{O}(1)$, in which case the answer to the question formulated above is obvious: while $\mathcal{B}_1 - \mathcal{B}_5$ may be expected to contribute with similar strength to the couplings in Eq. (7.2), the $d \geqslant 6$ operators of the linear expansion should be suppressed by powers of $v^2/\Lambda_{DM}^2 \ll 1$: in other words, the dominant, leading order effects of the linear expansion are expected to reduce exclusively to those of the standard portal in Eq. (7.1), in contrast to the plethora of phenomenological consequences of the leading-order non-linear portal.

It could be argued, though, that fine-tunings occur in nature: in a particular model the amplitude of a given leading operator of the linear expansion could be suppressed, or alternatively that of a higher-dimension operator enhanced. In such an hypothetical situation, is

5 Other bosonic operators are redundant in that they are related via equations of motion or a total derivative; for instance the operator $\partial_\mu S \partial^\mu S \Phi^\dagger \Phi$ can be reabsorbed by field redefinitions.

there a way to disentangle the origin of a putative signal of the non-linear basis with respect to that from a sibling linear operator? The answer is positive even if the procedure is involved: a further tool is provided by the comparison – for a given type of coupling – between a vertex with no h leg versus one or more additional h legs, because they are correlated in the linear case and not so in the non-linear one. For instance the Feynman Rules in Appendix B.1, and in particular FR.2 *vs.* FR.6, illustrate that the couplings $S-S-Z$ and $S-S-Z-h$ are correlated. This is not the case in the non-linear scenario, where these couplings are independent of one another. An analogous effect, due to the different orderings of the operators in the two expansions, is visible in FR.4 *vs.* FR.5: whilst the vertices $S-S-W-W$ and $S-S-Z-Z$ are proportional to each other in the linear description, they are no longer so in the non-linear case. In practice, such an analysis would be challenging from the experimental point of view, as the identification of these specific couplings is not straightforward with the observables considered here.

Note finally that while some apparent decorrelation may still happen in the linear expansion via a fine-tuned combination of couplings of different orders, with enough data on Higgs physics a global analysis should provide enough resolution on the nature of EWSB involved. Furthermore, that nature would also be expected to show up in other BSM couplings not involving the DM particle.

On a different realm, notice that the comparison between the non-linear portal and the $d \geqslant 6$ in Eq (7.25) implies a trivial relation between the Lagrangian coefficients of the two expansions, when comparing the intensity of the interactions:

$$c_i^L \frac{v^2}{\Lambda_{DM}^2} = c_i \qquad \text{for} \quad i = 1,2,4\,, \qquad\qquad c_i^L \frac{v^4}{\Lambda_{DM}^4} = c_i \qquad \text{for} \quad i = 3,5\,. \tag{7.26}$$

It is then straightforward to apply to the linear analysis the results in the plots presented in the previous sections for the non-linear scenario. A caveat should be kept in mind, though, given the limits of validity of the linear expansion: because $v/\Lambda_{DM} \ll 1$, only those examples explored in which the constraint imposed on the analysis translates into a non-linear coefficient $c_i^L < 4\pi$, and within the region $\Lambda_{DM} > m_S$, should be retained for consistency of the perturbative expansion, as far as no extra exotic light resonance is detected.

Furthermore, note that in the decoupling limit of the two expansions, $\Lambda \to \infty$ (corresponding to $c_i \to 0$ in the non-linear case), the effects of the operators $\mathcal{B}_i(h)$ (and of the $b \neq 1$ deviations) as well as of their linear siblings vanish. Equivalently, the profiles in the figures in the previous sections approach the standard linear DM portal as the values of the coefficients c_i (and of the b deviation) get smaller. This can be explicitly seen in Fig. B.3, where the excluded parameter space increases with the coefficient c_1 getting smaller in absolute value.

7.4 SUMMARY

In this chapter we have studied a new, more general scenario of scalar Higgs portals, with electroweak symmetry breaking non-linearly realised. Within this pattern of symmetry breaking, the physical Higgs particle does not behave as an exact $SU(2)_L$ doublet and in general its participation in couplings as powers of $v + h$ -characteristic of the SM and also of BSM linear realisations of the Higgs mechanism- breaks down. We have first noticed how this fact automatically transforms the standard scalar Dark Matter Higgs portal and impacts strongly on the relic abundance. We have then comprehensively described the non-linear Higgs portal to Dark Matter: the dominant effective couplings – those not explicitly suppressed by any beyond the SM scale – describing the interactions of a scalar singlet Dark Matter particle with the Higgs field when electroweak symmetry is non-linearly realised. A plethora of new couplings appear involving the SM bosonic sector. The new interactions are characterised by

- **Direct couplings to gauge bosons:** Dark Matter couples to all *Higgs degrees of freedom*, namely the Higgs and the longitudinal $W^{\pm}$ and Z, see Eqs. 1.52, **??** and 7.5.
- **De-correlation of single and double Higgs couplings:** The strength of Dark Matter couplings to one- and two-Higgs fields are are de-correlated in non-linear EWSB, see Eq. (7.6).
- **Novel kinematic features:** Non-trivial momentum dependence of Dark Matter interactions due to new derivative couplings provides handles to disentangle linear vs non-linear Higgs portals at colliders. These features can be extracted from the Lagrangian Eq. (7.5), and the Feynman rules derived in Appendix B.1.

We have exploited the features of non-linear Higgs portals using information from CMB measurements, Dark Matter direct detection experiments and LHC searches of visible objects recoiling against missing energy. The effect of non-linear interactions on these observables is summarised in Table 7.1.

As a general feature, in presence of non-linearity the space of parameters for Higgs portals is much less constrained than in the standard picture, see Fig. 7.5 for the current exclusion limits. In particular, none of the existing bounds limits the region of masses $m_S > 200\,\text{GeV}$ for couplings λ_S smaller than 1, except for small regions of the parameter space. Only a limited band within this region will be probed by the next generation of direct detection experiments, see Figs. 7.4a and 7.4b for XENON1T [201] prospects.

The viable parameter spaces differ so much between the two scenarios, that it may be possible to single out signals excluding the standard portal. Let us suppose, for example, that Xenon1T observes a DM signal at a mass $m_S \simeq 200\,\text{GeV}$, measuring a DM-nucleon scattering cross-section with some value $\hat{\sigma}_{SI}$. In the standard Higgs-portal interpretation, this would give a point in the (m_S, λ_S) plane: the coupling is uniquely determined by the values of the mass and of the cross-section. In a non-linear portal setting, instead, the measure would translate into a viable vertical line whose size depends on the values assumed for the non-linear coefficients. Now, it may happen that the point in the linear plane falls within a region which is already ruled out (for example by Planck or by some collider constraint), while the line in the non-linear plot is (at least partly) allowed. This kind of signals would represent a strong indication in favour of extra interactions beyond the standard Higgs portal.

Another characteristic aspect of non-linear portals is the enhancement of signal rates at colliders. In this paper we studied production of a pair of DM particles in association with a vector boson or a Higgs. In the standard Higgs portal, the production of DM particles is unique: a Higgs produced in gluon fusion radiating two DM particles. This production is very suppressed for DM heavier or around the Higgs mass, whereas light DM appears already excluded by a combination of Higgs invisible width, relic abundance and direct detection constraints. Non-linear interactions allow electroweak production of DM via couplings to vector bosons, leading to mono-W, mono-Z and mono-Higgs signatures with rates $\mathcal{O}(10^{1-4}) \times c_i^2$ bigger than the standard Higgs. Additionally, these new production modes exhibit specific kinematic features which may help in disentangling standard and non-linear production. We have shown that a smoking gun to distinguish the standard portal from the non-linear one is provided by the combined measurement of the cross-sections ratio $R_{WZ} = \sigma(pp \to ZSS)/\sigma(pp \to W^{\pm}SS)$ with that of m_S from transverse momentum distributions.

For comparative purposes between the linear and non-linear expansions, as part of the theoretical analysis we have determined the linear siblings of all couplings studied. We determined the complete basis of purely bosonic $d = 6$ operators of the linear realisation and also the subset of linear $d = 8$ operators which induce the same physical couplings as those in the non-linear portal, up to two Dark Matter fields. While all operators of the non-linear portal considered appear at leading order, their siblings are subleading corrections in the linear expansion and their amplitude should be duly suppressed. Nevertheless, we have discussed how to distinguish the impact of both expansions, in case the relative amplitude of a $d \geqslant 6$ linear operator becomes enhanced due to some fine-tuning. A tool to disentangle the impact of higher-dimension linear operators from the leading non-linear ones may result, in principle, from the analysis of (de)correlations of specific couplings: $S-S-Z$ *vs.* $S-S-Z-h$ and $S-S-Z-Z$ *vs.* $S-S-W-W$. Finally, note that the features and bounds obtained in the analysis of the non-linear portal apply equally well to the standard one, except in regions of the parameter space which undergo restrictions due to constraints on the cut-off of the theory.

The search for Dark Matter and the quest for the nature of electroweak symmetry breaking are major present challenges. We have discussed in this chapter their interplay within an effective approach, in the framework of the Higgs Dark Matter portal.

Part IV

CONCLUSIONS

SUMMARY AND CONCLUSIONS

This thesis has explored solutions to fundamental fine-tuning issues of the Standard Model. In so doing, spin zero particles, either (pseudo)Goldstone bosons (such as axions) or not, have been brought to the forefront.

From the theoretical perspective, we have taken two different approaches: that of model-building in one part of this work, and that of effective Lagrangians in another. In the model-building arena, two fine-tuning problems of the SM have been tackled simultaneously in a proposal that invokes an enlarged (spontaneously broken) global symmetry group to explain the non-observation of the QCD θ parameter and the "smallness" of the Higgs mass. One of the major drawbacks of invisible axion models is that they suffer from the EW hierarchy problem, since the axion scale f_a is phenomenologically orders of magnitude larger than the EW scale and feeds the Higgs mass through the scalar potential. One class of pre-existing solutions to the EW hierarchy problem endow the Higgs with a GB ancestry. Typically, their implementation requires exotic vectorial fermions, and light masses for the SM fermions are generated via partial compositeness. One of these models is the minimal $SO(5)/SO(4)$ linear σ model for a GB Higgs [59], which we have extended to make it PQ invariant *à la KSVZ*, benefitting from the fact that hadronic axion models also rely on exotic vectorial fermions. We have shown that it is enough to add a single complex PQ-charged scalar to the spectrum of the minimal $SO(5)/SO(4)$ linear σ model to make it PQ invariant. This result is rather general, as the minimal PQ invariant linear σ model built here can be interpreted as a low energy description of a plethora of PQ invariant composite Higgs models, also explored in this work.

In the GB Higgs framework, the Higgs mass remains protected with respect to the overall scale of the spontaneously broken global theory by construction. The question is, though, whether other parameters of the complete scalar potential, or the value of the global scale itself, can be destabilised in the presence of a very large axion scale f_a. We have shown that when all heavy exotic fermion mass eigenstates are assumed to remain at most of the order of the composite scale ($1 - 100$ TeV), all axion solutions found are technically natural as they are protected by a chiral symmetry under which some fermions transform but not the scalar singlet nor the Higgs..

The phenomenological predictions for the axion-photon-photon coupling, which is being actively searched for by many experiments, have also been studied here for these minimally extended pGB Higgs constructions. We showed that the predicted region in the $(m_a, g_{a\gamma\gamma})$ parameter space is restricted with respect to that of the standard invisible axion formulations [140, 244] as a consequence of the necessary relations amongst the PQ charges required by the partial compositeness mechanism. The expected coupling strength is shown to be within reach of future experiments.

Beyond this particular example of a solution to a fundamental fine-tuning problem, pseudo-GBs with anomalous couplings appear in numerous models: ALPs arise in solutions to other

SM problems which invoke spontaneously broken U(1)s, and there is a whole class of models –from GB and composite Higgs models to supersymmetry– which assume new physics in relation to the EW sector, for instance to explain the EW hierarchy problem. A model-independent phenomenological study of these solutions is implemented using the tool of effective Lagrangians. For an ALP, it is just required that its couplings are mainly derivative (and/or anomalous) and suppressed by the new physics scale f_a, a characteristic feature of GBs. While the effective Lagrangian had been derived long ago [16] for linear EWSB realisations (in the SMEFT formalism), this work is pioneer in analysing the general non-linear EWSB setup (using the HEFT formalism). As theoretical contribution, we have constructed the basis of operators describing the interactions of an ALP with the SM fields in the HEFT formalism at LO and NLO. Furthermore, we have also identified and explored its main phenomenological features and new signals in present and future experiments.

The EFT formulation of the problem makes one quite common shortcoming of previous ALP phenomenology stand out: while a gauge invariant formulation in terms of the electroweak gauge bosons shows that, in general, ALP couplings to W and Z bosons are expected to arise together with the coupling to photons, the former have been largely disregarded up to now. Those couplings are expected irrespectively of the effective Lagrangian –linear or non-linear– considered. As long as there are still many orders of magnitude between the sensitivity to $a\gamma\gamma$ and to couplings such as aZZ, $aZ\gamma$ or aW^+W^-, to pursue an improvement in the latter is of paramount importance.

Our first incursion to the task of testing the EFT parameter space orthogonal to the photon coupling is found in non-standard Z decays, proposed for the first time in the ALP context in this work. For example, $Z \to a\gamma$ already provides bounds on the corresponding couplings with LEP data –our work on Z decays to ALPS initiated a path that has already been followed in more recent works [165], showing an impressive sensitivity at LHC. Furthermore, we have shown that LHC provides stupendous sensitivity in signals which have never been used in the ALP context, for instance mono-Z signatures. A reanalysis of a CMS $Z + \not{E}_T$ search pushes the ALP scale to $f_a \gtrsim 4\,\text{TeV}$ and high-luminosity LHC will test up to $\sim 20\,\text{TeV}$ for operator coefficients involved in $aZ\gamma$ and aZZ couplings of order one, for (collider stable) sub-MeV ALPs. For heavier ALPs decaying in the detector, the equivalent work remains to be done. We have also set some new bounds on effective operators using low-energy precision tests such as rare-meson decays.

The above bounds and channels being valid for both the linear and non-linear Lagrangians, they do not serve to discriminate between these two scenarios. Yet, we have found other signals to be particularly effective in revealing the presence of non-linearity. Mono-W and $aW\gamma$ production both depend on the same limited set of linear and non-linear coefficients, and we have shown that a combined analysis using HL-LHC data would be sensitive to TeV-scale non-linear interactions. The latter show up as hard momentum tails in the energy distributions due to the derivative nature of the chiral expansion. However, in working in an EFT approach, issues concerning the validity of the EFT should be taken into account, as TeV-scale observables are measured in the tails of the distributions. We have implemented in this thesis a method that takes care of this issue by removing from the expected signal all events for which the invariant mass is beyond the validity of the EFT.

Finally, another type of striking signature has been explored here: ALP couplings to the Higgs boson, proposing novel avenues in the study of ALPs. These interactions had mostly

been ignored up to now because in the linear formulation they are extremely suppressed (they do not show up below $d = 7$ effective couplings), while we proved in this thesis that aZh interactions arise at leading order in the chiral expansion, due to to combined action of the derivative chiral expansion and the fact that the Higgs does not necessarily have to be part of an exact doublet at low energies (this non-doublet behaviour is typical of GB Higgs constructions). Axion or ALP couplings to the Higgs particle, if present, would show up in non-standard Higgs decays, whose limits we used to constrain the ALP scale from $Z \to ah$ channels to $f_a \gtrsim 3\,(6)$ TeV with present (future) LHC data, for operator coefficients of order one (and for $m_a \lesssim 34$ GeV). Furthermore, the mono-h channel, which is being used in the study of DM, is proposed in this work for the first time as a probe of ALP interactions. We demonstrated that it is sensitive to ALP-Higgs interactions up to NLO in the non-linear Lagrangian.

Our results join other recent publications [17, 18, 163] in launching a new program of ALP searches at the LHC which, as a consequence, has already started to be implemented by the ATLAS collaboration, who are planning searches for ALPs in mono-X signatures. More recent followups in this path can also be found in Ref. [165].

Yet another territory considered in this thesis is that of DM candidates that do not have a pGB character. These can also benefit from a more general formulation of their interactions in terms of the two types of effective Lagrangians. A real scalar particle with polynomial couplings (instead of derivative ones) has only one type of LO (and renormalisable) interaction with the SM fields in linear EWSB realisations, known as the standard Higgs portal. Previous studies in the literature had considered scalar DM interactions using linear effective Lagrangians. We have instead considered here those interactions in the context of non-linear EWSB using the HEFT Lagrangian, and the basis of interactions has been derived at LO.

When exploring the phenomenology stemming from that basis, we found that the experimental consequences of the linear and non-linear formulations are quite different. While the standard –linear– case is almost excluded by a combination of relic density, direct detection and collider constraints, the non-linear scenario remains wide open for a large region of parameter space. New interactions of the scalar DM with the EW gauge bosons and the Higgs appear at leading order and enhance DM annihilation into SM particles before freeze-out. As a consequence, the expected relic density and direct detection rates are reduced, and large parts of parameter space become viable: the portal is in general reopened for scalar DM masses $m_S > 80$ GeV. However, in another region of parameter space the effect might be the opposite. The new leading couplings with the Higgs enhance the SSh interactions, and in their presence, the non-observation of BSM invisible Higgs decays adds up in constraining new regions in parameter space for $m_S < m_h/2$.

Predictivity, however, is not lost as the appearance of new couplings and novel kinematic features at the renormalisable level provides handles to disentangle non-linear behaviour from the standard Higgs portal at colliders. Key probes of DM at colliders are again mono-X signatures. The presence of non-linear Higgs portal interactions has a dramatic impact, allowing EW production of DM via couplings to vector bosons, leading to mono-W, mono-Z and mono-Higgs signatures with rates $\mathcal{O}(10^{1-4}) \times c_i^2$ larger than the standard –linear– Higgs. Furthermore, the relative rate of mono-Z *vs.* mono-W is fixed as a function of m_S in the

standard setup while interactions in the non-linear DM portal predict deviations from these values.

What if a signal was to be found in searches such as mono-W, mono-Z or mono-h? In the light of an excess, for example in the form of missing energy, how to uncover its *raison d'être*? How to differentiate whether it may result from couplings of a new pGB or those of a general scalar? The Goldstone character of a scalar particle is revealed, for instance, in the derivative nature of its couplings, which translates into hard momentum tails in the energy distributions: this is one distinctive guideline. In this perspective, future facilities at higher energies would be illuminating. Other aspects such as the CP nature should show up in distributions of angular variables due to the difference in Lorentz structures at the level of the Lagrangian, a work which remains to be developed in the future.

Moreover, to what extent can the nature of EWSB impact the interpretation of this hypothetical signal? We have found that the correlations amongst channels differ in the linear and non-linear realisations of EWSB, a consideration which would need to be taken into account in the analysis. Furthermore, this thesis has uncovered that the Higgs may play a crucial role in interpreting new physics effects, as the strength of Higgs couplings to the spin zero BSM candidates may also depend essentially on the –linear or non-linear– nature of EWSB.

From the point of view of analysis of data in terms of EFTs, often a single signal is being used to constrain more than one coupling on a "one by one" basis. A global fit of parameters would be relevant in order to break the ambiguity inherent to the presence of many operators which should be ideally considered together. For this reason, the complementary measurements presented here will be useful to constrain the operators independently. Furthermore, it remains to extend the above analysis to higher (pseudo)scalar masses including signals from the decays of the spin zero candidate. This been initiated for the case of ALPs subsequent to our work [165], however, much remains to be done to constrain the effective Lagrangian (and it has not even started for the case of non-linear Lagrangians), as often the production and decay mechanisms involve different types of couplings.

The high-energies and momenta made now accessible by LHC, complemented formidably by low-energy and precision probes such as rare meson decays, are enabling the exploration of new phenomenological paths, in particular in probing the existence of an enlarged scalar sector beyond the SM. We have reviewed various scenarios in which scalars and pseudoscalars, Goldstone bosons or not, appear in solutions to the unanswered questions of the SM of particle physics: we have developed new theoretical tools and proposed unexplored experimental paths in their search. There is a long way to go as far as the exploration of the spin zero sector is concerned; this thesis has slightly opened new doors to portals which we hope can be explored in the near future.

RESUMEN Y CONCLUSIONES

Esta tesis ha explorado soluciones a problemas fundamentales del ME que involucran a partículas de espín cero, ya sean bosones de Goldstone pseudoecalares –axiones y partículas-tipo-axión (PTA)– o escalares genéricos.

Desde una perspectiva teórica hemos adoptado dos enfoques: el de la construcción de modelos en una parte de la tesis, y el de los Lagrangianos efectivos en otrs. Por la parte de costrucción de modelos se ha hecho frente a dos problemas de ajuste fino del ME simultáneamente en una propuesta que invoca una simetría global ampliada (espontáneamente rota) para explicar la no observación del parámetro θ de QCD y la ligereza del Higgs. Mientras que uno de los principales inconvenientes de los modelos de axión invisible es que sufren del problema de la jerarquía ED, puesto que la escala del axión f_a está fenomenológicamente a varios órdenes de magnitud de la escala ED, y puede alimentar a la masa del Higgs mediante el potencial escalar, una solución ya existente consiste en darle una ascendencia tipo BG al Higgs. Su implementación requiere típicamente de fermiones vectoriales exóticos, y la masa ligera de los fermiones del ME se genera mediante el "composicionamiento parcial". Uno de estos modelos es el modelo σ lineal para un Higgs BG, que hemos extendido mínimamente para hacerlo invariante PQ *à la KSVZ*, aprovechando el hecho de que los modelos hadrónicos de axión también cuentan con fermiones vectoriales exóticos. Hemos encontrado que basta con añadir un campo escalar complejo al espectro del modelo σ lineal para un Higgs BG. Es un resultado bastante general, ya que el modelo en cuestión se puede interpretar como la descripción efectiva a bajas energías de un sinfín de modelos que se han tenido en cuenta en este trabajo.

La masa del Higgs está protegida respecto de la escala alta asociada a la rotura global de simetría por construcción. La pregunta que queda es si otros parámetros del potencial escalar, o el valor de la escala global en sí mismo, se pueden desestabilizar en presencia de una escala alta asociada al axión, f_a. Hemos mostrado que manteniendo las masas de los fermiones a la escala de $1 - 100$ TeV, todas las soluciones axiónicas son técnicamente natural en el sentido de 'tHooft, porque están protegidas por una simetría quiral bajo la cual algunos fermiones transforman y los escalares no.

Se han estudiado las predicciones fenomenológicas del modelo en el acoplo a dos fotones, que está siendo activamente buscado por muchos experimentos. Mostramos que la región predicha en el espacio de parámetros de $(m_a, g_{a\gamma\gamma})$ queda restringida respecto a la del axión invisible en general [140, 244], como consecuencia del mecanismo de "comoposicionamiento parcial". Se muestra también que que el modelo en cuestión está al alcance de experimentos presentes y futuros.

Más allá de este ejemplo concreto de una solución a un problema fundamental de ajuste fino, los bosones (pseudo)Goldstone aparecen en numerosos modelos: las PTA aparecen en soluciones a otros problemas del ME que invocan simetrías $U(1)$ espontáneamente rotas, y hay toda una clase de modelos –desde modelos de Higgs compuesto o de naturaleza

Goldstone hasta supersimetría– que asumen que hay nueva física para explicar el problema de la jerarquía ED. Para un estudio con independencia del modelo concreto se ha utilizado la herramienta de los Lagrangianos efectivos. Por un lado, la PTA solamente requiere que sus acoplos sean derivativos (y/o anómalos) y que estén suprimidos por la escala de nueva física f_a. Mientras que el Lagrangiano efectivo de la PTA se derivó hace años [16] para el caso de RSED lineal (el el formalismo de SMEFT), este trabajo es pionero en analizar la construcción general del caso de RSED no-lineal (usando el formalismo HEFT). En un acercamiento teórico a la cuestión, hemos construido la base de operadores que describen las interacciones de la PTA con los campos del ME en el formalismo HEFT a orden dominante y a segundo orden. También hemos identificado y explorado sus principales características fenomenológicas y nuevas señales en experimentos presentes y futuros.

La formulación del problema en términos de teorías efectivas resalta una de las lagunas en la fenomenología axiónica: mientras que una formulación invariante gauge en términos de los bosones gauge ED muestra que, en general, los acoplos de la PTA a los bosones W y Z deberían aparecer junto con el acoplo a fotones, los primeros han sido ampliamente ignorados hasta ahora. Estos acoplos se esperan a independientemente del Lagrangiano en cuestión. Mientras que haya órdenes de magnitud entre la sensibilidad a $a\gamma\gamma$ y a acoplos tales como aZZ, $aZ\gamma$ or aW^+W^-, será prioritario perseguir una mejora en los últimos.

Nuestra primera incursión en la tarea de poner a prueba el espacio de parámetros de la TEC en una dirección ortogonal al acoplo a fotones se encuentra en los decaimientos no-estándar del bosón Z, propuestos aquí por primera vez en el contexto de las PTA. Por ejemplo, del estudio de $Z \to a\gamma$ ponemos cotas con datos de LEP –nuestro trabajo en decaimientos del Z a PPTA ha iniciado un camino que ya se está siguiendo en trabajos recientes [165], mostrando una sensibilidad impresionante en el LHC. Además, hemos mostrado que el LHC proporciona una sensibilidad fantástica en otras señales que nunca usadas en el contexto de las PPTA, por ejemplo en la señal llamada mono-Z. Un reanálisis de una búsqueda de $Z + \not{E}_T$ realizada por CMS, pone cotas a la escala de la PTA a $f_a \gtrsim 4\,\text{TeV}$ con datos actuales, mientras que en su fase de alta luminosidad podrá probar escalas de hasta $\sim 20\,\text{TeV}$ para coeficientes de operadores de orden uno en el caso de partículas-tipo axión (estables en el detector) de masas por debajo del MeV. También hemos puesto cotas nuevas en operadores efectivos utilizando experimentos de precisión a baja energía tales como decaimientos raros de mesones.

Estas cotas y canales son válidas tanto para los Lagrangianos lineal y no lineal, pero no sirven para discriminar entre ambos escenarios. Sin embargo, hemos encontrado otras señales que serían particularmente efectivas a la hora de revelar la presencia de no-linearidad. Mono-W y producción de $aW\gamma$ ambas dependen del mismo conjunto finito de coeficientes lineales y no lineales, y se ha comprobado que un análisis combinado de ambas señales sería sensible a interacciones no-lineales con escalas características del TeV. La no linearidad se muestra en la forma de fuertes colas en las distribuciones de momento, debidas a la naturaleza derivativa de la expansión quiral. No obstante, al estar trabajando con una teoría efectiva hay que prestar atención a la validez de la misma. En esta tesis se ha desarrollado un método que tiene en cuenta este asunto eliminando de la señal esperada todos los eventos para los cuales la masa invariante está por encima de la validez de la teoría.

Finalmente, en cuanto a las interacciones de axiones y PTA se refiere, esta tesis ha explorado una serie de señales llamativas, basadas en las interacciones de la PTA con el bosón de Higgs. Estas interacciones se han ignorado en su mayor parte porque en la formulación

lineal están extremadamente suprimidas (no apareciendo en el Lagrangiano hasta el nivel de $d = 7$), mientras que hemos comprobado que en la formulación no-lineal aparecen acoplos aZh incluso al nivel dominante. Esto se debe a la acción combinada de la expansión derivativa quiral y al hecho de que el Higgs no tiene necesariamente que formar parte de un doblete exacto a bajas energías (una característica de todas las construcciones de Higgs BG). Los acoplos del axión al Higgs, en caso de estar presentes, aparecerían en decaimientos no-estándar de Higgs, cuyas cotas se han usado sobre el proceso $Z \to ah$ para acotar la escala del axión a $f_a > 3\,(6)$ TeV con datos del LHC presentes (futuros) para coeficientes de orden uno (y para $m_a < 34$ GeV). También la señal de mono-h, que ya se está usando en búsquedas de materia oscura, se ha propuesto en este trabajo por primera vez como prueba de las interacciones de una PTA. Hemos demostrado que es sensible a interacciónes hasta segundo orden en el Lagrangiano no-lineal.

Estos resultados se unen a una serie de publicaciones anteriores [18, 163] en el lanzamiento de un nuevo programa de búsquedas en el LHC que, como consecuencia, ya ha empezado a llevarse a cabo por grupos de la colaboración de ATLAS, quienes están planeando búsquedas de PTA con señales mono-X. Entre otros trabajos subsiguientes en este camino se encuentra el de la Ref. [165].

Hay aún otro ámbito considerado en esta tesis que es el de candidatos a MO que no tienen un carácter BG. Éstas partículas también se pueden beneficiar de una formulación más general de sus interacciones en términos de estos dos tipos de Lagrangianos efectivos. Un escalar real con acoplos polinómicos (en lugar de derivativos) tiene una sola interacción dominante –renormalizable– con el ME en contextos de realización lineal de la rotura de la simetría electrodébil, conocida como el portal escalar de Higgs. De nuevo, el escalar MO solo se había considerado anteriormente en el contexto de RSED lineal. En cambio, aquí hemos derivado la base de interacciones dominantes de este candidato a materia oscura con los campos del ME en el caso del Lagrangiano ED quiral utilizando el formalismo de HEFT.

Hemos encontrando que el estado experimental de ambos es notablemente diferente. Mientras que el caso estándar –lineal– está casi completamente excluido por una combinación de medidas de la abundancia de materia oscura, búsquedas directas y cotas de aceleradores, el caso no-lineal permanece abierto. Nuevas interacciones de la materia oscura con los bosones gauge ED y con el Higgs que aparecen a orden dominante realzan la aniquilación de materia oscura a partículas del ME antes de su desacoplo. En consecuencia, se reduce el impacto de las cotas en abundancia y de detección directa, y grandes porciones del espacio de parámetros se vuelven viable: el portal está generalmente reabierto para masas del escalar en cuesión de $m_S > 80$ GeV. Sin embargo, en otras zonas del espacio de parámetros el efecto es el contrario. Las nuevas interacciones con el Higgs realzan las interacciones SSh, y en su presencia, la no observación de decaimientos invisibles del Higgs MAME acota regiones nuevas del especio de parámetros para $m_S < m_h/2$.

Sin embargo, no se pierde predictividad pues la aparición de nuevos acoplos y características kinemáticas al orden dominante aportará información que permite distinguir el portal de Higgs no lineal de estándar en colisionadores. Una señal clave en la búsqueda de las interacciones son las señales mono-X. La presencia de las interacciones no lineales tiene como efecto que las señales esperadas de mono-W, mono-Z y mono-h sean $\mathcal{O}(10^1 - 10^4 \times c_i^2)$ veces mayores que en el caso estándar –lineal. Además, la tasa relativa entre mono-W y mono-Z está

fijada en función de m_S para el caso lineal y mientras que el no-lineal predice desviaciones con respecto a la misma.

En resumen, las principales aportaciones de esta tesis han sido variadas: desde aportaciones teóricas, en el desarrollo de una clase de modelos que resuelven dos problemas de ajuste fino al mismo tiempo, y en la construcción de dos bases efectivas nuevas, hasta el desarrollo de nuevas señales fenomenológicas que acompañan a una serie muy reciente de trabajos en abrir un nuevo camino en la búsqueda de partículas de espín cero en el LHC.

¿Y si se encontrara una señal positiva en búsquedas tales como mono-W, mono-Z o mono-h? A la luz de un exceso, por ejemplo en forma de energía perdida, ¿cómo desvelar su *raison d'être*? ¿Cómo distinguir si proviene de acoplos de tipo pBG o acoplos generales escalares? El carácter Goldstone de una partícula escalar se manifiesta, por ejemplo, en la naturaleza derivativa de sus acoplos, que se traduce en colas fuertes de momentos en distribuciones de energía: este es un posible distintivo. Desde esta perspectiva, resultarán esclarecedoras las instalaciones futuras a energías más altas. Otros aspectos tales como la naturaleza CP deberán mostrarse en distribuciones de variables angulares debido a la diferencia en estructuras de Lorentz a nivel del Lagrangiano, un trabajo que queda para el futuro.

Por otra parte, ¿hasta qué punto podrá verse afectada la interpretación de esta hipotética señal en función de la naturaleza de la RSED? Hemos encontrado que la correlación entre canales difiere entre los casos se RSED lineal y no lineal, una cosideración que debería tenerse en cuenta en el análisis. Asimismo, esta tesis ha encontrado que el Higgs podría desempeñar un papel crucial en la interpretación de efectos de nueva física, pues la intensidad de los acoplos del Higgs al candidato MAME de espín cero depende esencialmente de la naturaleza –lineal o no lineal– de RSED.

Desde el punto de vista del análisis de datos en términos de TEC, a menudo se está usando una sola señal para acotar más de un acoplo, estudiándolos "de uno en uno". Un ajuste global de parámetros sería relevante para romper la ambigüedad inherente a la presencia de muchos operadores que se deberían idealmente considerar juntos. Por esta razón, se requieren medidas complementarias para acotar los operadores independientemente. Asimismo, queda pendiente extenter el análisis anterior masas de (pseudo)escalares mayores, incluyendo señales producidas el decaimiento de estas partículas. Para el caso de las PPTA, esta tarea se ha iniciado posteriormente a nuestro trabajo [165], sin embargo, aún queda mucho por hacer para acotar el Lagrangiano efectivo (y ni siquiera ha empezado en el caso de los Lagrangianos no lineales), pues a menudo la producción y decaimiento implican acoplos diferentes.

Más aún, desde el punto de vista del análisis, Las altas energías y momentos hechas accesibles ahora gracias al LHC, complementadas formidablemente por búsquedas de precisión a baja energía como decaimientos raros de menos, están permitiendo la exploración de nuevos caminos fenomenológicos, en particular en la búsqueda de un sector escalar ampliado respecto al del ME. Hemos revisado varios escenarios en los que escalares y pseudoescalares, bosones de Goldstone o no, aparecen en soluciones a las preguntas sin responder del ME: hemos desarrollado nuevas herramientas teóricas y propuesto caminos experimentales no explorados aún en su búsqueda. Queda un largo camino en lo que se refiere a la exploración del sector de espín cero; esta tesis ha abierto nuevas puertas a portales que esperemos se puedan seguir investigando en un futuro cercano.

Part V

APPENDIX

A

APPENDICES: ALPS EFT AND COLLIDER SIGNATURES

A.1 FERMIONIC CHIRAL ALP LAGRANGIAN AND COMPLETE BASIS

In what follows, a complete basis of operators -bosonic plus fermionic- which include an ALP insertion is determined, up to NLO for the chiral EWSB. Consider the following set of independent fermionic structures, assuming only one flavour family:

$$
\begin{aligned}
\mathcal{P}_1^q &= \bar{Q}_L \mathbf{U} Q_R \, \partial_\mu \frac{a}{f_a} \partial^\mu \mathcal{F}(h)\,, & \mathcal{P}_1^\ell &= \bar{L}_L \mathbf{U} L_R \, \partial_\mu \frac{a}{f_a} \partial^\mu \mathcal{F}(h)\,,\\
\mathcal{P}_2^q &= \bar{Q}_L \mathbf{T}\mathbf{U} Q_R \, \partial_\mu \frac{a}{f_a} \partial^\mu \mathcal{F}(h)\,, & &\\
\mathcal{P}_3^q &= \bar{Q}_L \mathbf{V}_\mu \mathbf{U} Q_R \, \partial^\mu \frac{a}{f_a} \mathcal{F}(h)\,, & &\\
\mathcal{P}_4^q &= \bar{Q}_L \{\mathbf{V}_\mu, \mathbf{T}\} \mathbf{U} Q_R \, \partial^\mu \frac{a}{f_a} \mathcal{F}(h)\,, & \mathcal{P}_2^\ell &= \bar{L}_L \{\mathbf{V}_\mu, \mathbf{T}\} \mathbf{U} L_R \, \partial^\mu \frac{a}{f_a} \mathcal{F}(h)\,,\\
\mathcal{P}_5^q &= \bar{Q}_L \, [\mathbf{V}_\mu, \mathbf{T}] \, \mathbf{U} Q_R \, \partial^\mu \frac{a}{f_a} \mathcal{F}(h)\,, & \mathcal{P}_3^\ell &= \bar{L}_L \, [\mathbf{V}_\mu, \mathbf{T}] \, \mathbf{U} L_R \, \partial^\mu \frac{a}{f_a} \mathcal{F}(h)\,,\\
\mathcal{P}_6^q &= \bar{Q}_L \mathbf{T}\mathbf{V}_\mu \mathbf{T}\mathbf{U} Q_R \, \partial^\mu \frac{a}{f_a} \mathcal{F}(h)\,, & &\\
\mathcal{P}_7^q &= \bar{Q}_L \sigma^{\mu\nu} \mathbf{V}_\mu \mathbf{U} Q_R \, \partial^\mu \frac{a}{f_a} \mathcal{F}(h)\,, & &\\
\mathcal{P}_8^q &= \bar{Q}_L \sigma^{\mu\nu} \{\mathbf{V}_\mu, \mathbf{T}\} \mathbf{U} Q_R \, \partial^\mu \frac{a}{f_a} \mathcal{F}(h)\,, & \mathcal{P}_4^\ell &= \bar{L}_L \sigma^{\mu\nu} \{\mathbf{V}_\mu, \mathbf{T}\} \mathbf{U} L_R \, \partial^\mu \frac{a}{f_a} \mathcal{F}(h)\,,\\
\mathcal{P}_9^q &= \bar{Q}_L \sigma^{\mu\nu} \, [\mathbf{V}_\mu, \mathbf{T}] \, \mathbf{U} Q_R \, \partial^\mu \frac{a}{f_a} \mathcal{F}(h)\,, & \mathcal{P}_5^\ell &= \bar{L}_L \sigma^{\mu\nu} \, [\mathbf{V}_\mu, \mathbf{T}] \, \mathbf{U} L_R \, \partial^\mu \frac{a}{f_a} \mathcal{F}(h)\,,\\
\mathcal{P}_{10}^q &= \bar{Q}_L \sigma^{\mu\nu} \mathbf{T}\mathbf{V}_\mu \mathbf{T}\mathbf{U} Q_R \, \partial^\mu \frac{a}{f_a} \mathcal{F}(h)\,, & &
\end{aligned}
\tag{A.1}
$$

Would the neutral components be added to the $SU(2)_R$ doublet $L_R \equiv (0, E_R)$, the number of leptonic operators above would double. When considering several generations, each of the structures in Eq. (A.1) encodes all possible independent flavour operators $\mathcal{P}^q_{i,\alpha\beta}$, where greek indices denote flavour.

A complete basis can be constructed combining the set of fermionic operators above with the bosonic Lagrangian in Eq. (6.12) while avoiding redundancies. This can be enforced using

the EOM which may relate some bosonic and fermionic operators. Given the form of the chiral LO Lagrangian in Eq. (6.2), the relevant EOMs read

$$\begin{aligned} i\not{D}\psi_L &= \frac{v}{\sqrt{2}}\mathbf{U}y_\psi(h)\psi_R + iv\sqrt{2}\frac{a}{f_a}c_{2D}\,\mathbf{U}y_\psi(h)\sigma^3\psi_R\,, \\ i\not{D}\psi_R &= \frac{v}{\sqrt{2}}y_\psi^\dagger(h)\mathbf{U}^\dagger\psi_L - iv\sqrt{2}\frac{a}{f_a}c_{2D}\,\sigma^3 y_\psi^\dagger(h)\mathbf{U}^\dagger\psi_L\,, \end{aligned} \tag{A.2}$$

$$(D^\mu W_{\mu\nu})^a = \sum_{\psi=Q,L}\frac{g}{2}\bar{\psi}_L\sigma^a\gamma_\nu\psi_L + \frac{igv^2}{4}\mathrm{Tr}[\mathbf{V}_\nu\sigma^a]\mathcal{F}_C(h)\,, \tag{A.3}$$

$$\partial^\mu B_{\mu\nu} = gc_\theta\sum_{\substack{i=L,R\\ \psi\\ Q,L}}\bar{\psi}_i\mathbf{h}_{\psi_i}\gamma_\nu\psi_i - \frac{igc_\theta v^2}{4}\mathrm{Tr}[\mathbf{T}\mathbf{V}_\mu]\mathcal{F}_C(h)\,, \tag{A.4}$$

$$\begin{aligned} \Box h =& -V'(h) - \frac{v^2}{4}\mathrm{Tr}[\mathbf{V}_\mu\mathbf{V}^\mu]\mathcal{F}_C'(h) + \\ &- \frac{v}{\sqrt{2}}\sum_{\psi=Q,L}\left(\bar{\psi}_L\mathbf{U}y_\psi'(h)\psi_R + \mathrm{h.c.}\right) + v^2c_T\mathrm{Tr}(\mathbf{T}\mathbf{V}_\mu)^2\mathcal{F}_T'(h) + \\ &+ ic_{2D}v^2\left[\mathrm{Tr}\left[\mathbf{T}\mathbf{V}_\mu\right]\frac{\partial^\mu a}{f_a}\hat{\mathcal{F}}_{2D}'(h) - \sqrt{2}v\frac{a}{f_a}\sum_{\psi=Q,L}\left(\bar{\psi}_L\mathbf{U}y_\psi'(h)\psi_R\right) + \mathrm{h.c.}\right]\,, \end{aligned} \tag{A.5}$$

$$\Box\frac{a}{f_a} = -ic_{2D}\frac{v^2}{f_a^2}\left[\partial_\mu\left(\mathrm{Tr}\left[\mathbf{T}\mathbf{V}_\mu\right]\hat{\mathcal{F}}_{2D}(h)\right) + \frac{\sqrt{2}}{v}\sum_{\psi=Q,L}\left(\bar{\psi}_L\mathbf{U}y_\psi(h)\psi_R\right) + \mathrm{h.c.}\right]\,, \tag{A.6}$$

where $y_\psi(h)$ has been defined in Eq. (1.58), $\hat{\mathcal{F}}_{2D}(h)$ is defined as $\mathcal{F}_{2D}(h)$ without its h-independent term and the prime on the $\mathcal{F}_i$ and y_ψ functions denotes the first derivative with respect to h. $\mathbf{h}_{\psi_i}$ in Eq. (A.4) are the hypercharges given in the 2×2 matrix notation

$$\begin{aligned} \mathbf{h}_{Q_L} &= \mathrm{diag}\,(1/6, 1/6)\,, & \mathbf{h}_{Q_R} &= \mathrm{diag}\,(2/3, -1/3)\,, \\ \mathbf{h}_{L_L} &= \mathrm{diag}\,(-1/2, -1/2)\,, & \mathbf{h}_{L_R} &= \mathrm{diag}\,(0, -1)\,. \end{aligned} \tag{A.7}$$

A consequence of Eqs. (A.2) and (A.3) is [15, 70]

$$\mathcal{D}_\mu\left(\mathbf{V}^\mu\mathcal{F}_C\right) = \frac{i}{v^2}D_\mu\left(\sum_{\psi=Q,L}\bar{\psi}_L\sigma^j\gamma^\mu\psi_L\right)\sigma^j = \frac{1}{\sqrt{2}v}\sum_{\psi=Q,L}\left(\bar{\psi}_L\sigma^j\mathbf{U}y_\psi(h)\psi_R - \bar{\psi}_R y_\psi^\dagger(h)\mathbf{U}^\dagger\sigma^j\psi_L\right)\sigma^j\,, \tag{A.8}$$

which can be recast as

$$\mathrm{Tr}(\sigma^j\mathcal{D}_\mu\mathbf{V}^\mu)\mathcal{F}_C(h) = \frac{\sqrt{2}}{v}\sum_{\psi=Q,L}\left(\bar{\psi}_L\sigma^j\mathbf{U}y_\psi(h)\psi_R - \bar{\psi}_R y_\psi^\dagger(h)\mathbf{U}^\dagger\sigma^j\psi_L\right) - \mathrm{Tr}(\sigma^j\mathbf{V}_\mu)\partial^\mu\mathcal{F}_C(h)\,, \tag{A.9}$$

and is valid order by order in the h expansion.

Applying the EOMs above, the operators $\mathcal{A}_8$, $\mathcal{A}_{11}$, $\mathcal{A}_{13}$, $\mathcal{A}_{17}$ in Eq. (6.6) can be removed as redundant, because tradable by flavour-blind structures of the type in Eq. (A.1). In summary, the complete basis of LO plus NLO operators of the EWSB chiral expansion which include an ALP insertion includes a total of 32 independent operators, considering only one fermion generation and disregarding the different coefficients inside the $\mathcal{F}_i(h)$ functions; the extension to three generations is obvious.

A.2 FEYNMAN RULES FOR THE BOSONIC BASIS

This section provides a complete list of the Feynman rules for vertices involving an ALP and resulting from the NLO linear Lagrangian Eq. (3.65) and the chiral one Eq. (6.12), up to four legs. The coefficients $\tilde{a}_i$ and $\tilde{b}_i$ have been defined in Eq. (6.7) in terms of the parameters in those Lagrangians; this is extended below for the operators $\mathcal{A}_{15}$ and $\mathcal{A}_{16}$, that contain two functions $\mathcal{F}_i(h)$ and $\mathcal{F}'_i(h)$, redefining $c_i a_i a'_i \to \tilde{a}_i$. The rules are computed:

- choosing the momenta to flow inwards in the vertices
- in unitary gauge
- neglecting flavor effects, *i.e.* assuming hermitian and diagonal Yukawa matrices ($\mathbf{Y}_\psi \equiv \mathbf{Y}_\psi^\dagger$) and $V_{CKM} \equiv \mathbb{1}$ (greek indices will indicate flavour).

The Feynman rules for the linear case be easily obtained from those for the non-linear Lagrangian, in the limit

$$c_1, \ldots, c_{17} \to 0\,, \qquad c_{\tilde{B}} \to c_{\tilde{B}}\,, \qquad c_{\tilde{W}} \to c_{\tilde{W}}\,, \qquad c_{\tilde{G}} \to c_{\tilde{G}}\,, \tag{A.10}$$

A final replacement, $c_{2D} \to -c_\Phi/2$, only applies for the fermionic couplings stemming from the corresponding chiral and linear operators. In the table of Feynman rules below, the left, center and middle columns show respectively the phenomenological vertex, the amplitude in the chiral case and that in the linear case when non-vanishing, up to NLO.

	Coupling	Chiral Lagrangian	Linear Lagrangian
(FR.1)	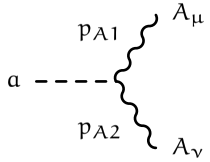	$-\frac{4i}{f_a} p_{A1\alpha} p_{A2\beta} \varepsilon^{\mu\nu\alpha\beta} \left(c_\theta^2 c_{\tilde{B}} + s_\theta^2 c_{\tilde{W}}\right)$	$-\frac{4i}{f_a} p_{A1\alpha} p_{A2\beta} \varepsilon^{\mu\nu\alpha\beta} \left(c_\theta^2 c_{\tilde{B}} + s_\theta^2 c_{\tilde{W}}\right)$
(FR.2)	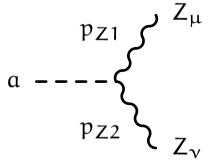	$-\frac{4i}{f_a} p_{Z1\alpha} p_{Z2\beta} \varepsilon^{\mu\nu\alpha\beta} \left(s_\theta^2 c_{\tilde{B}} + c_\theta^2 c_{\tilde{W}} + \frac{g}{16\pi}(c_2 + 2c_7 - 2t_\theta c_1)\right)$	$-\frac{4i}{f_a} p_{Z1\alpha} p_{Z2\beta} \varepsilon^{\mu\nu\alpha\beta} \left(s_\theta^2 c_{\tilde{B}} + c_\theta^2 c_{\tilde{W}}\right)$
(FR.3)	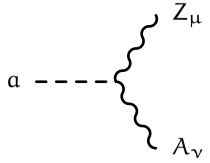	$\frac{i}{f_a} p_{Z\alpha} p_{A\beta} \varepsilon^{\mu\nu\alpha\beta} \left(2s_{2\theta}(c_{\tilde{B}} - c_{\tilde{W}}) - \frac{g}{8\pi}(2c_1 + t_\theta(c_2 + 2c_7))\right)$	$\frac{2is_{2\theta}}{f_a} p_{Z\alpha} p_{A\beta} \varepsilon^{\mu\nu\alpha\beta} \left(c_{\tilde{B}} - c_{\tilde{W}}\right)$

(FR.4)

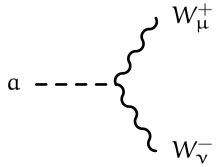

$$\frac{g}{4\pi f_a}\left[c_6 g^{\mu\nu}(p_+^2 - p_-^2) + \left(\frac{g}{4\pi}c_8 - c_6\right)\left(p_+^\mu p_+^\nu - p_-^\mu p_-^\nu\right)\right] +$$

$$-\frac{4i}{f_a}\left(c_{\tilde{W}} + \frac{g}{16\pi}c_2\right) p_{+\alpha} p_{-\beta}\, \varepsilon^{\mu\nu\alpha\beta}$$

$$-\frac{4i}{f_a} c_{\tilde{W}} p_{+\alpha} p_{-\beta}\, \varepsilon^{\mu\nu\alpha\beta}$$

(FR.5)

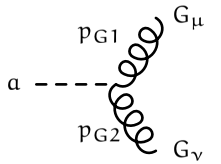

$$-\frac{4i}{f_a} c_{\tilde{G}}\, p_{G1\alpha} p_{G2\beta}\, \varepsilon^{\mu\nu\alpha\beta}$$

$$-\frac{4i}{f_a} c_{\tilde{G}}\, p_{G1\alpha} p_{G2\beta}\, \varepsilon^{\mu\nu\alpha\beta}$$

(FR.6)

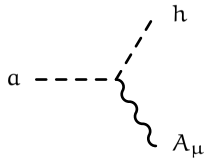

$$\frac{1}{2\pi v f_a}\left(\tilde{a}_3 c_\theta + \tilde{a}_{10} s_\theta\right)\left(p_A^\mu p_a \cdot p_A - p_A^2 p_a^\mu\right)$$

(FR.7)

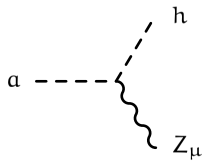

$$\frac{1}{4\pi^2 s_{2\theta} v f_a}\Big[e\,p_h^\mu(p_a^2\tilde{a}_{11}+p_a\cdot p_h\tilde{a}_{14})+e\,p_a^\mu(p_h^2\tilde{a}_{13}+p_a\cdot p_h\tilde{a}_{12})$$

$$+2\pi s_{2\theta}(\tilde{a}_3 s_\theta-\tilde{a}_{10}c_\theta)(p_Z^\mu p_h\cdot p_Z-p_h^\mu p_Z^2)$$

$$-e\,p_a^\mu(16\pi^2v^2\tilde{a}_{2D}-\tilde{a}_{17}p_a^2)\Big]$$

(FR.8)

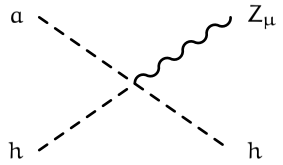

$$\frac{1}{4\pi^2 s_{2\theta} v^2 f_a}\Big[e\,(p_{h1}+p_{h2})^\mu(p_a^2\tilde{b}_{11}+p_a\cdot(p_{h1}+p_{h2})\tilde{b}_{14})$$

$$+e\,p_a^\mu((p_{h1}+p_{h2})^2\tilde{b}_{13}+p_a\cdot(p_{h1}+p_{h2})\tilde{b}_{12})$$

$$+2e\tilde{a}_{16}(p_{h1}^\mu p_a\cdot p_{h2}+p_{h2}^\mu p_a\cdot p_{h1})$$

$$+4e\tilde{a}_{15}p_a^\mu p_{h1}\cdot p_{h2}-e\,p_a^\mu(16\pi^2v^2\tilde{b}_{2D}-\tilde{b}_{17}p_a^2)$$

$$+2\pi s_{2\theta}(\tilde{b}_3 s_\theta-\tilde{b}_{10}c_\theta)(p_Z^2p_a^\mu-p_Z^\mu p_a\cdot p_Z)\Big]$$

(FR.9)

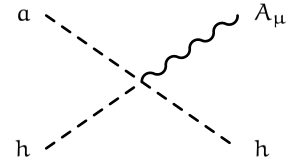

$$\frac{1}{2\pi v^2 f_a}\left(\tilde{b}_3 c_\theta + \tilde{b}_{10} s_\theta\right)\left(p_A^\mu p_a \cdot p_A - p_A^2 p_a^\mu\right)$$

(FR.10)

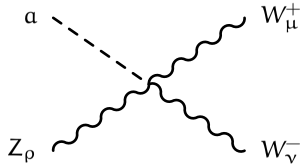

$$\frac{g^2}{4\pi c_\theta f_a}\left[2\left(\frac{g}{8\pi}c_5 + c_\theta^2 c_6\right) g^{\mu\nu} p_a^\rho + \left(\frac{g}{8\pi}c_4 - c_\theta^2 c_6 - \frac{e s_\theta}{4\pi}c_8\right)\left(g^{\mu\rho}p_a^\nu + g^{\nu\rho}p_a^\mu\right)\right] +$$

$$-\frac{4igc_\theta}{f_a}c_{\tilde{W}}\varepsilon^{\mu\nu\rho\alpha}p_{a\alpha}$$

$$-\frac{4igc_\theta}{f_a}\left(c_{\tilde{W}} + c_2\frac{g(1+2c_\theta^2)}{32\pi c_\theta^2} + \frac{g}{16\pi c_\theta^2}c_7\right)\varepsilon^{\mu\nu\rho\alpha}p_{a\alpha}$$

(FR.11)

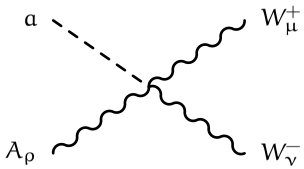

$$\frac{ge}{4\pi f_a}\left[\left(\frac{g}{4\pi}c_8 - c_6\right)\left(g^{\mu\rho}p_a^\nu + g^{\nu\rho}p_a^\mu\right) + 2c_6 g^{\mu\nu}p_a^\rho\right] +$$

$$-\frac{4ig}{f_a}c_{\tilde{W}}\varepsilon^{\mu\nu\rho\alpha}p_{a\alpha}$$

$$-\frac{4ig}{f_a}\left(c_{\tilde{W}} + \frac{g}{16\pi}c_2\right)\varepsilon^{\mu\nu\rho\alpha}p_{a\alpha}$$

(FR.12)

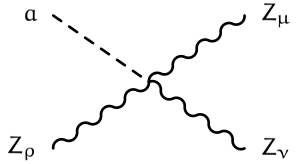

$$\frac{g^3}{16\pi^2 c_\theta^3 f_a}(c_4 + c_5 + 2c_9)\left(g^{\mu\nu}p_a^\rho + g^{\mu\rho}p_a^\nu + g^{\nu\rho}p_a^\mu\right)$$

(FR.13)

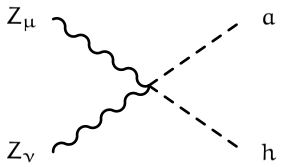

$$-\frac{ig}{4\pi v f_a}p_{a\alpha}(p_{Z1-}p_{Z2})_\beta\,\varepsilon^{\mu\nu\alpha\beta}\,(\tilde{a}_2 + 2\tilde{a}_7 - 2t_\theta\tilde{a}_1)$$

(FR.14)

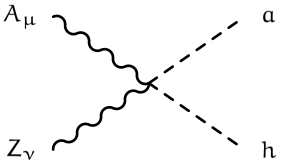

$$-\frac{ig}{4\pi v f_a}p_{a\alpha}p_{A\beta}\,\varepsilon^{\mu\nu\alpha\beta}\,(2\tilde{a}_1 + t_\theta(\tilde{a}_2 + 2\tilde{a}_7))$$

(FR.15)

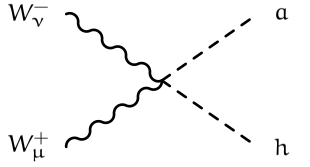

$$\frac{g}{2\pi v f_a}\left[\tilde{a}_6 g^{\mu\nu}p_a\cdot(p_+ - p_-) + \left(\frac{g}{4\pi}\tilde{a}_8 - \tilde{a}_6\right)\left(p_a^\mu p_+^\nu - p_-^\mu p_a^\nu\right)\right] +$$

$$-\frac{ig}{4\pi v f_a}\tilde{a}_2 p_{a\alpha}(p_+ - p_-)_\beta\,\varepsilon^{\mu\nu\alpha\beta} + \frac{g}{2\pi v f_a}\left(\tilde{a}_{10} - \frac{g}{4\pi}\tilde{a}_8\right)\left(p_a^\mu p_h^\nu - p_a^\nu p_h^\mu\right)$$

(FR.16) 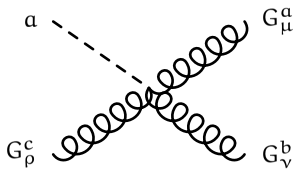

$\frac{4g_s}{f_a} c_{\tilde{G}} f^{abc} \varepsilon^{\mu\nu\rho\alpha} p_{a\alpha}$ $\frac{4g_s}{f_a} c_{\tilde{G}} f^{abc} \varepsilon^{\mu\nu\rho\alpha} p_{a\alpha}$

(FR.17) 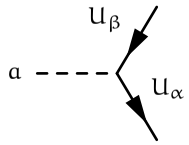

$\frac{2\sqrt{2}v}{f_a} \left(c_{2D} - \frac{c_{17}}{16\pi^2} \frac{p_a^2}{v^2} \right) (\mathbf{Y}_u)_\alpha \delta_{\alpha\beta} \gamma_5$ $-\frac{\sqrt{2}v}{f_a} c_{a\Phi} (Y_u)_\alpha \delta_{\alpha\beta} \gamma_5$

(FR.18) 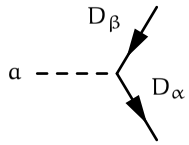

$-\frac{2\sqrt{2}v}{f_a} \left(c_{2D} - \frac{c_{17}}{16\pi^2} \frac{p_a^2}{v^2} \right) (Y_D)_\alpha \delta_{\alpha\beta} \gamma_5$ $\frac{\sqrt{2}v}{f_a} c_{a\Phi} (Y_D)_\alpha \delta_{\alpha\beta} \gamma_5$

(FR.19) 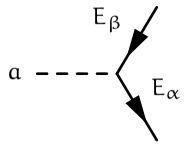

$-\frac{2\sqrt{2}v}{f_a} \left(c_{2D} - \frac{c_{17}}{16\pi^2} \frac{p_a^2}{v^2} \right) (Y_E)_\alpha \delta_{\alpha\beta} \gamma_5$ $\frac{\sqrt{2}v}{f_a} c_{a\Phi} (Y_E)_\alpha \delta_{\alpha\beta} \gamma_5$

(FR.20)

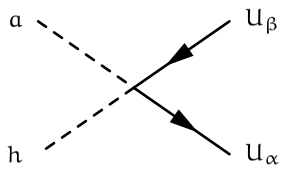

$$\frac{4\sqrt{2}}{f_a} a_U \left(c_{2D} - \frac{c_{17}}{16\pi^2} \frac{p_a^2}{v^2} \right) (Y_U)_\alpha \delta_{\alpha\beta} \gamma_5 \qquad -\frac{\sqrt{2}}{f_a} c_{a\Phi} (Y_U)_\alpha \delta_{\alpha\beta} \gamma_5$$

(FR.21)

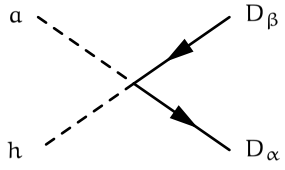

$$-\frac{4\sqrt{2}}{f_a} a_D \left(c_{2D} - \frac{c_{17}}{16\pi^2} \frac{p_a^2}{v^2} \right) (Y_D)_\alpha \delta_{\alpha\beta} \gamma_5 \qquad \frac{\sqrt{2}}{f_a} c_{a\Phi} (Y_D)_\alpha \delta_{\alpha\beta} \gamma_5$$

(FR.22)

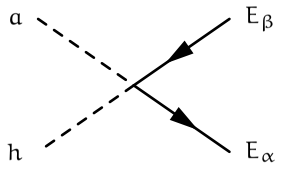

$$-\frac{4\sqrt{2}}{f_a} a_E \left(c_{2D} - \frac{c_{17}}{16\pi^2} \frac{p_a^2}{v^2} \right) (Y_E)_\alpha \delta_{\alpha\beta} \gamma_5 \qquad \frac{\sqrt{2}}{f_a} c_{a\Phi} (Y_E)_\alpha \delta_{\alpha\beta} \gamma_5$$

A.3 LINEAR SIBLINGS

The interaction vertices described by the chiral operators in Sect. 6.1 can also be described in the context of linearly realized EWSB, through linear operators in which the Higgs resonance is embedded within the SM Higgs doublet. In this section, the connection between the two expansions is shown. Operators up to NNLO of the linear expansion have to be taken into account in order to encompass all the interaction vertices appearing in the chiral framework up to NLO. The chiral couplings involving an ALP discussed in this work can be grouped as those

CONNECTED TO $d = 5$ OPERATORS IN THE LINEAR EXPANSION

$$\begin{aligned}
\mathcal{A}_{2D} &\longrightarrow \frac{-i}{2}(\Phi^\dagger \overleftrightarrow{D}^\mu \Phi)\frac{\partial_\mu a}{f_a} \\
\mathcal{A}_{\tilde{B}} &\longrightarrow -B_{\mu\nu}\tilde{B}^{\mu\nu}\frac{a}{f_a} \\
\mathcal{A}_{\tilde{W}} &\longrightarrow -W^a_{\mu\nu}\tilde{W}^{a\mu\nu}\frac{a}{f_a} \\
\mathcal{A}_{\tilde{G}} &\longrightarrow -G^a_{\mu\nu}\tilde{G}^{a\mu\nu}\frac{a}{f_a}
\end{aligned} \tag{A.11}$$

CONNECTED TO $d = 7$ OPERATORS IN THE LINEAR EXPANSION

$$\begin{aligned}
\mathcal{A}_1 &\longrightarrow -\tfrac{2i}{(4\pi)v^2}{}'\tilde{B}_{\mu\nu}(\Phi^\dagger \overleftrightarrow{D}_\mu \Phi)\partial_\nu \tfrac{a}{f_a} \\
\mathcal{A}_2 &\longrightarrow -\tfrac{i}{(4\pi)v^2}(D_\mu\Phi^\dagger \tilde{W}^{\mu\nu}\Phi - \Phi^\dagger\tilde{W}^{\mu\nu}D_\mu\Phi)\tfrac{\partial^\nu a}{f_a} \\
\mathcal{A}_3 &\longrightarrow \tfrac{-2}{(4\pi)v^2}B_{\mu\nu}\tfrac{\partial^\mu a}{f_a}D^(\Phi^\dagger\Phi) \\
\mathcal{A}_4, \mathcal{A}_8 &\longrightarrow \tfrac{4i}{(4\pi)^2v^2}(D^\mu\Phi^\dagger D_\mu D_\nu\Phi - D_\mu D_\nu\Phi^\dagger D^\mu\Phi)\tfrac{\partial^\nu a}{f_a} \\
\mathcal{A}_5 &\longrightarrow \tfrac{4i}{(4\pi)^2v^2}(D^\nu\Phi^\dagger\Box\Phi - \Box\Phi^\dagger D^\mu\Phi)\tfrac{\partial_\nu a}{f_a} \\
\mathcal{A}_6 &\longrightarrow -\tfrac{4}{(4\pi)iv^2}(\Phi^\dagger W_{\mu\nu}D^\mu\Phi + D^\mu\Phi^\dagger W_{\mu\nu}\Phi)\tfrac{\partial^\nu a}{f_a} \\
\mathcal{A}_{10} &\longrightarrow \tfrac{4}{(4\pi)v^2}(\Phi^\dagger W_{\mu\nu}D^\mu\Phi + D^\mu\Phi^\dagger W_{\mu\nu}\Phi)\tfrac{\partial^\nu a}{f_a} \\
\mathcal{A}_{11} &\longrightarrow -\tfrac{2i}{(4\pi)^2v^2}(\Phi^\dagger\Box\Phi - \Phi\Box\Phi^\dagger)\tfrac{\Box a}{f_a} \\
\mathcal{A}_{12} &\longrightarrow -\tfrac{2i}{(4\pi)^2v^2}(\Phi^\dagger \overleftarrow{D_\mu D_\nu}\Phi)\tfrac{\partial^\mu\partial^\nu a}{f_a} \\
\mathcal{A}_{15}, \mathcal{A}_{16} &\longrightarrow -\tfrac{8i}{(4\pi)^2v^2}(D^\mu\Phi^\dagger D_\mu D_\nu\Phi - D_\mu D_\nu\Phi^\dagger D^\mu\Phi)\tfrac{\partial^\nu a}{f_a} \\
\mathcal{A}_{17} &\longrightarrow 2\tfrac{2i}{(4\pi)^2v^2}(\Phi^\dagger D_\mu\Phi)\tfrac{\partial^\mu\Box a}{f_a}
\end{aligned} \tag{A.12}$$

CONNECTED TO $d = 9$ OPERATORS IN THE LINEAR EXPANSION

$$\begin{aligned}
\mathcal{A}_7 &\longrightarrow \tfrac{8i}{(4\pi)^2v^4}(\Phi^\dagger\tilde{W}_{\mu\nu}\Phi)(\Phi^\dagger\overleftrightarrow{D^\mu}\Phi)\tfrac{\partial^\nu a}{f_a} \\
\mathcal{A}_{13} &\longrightarrow -\tfrac{4i}{(4\pi)^2v^4}(\Phi^\dagger\overleftrightarrow{D}_\mu\Phi)\Box[\Phi^\dagger\Phi]\tfrac{\partial^\mu a}{f_a} \\
\mathcal{A}_{14} &\longrightarrow -\tfrac{4i}{(4\pi)^2v^4}(\Phi^\dagger\overleftrightarrow{D}_\mu\Phi)\partial^\mu\partial^\nu[\Phi^\dagger\Phi]\tfrac{\partial_\nu a}{f_a}
\end{aligned} \tag{A.13}$$

CONNECTED TO $d = 11$ OPERATORS IN THE LINEAR EXPANSION

$$\mathcal{A}_9 \longrightarrow -\tfrac{i}{2\pi v^6}(\Phi^\dagger D_\mu\Phi)(\Phi^\dagger D^\mu\Phi)(\Phi^\dagger D_\nu\Phi)\tfrac{\partial^\nu a}{f_a} \tag{A.14}$$

This shows that operators of the linear expansion up to $d = 11$ "collapse" into NLO or LO operators of the chiral one. Note that the leading corrections of the non-linear bosonic set encompass 1 (2 derivatives) + 20 (4 derivatives) = 21 couplings while the linear $d = 5$ level has only 4.

A.4 EFFECTS OF FIELDS REDEFINITIONS

The field redefinitions performed to remove the a-Z two-point function stemming from the operator $\mathbf{O}_{a\Phi}$ in the linear EFT, Eq. (3.57), and from its sibling $\mathcal{A}_{2D}$ in the chiral EFT, Eq. (6.4), can be generalized. The effects of generic redefinitions of the GB matrix $\mathbf{U}$ and of fermionic fields in both the linear and chiral cases will be discussed and compared next.

A.4.1 *Chiral EFT*

In the chiral EFT case, the most general redefinition of the GB matrix $\mathbf{U}$ and of fermionic fields can be schematically written as:

$$\mathbf{U} \to \mathbf{U} \exp\left\{ i x_U \frac{a}{f_a} \sigma^3 \right\}, \tag{A.15a}$$

$$\psi_L \to \exp\left\{ i x_{\psi L} \frac{a}{f_a} \right\} \psi_L, \qquad \psi = \{Q,\, L\}, \tag{A.15b}$$

$$Q_R \to \exp\left\{ i \left((x_{uR} + x_{dR}) \frac{\mathbf{1}}{2} + (x_{uR} - x_{dR}) \frac{\sigma^3}{2} \right) \frac{a}{f_a} \right\} Q_R, \tag{A.15c}$$

$$L_R \to \exp\left\{ i x_{eR} \frac{(\mathbf{1} - \sigma^3)}{2} \frac{a}{f_a} \right\} L_R. \tag{A.15d}$$

Although the parameters $x_{\psi L,R}$ are generically 3×3 hermitian matrices in flavor space, they will be taken to be flavor universal, $x_{\psi L,R} \equiv x_{\psi L,R} \mathbb{1}$. Moreover, without loss of generality, all the arbitrary x_i parameters are taken to be real, and $f = v$ will be assumed in oder to simplify the notation.

Applying the redefinitions in Eq. (A.15) on the leading order Lagrangian $\mathcal{L}^{LO}_{HEFT}$ in Eq. (**??**) leads to additional terms:

$$\mathcal{L}^{LO}_{HEFT} \to \mathcal{L}^{LO}_{HEFT} + \Delta\mathcal{L}^{LO}_{HEFT}, \tag{A.16}$$

with

$$\begin{aligned}
\Delta\mathcal{L}^{LO}_{HEFT} = &- \frac{i v^2}{2} x_U \mathrm{Tr}(\mathbf{T}\mathbf{V}_\mu) \frac{\partial^\mu a}{f_a} \mathcal{F}_C(h) + \\
&- \frac{v}{2\sqrt{2}} \frac{i a}{f_a} \Big[\bar{Q}_L \mathcal{Y}_Q(h) \mathbf{U} \sigma^3 Q_R \, (2x_U + x_{uR} - x_{dR}) + \bar{Q}_L \mathcal{Y}_Q(h) \mathbf{U} Q_R \, (x_{uR} + x_{dR} - 2x_{QL}) + \\
&\qquad + \bar{L}_L \mathcal{Y}_L(h) \mathbf{U} \sigma^3 L_R \, (2x_U - x_{eR}) + \bar{L}_L \mathcal{Y}_L(h) \mathbf{U} L_R \, (x_{eR} - 2x_{LL}) + \mathrm{h.c.} \Big] + \\
&+ \frac{\partial_\mu a}{f_a} \Big[(\bar{Q}_L \gamma^\mu Q_L) \, (x_{QL} - x_{uR} - x_{dR}) + (\bar{L}_L \gamma^\mu L_L) \, (x_{LL} - x_{eR}) \Big] + \\
&- \frac{\alpha_1}{8\pi} B_{\mu\nu} \tilde{B}^{\mu\nu} \frac{a}{f_a} \sum \left(\frac{1}{3} x_{QL} - \frac{8}{3} x_{uR} - \frac{2}{3} x_{dR} + x_{LL} - 2x_{eR} \right) + \\
&- \frac{\alpha_2}{8\pi} W^a_{\mu\nu} \tilde{W}^{a\mu\nu} \frac{a}{f_a} \sum \left(3x_{QL} + x_{LL} \right) + \\
&- \frac{\alpha_3}{8\pi} G^a_{\mu\nu} \tilde{G}^{a\mu\nu} \frac{a}{f_a} \sum \left(2x_{QL} - x_{uR} - x_{dR} \right),
\end{aligned} \tag{A.17}$$

where $\alpha_i \equiv g_i^2/4\pi$. The contributions in the last three lines, proportional to $aX_{\mu\nu}\tilde{X}^{\mu\nu}$, arise from the anomaly triangle and the sum runs over the three fermion generations. This is consistent with the result shown in Ref. [160].

The a-Z two-point function stemming from the operator $\mathcal{A}_{2D}$ can be completely removed by choosing $x_U = 2c_{2D}$: this corresponds to the procedure described in Sect. 6.1.2. In addition, it remains the freedom to choose the six fermionic transformations so as to remove two fermionic terms among $(\bar{\psi}_L\gamma_\mu\psi_L)\partial^\mu a$, $(\bar{\psi}_L\gamma_\mu\sigma^3\psi_L)\partial^\mu a$ and $ia(\bar{\psi}_L\mathbf{U}\psi_R)$. For example, requiring that

$$\begin{gathered} x_{uR} - x_{dR} = -2x_U = -x_{eR} = -2x_{LL} = -4c_{2D} \\ x_{uR} + x_{dR} - 2x_{QL} = 0 \end{gathered} \tag{A.18}$$

it results

$$\begin{aligned} \Delta\mathcal{L}^{LO}_{HEFT} = &- iv^2 c_{2D}\,\mathrm{Tr}(\mathbf{T}\mathbf{V}_\mu)\partial^\mu\frac{a}{f_a}\mathcal{F}_C(h) - 2\frac{\partial_\mu a}{f_a}c_{2D}\left(\bar{Q}_L\gamma^\mu\sigma^3 Q_L + \bar{L}_L\gamma^\mu\sigma^3 L_L\right) + \\ &+ \frac{\alpha_2}{8\pi}W^a_{\mu\nu}\tilde{W}^{a\mu\nu}\frac{a}{f_a}\sum\left(3x_{QL} + 2c_{2D}\right) + \frac{\alpha_1}{8\pi}B_{\mu\nu}\tilde{B}^{\mu\nu}\frac{a}{f_a}\sum\left(-\frac{3}{2}x_{QL} - c_{2D}\right). \end{aligned} \tag{A.19}$$

The parameter x_{QL} is still free and can be set to zero: this corresponds to recasting the impact of the a-Z two-point function into a redefinition of the coupling $c_{\tilde{W}}$ plus the insertion of the fermionic term $(\partial_\mu a)(\bar{\psi}\gamma^\mu\gamma_5\sigma^3\psi)$. This result is equivalent to that reported in Eq. (6.11).

A.4.2 *Linear EFT*

It is useful to reformulate the discussion of the previous paragraph for the linear EFT, in order to point out a few worthy differences. The most general field redefinition for this case is

$$\Phi \to \exp\{ix_\Phi\, a/f_a\}\,\Phi\,, \tag{A.20a}$$

$$\psi_L \to \exp\{ix_{\psi L}\, a/f_a\}\psi_L\,, \tag{A.20b}$$

$$\psi_R \to \exp\{ix_{\psi R}\, a/f_a\}\psi_R\,, \tag{A.20c}$$

for $\psi_L = \{Q_L, L_L\}$, $\psi_R = \{u_R, d_R, e_R\}$. As above, the fermion redefinitions generically act as 3×3 hermitian matrices in flavor space, while $x_\Phi \in \mathbb{R}$ is chosen $x_\Phi \in \mathbb{R}$. The action of these redefinitions on the LO linear Lagrangian, $\mathcal{L}_{SM}$, Eq. (3.50), is

$$\begin{aligned}
\mathcal{L}_{SM} \to \mathcal{L}_{SM} &+ \frac{ia}{f_a} \sum_{\psi=Q,L} \left[\bar{\psi}_L \check{} \left(x_\Phi \sigma^3 \mathbf{Y}_\psi + x_{\psi L} \mathbf{Y}_\psi - \mathbf{Y}_\psi x_{\psi R}\right) \psi_R + \text{h.c.}\right] + \\
&+ \sum_{\psi=u,d,e,\nu} \frac{\partial_\mu a}{2f_a} (\bar{\psi}_\alpha \gamma^\mu \gamma_5 \psi_\beta)(x_{\psi L} - x_{\psi R})_{\alpha\beta} + \\
&- i x_\Phi (\Phi^\dagger \overleftrightarrow{D}_\mu \Phi) \frac{\partial^\mu a}{f_a} + \\
&- \frac{\alpha_1}{8\pi} B_{\mu\nu} \tilde{B}^{\mu\nu} \frac{a}{f_a} \sum \left(\frac{1}{3} x_{QL} - \frac{8}{3} x_{uR} - \frac{2}{3} x_{dR} + x_{LL} - 2 x_{eR}\right) + \\
&- \frac{\alpha_2}{8\pi} W^a_{\mu\nu} \tilde{W}^{a\mu\nu} \frac{a}{f_a} \sum \left(3 x_{QL} + x_{LL}\right) + \\
&- \frac{\alpha_3}{8\pi} G^a_{\mu\nu} \tilde{G}^{a\mu\nu} \frac{a}{f_a} \sum \left(2 x_{QL} - x_{uR} - x_{dR}\right) ,
\end{aligned} \tag{A.21}$$

where $\Phi^\dagger \overleftrightarrow{D}_\mu \Phi \equiv \Phi^\dagger D_\mu \Phi - (D_\mu \Phi)^\dagger \Phi$, and the last three lines are identical to those for non-linear case, Eq. (A.17).

The parameter x_Φ can be conveniently chosen so as to remove the a-Z two-point function contained in the operator $\mathbf{O}_{a\Phi} = (\Phi^\dagger \overleftrightarrow{D}_\mu \Phi)\partial^\mu a$: this is similar to what happened in the chiral case choosing conveniently the parameter x_U. Moreover, it is also possible to choose in this linear case only one of the two axion-fermion operators (either the Yukawa-like or the vector-axial structure) by tuning the fermion field redefinitions, as described for the chiral case. For instance, focusing on the $a\bar{d}d$ vertex, it is possible to retain the structure $ia(\bar{Q}_L \Phi d_R)$ choosing $x_{QL} = x_{dR}$; alternatively, the coupling $\partial_\mu a(\bar{d}\gamma^\mu \gamma_5 d)$ can be selected setting $x_\Phi Y_D - x^T_{QL} Y_D + Y_D x_{dR} \equiv 0$.

The major difference of the impact of the field redefinitions on the linear and chiral EFTs resides instead in the Higgs couplings: while in the linear case the operator $\mathbf{O}_{a\Phi}$ is completely removed from the Lagrangian, including its couplings containing Higgs legs, this is not the case in the chiral case where only the pure a-Z two-point coupling is redefined away, as illustrated in Sect. 6.1.2, but in general not those involving the ALP, gauge bosons and Higgs legs. This follows from the fact that Higgs couplings and pure-gauge interactions are correlated in the linear case, while they are independent in the chiral one. The presence of couplings with the structure $(Z_\mu \partial^\mu a)h^n$, $n \geqslant 1$, among the dominant deviations from the SM expectations, is a smoking gun of non-linearity, as such vertices appear in the linear EFT case only at NNLO (operators with $d \geqslant 7$, see Sect. 6.2).

B

APPENDICES: NON-LINEAR HIGGS PORTAL TO DARK MATTER

B.1 FEYNMAN RULES

This Appendix provides a complete list of the Feynman rules resulting from the non-linear Higgs portal effective Lagrangian, Eq. (7.6), computed in unitary gauge and with momenta understood to flow inwards. The right column shows for comparison the Feynman rules for the case of the linear Higgs portal $\lambda_S\, S^2\,(2v h + h^2)$.

		Standard	**Non-linear**	**Linear** $d \leqslant 6$
(FR.1)	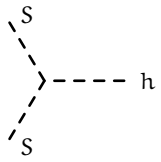	$-4i\lambda_S v$	$-4i\left(\lambda_S v + \frac{c_2 a_2 p_h^2}{v}\right)$	$-4i\left(\lambda_S v + \frac{2 v c_2^L p_h^2}{\Lambda^2}\right)$
(FR.2)	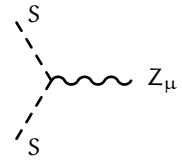	–	$\frac{2 g c_4}{c_\theta} p_Z^\mu$	$-\frac{4 v^2 g c_d^L}{c_\theta \Lambda^2} p_Z^\mu$
(FR.3)	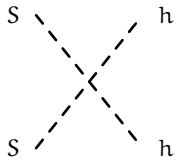	$-4i\lambda_S$	$-4i\left(\lambda_S b + \frac{c_2 b_2 (p_{h1}+p_{h2})^2}{v^2}\right)$	$-4i\left(\lambda_S + \frac{3 v^2 c_b}{2\Lambda^2} + \frac{2 c_2^L (p_{h1}+p_{h2})^2}{\Lambda^2}\right)$
(FR.4)	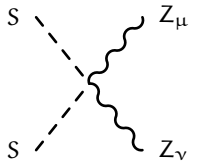	–	$-\frac{2 i g^2 (c_1+2c_3)}{c_\theta^2} g_{\mu\nu}$	$-\frac{8 v^2 i g^2 c_1^L}{c_\theta^2 \Lambda^2} g_{\mu\nu}$
(FR.5)	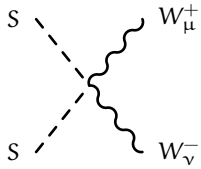	–	$-2 i g^2 c_1 g_{\mu\nu}$	$-8\frac{v^2}{\Lambda^2} i g^2 c_1^L g_{\mu\nu}$
(FR.6)	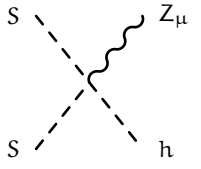	–	$\frac{4g}{v c_\theta}\left(c_4 a_4 (p_Z + p_h)^\mu - c_5 a_5 p_h^\mu\right)$	$-\frac{8 v g}{\Lambda^2 c_\theta}\left(c_4^L (p_Z + p_h)^\mu\right)$

B.2 CONTRIBUTIONS TO THE DARK MATTER RELIC ABUNDANCE

The Feynman diagrams contributing to the main Higgs portal DM annihilation processes are shown next. The labels indicate the parameters entering each vertex (see Appendix B.1 for signs and numerical factors). λ_h in B.1d stands for the SM Higgs self-coupling.

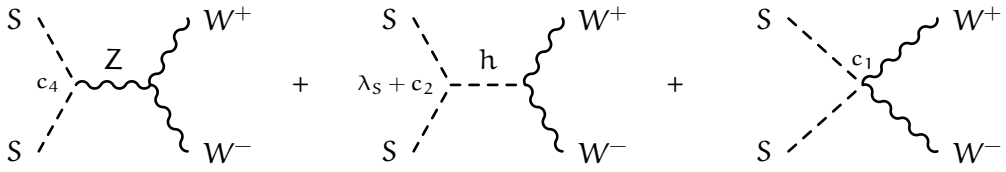

(a) Dark Matter annihilation to Higgs bosons.

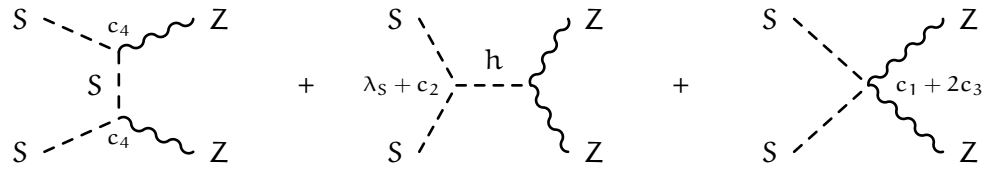

(b) Dark Matter annihilation to W bosons.

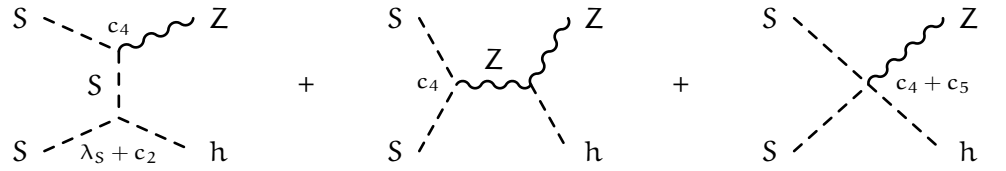

(c) Dark Matter annihilation to Z bosons.

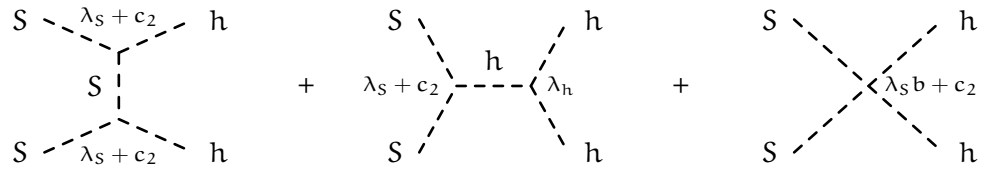

(d) Dark Matter annihilation to Z and Higgs bosons.

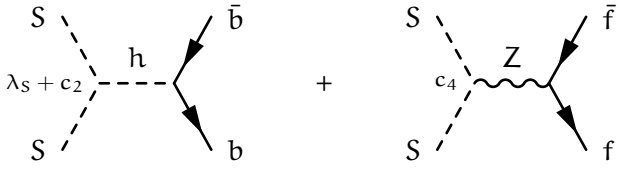

(e) Dark Matter annihilation to $f\bar{f}$.

Figure B.1: Main Higgs portal DM annihilation processes.

B.3 IMPACT OF $\mathcal{B}_1$ AND $\mathcal{B}_2$ FOR OTHER CHOICES OF c_i

The analysis of the current constraints on the parameter space of non-linear Higgs portals described in Section 7.2 is restricted to two specific non-linear setups: fixing either c_1 or c_2 to 0.1 (see Figure 7.4). Although the main features of non-linearity are quite exhaustively illustrated by these two examples, it is interesting to explore further scenarios, where the coefficients c_1 and c_2 are assigned different values in the range $[-1, 1]$. In this Appendix we show the exclusion regions obtained for $c_i = \{\pm 1, -0.1, -0.01\}$ and $c_2 = \pm 1$. These figures shall be compared with Figure 7.3, where the same constraints have been applied to the linear Higgs-portal scenario.

As a general feature, it is worth noticing that in presence of non-linearity, even conveyed by a coefficient of order 0.1 (Figures 7.4 and B.2c) or 0.01 (Figure B.2d), the space of parameters for Higgs portals is much less constrained than in the standard picture. In particular, none of the existing bounds limit the region of masses $m_S > 200\,\text{GeV}$ for couplings λ_S smaller than 1, except for small regions of the parameter space. Only a limited band within this region will be probed by the next generation of direct detection experiments (the plots show the reach of XENON1T [201]).

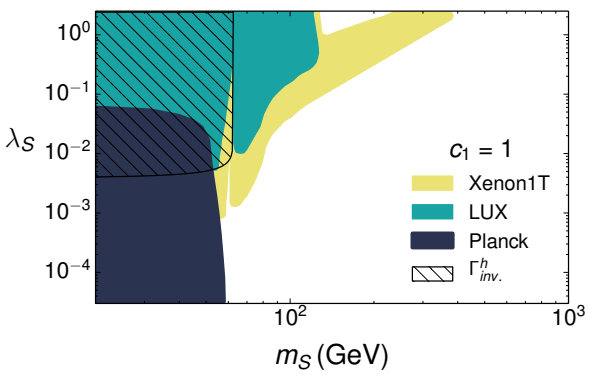

(a) $c_1 = 1$

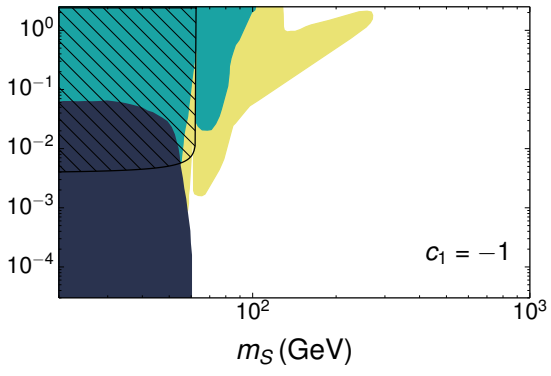

(b) $c_1 = -1$

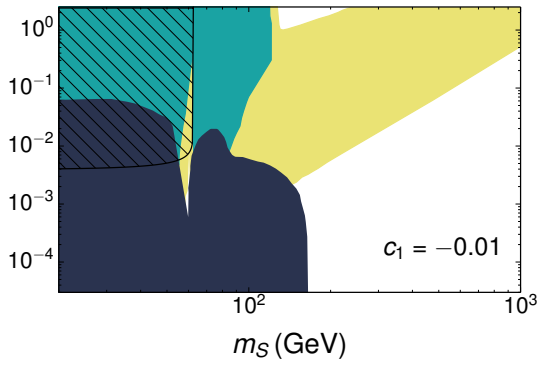

(c) $c_1 = -0.1$

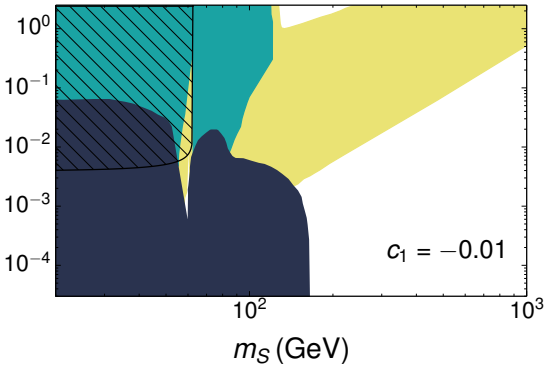

(d) $c_1 = -0.01$

Figure B.2: Results obtained considering the non-linear operator $\mathcal{B}_1$ with $\mathcal{F}_1(h) = (1 + h/v)^2$ and for different values of the coefficient c_1. The blue region is excluded by current bounds from Planck, the green one is excluded by LUX, while the area in yellow is within the projected reach of XENON1T. The black hatched region represents the bound from invisible Higgs width (same as in the linear scenario).

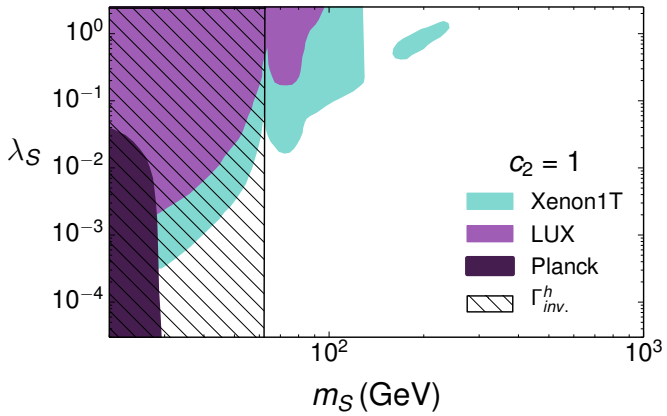

(a) $c_2 = 1$

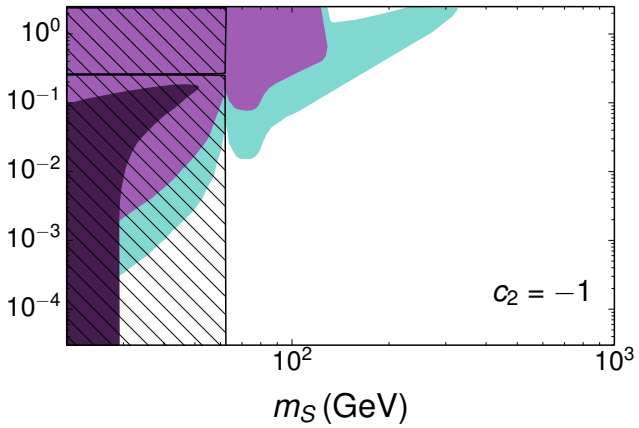

(b) $c_2 = -1$

Figure B.3: Results obtained considering the non-linear operator $\mathcal{B}_2$ with $\mathcal{F}_2(h) = (1 + h/v)^2$ and for $c_2 = \pm 1$. The darkest region is excluded by current bounds from Planck, the purple one is excluded by LUX, while the area in light blue is within the projected reach of XENON1T. The black hatched region represents the bound from invisible Higgs width.

BIBLIOGRAPHY

[1] I. Brivio, M. B. Gavela, L. Merlo, K. Mimasu, J. M. No, R. del Rey, and V. Sanz. "Non-Linear Higgs Portal to Dark Matter." In: *JHEP* 04 (2016), p. 141. DOI: 10.1007/JHEP04(2016)141. arXiv: 1511.01099 [hep-ph].

[2] I. Brivio, M. B. Gavela, L. Merlo, K. Mimasu, J. M. No, R. del Rey, and V. Sanz. "ALPs Effective Field Theory and Collider Signatures." In: *Eur. Phys. J.* C77.8 (2017), p. 572. DOI: 10.1140/epjc/s10052-017-5111-3. arXiv: 1701.05379 [hep-ph].

[3] I. Brivio, M. B. Gavela, S. Pascoli, R. del Rey, and S. Saa. "The Axion and the Goldstone Higgs." In: (2017). arXiv: 1710.07715 [hep-ph].

[4] Rocío del Rey Bajo. "Non-linear Higgs portal to Dark Matter." In: *Proceedings, 51st Rencontres de Moriond on Electroweak Interactions and Unified Theories: La Thuile, Italy, March 12-19, 2016*. 2016, pp. 619–622. arXiv: 1605.06388 [hep-ph]. URL: http://inspirehep.net/record/1463294/files/arXiv:1605.06388.pdf.

[5] Rocio del Rey. "ALPs EFT & Collider Signatures." In: *13th Patras Workshop on Axions, WIMPs and WISPs (AXION-WIMP 2017) CHALKIDIKI TBC, GREECE, May 15-19, 2017*. 2017. arXiv: 1711.04517 [hep-ph]. URL: https://inspirehep.net/record/1635920/files/arXiv:1711.04517.pdf.

[6] Gerard 't Hooft. "Naturalness, chiral symmetry, and spontaneous chiral symmetry breaking." In: *NATO Sci. Ser. B* 59 (1980), pp. 135–157. DOI: 10.1007/978-1-4684-7571-5_9.

[7] R. D. Peccei and Helen R. Quinn. "CP Conservation in the Presence of Instantons." In: *Phys. Rev. Lett.* 38 (1977), pp. 1440–1443. DOI: 10.1103/PhysRevLett.38.1440.

[8] David B. Kaplan and Howard Georgi. "SU(2) $\times$ U(1) Breaking by Vacuum Misalignment." In: *Phys. Lett.* B136 (1984), pp. 183–186. DOI: 10.1016/0370-2693(84)91177-8.

[9] Jihn E. Kim. "Weak Interaction Singlet and Strong CP Invariance." In: *Phys.Rev.Lett.* 43 (1979), p. 103. DOI: 10.1103/PhysRevLett.43.103.

[10] Mikhail A. Shifman, A. I. Vainshtein, and Valentin I. Zakharov. "Can Confinement Ensure Natural CP Invariance of Strong Interactions?" In: *Nucl. Phys.* B166 (1980), pp. 493–506. DOI: 10.1016/0550-3213(80)90209-6.

[11] W. Buchmuller and D. Wyler. "Effective Lagrangian Analysis of New Interactions and Flavor Conservation." In: *Nucl. Phys.* B268 (1986), pp. 621–653. DOI: 10.1016/0550-3213(86)90262-2.

[12] B. Grzadkowski, M. Iskrzynski, M. Misiak, and J. Rosiek. "Dimension-Six Terms in the Standard Model Lagrangian." In: *JHEP* 10 (2010), p. 085. DOI: 10.1007/JHEP10(2010)085. arXiv: 1008.4884 [hep-ph].

[13] Roberto Contino. "The Higgs as a Composite Nambu-Goldstone Boson." In: *Physics of the Large and the Small, Tasi 09, Proceedings of the Theoretical Advanced Study Institute in Elementary Particle Physics, Boulder, Colorado, Usa, 1-26 June 2009*. 2011, pp. 235–306. DOI: 10.1142/9789814327183_0005. arXiv: 1005.4269 [hep-ph]. URL: http://inspirehep.net/record/856065/files/arXiv:1005.4269.pdf.

[14] R. Alonso, M. B. Gavela, L. Merlo, S. Rigolin, and J. Yepes. "The Effective Chiral Lagrangian for a Light Dynamical "Higgs Particle"." In: *Phys. Lett.* B722 (2013). [Erratum: Phys. Lett.B726,926(2013)], pp. 330–335. DOI: 10.1016/j.physletb.2013.04.037,10.1016/j.physletb.2013.09.028. arXiv: 1212.3305 [hep-ph].

[15] I. Brivio, J. Gonzalez-Fraile, M. C. Gonzalez-Garcia, and L. Merlo. "The Complete Heft Lagrangian After the LHC Run I." In: (2016). arXiv: 1604.06801 [hep-ph].

[16] Howard Georgi, David B. Kaplan, and Lisa Randall. "Manifesting the Invisible Axion at Low-energies." In: *Phys.Lett.* B169 (1986), p. 73. DOI: 10.1016/0370-2693(86)90688-X.

[17] Eder Izaguirre, Tongyan Lin, and Brian Shuve. "A New Flavor of Searches for Axion-Like Particles." In: (2016). arXiv: 1611.09355 [hep-ph].

[18] Joerg Jaeckel and Michael Spannowsky. "Probing MeV to 90 GeV Axion-Like Particles with Lep and Lhc." In: *Phys. Lett.* B753 (2016), pp. 482–487. DOI: 10.1016/j.physletb.2015.12.037. arXiv: 1509.00476 [hep-ph].

[19] Brian Patt and Frank Wilczek. "Higgs-Field Portal into Hidden Sectors." In: (2006). arXiv: hep-ph/0605188 [hep-ph].

[20] Serguei Chatrchyan et al. "Observation of a new boson at a mass of 125 GeV with the CMS experiment at the LHC." In: *Phys. Lett.* B716 (2012), pp. 30–61. DOI: 10.1016/j.physletb.2012.08.021. arXiv: 1207.7235 [hep-ex].

[21] Georges Aad et al. "Observation of a new particle in the search for the Standard Model Higgs boson with the ATLAS detector at the LHC." In: *Phys. Lett.* B716 (2012), pp. 1–29. DOI: 10.1016/j.physletb.2012.08.020. arXiv: 1207.7214 [hep-ex].

[22] V. L. Ginzburg and L. D. Landau. "On the Theory of Superconductivity." In: *Zh. Eksp. Teor. Fiz.* 20 (1950), pp. 1064–1082.

[23] Yoichiro Nambu. "Quasiparticles and Gauge Invariance in the Theory of Superconductivity." In: *Phys. Rev.* 117 (1960), pp. 648–663. DOI: 10.1103/PhysRev.117.648.

[24] J. Goldstone. "Field Theories with Superconductor Solutions." In: *Nuovo Cim.* 19 (1961), pp. 154–164. DOI: 10.1007/BF02812722.

[25] Jeffrey Goldstone, Abdus Salam, and Steven Weinberg. "Broken Symmetries." In: *Phys. Rev.* 127 (1962), pp. 965–970. DOI: 10.1103/PhysRev.127.965.

[26] F. Englert and R. Brout. "Broken Symmetry and the Mass of Gauge Vector Mesons." In: *Phys. Rev. Lett.* 13 (1964), pp. 321–323. DOI: 10.1103/PhysRevLett.13.321.

[27] Peter W. Higgs. "Broken Symmetries and the Masses of Gauge Bosons." In: *Phys. Rev. Lett.* 13 (1964), pp. 508–509. DOI: 10.1103/PhysRevLett.13.508.

[28] G. S. Guralnik, C. R. Hagen, and T. W. B. Kibble. "Global Conservation Laws and Massless Particles." In: *Phys. Rev. Lett.* 13 (1964), pp. 585–587. DOI: 10.1103/PhysRevLett.13.585.

[29] Steven Weinberg. "A Model of Leptons." In: *Phys. Rev. Lett.* 19 (1967), pp. 1264–1266. DOI: 10.1103/PhysRevLett.19.1264.

[30] Abdus Salam. "Weak and Electromagnetic Interactions." In: *Conf. Proc.* C680519 (1968), pp. 367–377.

[31] S.L. Glashow. "Partial Symmetries of Weak Interactions." In: *Nucl.Phys.* 22 (1961), pp. 579–588. DOI: 10.1016/0029-5582(61)90469-2.

[32] Gerard 't Hooft and M. J. G. Veltman. "Regularization and Renormalization of Gauge Fields." In: *Nucl. Phys.* B44 (1972), pp. 189–213. DOI: 10.1016/0550-3213(72)90279-9.

[33] C. Patrignani et al. "Review of Particle Physics." In: *Chin. Phys.* C40.10 (2016), p. 100001. DOI: 10.1088/1674-1137/40/10/100001.

[34] Nicola Cabibbo. "Unitary Symmetry and Leptonic Decays." In: *Phys. Rev. Lett.* 10 (1963). [,648(1963)], pp. 531–533. DOI: 10.1103/PhysRevLett.10.531.

[35] Makoto Kobayashi and Toshihide Maskawa. "CP Violation in the Renormalizable Theory of Weak Interaction." In: *Prog. Theor. Phys.* 49 (1973), pp. 652–657. DOI: 10.1143/PTP.49.652.

[36] B. Pontecorvo. "Inverse beta processes and nonconservation of lepton charge." In: *Sov. Phys. JETP* 7 (1958). [Zh. Eksp. Teor. Fiz.34,247(1957)], pp. 172–173.

[37] Ziro Maki, Masami Nakagawa, and Shoichi Sakata. "Remarks on the unified model of elementary particles." In: *Prog. Theor. Phys.* 28 (1962), pp. 870–880. DOI: 10.1143/PTP.28.870.

[38] Georges Aad et al. "Combined Measurement of the Higgs Boson Mass in pp Collisions at $\sqrt{s} = 7$ and 8 TeV with the ATLAS and CMS Experiments." In: *Phys. Rev. Lett.* 114 (2015), p. 191803. DOI: 10.1103/PhysRevLett.114.191803. arXiv: 1503.07589 [hep-ex].

[39] Eldad Gildener. "Gauge Symmetry Hierarchies." In: *Phys. Rev.* D14 (1976), p. 1667. DOI: 10.1103/PhysRevD.14.1667.

[40] Steven Weinberg. "Gauge Hierarchies." In: *Phys. Lett.* 82B (1979), pp. 387–391. DOI: 10.1016/0370-2693(79)90248-X.

[41] Leonard Susskind. "Dynamics of Spontaneous Symmetry Breaking in the Weinberg-Salam Theory." In: *Phys. Rev.* D20 (1979), pp. 2619–2625. DOI: 10.1103/PhysRevD.20.2619.

[42] Kenneth G. Wilson. "The Renormalization Group and Strong Interactions." In: *Phys. Rev.* D3 (1971), p. 1818. DOI: 10.1103/PhysRevD.3.1818.

[43] Gian Francesco Giudice. "Naturally Speaking: the Naturalness Criterion and Physics at the Lhc." In: (2008). DOI: 10.1142/9789812779762_0010. arXiv: 0801.2562 [hep-ph].

[44] M. K. Gaillard and Benjamin W. Lee. "Rare Decay Modes of the K-Mesons in Gauge Theories." In: *Phys. Rev.* D10 (1974), p. 897. DOI: 10.1103/PhysRevD.10.897.

[45] S. L. Glashow, J. Iliopoulos, and L. Maiani. "Weak Interactions with Lepton-Hadron Symmetry." In: *Phys. Rev.* D2 (1970), pp. 1285–1292. DOI: 10.1103/PhysRevD.2.1285.

[46] O. M. Bilaniuk and E. C. G. Sudarshan. "Particles Beyond the Light Barrier." In: *Phys. Today* 22N5 (1969), pp. 43–51. DOI: 10.1063/1.3035574.

[47] Steven Weinberg. "Implications of Dynamical Symmetry Breaking." In: *Phys. Rev.* D13 (1976). [Addendum: Phys. Rev.D19,1277(1979)], pp. 974–996. DOI: 10.1103/PhysRevD.19.1277,10.1103/PhysRevD.13.974.

[48] Aneesh Manohar and Howard Georgi. "Chiral Quarks and the Nonrelativistic Quark Model." In: *Nucl.Phys.* B234 (1984), p. 189. DOI: 10.1016/0550-3213(84)90231-1.

[49] David B. Kaplan and Howard Georgi. "SU(2) x U(1) Breaking by Vacuum Misalignment." In: *Phys.Lett.* B136 (1984), p. 183. DOI: 10.1016/0370-2693(84)91177-8.

[50] David B. Kaplan, Howard Georgi, and Savas Dimopoulos. "Composite Higgs Scalars." In: *Phys. Lett.* B136 (1984), p. 187. DOI: 10.1016/0370-2693(84)91178-X.

[51] Tom Banks. "CONSTRAINTS ON SU(2) x U(1) BREAKING BY VACUUM MISALIGNMENT." In: *Nucl.Phys.* B243 (1984), p. 125. DOI: 10.1016/0550-3213(84)90389-4.

[52] Howard Georgi, David B. Kaplan, and Peter Galison. "Calculation of the Composite Higgs Mass." In: *Phys.Lett.* B143 (1984), p. 152. DOI: 10.1016/0370-2693(84)90823-2.

[53] Howard Georgi and David B. Kaplan. "Composite Higgs and Custodial SU(2)." In: *Phys.Lett.* B145 (1984), p. 216. DOI: 10.1016/0370-2693(84)90341-1.

[54] Kaustubh Agashe, Roberto Contino, and Alex Pomarol. "The Minimal Composite Higgs Model." In: *Nucl. Phys.* B719 (2005), pp. 165–187. DOI: 10.1016/j.nuclphysb.2005.04.035. arXiv: hep-ph/0412089 [hep-ph].

[55] Rodrigo Alonso, Ilaria Brivio, Belen Gavela, Luca Merlo, and Stefano Rigolin. "Sigma Decomposition." In: (2014). arXiv: 1409.1589 [hep-ph].

[56] Roberto Contino, Leandro Da Rold, and Alex Pomarol. "Light Custodians in Natural Composite Higgs Models." In: *Phys. Rev.* D75 (2007), p. 055014. DOI: 10.1103/PhysRevD.75.055014. arXiv: hep-ph/0612048 [hep-ph].

[57] Aneesh Manohar and Howard Georgi. "Chiral Quarks and the Nonrelativistic Quark Model." In: *Nucl. Phys.* B234 (1984), pp. 189–212. DOI: 10.1016/0550-3213(84)90231-1.

[58] Riccardo Barbieri, B. Bellazzini, Vyacheslav S. Rychkov, and Alvise Varagnolo. "The Higgs Boson from an Extended Symmetry." In: *Phys. Rev.* D76 (2007), p. 115008. DOI: 10.1103/PhysRevD.76.115008. arXiv: 0706.0432 [hep-ph].

[59] Ferruccio Feruglio, Belen Gavela, Kirill Kanshin, Pedro Accioly Nogueira Machado, Stefano Rigolin, and Sara Saa. "The Minimal Linear Sigma Model for the Goldstone Higgs." In: *JHEP* 06 (2016), p. 038. DOI: 10.1007/JHEP06(2016)038. arXiv: 1603.05668 [hep-ph].

[60] Steven Weinberg. "Baryon and Lepton Nonconserving Processes." In: *Phys. Rev. Lett.* 43 (1979), pp. 1566–1570. DOI: 10.1103/PhysRevLett.43.1566.

[61] F. Gürsey. "On the symmetries of strong and weak interactions." In: *Il Nuovo Cimento* 16.2 (1960), pp. 230–240. ISSN: 0029-6341. DOI: 10.1007/BF02860276. URL: http://dx.doi.org/10.1007/BF02860276.

[62] Thomas Appelquist and Claude W. Bernard. "Strongly Interacting Higgs Bosons." In: *Phys. Rev.* D22 (1980), p. 200. DOI: 10.1103/PhysRevD.22.200.

[63] Anthony C. Longhitano. "Heavy Higgs Bosons in the Weinberg-Salam Model." In: *Phys. Rev.* D22 (1980), p. 1166. DOI: 10.1103/PhysRevD.22.1166.

[64] Anthony C. Longhitano. "Low-Energy Impact of a Heavy Higgs Boson Sector." In: *Nucl. Phys.* B188 (1981), p. 118. DOI: 10.1016/0550-3213(81)90109-7.

[65] F. Feruglio. "The Chiral Approach to the Electroweak Interactions." In: *Int. J. Mod. Phys.* A8 (1993), pp. 4937–4972. DOI: 10.1142/S0217751X93001946. arXiv: hep-ph/9301281 [hep-ph].

[66] R. Alonso, M.B. Gavela, L. Merlo, S. Rigolin, and J. Yepes. "Minimal Flavour Violation with Strong Higgs Dynamics." In: *JHEP* 1206 (2012), p. 076. DOI: 10.1007/JHEP06(2012)076. arXiv: 1201.1511 [hep-ph].

[67] Aleksandr Azatov, Roberto Contino, and Jamison Galloway. "Model-Independent Bounds on a Light Higgs." In: *JHEP* 04 (2012). [Erratum: JHEP04,140(2013)], p. 127. DOI: 10.1007/JHEP04(2012)127,10.1007/JHEP04(2013)140. arXiv: 1202.3415 [hep-ph].

[68] R. Alonso, M. B. Gavela, L. Merlo, S. Rigolin, and J. Yepes. "Flavor with a Light Dynamical "Higgs Particle"." In: *Phys. Rev.* D87.5 (2013), p. 055019. DOI: 10.1103/PhysRevD.87.055019. arXiv: 1212.3307 [hep-ph].

[69] Gerhard Buchalla, Oscar Cata, and Claudius Krause. "Complete Electroweak Chiral Lagrangian with a Light Higgs at NLO." In: *Nucl. Phys.* B880 (2015). [Erratum: Nucl. Phys.B915,475(2016)], pp. 552–573. DOI: 10.1017/j.nuclphysb.2017.09.010,10.1017/j.nuclphysb.2015.01.018. arXiv: 1507.5017 [hep-ph].

[70] I. Brivio, T. Corbett, O. J. P. Eboli, M. B. Gavela, J. Gonzalez-Fraile, M. C. Gonzalez-Garcia, L. Merlo, and S. Rigolin. "Disentangling a Dynamical Higgs." In: *JHEP* 03 (2014), p. 024. DOI: 10.1007/JHEP03(2014)024. arXiv: 1311.1823 [hep-ph].

[71] M.B. Gavela, J. Gonzalez-Fraile, M.C. Gonzalez-Garcia, L. Merlo, S. Rigolin, et al. "CP Violation with a Dynamical Higgs." In: *JHEP* 1410 (2014), p. 44. DOI: 10.1007/JHEP10(2014)044. arXiv: 1406.6367 [hep-ph].

[72] M. B. Gavela, K. Kanshin, P. A. N. Machado, and S. Saa. "On the Renormalization of the Electroweak Chiral Lagrangian with a Higgs." In: *JHEP* 03 (2015), p. 043. DOI: 10.1007/JHEP03(2015)043. arXiv: 1409.1571 [hep-ph].

[73] I. Brivio, O. J. P. Eboli, M. B. Gavela, M. C. Gonzalez-Garcia, L. Merlo, and S. Rigolin. "Higgs Ultraviolet Softening." In: *JHEP* 12 (2014), p. 004. DOI: 10.1007/JHEP12(2014)004. arXiv: 1405.5412 [hep-ph].

[74] Rodrigo Alonso, Ilaria Brivio, Belen Gavela, Luca Merlo, and Stefano Rigolin. "Sigma Decomposition." In: *JHEP* 1412 (2014), p. 034. DOI: 10.1007/JHEP12(2014)034. arXiv: 1409.1589 [hep-ph].

[75] I. M. Hierro, L. Merlo, and S. Rigolin. "Sigma Decomposition: the CP-Odd Lagrangian." In: *JHEP* 04 (2016), p. 016. DOI: 10.1007/JHEP04(2016)016. arXiv: 1510.07899 [hep-ph].

[76] Luca Merlo, Sara Saa, and Mario Sacristan Barbero. "Baryon Non-Invariant Couplings in Higgs Effective Field Theory." In: (2016). arXiv: 1612.04832 [hep-ph].

[77] Thomas Appelquist and Claude W. Bernard. "Strongly Interacting Higgs Bosons." In: *Phys. Rev.* D22 (1980), p. 200. DOI: 10.1103/PhysRevD.22.200.

[78] Anthony C. Longhitano. "Heavy Higgs Bosons in the Weinberg-Salam Model." In: *Phys. Rev.* D22 (1980), p. 1166. DOI: 10.1103/PhysRevD.22.1166.

[79] Anthony C. Longhitano. "Low-Energy Impact of a Heavy Higgs Boson Sector." In: *Nucl. Phys.* B188 (1981), pp. 118–154. DOI: 10.1016/0550-3213(81)90109-7.

[80] Benjamin Grinstein and Michael Trott. "A Higgs-Higgs Bound State Due to New Physics at a TeV." In: *Phys. Rev.* D76 (2007), p. 073002. DOI: 10.1103/PhysRevD.76.073002. arXiv: 0704.1505 [hep-ph].

[81] Steven Weinberg. "Phenomenological Lagrangians." In: *Physica* A96 (1979), pp. 327–340. DOI: 10.1016/0378-4371(79)90223-1.

[82] Markus A. Luty. "Naive Dimensional Analysis and Supersymmetry." In: *Phys. Rev.* D57 (1998), pp. 1531–1538. DOI: 10.1103/PhysRevD.57.1531. arXiv: hep-ph/9706235 [hep-ph].

[83] Andrew G. Cohen, David B. Kaplan, and Ann E. Nelson. "Counting 4 Pis in Strongly Coupled Supersymmetry." In: *Phys. Lett.* B412 (1997), pp. 301–308. DOI: 10.1016/S0370-2693(97)00995-7. arXiv: hep-ph/9706275 [hep-ph].

[84] B. M. Gavela, E. E. Jenkins, A. V. Manohar, and L. Merlo. "Analysis of General Power Counting Rules in Effective Field Theory." In: (2016). arXiv: 1601.07551 [hep-ph].

[85] G. F. Giudice, C. Grojean, A. Pomarol, and R. Rattazzi. "The Strongly-Interacting Light Higgs." In: *JHEP* 06 (2007), p. 045. DOI: 10.1088/1126-6708/2007/06/045. arXiv: hep-ph/0703164 [hep-ph].

[86] David B. Kaplan, Howard Georgi, and Savas Dimopoulos. "Composite Higgs Scalars." In: *Phys. Lett.* B136 (1984), pp. 187–190. DOI: 10.1016/0370-2693(84)91178-X.

[87] Tom Banks. "Constraints on SU(2) × U(1) Breaking by Vacuum Misalignment." In: *Nucl. Phys.* B243 (1984), pp. 125–130. DOI: 10.1016/0550-3213(84)90389-4.

[88] Roberto Contino, Christophe Grojean, Mauro Moretti, Fulvio Piccinini, and Riccardo Rattazzi. "Strong Double Higgs Production at the Lhc." In: *JHEP* 05 (2010), p. 089. DOI: 10.1007/JHEP05(2010)089. arXiv: 1002.1011 [hep-ph].

[89] Juan Yepes. "Spin-1 Resonances in a Non-Linear Left-Right Dynamical Higgs Context." In: *PoS* CORFU2015 (2016), p. 063. arXiv: 1507.03974 [hep-ph].

[90] Kun-Ming Ruan, Jing Shu, and Juan Yepes. "CP Violation from Spin-1 Resonances in a Left-Right Dynamical Higgs Context." In: *Commun. Theor. Phys.* 66.1 (2016), pp. 93–103. DOI: 10.1088/0253-6102/66/1/093. arXiv: 1507.04745 [hep-ph].

[91] Steven Weinberg. "The U(1) Problem." In: *Phys. Rev.* D11 (1975), pp. 3583–3593. DOI: 10.1103/PhysRevD.11.3583.

[92] Steven Weinberg. "The U(1) Problem." In: *Phys. Rev.* D11 (1975), pp. 3583–3593. DOI: 10.1103/PhysRevD.11.3583.

[93] Gerard 't Hooft. "How Instantons Solve the U(1) Problem." In: *Phys. Rept.* 142 (1986), pp. 357–387. DOI: 10.1016/0370-1573(86)90117-1.

[94] Steven Weinberg. *The Quantum Theory of Fields. Vol. 2: Modern Applications*. Cambridge University Press, 2013. ISBN: 9781139632478, 9780521670548, 9780521550024.

[95] Jihn E. Kim. "Light Pseudoscalars, Particle Physics and Cosmology." In: *Phys. Rept.* 150 (1987), pp. 1–177. DOI: 10.1016/0370-1573(87)90017-2.

[96] Gerard 't Hooft. "Symmetry Breaking Through Bell-Jackiw Anomalies." In: *Phys. Rev. Lett.* 37 (1976), pp. 8–11. DOI: 10.1103/PhysRevLett.37.8.

[97] Gerard 't Hooft. "Computation of the Quantum Effects Due to a Four-Dimensional Pseudoparticle." In: *Phys. Rev.* D14 (1976). [Erratum: Phys. Rev.D18,2199(1978)], pp. 3432–3450. DOI: 10.1103/PhysRevD.18.2199.3,10.1103/PhysRevD.14.3432.

[98] Stephen L. Adler. "Axial Vector Vertex in Spinor Electrodynamics." In: *Phys. Rev.* 177 (1969), pp. 2426–2438. DOI: 10.1103/PhysRev.177.2426.

[99] J. S. Bell and R. Jackiw. "A PCAC Puzzle: Pio –≫ Gamma Gamma in the Sigma Model." In: *Nuovo Cim.* A60 (1969), pp. 47–61. DOI: 10.1007/BF02823296.

[100] William A. Bardeen. "Anomalous Ward Identities in Spinor Field Theories." In: *Phys. Rev.* 184 (1969), pp. 1848–1857. DOI: 10.1103/PhysRev.184.1848.

[101] Varouzhan Baluni. "CP Violating Effects in QCD." In: *Phys. Rev.* D19 (1979), pp. 2227–2230. DOI: 10.1103/PhysRevD.19.2227.

[102] R.J. Crewther, P. Di Vecchia, G. Veneziano, and Edward Witten. "Chiral Estimate of the Electric Dipole Moment of the Neutron in Quantum Chromodynamics." In: *Phys.Lett.* B88 (1979), p. 123. DOI: 10.1016/0370-2693(79)90128-X.

[103] Kazuyuki Kanaya and Makoto Kobayashi. "Strong Cp Violation in the Chiral σ Model." In: *Prog. Theor. Phys.* 66 (1981), p. 2173. DOI: 10.1143/PTP.66.2173.

[104] Howard J. Schnitzer. "The Soft Pion Skyrmion Lagrangian and Strong Cp Violation." In: *Phys. Lett.* 139B (1984), pp. 217–222. DOI: 10.1016/0370-2693(84)91248-6.

[105] P. Cea and G. Nardulli. "A Realistic Calculation of the Electric Dipole Moment of the Neutron Induced by Strong Cp Violation." In: *Phys. Lett.* 144B (1984), pp. 115–118. DOI: 10.1016/0370-2693(84)90187-4.

[106] M. M. Musakhanov and Z. Z. Israilov. "The Electric Dipole Moment of the Neutron in the Chiral Bag Model." In: *Phys. Lett.* 137B (1984), pp. 419–421. DOI: 10.1016/0370-2693(84)91747-7.

[107] Michael A. Morgan and Gerald A. Miller. "The Neutron Electric Dipole Moment in the Cloudy Bag Model." In: *Phys. Lett.* B179 (1986), pp. 379–384. DOI: 10.1016/0370-2693(86)90497-1.

[108] Jihn E. Kim and Gianpaolo Carosi. "Axions and the Strong CP Problem." In: *Rev. Mod. Phys.* 82 (2010), pp. 557–602. DOI: 10.1103/RevModPhys.82.557. arXiv: 0807.3125 [hep-ph].

[109] K. A. Olive et al. "Review of Particle Physics." In: *Chin. Phys.* C38 (2014), p. 090001. DOI: 10.1088/1674-1137/38/9/090001.

[110] J. Tran Thanh Van, ed. *Flavor Mixing and CP Violation. Proceedings, 5Th Moriond Workshop, La Plagne, France, January 13-19, 1985*. Ed. Frontieres. Gif-Sur-Yvette: Ed. Frontieres, 1985. URL: http://inspirehep.net/record/225470/files/C85-01-13_Proceedings.pdf.

[111] John R. Ellis, Mary K. Gaillard, and Dimitri V. Nanopoulos. "Lefthanded Currents and CP Violation." In: *Nucl. Phys.* B109 (1976), pp. 213–243. DOI: 10.1016/0550-3213(76)90203-0.

[112] John R. Ellis and Mary K. Gaillard. "Strong and Weak CP Violation." In: *Nucl. Phys.* B150 (1979), pp. 141–162. DOI: 10.1016/0550-3213(79)90297-9.

[113] E. P. Shabalin. "Electric Dipole Moment of Quark in a Gauge Theory with Left-Handed Currents." In: *Sov. J. Nucl. Phys.* 28 (1978). [Yad. Fiz.28,151(1978)], p. 75.

[114] E. P. Shabalin. "Electric Dipole Moment of Quark in the Kobayashi-Maskawa Theory with Account of the Gluonic Corrections. (In Russian)." In: *Yad. Fiz.* 31 (1980), pp. 1665–1679.

[115] D.V. Nanopoulos, Asim Yildiz, and Paul H. Cox. "On the electric dipole moment of the neutron." In: *Physics Letters B* 87.1â2 (1979), pp. 53 –56. ISSN: 0370-2693. DOI: http://dx.doi.org/10.1016/0370-2693(79)90016-9. URL: http://www.sciencedirect.com/science/article/pii/0370269379900169.

[116] M.B. Gavela, A. Le Yaouanc, L. Oliver, O. Pene, J.C. Raynal, et al. "CP Violation Induced by Penguin Diagrams and the Neutron Electric Dipole Moment." In: *Phys.Lett.* B109 (1982), p. 215. DOI: 10.1016/0370-2693(82)90756-0.

[117] John R. Ellis, Sergio Ferrara, and Dimitri V. Nanopoulos. "CP Violation and Supersymmetry." In: *Phys.Lett.* B114 (1982), p. 231. DOI: 10.1016/0370-2693(82)90484-1.

[118] W. Buchmuller and D. Wyler. "CP Violation and R Invariance in Supersymmetric Models of Strong and Electroweak Interactions." In: *Phys.Lett.* B121 (1983), p. 321. DOI: 10.1016/0370-2693(83)91378-3.

[119] Pran Nath. "CP." In: *Phys. Rev. Lett.* 66 (20 1991), pp. 2565–2568. DOI: 10.1103/PhysRevLett.66.2565. URL: http://link.aps.org/doi/10.1103/PhysRevLett.66.2565.

[120] Tarek Ibrahim and Pran Nath. "The Neutron and the lepton EDMs in MSSM, large CP violating phases, and the cancellation mechanism." In: *Phys.Rev.* D58 (1998), p. 111301. DOI: 10.1103/PhysRevD.60.099902, 10.1103/PhysRevD.58.111301. arXiv: hep-ph/9807501 [hep-ph].

[121] David B. Kaplan and Aneesh V. Manohar. "Current Mass Ratios of the Light Quarks." In: *Phys. Rev. Lett.* 56 (1986), p. 2004. DOI: 10.1103/PhysRevLett.56.2004.

[122] A. V. Manohar and C. T. Sachrajda. "Quark Masses." In: (2008).

[123] Kiwoon Choi and Jihn E. Kim. "Dynamical Axion." In: *Phys. Rev.* D32 (1985), p. 1828. DOI: 10.1103/PhysRevD.32.1828.

[124] Anson Hook. "Anomalous Solutions to the Strong CP Problem." In: *Phys. Rev. Lett.* 114.14 (2015), p. 141801. DOI: 10.1103/PhysRevLett.114.141801. arXiv: 1411.3325 [hep-ph].

[125] Ann E. Nelson. "Naturally Weak CP Violation." In: *Phys. Lett.* 136B (1984), pp. 387–391. DOI: 10.1016/0370-2693(84)92025-2.

[126] Stephen M. Barr. "A Natural Class of Nonpeccei-Quinn Models." In: *Phys. Rev.* D30 (1984), p. 1805. DOI: 10.1103/PhysRevD.30.1805.

[127] Michael Dine and Patrick Draper. "Challenges for the Nelson-Barr Mechanism." In: *JHEP* 08 (2015), p. 132. DOI: 10.1007/JHEP08(2015)132. arXiv: 1506.05433 [hep-ph].

[128] Steven Weinberg. "A New Light Boson?" In: *Phys. Rev. Lett.* 40 (1978), pp. 223–226. DOI: 10.1103/PhysRevLett.40.223.

[129] Frank Wilczek. "Problem of Strong P and T Invariance in the Presence of Instantons." In: *Phys. Rev. Lett.* 40 (1978), pp. 279–282. DOI: 10.1103/PhysRevLett.40.279.

[130] Michael Dine, Willy Fischler, and Mark Srednicki. "A Simple Solution to the Strong CP Problem with a Harmless Axion." In: *Phys.Lett.* B104 (1981), p. 199. DOI: 10.1016/0370-2693(81)90590-6.

[131] A. R. Zhitnitsky. "On Possible Suppression of the Axion Hadron Interactions. (In Russian)." In: *Sov. J. Nucl. Phys.* 31 (1980). [Yad. Fiz.31,497(1980)], p. 260.

[132] V. A. Rubakov. "Grand Unification and Heavy Axion." In: *JETP Lett.* 65 (1997), pp. 621–624. DOI: 10.1134/1.567390. arXiv: hep-ph/9703409 [hep-ph].

[133] Zurab Berezhiani, Leonida Gianfagna, and Maurizio Giannotti. "Strong CP Problem and Mirror World: the Weinberg-Wilczek Axion Revisited." In: *Phys. Lett.* B500 (2001), pp. 286–296. DOI: 10.1016/S0370-2693(00)01392-7. arXiv: hep-ph/0009290 [hep-ph].

[134] Tony Gherghetta, Natsumi Nagata, and Mikhail Shifman. "A Visible QCD Axion from an Enlarged Color Group." In: *Phys. Rev.* D93.11 (2016), p. 115010. DOI: 10.1103/PhysRevD.93.115010. arXiv: 1604.01127 [hep-ph].

[135] Savas Dimopoulos, Anson Hook, Junwu Huang, and Gustavo Marques-Tavares. "A Collider Observable QCD Axion." In: *JHEP* 11 (2016), p. 052. DOI: 10.1007/JHEP11(2016)052. arXiv: 1606.03097 [hep-ph].

[136] Prateek Agrawal and Kiel Howe. "Factoring the Strong CP Problem." In: *Submitted to: JHEP* (2017). arXiv: 1710.04213 [hep-ph].

[137] Daniele S. M. Alves and Neal Weiner. "A Viable QCD Axion in the MeV Mass Range." In: (2017). arXiv: 1710.03764 [hep-ph].

[138] David B. Kaplan. "Opening the Axion Window." In: *Nucl. Phys.* B260 (1985), pp. 215–226. DOI: 10.1016/0550-3213(85)90319-0.

[139] Mark Srednicki. "Axion Couplings to Matter. 1. CP Conserving Parts." In: *Nucl. Phys.* B260 (1985), pp. 689–700. DOI: 10.1016/0550-3213(85)90054-9.

[140] Luca Di Luzio, Federico Mescia, and Enrico Nardi. "The Window for Preferred Axion Models." In: (2017). arXiv: 1705.05370 [hep-ph].

[141] Giovanni Grilli di Cortona, Edward Hardy, Javier Pardo Vega, and Giovanni Villadoro. "The QCD Axion, Precisely." In: *JHEP* 01 (2016), p. 034. DOI: 10.1007/JHEP01(2016)034. arXiv: 1511.02867 [hep-ph].

[142] Kiwoon Choi, Kyungsik Kang, and Jihn E. Kim. "Effects of η' in Low-Energy Axion Physics." In: *Phys. Lett.* B181 (1986), pp. 145–149. DOI: 10.1016/0370-2693(86)91273-6.

[143] Y. Asano, E. Kikutani, S. Kurokawa, T. Miyachi, M. Miyajima, Y. Nagashima, T. Shinkawa, S. Sugimoto, and Y. Yoshimura. "Search for a Rare Decay Mode K+ —≫ Pi+ Neutrino Anti-Neutrino and Axion." In: *Phys. Lett.* 107B (1981). [,411(1981)], p. 159. DOI: 10.1016/0370-2693(81)91172-2.

[144] William A. Bardeen, R. D. Peccei, and T. Yanagida. "Constraints on Variant Axion Models." In: *Nucl. Phys.* B279 (1987), pp. 401–428. DOI: 10.1016/0550-3213(87)90003-4.

[145] J. M. Frere, J. A. M. Vermaseren, and M. B. Gavela. "The Elusive Axion." In: *Phys. Lett.* 103B (1981), pp. 129–133. DOI: 10.1016/0370-2693(81)90686-9.

[146] R. D. Peccei. "The Strong Cp Problem." In: *Adv. Ser. Direct. High Energy Phys.* 3 (1989), pp. 503–551. DOI: 10.1142/9789814503280_0013.

[147] V. Anastassopoulos et al. "New CAST Limit on the Axion-Photon Interaction." In: *Nature Phys.* 13 (2017), pp. 584–590. DOI: 10.1038/nphys4109. arXiv: 1705.02290 [hep-ex].

[148] S. J. Asztalos et al. "A Squid-Based Microwave Cavity Search for Dark-Matter Axions." In: *Phys. Rev. Lett.* 104 (2010), p. 041301. DOI: 10.1103/PhysRevLett.104.041301. arXiv: 0910.5914 [astro-ph.CO].

[149] G. Carosi, A. Friedland, M. Giannotti, M. J. Pivovaroff, J. Ruz, and J. K. Vogel. "Probing the Axion-Photon Coupling: Phenomenological and Experimental Perspectives. a Snowmass White Paper." In: *Proceedings, 2013 Community Summer Study on the Future of U.S. Particle Physics: Snowmass on the Mississippi (CsS^{2}013): Minneapolis, Mn, Usa, July 29-August 6, 2013*. 2013. arXiv: 1309.7035 [hep-ph]. URL: http://www.slac.stanford.edu/econf/C1307292/docs/submittedArxivFiles/1309.7035.pdf.

[150] S. De Panfilis, A. C. Melissinos, B. E. Moskowitz, J. T. Rogers, Y. K. Semertzidis, Walter Wuensch, H. J. Halama, A. G. Prodell, W. B. Fowler, and F. A. Nezrick. "Limits on the Abundance and Coupling of Cosmic Axions at 4.5-Microev ≪ M(A) ≪ 5.0-Microev." In: *Phys. Rev. Lett.* 59 (1987), p. 839. DOI: 10.1103/PhysRevLett.59.839.

[151] Walter Wuensch, S. De Panfilis-Wuensch, Y. K. Semertzidis, J. T. Rogers, A. C. Melissinos, H. J. Halama, B. E. Moskowitz, A. G. Prodell, W. B. Fowler, and F. A. Nezrick. "Results of a Laboratory Search for Cosmic Axions and Other Weakly Coupled Light Particles." In: *Phys. Rev.* D40 (1989), p. 3153. DOI: 10.1103/PhysRevD.40.3153.

[152] C. Hagmann, P. Sikivie, N. S. Sullivan, and D. B. Tanner. "Results from a Search for Cosmic Axions." In: *Phys. Rev.* D42 (1990), pp. 1297–1300. DOI: 10.1103/PhysRevD.42.1297.

[153] C. Patrignani et al. "Review of Particle Physics." In: *Chin. Phys.* C40.10 (2016), p. 100001. DOI: 10.1088/1674-1137/40/10/100001.

[154] Adrian Ayala, Inma Domínguez, Maurizio Giannotti, Alessandro Mirizzi, and Oscar Straniero. "Revisiting the bound on axion-photon coupling from Globular Clusters." In: *Phys. Rev. Lett.* 113.19 (2014), p. 191302. DOI: 10.1103/PhysRevLett.113.191302. arXiv: 1406.6053 [astro-ph.SR].

[155] Robin BÃ□hre et al. "Any Light Particle Search II âTechnical Design Report." In: *JINST* 8 (2013), T09001. DOI: 10.1088/1748-0221/8/09/T09001. arXiv: 1302.5647 [physics.ins-det].

[156] I. G. Irastorza et al. "Towards a new generation axion helioscope." In: *JCAP* 1106 (2011), p. 013. DOI: 10.1088/1475-7516/2011/06/013. arXiv: 1103.5334 [hep-ex].

[157] Stephen J. Asztalos et al. "An Improved Rf Cavity Search for Halo Axions." In: *Phys. Rev.* D69 (2004), p. 011101. DOI: 10.1103/PhysRevD.69.011101. arXiv: astro-ph/0310042 [astro-ph].

[158] Allen Caldwell, Gia Dvali, BÃ©la Majorovits, Alexander Millar, Georg Raffelt, Javier Redondo, Olaf Reimann, Frank Simon, and Frank Steffen. "Dielectric Haloscopes: a New Way to Detect Axion Dark Matter." In: *Phys. Rev. Lett.* 118.9 (2017), p. 091801. DOI: 10.1103/PhysRevLett.118.091801. arXiv: 1611.05865 [physics.ins-det].

[159] Howard M. Georgi, Lawrence J. Hall, and Mark B. Wise. "Grand Unified Models with an Automatic Peccei-Quinn Symmetry." In: *Nucl. Phys.* B192 (1981), pp. 409–416. DOI: 10.1016/0550-3213(81)90433-8.

[160] Alberto Salvio, Alessandro Strumia, and Wei Xue. "Thermal Axion Production." In: *JCAP* 1401 (2014), p. 011. DOI: 10.1088/1475-7516/2014/01/011. arXiv: 1310.6982 [hep-ph].

[161] Georg G. Raffelt. *Stars as Laboratories for Fundamental Physics : The Astrophysics of Neutrinos, Axions, and Other Weakly Interacting Particles (Theoretical Astrophysics)*. University Of Chicago Press, May 1996. ISBN: 0226702723. URL: http://www.amazon.com/exec/obidos/redirect?tag=citeulike07-20\&path=ASIN/0226702723.

[162] Georg G. Raffelt. "Astrophysical Axion Bounds." In: *Lect. Notes Phys.* 741 (2008). [,51(2006)], pp. 51–71. DOI: 10.1007/978-3-540-73518-2_3. arXiv: hep-ph/0611350 [hep-ph].

[163] Ken Mimasu and Veronica Sanz. "Alps at Colliders." In: *JHEP* 06 (2015), p. 173. DOI: 10.1007/JHEP06(2015)173. arXiv: 1409.4792 [hep-ph].

[164] Joerg Jaeckel and Andreas Ringwald. "The Low-Energy Frontier of Particle Physics." In: *Ann. Rev. Nucl. Part. Sci.* 60 (2010), pp. 405–437. DOI: 10.1146/annurev.nucl.012809.104433. arXiv: 1002.0329 [hep-ph].

[165] Martin Bauer, Matthias Neubert, and Andrea Thamm. "Collider Probes of Axion-Like Particles." In: *JHEP* 12 (2017), p. 044. DOI: 10.1007/JHEP12(2017)044. arXiv: 1708.00443 [hep-ph].

[166] S. Adler et al. "Further search for the decay K+ —> pi+ nu anti-nu in the momentum region P < 195-MeV/c." In: *Phys. Rev.* D70 (2004), p. 037102. DOI: 10.1103/PhysRevD.70.037102. arXiv: hep-ex/0403034 [hep-ex].

[167] Marcela Carena and R. D. Peccei. "The Effective Lagrangian for Axion Emission from Sn1987A." In: *Phys. Rev.* D40 (1989), p. 652. DOI: 10.1103/PhysRevD.40.652.

[168] Hajime Fukuda, Keisuke Harigaya, Masahiro Ibe, and Tsutomu T. Yanagida. "A Model of Visible QCD Axion." In: (2015). arXiv: 1504.06084 [hep-ph].

[169] Vardan Khachatryan et al. "Search for Dark Matter, Extra Dimensions, and Unparticles in Monojet Events in Proton-Proton Collisions at $\sqrt{s} = 8$ TeV." In: *Eur. Phys. J.* C75.5 (2015), p. 235. DOI: 10.1140/epjc/s10052-015-3451-4. arXiv: 1408.3583 [hep-ex].

[170] Georges Aad et al. "Search for New Phenomena in Final States with an Energetic Jet and Large Missing Transverse Momentum in PP Collisions at $\sqrt{s}$ =8 TeV with the Atlas Detector." In: *Eur. Phys. J.* C75.7 (2015). [Erratum: Eur. Phys. J.C75,no.9,408(2015)], p. 299. DOI: 10.1140/epjc/s10052-015-3517-3, 10.1140/epjc/s10052-015-3639-7. arXiv: 1502.01518 [hep-ex].

[171] Wolfgang Keil, Hans-Thomas Janka, David N. Schramm, Gunter Sigl, Michael S. Turner, and John R. Ellis. "A Fresh Look at Axions and Sn-1987A." In: *Phys. Rev.* D56 (1997), pp. 2419–2432. DOI: 10.1103/PhysRevD.56.2419. arXiv: astro-ph/9612222 [astro-ph].

[172] Georg G. Raffelt. "Axion Constraints from White Dwarf Cooling Times." In: *Phys. Lett.* 166B (1986), pp. 402–406. DOI: 10.1016/0370-2693(86)91588-1.

[173] J. Isern, S. Catalan, E. García--Berro, M. Salaris, and S. Torres. "Axion Cooling of White Dwarfs." In: 2013. arXiv: 1304.7652 [astro-ph.SR]. URL: http://inspirehep.net/record/1230903/files/arXiv:1304.7652.pdf.

[174] Nicolas Viaux, Marcio Catelan, Peter B. Stetson, Georg Raffelt, Javier Redondo, Aldo A. R. Valcarce, and Achim Weiss. "Neutrino and Axion Bounds from the Globular ClusterM **5** (Ngc 5904)." In: *Phys. Rev. Lett.* 111 (2013), p. 231301. DOI: 10.1103/PhysRevLett.111.231301. arXiv: 1311.1669 [astro-ph.SR].

[175] E. Aprile et al. "First Axion Results from the Xenon100 Experiment." In: *Phys. Rev.* D90.6 (2014), p. 062009. DOI: 10.1103/PhysRevD.90.062009. arXiv: 1404.1455 [astro-ph.CO].

[176] Gordan Krnjaic. "Probing Light Thermal Dark-Matter with a Higgs Portal Mediator." In: *Phys. Rev.* D94.7 (2016), p. 073009. DOI: 10.1103/PhysRevD.94.073009. arXiv: 1512.04119 [hep-ph].

[177] F. Bergsma et al. "Search for Axion Like Particle Production in 400-GeV Proton - Copper Interactions." In: *Phys. Lett.* 157B (1985), pp. 458–462. DOI: 10.1016/0370-2693(85)90400-9.

[178] Matthew J. Dolan, Felix Kahlhoefer, Christopher McCabe, and Kai Schmidt-Hoberg. "A Taste of Dark Matter: Flavour Constraints on Pseudoscalar Mediators." In: *JHEP* 03 (2015). [Erratum: JHEP07,103(2015)], p. 171. DOI: 10.1007/JHEP07(2015)103, 10.1007/JHEP03(2015)171. arXiv: 1412.5174 [hep-ph].

[179] F. Zwicky. "Die Rotverschiebung Von Extragalaktischen Nebeln." In: *Helv. Phys. Acta* 6 (1933). [Gen. Rel. Grav.41,207(2009)], pp. 110–127. DOI: 10.1007/s10714-008-0707-4.

[180] F. Zwicky. "On the Masses of Nebulae and of Clusters of Nebulae." In: *Astrophys. J.* 86 (1937), pp. 217–246. DOI: 10.1086/143864.

[181] Gianfranco Bertone and Dan Hooper. "A History of Dark Matter." In: *Submitted to: Rev. Mod. Phys.* (2016). arXiv: 1605.04909 [astro-ph.CO].

[182] Paul Gorenstein and Wallace Tucker. "Astronomical Signatures of Dark Matter." In: *Adv. High Energy Phys.* 2014 (2014), p. 878203. DOI: 10.1155/2014/878203.

[183] Andrew B. Newman, Tommaso Treu, Richard S. Ellis, David J. Sand, Carlo Nipoti, Johan Richard, and Eric Jullo. "The Density Profiles of Massive, Relaxed Galaxy Clusters: I. the Total Density over 3 Decades in Radius." In: *Astrophys. J.* 765 (2013), p. 24. DOI: 10.1088/0004-637X/765/1/24. arXiv: 1209.1391 [astro-ph.CO].

[184] Vera C. Rubin and W. Kent Ford Jr. "Rotation of the Andromeda Nebula from a Spectroscopic Survey of Emission Regions." In: *Astrophys. J.* 159 (1970), pp. 379–403. DOI: 10.1086/150317.

[185] M. S. Roberts and R. N. Whitehurst. "The rotation curve and geometry of M31 at large galactocentric distances." In: *Astrophysical Journal* 201 (2007), pp. 327 –346.

[186] Begeman, K.G., Broeils, A. H., and Sanders, R. H. "Extended rotation curves of spiral galaxies - Dark haloes and modified dynamics." In: *Monthly Notices of the Royal Astronomical Society* 249 (1991), pp. 523–537.

[187] P. A. R. Ade et al. "Planck 2015 results. XIII. Cosmological parameters." In: *Astron. Astrophys.* 594 (2016), A13. DOI: 10.1051/0004-6361/201525830. arXiv: 1502.01589 [astro-ph.CO].

[188] Kim Griest. "Galactic Microlensing as a Method of Detecting Massive Compact Halo Objects." In: *Astrophys. J.* 366 (1991), pp. 412–421. DOI: 10.1086/169575.

[189] P. Ivanov, P. Naselsky, and I. Novikov. "Inflation and Primordial Black Holes as Dark Matter." In: *Phys. Rev.* D50 (1994), pp. 7173–7178. DOI: 10.1103/PhysRevD.50.7173.

[190] S. S. Gershtein and Ya. B. Zeldovich. "Rest Mass of Muonic Neutrino and Cosmology." In: *JETP Lett.* 4 (1966). [Pisma Zh. Eksp. Teor. Fiz.4,174(1966)], pp. 120–122.

[191] J. Bonn et al. "The Mainz neutrino mass experiment." In: *Nucl. Phys. Proc. Suppl.* 91 (2001). [PoShep2001,192(2001)], pp. 273–279. DOI: 10.1016/S0920-5632(00)00951-8.

[192] Gianfranco Bertone, Dan Hooper, and Joseph Silk. "Particle Dark Matter: Evidence, Candidates and Constraints." In: *Phys. Rept.* 405 (2005), pp. 279–390. DOI: 10.1016/j.physrep.2004.08.031. arXiv: hep-ph/0404175 [hep-ph].

[193] S. L. Dubovsky, D. S. Gorbunov, and G. I. Rubtsov. "Narrowing the Window for Millicharged Particles by Cmb Anisotropy." In: *JETP Lett.* 79 (2004). [Pisma Zh. Eksp. Teor. Fiz.79,3(2004)], pp. 1–5. DOI: 10.1134/1.1675909. arXiv: hep-ph/0311189 [hep-ph].

[194] Kenji Kadota, Toyokazu Sekiguchi, and Hiroyuki Tashiro. "A New Constraint on Millicharged Dark Matter from Galaxy Clusters." In: (2016). arXiv: 1602.04009 [astro-ph.CO].

[195] Park. E.-K. "DMSAG Report on the Direct Detection and Study of Dark Matter." In: (2007).

[196] C. Boehm and Pierre Fayet. "Scalar Dark Matter Candidates." In: *Nucl. Phys.* B683 (2004), pp. 219–263. DOI: 10.1016/j.nuclphysb.2004.01.015. arXiv: hep-ph/0305261 [hep-ph].

[197] Edward W. Kolb and Richard Slansky. "Dimensional Reduction in the Early Universe: Where Have the Massive Particles Gone?" In: *Phys. Lett.* 135B (1984), p. 378. DOI: 10.1016/0370-2693(84)90298-3.

[198] John R. Ellis. "Particle Candidates for Dark Matter." In: *Phys. Scripta* T85 (2000), pp. 221–230. DOI: 10.1238/Physica.Topical.085a00221. arXiv: astro-ph/9812211 [astro-ph].

[199] Lars BergstrÃPm. "Nonbaryonic Dark Matter: Observational Evidence and Detection Methods." In: *Rept. Prog. Phys.* 63 (2000), p. 793. DOI: 10.1088/0034-4885/63/5/2r3. arXiv: hep-ph/0002126 [hep-ph].

[200] D. S. Akerib et al. "First results from the LUX dark matter experiment at the Sanford Underground Research Facility." In: *Phys. Rev. Lett.* 112 (2014), p. 091303. DOI: 10.1103/PhysRevLett.112.091303. arXiv: 1310.8214 [astro-ph.CO].

[201] Elena Aprile. "The Xenon1T Dark Matter Search Experiment." In: *Springer Proc. Phys.* 148 (2013), pp. 93–96. DOI: 10.1007/978-94-007-7241-0_14. arXiv: 1206.6288 [astro-ph.IM].

[202] Vanda Silveira and A. Zee. "Scalar Phantoms." In: *Phys. Lett.* 161B (1985), pp. 136–140. DOI: 10.1016/0370-2693(85)90624-0.

[203] M. J. G. Veltman and F. J. Yndurain. "Radiative Corrections to W W Scattering." In: *Nucl. Phys.* B325 (1989), pp. 1–17. DOI: 10.1016/0550-3213(89)90369-6.

[204] Yeong Gyun Kim and Kang Young Lee. "The Minimal Model of Fermionic Dark Matter." In: *Phys. Rev.* D75 (2007), p. 115012. DOI: 10.1103/PhysRevD.75.115012. arXiv: hep-ph/0611069 [hep-ph].

[205] John March-Russell, Stephen M. West, Daniel Cumberbatch, and Dan Hooper. "Heavy Dark Matter Through the Higgs Portal." In: *JHEP* 07 (2008), p. 058. DOI: 10.1088/1126-6708/2008/07/058. arXiv: 0801.3440 [hep-ph].

[206] Yeong Gyun Kim, Kang Young Lee, and Seodong Shin. "Singlet Fermionic Dark Matter." In: *JHEP* 05 (2008), p. 100. DOI: 10.1088/1126-6708/2008/05/100. arXiv: 0803.2932 [hep-ph].

[207] Markus Ahlers, Joerg Jaeckel, Javier Redondo, and Andreas Ringwald. "Probing Hidden Sector Photons Through the Higgs Window." In: *Phys. Rev.* D78 (2008), p. 075005. DOI: 10.1103/PhysRevD.78.075005. arXiv: 0807.4143 [hep-ph].

[208] Jonathan L. Feng, Huitzu Tu, and Hai-Bo Yu. "Thermal Relics in Hidden Sectors." In: *JCAP* 0810 (2008), p. 043. DOI: 10.1088/1475-7516/2008/10/043. arXiv: 0808.2318 [hep-ph].

[209] Sarah Andreas, Thomas Hambye, and Michel H. G. Tytgat. "WIMP Dark Matter, Higgs Exchange and Dama." In: *JCAP* 0810 (2008), p. 034. DOI: 10.1088/1475-7516/2008/10/034. arXiv: 0808.0255 [hep-ph].

[210] Vernon Barger, Paul Langacker, Mathew McCaskey, Michael Ramsey-Musolf, and Gabe Shaughnessy. "Complex Singlet Extension of the Standard Model." In: *Phys. Rev.* D79 (2009), p. 015018. DOI: 10.1103/PhysRevD.79.015018. arXiv: 0811.0393 [hep-ph].

[211] Mario Kadastik, Kristjan Kannike, Antonio Racioppi, and Martti Raidal. "Ewsb from the Soft Portal into Dark Matter and Prediction for Direct Detection." In: *Phys. Rev. Lett.* 104 (2010), p. 201301. DOI: 10.1103/PhysRevLett.104.201301. arXiv: 0912.2729 [hep-ph].

[212] Shinya Kanemura, Shigeki Matsumoto, Takehiro Nabeshima, and Nobuchika Okada. "Can WIMP Dark Matter Overcome the Nightmare Scenario?" In: *Phys. Rev.* D82 (2010), p. 055026. DOI: 10.1103/PhysRevD.82.055026. arXiv: 1005.5651 [hep-ph].

[213] Federico Piazza and Maxim Pospelov. "Sub-Ev Scalar Dark Matter Through the Super-Renormalizable Higgs Portal." In: *Phys. Rev.* D82 (2010), p. 043533. DOI: 10.1103/PhysRevD.82.043533. arXiv: 1003.2313 [hep-ph].

[214] Chiara Arina, Francois-Xavier Josse-Michaux, and Narendra Sahu. "A Tight Connection Between Direct and Indirect Detection of Dark Matter Through Higgs Portal Couplings to a Hidden Sector." In: *Phys. Rev.* D82 (2010), p. 015005. DOI: 10.1103/PhysRevD.82.015005. arXiv: 1004.3953 [hep-ph].

[215] Ian Low, Pedro Schwaller, Gabe Shaughnessy, and Carlos E. M. Wagner. "The Dark Side of the Higgs Boson." In: *Phys. Rev.* D85 (2012), p. 015009. DOI: 10.1103/PhysRevD.85.015009. arXiv: 1110.4405 [hep-ph].

[216] Abdelhak Djouadi, Oleg Lebedev, Yann Mambrini, and Jeremie Quevillon. "Implications of Lhc Searches for Higgs–Portal Dark Matter." In: *Phys. Lett.* B709 (2012), pp. 65–69. DOI: 10.1016/j.physletb.2012.01.062. arXiv: 1112.3299 [hep-ph].

[217] Christoph Englert, Tilman Plehn, Dirk Zerwas, and Peter M. Zerwas. "Exploring the Higgs Portal." In: *Phys. Lett.* B703 (2011), pp. 298–305. DOI: 10.1016/j.physletb.2011.08.002. arXiv: 1106.3097 [hep-ph].

[218] Jernej F. Kamenik and Christopher Smith. "Could a Light Higgs Boson Illuminate the Dark Sector?" In: *Phys. Rev.* D85 (2012), p. 093017. DOI: 10.1103/PhysRevD.85.093017. arXiv: 1201.4814 [hep-ph].

[219] Matthew Gonderinger, Hyungjun Lim, and Michael J. Ramsey-Musolf. "Complex Scalar Singlet Dark Matter: Vacuum Stability and Phenomenology." In: *Phys. Rev.* D86 (2012), p. 043511. DOI: 10.1103/PhysRevD.86.043511. arXiv: 1202.1316 [hep-ph].

[220] Oleg Lebedev. "On Stability of the Electroweak Vacuum and the Higgs Portal." In: *Eur. Phys. J.* C72 (2012), p. 2058. DOI: 10.1140/epjc/s10052-012-2058-2. arXiv: 1203.0156 [hep-ph].

[221] Nathaniel Craig, Hou Keong Lou, Matthew McCullough, and Arun Thalapillil. "The Higgs Portal Above Threshold." In: *JHEP* 02 (2016), p. 127. DOI: 10.1007/JHEP02(2016)127. arXiv: 1412.0258 [hep-ph].

[222] Georges Aad et al. "Constraints on New Phenomena via Higgs Boson Couplings and Invisible Decays with the Atlas Detector." In: *JHEP* 11 (2015), p. 206. DOI: 10.1007/JHEP11(2015)206. arXiv: 1509.00672 [hep-ex].

[223] M. L. Ahnen et al. "Limits to dark matter annihilation cross-section from a combined analysis of MAGIC and Fermi-LAT observations of dwarf satellite galaxies." In: *JCAP* 1602.02 (2016), p. 039. DOI: 10.1088/1475-7516/2016/02/039. arXiv: 1601.06590 [astro-ph.HE].

[224] M. Ackermann et al. "Updated search for spectral lines from Galactic dark matter interactions with pass 8 data from the Fermi Large Area Telescope." In: *Phys. Rev.* D91.12 (2015), p. 122002. DOI: 10.1103/PhysRevD.91.122002. arXiv: 1506.00013 [astro-ph.HE].

[225] Michael Duerr, Pavel Fileviez PÃ©rez, and Juri Smirnov. "Scalar Dark Matter: Direct Vs. Indirect Detection." In: *JHEP* 06 (2016), p. 152. DOI: 10.1007/JHEP06(2016)152. arXiv: 1509.04282 [hep-ph].

[226] J. Alberto Casas, David G. CerdeÃ±o, JesusM.Moreno, AndJavierQuilis. "Reopening the Higgs Portal for Single Scalar Dark Matter." In: *JHEP* 05 (2017), p. 036. DOI: 10.1007/JHEP05(2017)036. arXiv: 1701.08134 [hep-ph].

[227] P. Sikivie and Q. Yang. "Bose-Einstein Condensation of Dark Matter Axions." In: *Phys. Rev. Lett.* 103 (2009), p. 111301. DOI: 10.1103/PhysRevLett.103.111301. arXiv: 0901.1106 [hep-ph].

[228] John Preskill, Mark B. Wise, and Frank Wilczek. "Cosmology of the Invisible Axion." In: *Phys. Lett.* B120 (1983), pp. 127–132. DOI: 10.1016/0370-2693(83)90637-8.

[229] L. F. Abbott and P. Sikivie. "A Cosmological Bound on the Invisible Axion." In: *Phys. Lett.* B120 (1983), pp. 133–136. DOI: 10.1016/0370-2693(83)90638-X.

[230] Michael Dine and Willy Fischler. "The Not So Harmless Axion." In: *Phys. Lett.* B120 (1983), pp. 137–141. DOI: 10.1016/0370-2693(83)90639-1.

[231] Steen Hannestad, Alessandro Mirizzi, and Georg Raffelt. "New Cosmological Mass Limit on Thermal Relic Axions." In: *JCAP* 0507 (2005), p. 002. DOI: 10.1088/1475-7516/2005/07/002. arXiv: hep-ph/0504059 [hep-ph].

[232] Pierre Sikivie. "Axion Cosmology." In: *Lect. Notes Phys.* 741 (2008). [,19(2006)], pp. 19–50. DOI: 10.1007/978-3-540-73518-2_2. arXiv: astro-ph/0610440 [astro-ph].

[233] Pierre Sikivie. "Axion Cosmology." In: *Lect.Notes Phys.* 741 (2008), pp. 19–50. DOI: 10.1007/978-3-540-73518-2_2. arXiv: astro-ph/0610440 [astro-ph].

[234] John Preskill, Mark B. Wise, and Frank Wilczek. "Cosmology of the Invisible Axion." In: *Phys.Lett.* B120 (1983), pp. 127–132. DOI: 10.1016/0370-2693(83)90637-8.

[235] L.F. Abbott and P. Sikivie. "A Cosmological Bound on the Invisible Axion." In: *Phys.Lett.* B120 (1983), pp. 133–136. DOI: 10.1016/0370-2693(83)90638-X.

[236] Michael Dine and Willy Fischler. "The Not So Harmless Axion." In: *Phys.Lett.* B120 (1983), pp. 137–141. DOI: 10.1016/0370-2693(83)90639-1.

[237] Takashi Hiramatsu, Masahiro Kawasaki, Ken'ichi Saikawa, and Toyokazu Sekiguchi. "Production of Dark Matter Axions from Collapse of String-Wall Systems." In: *Phys. Rev.* D85 (2012). [Erratum: Phys. Rev.D86,089902(2012)], p. 105020. DOI: 10.1103/PhysRevD.86.089902,10.1103/PhysRevD.85.105020. arXiv: 1202.5851 [hep-ph].

[238] Masahiro Kawasaki, Ken'ichi Saikawa, and Toyokazu Sekiguchi. "Axion Dark Matter from Topological Defects." In: *Phys. Rev.* D91.6 (2015), p. 065014. DOI: 10.1103/PhysRevD.91.065014. arXiv: 1412.0789 [hep-ph].

[239] Vincent B.. Klaer and Guy D.. Moore. "The Dark-Matter Axion Mass." In: *JCAP* 1711.11 (2017), p. 049. DOI: 10.1088/1475-7516/2017/11/049. arXiv: 1708.07521 [hep-ph].

[240] Vincent B. Klaer and Guy D. Moore. "How to Simulate Global Cosmic Strings with Large String Tension." In: *JCAP* 1710 (2017), p. 043. DOI: 10.1088/1475-7516/2017/10/043. arXiv: 1707.05566 [hep-ph].

[241] Ken'ichi Saikawa. "Axion as a non-WIMP dark matter candidate." In: *2017 European Physical Society Conference on High Energy Physics (EPS-HEP 2017) Venice, Italy, July 5-12, 2017*. 2017. arXiv: 1709.07091 [hep-ph]. URL: http://inspirehep.net/record/1624646/files/arXiv:1709.07091.pdf.

[242] Guillermo Ballesteros, Javier Redondo, Andreas Ringwald, and Carlos Tamarit. "Standard ModelâAxionâSeesawâHiggs Portal Inflation. Five Problems of Particle Physics and Cosmology Solved in One Stroke." In: *JCAP* 1708.08 (2017), p. 001. DOI: 10.1088/1475-7516/2017/08/001. arXiv: 1610.01639 [hep-ph].

[243] Nuria Vinyoles, Aldo Serenelli, Francesco L. Villante, Sarbani Basu, Javier Redondo, and Jordi Isern. "New Axion and Hidden Photon Constraints from a Solar Data Global Fit." In: *JCAP* 1510.10 (2015), p. 015. DOI: 10.1088/1475-7516/2015/10/015. arXiv: 1501.01639 [astro-ph.SR].

[244] Luca Di Luzio, Federico Mescia, and Enrico Nardi. "Redefining the Axion Window." In: *Phys. Rev. Lett.* 118.3 (2017), p. 031801. DOI: 10.1103/PhysRevLett.118.031801. arXiv: 1610.07593 [hep-ph].

[245] Howard Georgi and David B. Kaplan. "Composite Higgs and Custodial SU(2)." In: *Phys. Lett.* 145B (1984), pp. 216–220. DOI: 10.1016/0370-2693(84)90341-1.

[246] Michael J. Dugan, Howard Georgi, and David B. Kaplan. "Anatomy of a Composite Higgs Model." In: *Nucl. Phys.* B254 (1985), pp. 299–326. DOI: 10.1016/0550-3213(85)90221-4.

[247] Alex Pomarol and Francesco Riva. "The Composite Higgs and Light Resonance Connection." In: *JHEP* 08 (2012), p. 135. DOI: 10.1007/JHEP08(2012)135. arXiv: 1205.6434 [hep-ph].

[248] Marcela Carena, Leandro Da Rold, and Eduardo PontÃ³n. "Minimal Composite Higgs Models at the Lhc." In: *JHEP* 06 (2014), p. 159. DOI: 10.1007/JHEP06(2014)159. arXiv: 1402.2987 [hep-ph].

[249] Alexandre Alves, Alex G. Dias, and Kuver Sinha. "Diphotons at the Z-pole in Models of the 750 GeV Resonance Decaying to Axion-Like Particles." In: *JHEP* 08 (2016), p. 060. DOI: 10.1007/JHEP08(2016)060. arXiv: 1606.06375 [hep-ph].

[250] Martin Bauer, Matthias Neubert, and Andrea Thamm. "Analyzing the CP Nature of a New Scalar Particle via S-≫Zh Decay." In: *Phys. Rev. Lett.* 117 (2016), p. 181801. DOI: 10.1103/PhysRevLett.117.181801. arXiv: 1610.00009 [hep-ph].

[251] Alexander Friedland, Maurizio Giannotti, and Michael Wise. "Constraining the Axion-Photon Coupling with Massive Stars." In: *Phys. Rev. Lett.* 110.6 (2013), p. 061101. DOI: 10.1103/PhysRevLett.110.061101. arXiv: 1210.1271 [hep-ph].

[252] J. D. Bjorken, S. Ecklund, W. R. Nelson, A. Abashian, L. Mo, P. Rassmann, C. Church, and T. Nunamaker. "Search for Neutral, Penetrating, Metastable Particles Produced in the Slac Beam Dump." In: *Massive Neutrinos in Astrophysics and in Particle Physics. Proceedings, 4Th Moriond Workshop, La Plagne, France, January 15-21, 1984*. 1984, pp. 227–242. URL: http://lss.fnal.gov/cgi-bin/finD_{p}aper.pl?conf-84-33.

[253] Marius Millea, Lloyd Knox, and Brian Fields. "New Bounds for Axions and Axion-Like Particles with Kev-Gev Masses." In: *Phys. Rev.* D92.2 (2015), p. 023010. DOI: 10.1103/PhysRevD.92.023010. arXiv: 1501.04097 [astro-ph.CO].

[254] F. Pobbe, A. Wulzer, and M. Zanetti. "Setting Limits on Effective Field Theories: the Case of Dark Matter." In: *JHEP* 08 (2017), p. 074. DOI: 10.1007/JHEP08(2017)074. arXiv: 1704.00736 [hep-ph].

[255] Georges Aad et al. "Measurements of the Higgs boson production and decay rates and constraints on its couplings from a combined ATLAS and CMS analysis of the LHC pp collision data at $\sqrt{s} = 7$ and 8 TeV." In: *JHEP* 08 (2016), p. 045. DOI: 10.1007/JHEP08(2016)045. arXiv: 1606.02266 [hep-ex].

[256] A. Denner, S. Heinemeyer, I. Puljak, D. Rebuzzi, and M. Spira. "Standard Model Higgs-Boson Branching Ratios with Uncertainties." In: *Eur. Phys. J.* C71 (2011), p. 1753. DOI: 10.1140/epjc/s10052-011-1753-8. arXiv: 1107.5909 [hep-ph].

[257] *Projections for measurements of Higgs boson signal strengths and couplings parameters with the ATLAS detector at a HL-LHC*. Tech. rep. ATL-PHYS-PUB-2014-016. Geneva: CERN, 2014. URL: https://cds.cern.ch/record/1956710.

[258] Georges Aad et al. "Search for Invisible Decays of a Higgs Boson Using Vector-Boson Fusion in pp Collisions at $\sqrt{s} = 8$ TeV with the Atlas Detector." In: *JHEP* 01 (2016), p. 172. DOI: 10.1007/JHEP01(2016)172. arXiv: 1508.07869 [hep-ex].

[259] Serguei Chatrchyan et al. "Search for Invisible Decays of Higgs Bosons in the Vector Boson Fusion and Associated Zh Production Modes." In: *Eur. Phys. J.* C74 (2014), p. 2980. DOI: 10.1140/epjc/s10052-014-2980-6. arXiv: 1404.1344 [hep-ex].

[260] *Projections for measurements of Higgs boson cross sections, branching ratios and coupling parameters with the ATLAS detector at a HL-LHC*. Tech. rep. ATL-PHYS-PUB-2013-014. Geneva: CERN, 2013. URL: https://cds.cern.ch/record/1611186.

[261] Yang Bai and Tim M. P. Tait. "Searches with Mono-Leptons." In: *Phys. Lett.* B723 (2013), pp. 384–387. DOI: 10.1016/j.physletb.2013.05.057. arXiv: 1208.4361 [hep-ph].

[262] Nicole F. Bell, James B. Dent, Ahmad J. Galea, Thomas D. Jacques, Lawrence M. Krauss, and Thomas J. Weiler. "Searching for Dark Matter at the Lhc with a Mono-Z." In: *Phys. Rev.* D86 (2012), p. 096011. DOI: 10.1103/PhysRevD.86.096011. arXiv: 1209.0231 [hep-ph].

[263] Linda M. Carpenter, Andrew Nelson, Chase Shimmin, Tim M. P. Tait, and Daniel Whiteson. "Collider Searches for Dark Matter in Events with a Z Boson and Missing Energy." In: *Phys. Rev.* D87.7 (2013), p. 074005. DOI: 10.1103/PhysRevD.87.074005. arXiv: 1212.3352 [hep-ex].

[264] Alexandre Alves and Kuver Sinha. "Searches for Dark Matter at the Lhc: a Multivariate Analysis in the Mono-Z Channel." In: *Phys. Rev.* D92.11 (2015), p. 115013. DOI: 10.1103/PhysRevD.92.115013. arXiv: 1507.08294 [hep-ph].

[265] Jose Miguel No. "Looking Through the Pseudoscalar Portal into Dark Matter: Novel Mono-Higgs and Mono-Z Signatures at the Lhc." In: *Phys. Rev.* D93.3 (2016), p. 031701. DOI: 10.1103/PhysRevD.93.031701. arXiv: 1509.01110 [hep-ph].

[266] Matthias Neubert, Jian Wang, and Cen Zhang. "Higher-Order QCD Predictions for Dark Matter Production in Mono-Z Searches at the Lhc." In: *JHEP* 02 (2016), p. 082. DOI: 10.1007/JHEP02(2016)082. arXiv: 1509.05785 [hep-ph].

[267] J. Alwall, R. Frederix, S. Frixione, V. Hirschi, F. Maltoni, O. Mattelaer, H. S. Shao, T. Stelzer, P. Torrielli, and M. Zaro. "The automated computation of tree-level and next-to-leading order differential cross sections, and their matching to parton shower simulations." In: *JHEP* 07 (2014), p. 079. DOI: 10.1007/JHEP07(2014)079. arXiv: 1405.0301 [hep-ph].

[268] *Search for new resonances in events with one lepton and missing transverse momentum in pp collisions at sqrt(s) = 13 TeV with the ATLAS detector*. Tech. rep. ATLAS-CONF-2015-063. Geneva: CERN, 2015. URL: https://cds.cern.ch/record/2114829/.

[269] Morad Aaboud et al. "Search for New Resonances in Events with One Lepton and Missing Transverse Momentum in pp Collisions at $\sqrt{s} = 13$ TeV with the Atlas Detector." In: *Phys. Lett.* B762 (2016), pp. 334–352. DOI: 10.1016/j.physletb.2016.09.040. arXiv: 1606.03977 [hep-ex].

[270] CMS Collaboration. "Search for Dark Matter and Unparticles in Events with a Z Boson and Missing Transverse Momentum in Proton-Proton Collisions at $\sqrt{s} = 13$ TeV." In: (2016).

[271] D. de Florian et al. "Handbook of Lhc Higgs Cross Sections: 4. Deciphering the Nature of the Higgs Sector." In: (2016). arXiv: 1610.07922 [hep-ph].

[272] Georges Aad et al. "Measurements of $W\gamma$ and $Z\gamma$ Production in pp Collisions at $\sqrt{s} = 7$ TeV with the Atlas Detector at the LHC." In: *Phys. Rev.* D87.11 (2013). [Erratum: Phys. Rev.D91,no.11,119901(2015)], p. 112003. DOI: 10.1103/PhysRevD.87.112003,10.1103/PhysRevD.91.119901. arXiv: 1302.1283 [hep-ex].

[273] Serguei Chatrchyan et al. "Measurement of the $W\gamma$ and $Z\gamma$ Inclusive Cross Sections in pp Collisions at $\sqrt{s} = 7$ TeV and Limits on Anomalous Triple Gauge Boson Couplings." In: *Phys. Rev.* D89.9 (2014), p. 092005. DOI: 10.1103/PhysRevD.89.092005. arXiv: 1308.6832 [hep-ex].

[274] Glen Cowan, Kyle Cranmer, Eilam Gross, and Ofer Vitells. "Asymptotic Formulae for Likelihood-Based Tests of New Physics." In: *Eur. Phys. J.* C71 (2011). [Erratum: Eur. Phys. J.C73,2501(2013)], p. 1554. DOI: 10.1140/epjc/s10052-011-1554-0,10.1140/epjc/s10052-013-2501-z. arXiv: 1007.1727 [physics.data-an].

[275] C. G. Lester and D. J. Summers. "Measuring Masses of Semiinvisibly Decaying Particles Pair Produced at Hadron Colliders." In: *Phys. Lett.* B463 (1999), pp. 99–103. DOI: 10.1016/S0370-2693(99)00945-4. arXiv: hep-ph/9906349 [hep-ph].

[276] Alan Barr, Christopher Lester, and P. Stephens. "M(T2): the Truth Behind the Glamour." In: *J. Phys.* G29 (2003), pp. 2343–2363. DOI: 10.1088/0954-3899/29/10/304. arXiv: hep-ph/0304226 [hep-ph].

[277] G. Brooijmans et al. "Les Houches 2015: Physics at TeV Colliders - New Physics Working Group Report." In: *9Th Les Houches Workshop on Physics at TeV Colliders (Phystev 2015) Les Houches, France, June 1-19, 2015*. 2016. arXiv: 1605.02684 [hep-ph]. URL: http://inspirehep.net/record/1456803/files/arXiv:1605.02684.pdf.

[278] Torbjorn Sjostrand, Stephen Mrenna, and Peter Z. Skands. "A Brief Introduction to PYTHIA 8.1." In: *Comput. Phys. Commun.* 178 (2008), pp. 852–867. DOI: 10.1016/j.cpc.2008.01.036. arXiv: 0710.3820 [hep-ph].

[279] Matteo Cacciari, Gavin P. Salam, and Gregory Soyez. "FastJet User Manual." In: *Eur. Phys. J.* C72 (2012), p. 1896. DOI: 10.1140/epjc/s10052-012-1896-2. arXiv: 1111.6097 [hep-ph].

[280] *Search for the Supersymmetric Partner of the Top Quark in the Jets+Emiss Final State at sqrt(s) = 13 TeV*. Tech. rep. ATLAS-CONF-2016-077. Geneva: CERN, 2016. URL: http://cds.cern.ch/record/2206250.

[281] Michele Frigerio, Alex Pomarol, Francesco Riva, and Alfredo Urbano. "Composite Scalar Dark Matter." In: *JHEP* 07 (2012), p. 015. DOI: 10.1007/JHEP07(2012)015. arXiv: 1204.2808 [hep-ph].

[282] David Marzocca and Alfredo Urbano. "Composite Dark Matter and Lhc Interplay." In: *JHEP* 07 (2014), p. 107. DOI: 10.1007/JHEP07(2014)107. arXiv: 1404.7419 [hep-ph].

[283] Nayara Fonseca, Renata Zukanovich Funchal, Andre Lessa, and Laura Lopez-Honorez. "Dark Matter Constraints on Composite Higgs Models." In: *JHEP* 06 (2015), p. 154. DOI: 10.1007/JHEP06(2015)154. arXiv: 1501.05957 [hep-ph].

[284] Thomas Appelquist and Guo-Hong Wu. "The Electroweak Chiral Lagrangian and New Precision Measurements." In: *Phys. Rev.* D48 (1993), pp. 3235–3241. DOI: 10.1103/PhysRevD.48.3235. arXiv: hep-ph/9304240 [hep-ph].

[285] Gino Isidori and Michael Trott. "Higgs Form Factors in Associated Production." In: *JHEP* 02 (2014), p. 082. DOI: 10.1007/JHEP02(2014)082. arXiv: 1307.4051 [hep-ph].

[286] E. Aprile et al. "Dark Matter Results from 225 Live Days of XENON100 Data." In: *Phys. Rev. Lett.* 109 (2012), p. 181301. DOI: 10.1103/PhysRevLett.109.181301. arXiv: 1207.5988 [astro-ph.CO].

[287] Adam Alloul, Neil D. Christensen, CÃ©line Degrande, Claude Duhr, and Benjamin Fuks. "Feynrules 2.0 - a Complete Toolbox for Tree-Level Phenomenology." In: *Comput. Phys. Commun.* 185 (2014), pp. 2250–2300. DOI: 10.1016/j.cpc.2014.04.012. arXiv: 1310.1921 [hep-ph].

[288] G. BÃ©langer, F. Boudjema, A. Pukhov, and A. Semenov. "Micromegas4.1: Two Dark Matter Candidates." In: *Comput. Phys. Commun.* 192 (2015), pp. 322–329. DOI: 10.1016/j.cpc.2015.03.003. arXiv: 1407.6129 [hep-ph].

[289] Olivier Mattelaer and Eleni Vryonidou. "Dark Matter Production Through Loop-Induced Processes at the Lhc: the S-Channel Mediator Case." In: *Eur. Phys. J.* C75.9 (2015), p. 436. DOI: 10.1140/epjc/s10052-015-3665-5. arXiv: 1508.00564 [hep-ph].

[290] James M. Cline, Kimmo Kainulainen, Pat Scott, and Christoph Weniger. "Update on Scalar Singlet Dark Matter." In: *Phys. Rev.* D88 (2013). [Erratum: Phys. Rev.D92,no.3,039906(2015)], p. 055025. DOI: 10.1103/PhysRevD.92.039906,10.1103/PhysRevD.88.055025. arXiv: 1306.4710 [hep-ph].

[291] Michael Duerr, Pavel Fileviez Perez, and Juri Smirnov. "Scalar Singlet Dark Matter and Gamma Lines." In: *Phys. Lett.* B751 (2015), pp. 119–122. DOI: 10.1016/j.physletb.2015.10.034. arXiv: 1508.04418 [hep-ph].

[292] Huayong Han and Sibo Zheng. "New Constraints on Higgs-Portal Scalar Dark Matter." In: *JHEP* 12 (2015), p. 044. DOI: 10.1007/JHEP12(2015)044. arXiv: 1509.01765 [hep-ph].

[293] Mihailo BackoviÄ, Antony Martini, Olivier Mattelaer, Kyoungchul Kong, and Gopolang Mohlabeng. "Direct Detection of Dark Matter with Maddm V.2.0." In: *Phys. Dark Univ.* 9-10 (2015), pp. 37–50. DOI: 10.1016/j.dark.2015.09.001. arXiv: 1505.04190 [hep-ph].

[294] Celine Degrande. "Automatic Evaluation of UV and R2 Terms for Beyond the Standard Model Lagrangians: a Proof-Of-Principle." In: *Comput. Phys. Commun.* 197 (2015), pp. 239–262. DOI: 10.1016/j.cpc.2015.08.015. arXiv: 1406.3030 [hep-ph].

[295] Valentin Hirschi, Rikkert Frederix, Stefano Frixione, Maria Vittoria Garzelli, Fabio Maltoni, and Roberto Pittau. "Automation of One-Loop QCD Corrections." In: *JHEP* 05 (2011), p. 044. DOI: 10.1007/JHEP05(2011)044. arXiv: 1103.0621 [hep-ph].

[296] Valentin Hirschi and Olivier Mattelaer. "Automated Event Generation for Loop-Induced Processes." In: *JHEP* 10 (2015), p. 146. DOI: 10.1007/JHEP10(2015)146. arXiv: 1507.00020 [hep-ph].

[297] Alexey A. Petrov and William Shepherd. "Searching for Dark Matter at Lhc with Mono-Higgs Production." In: *Phys. Lett.* B730 (2014), pp. 178–183. DOI: 10.1016/j.physletb.2014.01.051. arXiv: 1311.1511 [hep-ph].

[298] Linda Carpenter, Anthony DiFranzo, Michael Mulhearn, Chase Shimmin, Sean Tulin, and Daniel Whiteson. "Mono-Higgs-Boson: a New Collider Probe of Dark Matter." In: *Phys. Rev.* D89.7 (2014), p. 075017. DOI: 10.1103/PhysRevD.89.075017. arXiv: 1312.2592 [hep-ph].

[299] Asher Berlin, Tongyan Lin, and Lian-Tao Wang. "Mono-Higgs Detection of Dark Matter at the Lhc." In: *JHEP* 06 (2014), p. 078. DOI: 10.1007/JHEP06(2014)078. arXiv: 1402.7074 [hep-ph].

[300] Georges Aad et al. "Search for Dark Matter in Events with Missing Transverse Momentum and a Higgs Boson Decaying to Two Photons in pp Collisions at $\sqrt{s} = 8$ TeV with the ATLAS Detector." In: *Phys. Rev. Lett.* 115.13 (2015), p. 131801. DOI: 10.1103/PhysRevLett.115.131801. arXiv: 1506.01081 [hep-ex].

[301] Georges Aad et al. "Search for dark matter produced in association with a Higgs boson decaying to two bottom quarks in pp collisions at $\sqrt{s} = 8$ TeV with the ATLAS detector." In: *Phys. Rev.* D93.7 (2016), p. 072007. DOI: 10.1103/PhysRevD.93.072007. arXiv: 1510.06218 [hep-ex].

[302] Georges Aad et al. "Search for dark matter in events with a Z boson and missing transverse momentum in pp collisions at $\sqrt{s}$=8 TeV with the ATLAS detector." In: *Phys. Rev.* D90.1 (2014), p. 012004. DOI: 10.1103/PhysRevD.90.012004. arXiv: 1404.0051 [hep-ex].

[303] Vincenzo Vitale and Aldo Morselli. "Indirect Search for Dark Matter from the Center of the Milky Way with the Fermi-Large Area Telescope." In: *Fermi Gamma-Ray Space Telescope. Proceedings, 2Nd Fermi Symposium, Washington, Usa, November 2-5, 2009*. 2009. arXiv: 0912.3828 [astro-ph.HE]. URL: http://inspirehep.net/record/840760/files/arXiv:0912.3828.pdf.

[304] Dan Hooper, Chris Kelso, and Farinaldo S. Queiroz. "Stringent and Robust Constraints on the Dark Matter Annihilation Cross Section from the Region of the Galactic Center." In: *Astropart. Phys.* 46 (2013), pp. 55–70. DOI: 10.1016/j.astropartphys.2013.04.007. arXiv: 1209.3015 [astro-ph.HE].